



## Durham E-Theses

---

### *A search for massive particles in the cosmic radiation*

Kelly, G. N.

#### How to cite:

---

Kelly, G. N. (1969) *A search for massive particles in the cosmic radiation*, Durham theses, Durham University. Available at Durham E-Theses Online: <http://etheses.dur.ac.uk/8693/>

#### Use policy

---

The full-text may be used and/or reproduced, and given to third parties in any format or medium, without prior permission or charge, for personal research or study, educational, or not-for-profit purposes provided that:

- a full bibliographic reference is made to the original source
- a [link](#) is made to the metadata record in Durham E-Theses
- the full-text is not changed in any way

The full-text must not be sold in any format or medium without the formal permission of the copyright holders.

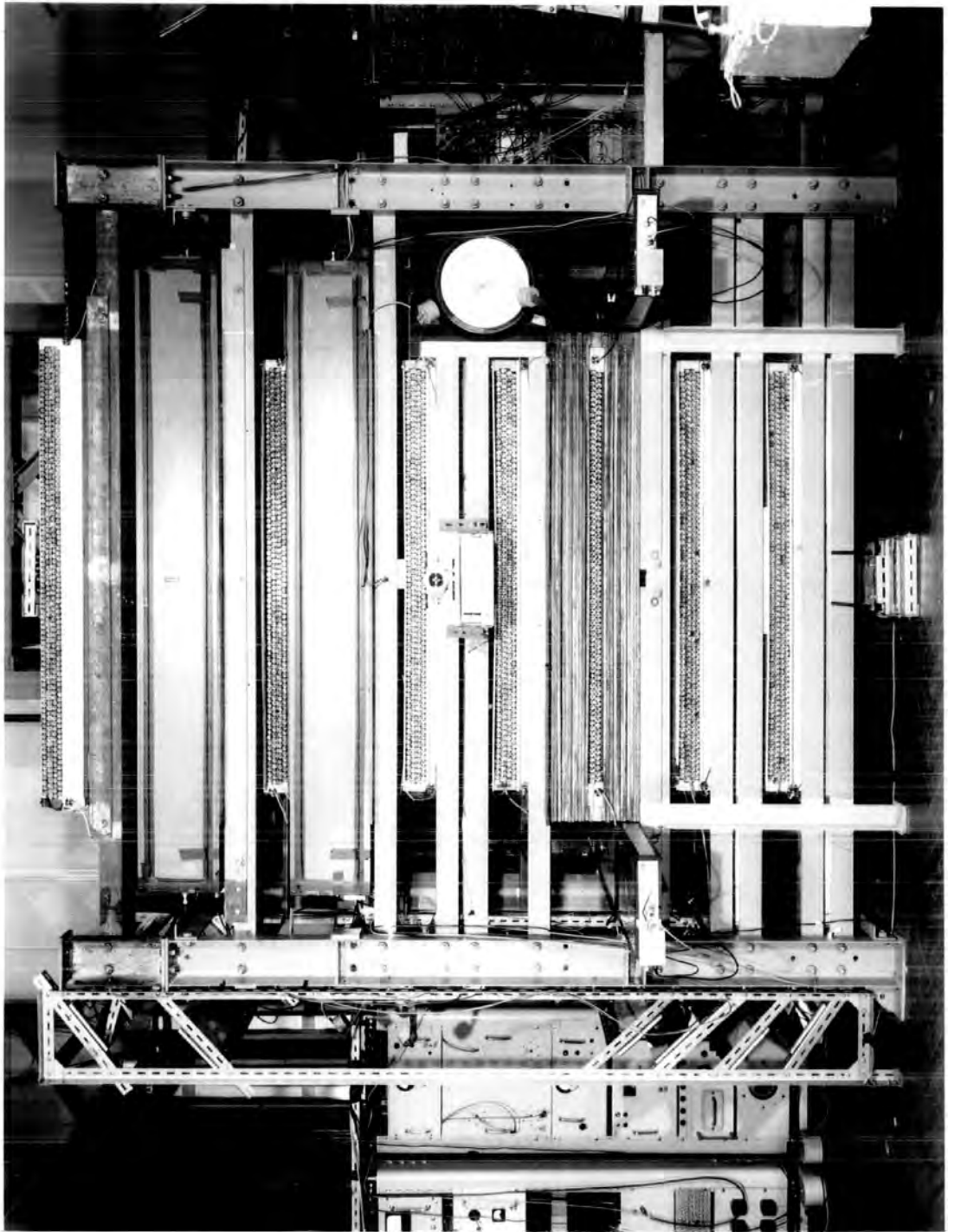
Please consult the [full Durham E-Theses policy](#) for further details.

PLATE I

FRONTISPIECE

THE 'HEAVY MASS'

TELESCOPE



A SEARCH FOR MASSIVE PARTICLES  
IN THE COSMIC RADIATION

by

G.N. Kelly, B.Sc.

A Thesis submitted to the  
University of Durham  
for the Degree of Doctor of Philosophy.

July, 1969.



ABSTRACT

Two large area ( $1.29\text{m}^2$ ) thin water Cerenkov counters have been developed and their properties investigated when amino G acid (a wavelength shifter) is added to the water. With a concentration of  $16\text{mg./litre}$  of the acid an increased response of  $\sim 5$  is achieved, as well as the uniformity improving by a factor of 2, compared with that of a pure water counter. The efficiency of the acid, however, has been found to deteriorate at a rate of  $\sim 3.5\%/month$ . The velocity response of the counters has been studied and it is found that, for counters of the present geometry, the addition of the acid is essential to maintain the inherent property of Cerenkov counters: that of a sharp velocity cut off.

The counters, together with plastic scintillators, neon flash tubes and suitable amounts of absorber have been combined to form a large aperture ( $\sim 0.1\text{ m}^2\text{sterad.}$ ) telescope capable of mass discrimination over a range of several  $\text{Gev}/c^2$ . The properties of, and mass resolution attainable with such a system have been investigated by selecting sub-relativistic sea level cosmic ray protons to traverse the telescope. The mass resolution achieved for protons was a full width at half height of  $350\text{ Mev}/c^2$ , and the intensities of observed protons were found to be in good agreement with measurements of other workers in the same energy region.

The telescope has been operated in a search for sub-relativistic massive particles, having integral or fractional charge ('quarks'), in the sea level cosmic radiation (typically  $M > 1.3\text{ Gev}/c^2$  for  $z = 1$ ; a lower value applying for  $z < 1$ ). One anomalous event has been observed for which an interpretation

in terms of the conventional particles is not forthcoming. The most plausible interpretation appears to be in terms of a unit charged particle having a mass significantly greater than  $3.3 \text{ Gev}/c^2$ . However the finite, but small, probability of  $\sim 10^{-5}$  of the event being spurious, due to the relatively long sensitive time of the neon flash tubes, precludes a definite conclusion as to the existence of massive particles and this one observation has been used to set an upper limit, at the 90% confidence level, to their presence in the sea level cosmic radiation of

$$< 1.01 \cdot 10^{-9} \text{ cm.}^{-2} \text{ sec.}^{-1} \text{ sterad}^{-1}$$

the limit referring to particles incident within well defined velocity bands, these being a function of the particle mass and charge.

The implications on the quark intensity at various levels in the atmosphere have been investigated subject to two models of quark production and four plausible, yet widely differing, models of quark propagation. The intensity limit imposed by the present work, and those reported by other workers searching via different methods, have been used to summarise the limits that can be placed on the quark production cross section subject to each of the production and propagation models, and conclusions have been drawn as to the most profitable areas for future quark searches.

The present work has also allowed a limit of  $\sim 10^{-7}$ , in the mass range  $2\text{-}50 \text{ Gev}/c^2$ , to be placed on the fraction of U particles in the primary radiation at low energies (the U particle being suggested by Callan and Glashow, 1968, to be massive ( $M > 4 \text{ Gev}/c^2$ ), weakly interacting and to comprise  $\sim 10^{-3}$  of the primary radiation).

Deuterons have been detected at various stages of the work and their intensity in the sea level cosmic radiation has been evaluated as

$$(4.2^{+3.0}_{-2.4}) \cdot 10^{-9} \text{cm.}^{-2} \text{sec.}^{-1} \text{sterad}^{-1} (\text{Mev/c})^{-1} \quad \text{for } p_d = 1.65 \text{ Gev/c}$$

$$\text{and } (4.8^{+6.8}_{-3.3}) \cdot 10^{-10} \text{cm.}^{-2} \text{sec.}^{-1} \text{sterad}^{-1} (\text{Mev/c})^{-1} \quad \text{for } p_d = 2.45 \text{ Gev/c}$$

The measured intensities have been shown to be an order of magnitude too large to be consistent with the bulk of production coming through reactions such as  $NN \rightarrow d\pi$ , but they are apparently consistent with what would be expected from 'pick-up' reactions.

The 'heavy mass telescope' has been modified to investigate the possibility of the direct production of muons, from the interactions of neutral primaries, at a rate much greater than that expected from neutrinos having their 'normal' cross section. The results of a series of experiments that were performed were suggestive of a very high pion and proton background, and within the uncertainties in the sea level neutron spectrum the observed rates of events were not inconsistent with all of them having been neutron induced. It is concluded that there is no evidence for an excess of muons induced by neutral primaries as has repeatedly been reported by Cowan et al., (1964 - 1969).

## PREFACE

This thesis describes the work performed by the author in the Physics Department of the University of Durham while he was a Research Student under the supervision of Professor A.W. Wolfendale.

It describes the development of a large aperture Cerenkov counter - scintillation counter - neon flash tube telescope, which was capable of mass discrimination and of enabling the mass of an incident particle to be determined. The telescope has been used in a search for massive sub-relativistic particles (quarks, U particles and deuterons) having unit or fractional charge. A theoretical analysis of quark production and propagation has been made subject to various plausible models, and from a review of cosmic ray quark searches cross section limits have been derived for quark production, and as a consequence of these the most profitable areas for future quark searches have been determined. The telescope was modified to carry out a search for muons produced directly in the interactions of neutral primaries at a rate much greater than that expected from neutrinos having their 'normal' cross section.

The development of the Cerenkov counters, the design, construction and modifications of the telescope, its day to day operation and the data analyses of the various experiments have been the responsibility of the author, with assistance from Mrs. H.J. Edwards during the latter stages of the work. The author has been solely responsible for the theoretical analysis of quark production and propagation, and the derivation of the summary of the upper limits that can presently be imposed on the quark production cross section.

The work which has been published, in which the present author was a

co-author is briefly summarised. Other work carried out by the author but not referred to in this thesis comprises: a study of the interactions of cosmic ray muons in the energy range 5-1000 Gev (Kelly et al., 1967a); a study of the fine structure in the muon charge ratio at large zenith angles (Kelly et al., 1967b); and a report on the relative merits of large area scintillation counters and gas proportional counters (Ashton et al., 1967b). All three papers were presented at the Calgary Cosmic Ray Conference.

The results of a search for relativistic fractionally charged quarks in the cosmic radiation have been published in the Journal of Physics (Ashton et al., 1968a). Evidence against the presence of U particles in the primary radiation has been published in Physical Review Letters (Ashton et al; 1968b). Preliminary results on the search for neutrally induced directly produced muons were presented at a CERN Neutrino Meeting and are to be published in a CERN report (Ashton et al., 1969a). Preliminary results of the search for massive sub-relativistic particles have been published in Physics Letters (Ashton et al., 1969b).

The results of the most recent work described in this thesis are to be presented at the International Conference on Cosmic Rays at Budapest in August, 1969. These include a paper on the development and uses of large area water Cerenkov counters (Ashton and Kelly); the deuteron intensity in the sea level cosmic radiation (Ashton et al.); final results on the search for neutrally induced muons (Ashton et al); and a review of the quark production cross section limits that can be imposed from cosmic ray searches, as well as an appraisal of the future of cosmic ray searches as opposed to those proposed for the CERN I.S.R. (Ashton and Kelly).

## CONTENTS.

	Page.
ABSTRACT	i.
PREFACE	iv.
CHAPTER 1 INTRODUCTION	1.
1.1 Particle symmetry and the quark model.	1.
1.2 The quark search.	6.
1.3 The present quark search.	8.
1.4 The Glashow U particle.	10.
1.5 Muons from neutral primaries.	11.
CHAPTER 2 THE BASIC PROPERTIES OF THE DETECTORS	14.
2.1 Introduction.	14.
2.2 The neon flash tubes	14.
2.2.1 The flash tube trays.	14.
2.2.2 Efficiency of the neon flash tubes.	15.
2.3 The scintillation counters.	16.
2.3.1. Design of the counters.	16.
2.3.2 Linearity of the scintillation counter.	17.
2.3.3 Pulse height distributions for muons traversing the scintillators.	18.
2.4. The Cerenkov counters.	19.
2.4.1 Introduction.	19.
2.4.2 Design of the Cerenkov counters.	20.
2.4.3 Response of the counter containing pure water.	20.
2.4.4 Inadequacies of a pure water counter of the present geometry.	21.
2.4.5 Increased efficiency due to the addition of amino acid G.	23.

	Page.
2.4.6 Pulse height distributions for muons traversing the counter.	24.
2.4.7 Efficiency of amino acid G as a function of time.	24.
2.4.8 Comparison with results of other workers.	25.
CHAPTER 3 THE PROTON EXPERIMENT - CALIBRATION OF THE DETECTOR	27.
3.1. Introduction.	27.
3.2 The scintillation counter - Cerenkov counter -neon flash tube telescope.	27.
3.3 Selection, display and recording system.	27.
3.4 Energy loss in the scintillation counter.	29.
3.4.1 Most probable energy loss as a function of particle velocity.	29.
3.4.2 Most probable energy loss recorded by a muon calibration of the scintillators.	31.
3.5 Expected velocity response of the Cerenkov counter.	33.
3.5.1 Cerenkov light from the water.	33.
3.5.2 Cerenkov light from the perspex box.	34.
3.5.3 Cerenkov light from knock on electrons.	36.
3.5.4 Median pulse height recorded by a muon calibration of the Cerenkov counters.	38.
3.6 Normalisation of the telescope material for ionisation purposes.	38.
3.7. Selection criteria and analysis of events.	40.
3.7.1 Initial selection of events from the film.	40.
3.7.2 The basic data.	42.
3.7.3 Initial analysis of events.	43.
3.7.4 Mass determination of an event.	44.
3.7.5 Weighting of the equations.	46.
3.7.6 A more precise estimate of the residual range.	49.
3.8. Experimental mass distributions obtained from the P,Q and R series.	50.

	Page.
3.9. Measurements on the Cerenkov counters.	53.
3.9.1 The measured velocity response.	53.
3.9.2 Scintillation light from the solute.	55.
3.10 The proton spectrum at low energies.	55.
3.10.1 The telescope acceptance functions.	55.
3.10.2 Angular distributions of accepted particles.	56.
3.10.3 The observed rates of stopping protons.	57.
3.10.4 Correction of the observed rates due to proton interactions in the telescope.	58.
3.10.5 Comparison with other workers.	61.
3.11 Response of the scintillators as a function of velocity.	62.
3.12 Estimate of the deuteron intensity at sea level.	62.
3.12.1 Extraction of deuterons from the tail of the mass distributions.	62.
3.12.2 Correction of the deuteron intensity for interactions in the telescope.	64.
3.13 Summary.	66.
CHAPTER 4. THE HEAVY MASS SEARCH	68.
4.1. Introduction.	68.
4.2 The heavy mass telescope.	69.
4.3 Selection, display and recording system.	70.
4.4 The basic data.	72.
4.5 Analysis of the heavy mass candidates.	73.
4.5.1 Mass determination of the events.	73.
4.5.2 Individual analysis of the possible candidates.	74.
(a) Event H8/18.	74.
(b) Event H32/99.	75.
(c) Event H9/64.	75.
(d) Event H40/6.	78.
(e) Summary.	86.

	Page.	
4.6	The incident momentum bands accepted by the telescope.	87.
4.7	Aperture of the telescope.	88.
4.8.	Limits on the intensity of quarks.	88.
4.9.	The deuteron intensity at sea level.	90.
4.9.1	The observed intensity.	90.
4.9.2	Corrections to the observed intensity.	90.
4.9.3	Comparison with measurements of other workers.	93.
4.10	The Glashow U particle.	96.
4.10.1	Introduction.	96.
4.10.2	Limits on the intensity of U particles.	97.
4.10.3	Further evidence against the U particle.	99.
4.11	Summary.	100.
CHAPTER 5	PROPAGATION OF QUARKS IN THE ATMOSPHERE	102.
5.1	Introduction.	102.
5.2	Quark production in the atmosphere.	103.
5.3	Quark interactions with matter.	107.
5.4	Method of calculation.	110.
5.5	Results of the calculations.	112.
5.6	Limits on the quark production cross section, imposed by the present work.	112.
5.7	Quark production via nucleon dissociation.	115.
5.8	Summary.	117.
CHAPTER 6	REVIEW OF QUARK SEARCHES.	119.
6.1.	Introduction.	119.
6.2	Review of quark searches.	119.
6.2.1	Searches at the proton accelerators.	119.

	Page.
6.2.2 Searches at the electron accelerators.	121.
6.2.3 Searches in the cosmic radiation.	124.
(a) Relativistic fractionally charged particles.	124.
(b) Delayed particles in air showers.	130.
Chatterjee et al., 1965.	132.
Damgaard et al., 1965.	133.
Jones et al., 1967.	133.
Bjornboe et al., 1968.	134.
Dardo et al., 1968.	137.
(c) Searches for sub-relativistic massive particles.	143.
6.2.4 Searches for fractionally charged quarks. concentrated in matter.	143.
6.3. Summary of the experimental quark production cross section limits.	145.
6.4 Theoretical estimates of the quark production cross section.	147.
6.5 Conclusions and possible future quark searches.	149.
CHAPTER 7 MUONS FROM NEUTRAL PRIMARIES	155.
7.1. Introduction.	155.
7.2 A study of penetrating charged secondaries from neutral primaries.	156.
7.2.1 Modifications to the heavy mass telescope.	156.
7.2.2. Selection of events: N and M series.	157.
7.2.3 The basic data.	158.
7.2.4 The observed rate of events.	159.
7.2.5 Preliminary conclusions and a more refined analysis.	162.
7.3. Muons resulting from the interactions of neutral primaries.	167.
7.3.1. The experimental arrangement and electronic selection.	167.
7.3.2 The basic data and film analysis.	168.
7.3.3 Calibration of the telescope with stopping- atmospheric muons.	169.
7.3.4 The analysis and identity of the neutral induced events.	173.

	Page.	
7.4	Summary of the N, M and C series.	175.
7.5	Comparison with the work of Cowan et al.	176.
7.6	Limits on the suggested neutrino resonance cross section.	180.
7.7	Interpretation of the present results in terms of neutron induced protons and pions.	182.
7.7.1.	The sea level neutron spectrum.	183.
7.7.2	The expected number of neutron induced single protons.	183.
7.7.3	The expected number of neutron induced single pions.	185.
7.7.4	Comparison between the observed and predicted numbers.	187.
7.8	Conclusions.	187.
APPENDIX A	A SEARCH FOR RELATIVISTIC FRACTIONALLY CHARGED PARTICLES IN THE COSMIC RADIATION AT SEA LEVEL	191.
APPENDIX B	DEUTERON PRODUCTION THROUGH THE REACTIONS $NN \rightarrow d\pi$ .	194.
B.1	The deuteron production momentum as a function of the primary nucleon energy.	194.
B.2	The observed cross section for deuteron production.	196.
APPENDIX C	DISCUSSION OF RECENTLY PUBLISHED QUARK SEARCHES	199.
ACKNOWLEDGEMENTS		202.
REFERENCES		203.

## CHAPTER 1.

### INTRODUCTION

#### 1.1. Particle symmetry and the quark model.

The advent of the high energy proton accelerators and the refined techniques for studying the products of nucleon interactions has led to the discovery of approximately two hundred particles, and has confused the long held concept of a 'few fundamental particles'. However, this great profusion of particles and the subsequent attempts to establish some underlying order among them have suggested that in fact there may be a triplet of truly fundamental particles from which all the others can be constructed.

Before 1930 all physical phenomena, ignoring the structure of atomic nuclei, were explained in terms of three elementary particles, the proton, electron and photon, interacting through two basic types of force, electromagnetic and gravitational. However to explain the stability of nuclei Yukawa, in 1935, postulated the existence of a new nuclear force acting between nucleons in the nucleus which must be of short range, and be some hundred times greater in strength than the Coulomb force to overcome the enormous Coulomb repulsion. From the range of this force,  $\sim 10^{-13}$  cm., he deduced that it was due to the virtual exchange of a particle between the nucleons which had a mass some 200 times that of the electron. The subsequent observation of such a particle, the  $\pi$  meson, in the cosmic radiation by Lattes et al., 1947, substantiated this prediction which formed the basis of the model of the nucleons which has since emerged. Since that time many new particles have been discovered, the rate of discovery increasing as time

progressed, particularly around 1960 when the higher energy CERN and Brookhaven accelerators came into operation. With so many particles it was clear that they cannot all be 'fundamental' and in the last decade much work has been done to find some apparent order in this sub-nuclear world.

In the fields of classical, atomic and nuclear physics the discovery of symmetry principles or invariances under certain types of transformations has led to conservation laws which greatly reduce the multiplicity of processes and states which might be possible (e.g. in classical physics invariance under space and time translations leads to the conservation of momentum and energy respectively). Likewise in the domain of elementary particles it has been internal symmetry principles which have been the richest source of new conservation laws which have helped to bring order into its understanding. Such new symmetries include the baryon (B) and hypercharge (Y) gauge transformations which give the conservation of baryonic charge (a consequence of the stability and abundance of the proton) and hypercharge (a consequence of the observations of strange particle production), the latter however not holding for weak interactions. With these two conservation laws and the conservation of electric charge (Q) efforts were made to establish what mechanism could most simply give rise to the observed regularities among the particles. Such a scheme is to suppose that the particles themselves are all made up from sub-nuclear particles, 'quarks' as they were later termed, which carry different charges. Because of the three types of charge there must be at least three particles, and the original suggestion by Sakata, 1956, was that all three should have baryonic charge, two should have hypercharge, and only one should have an electric charge. Combining this triplet with its anti-triplet particles can be formed with any

combination of charges. In this model of Sakata the proton, neutron and  $\Lambda^0$  were identified with the triplet, the mesons being formed through quark-antiquark pairs and the heavier baryons,  $\Sigma$  and  $\Xi$ , being more complicated mixtures of two quarks and an antiquark. This model while accounting for the various charges on the particles did not account for the conservation laws.

The application, however, of a further new symmetry principle, that of unitary symmetry, has met with the greatest success in further classifying the 'fundamental particles'. It states effectively that the forces binding the quarks are approximately invariant under the unitary symmetry group  $U(3)$ , this invariance leading directly to the conservation laws of  $Q$ ,  $B$  and  $Y$  (due to requiring the quark content of a system to remain unchanged in a collision) and to the existence of multiplets of particle states that transform into each other under the group operation. Taking a triplet of quarks and its antitriplet, nine combinations can be obtained, one which transforms into itself and the other eight transforming into each other under the operators of the unitary group. The charges of this multiplet are obtained by adding the respective charges of the constituent quarks and this leads to an octet of mesons with well defined  $Q$ ,  $B$  and  $Y$  content. In 1959 the then known seven mesons fitted into this scheme and the missing  $\eta^0$  was later discovered in 1961.

It should be noted at this stage that the proton, neutron and  $\Lambda^0$  could still be identified with the quarks and also that  $U(3)$  can be no more than an approximate symmetry, since if all the quarks are supposed to be dynamically interchangeable they should all have the same mass, and as a consequence all the particles in the meson octet should have the same mass, whereas experimental observation shows that this is not so. The octet of mesons can in fact be

broken into three sub-multiplets ( $\pi$ , K and  $\eta$ ) of approximately equal mass and to satisfy their observed mass splitting it is necessary to assume that two of the quarks have the same mass, while the third should have a slightly greater mass.

Further interest was stimulated in unitary symmetry in 1961 when a new group of mesons having spin 1 was observed in bubble chamber experiments, and when Neeman, 1961, and Gell-Mann, 1962, independently pointed out that the octet of spin  $\frac{1}{2}$  baryons formed themselves into the same charge-hypercharge pattern as the meson octet. The effect on the underlying quarks of suggesting that the spin  $\frac{1}{2}$  baryons formed an unitary octet was revolutionary. The simplest configuration from which both the meson ( $B=0$ ) and baryon octets ( $B=1$ ) could be constructed was again a triplet of quarks; however a difficulty then arose in that if the quarks were assigned unit baryon number then one was left with the octet of baryons having a baryon number of three, since for all the baryons to have the same structure they must each contain three quarks. To overcome this anomaly it was necessary to attribute a baryon number of  $\frac{1}{3}$  to each of the quarks (Gell-Mann, 1964; Zweig, 1964) with the results that their electric charges must be  $\frac{2}{3}$ ,  $-\frac{1}{3}$  and  $-\frac{1}{3}e$ , a rather dramatic suggestion. Possible properties and quantum numbers of the quark triplet (a, b, c) are given in Table 1.1.

The success of unitary symmetry was further demonstrated when attention was turned to the baryonic states having spin  $3/2$ . By 1962 nine such states had been discovered which fitted neatly into the scheme of a unitary decuplet and this allowed predictions to be made regarding the charges and reactions in which the missing one, the  $\Omega^-$ , should be found. Its subsequent observation in 1964 confirmed that strong interactions did satisfy a U(3) symmetry, albeit a slightly broken one. The construction of the baryon octet and decuplet are

Table 1.1

Possible properties of the quark triplet

Designation	Mass	Q	B	Y	Spin	Possible decay schemes
a	several Gev/c <sup>2</sup>	$+\frac{2}{3}$	$\frac{1}{3}$	$\frac{1}{3}$	$\frac{1}{2}$	stable
b	as above	$-\frac{1}{3}$	$\frac{1}{3}$	$\frac{1}{3}$	$\frac{1}{2}$	$a + e^- + \bar{\nu}_e$ $\tau \sim \text{mins.}$
c	as above +146 Mev/c <sup>2</sup>	$-\frac{1}{3}$	$\frac{1}{3}$	$-\frac{2}{3}$	$\frac{1}{2}$	$a + \pi^-$ $\tau \sim 10^{-10} \text{secs.}$



shown in Figure 1.1. in terms of the quark triplet whose properties are listed in Table 1.1. More recently extensions of  $SU(3)$  to higher symmetries have been made and at present  $SU(6)$  appears to be the most in favour. Essentially it is  $SU(3)$  extended to take into account that a particle of spin  $S$  can exist in  $(2S + 1)$  different states and hence predicts larger groups as well as giving a more unified view of the nuclear world.

Attempts by several workers (e.g. Gursey et al., 1964) have been made to overcome the perhaps distasteful notion of fractional charges. These workers suggest the existence of the hadron states as being composites of two fundamental groups of particles exhibiting integral charges. The two groups, commonly referred to as  $\alpha$  and  $\beta$ , are of two types, one being baryonic ( $\alpha$ ) and the other leptonic ( $\beta$ ) and they are distinguished by a new quantum number termed 'supercharge' or 'charm' which is subject to new conservation laws. The group  $\alpha$  is required to be a triplet while  $\beta$  can be any odd multiplet and both groups are irreducible representations of  $SU(3)$ . However, while remaining a plausible interpretation, this suggestion is not as successful as that based on a triplet of fractional charges when used as a model to predict various hadron properties.

Recently, Morpurgo, 1968, has reviewed the status of the quark model (based on the fractionally charged triplet) with respect to its successes and difficulties. Some of its successes include its predictions of the ratio of the proton to neutron magnetic moment, the branching ratios of leptonic baryon decays and the electromagnetic properties of the baryons. The most serious difficulty of the model is suggested to be that of saturation; that is to say why quark-antiquark states and three quark states are strongly bound so as to produce the total mass of a meson or baryon, while four quarks are certainly much less strongly bound. A possible way around this problem

is to conclude that quarks are not particles but simply collective degrees of freedom which can be easily excited and therefore give rise to the excitation spectrum of the lower states of particles. Then if there were only three such degrees of freedom the saturation problem would not arise. However one is then left with the problem of why these degrees of freedom should behave as particles with fractional charge and half-integral spin. At present no answer to this difficulty is forthcoming.

The result of this uncertain theoretical aspect is that the experimental searches for real quarks still remain particularly important in attempting to resolve whether quarks really exist or are only a convenient mathematical device facilitating the computation of the consequences of  $U(3)$ , which has been so successful in returning order to the domain of the 'fundamental particles' at a time when the profusion of newly observed particles appeared to be bringing chaos to the field.

### 1.2. The quark search.

The success of unitary symmetry and the underlying suggestion of the existence of truly fundamental sub-nuclear particles resulted in a wide variety of experiments, all searching for massive particles of fractional or integral charge.

Naturally the first intensive searches were carried out at the proton accelerators where carefully controlled experiments could be performed. The negative results obtained there had one of two implications (apart from the non-existence of quarks as physical realities); the quark production cross section was lower than the measured upper limit or the quark mass was greater than the maximum kinematically possible from presently available proton energies. It was because of this latter reason that attention was focused on searches

being performed in the cosmic radiation where the difficulty of the maximum attainable quark mass is resolved by a primary proton energy spectrum extending effectively to infinity. However the situation with regard to the intensity of produced particles is much less satisfactory. With the integral energy spectrum of primary protons varying approximately as  $E_p^{-1.5}$  and the minimum proton energy required for quark-antiquark production (of mass  $M_q$ ) in a nucleon-nucleon collision varying as  $\sim M_q^2$ , where  $M_q$  is in units of the nucleon mass, the possible intensity of produced quarks is going to vary with  $M_q$  very approximately as  $M_q^{-3}$ , that is a reduction in intensity of 1000 in going from a mass of  $M_p$  to  $10 M_p$ . Thus to achieve results comparable with the accelerators at low masses, as well as useful results at higher masses, the cosmic ray detectors had to be relatively large and be operated for a considerable time.

Unfortunately cosmic ray experiments cannot be controlled like the accelerator experiments which are capable of giving direct limits on the quark production cross section. In the cosmic ray case such limits cannot be obtained directly, the only directly measurable parameter being the intensity of particles at the detector (although a detailed knowledge of the energy spectra of the other cosmic ray components does help). In general quarks produced in the primary proton interactions have to diffuse through the remainder of the atmosphere ( $\sim$  all nucleon interaction lengths) before reaching the detector, and it is thus easily seen that the measurements are particularly sensitive to the properties of the quark interaction with matter. It is for this reason that the searches in the cosmic radiation have been of several types: searching for relativistic fractional charges; delayed particles in air showers and sub-relativistic massive particles. The results of these separate experiments may be combined with each other in such a way

as to be relatively insensitive to the mode of quark propagation in the atmosphere, and to the degree of accompaniment at the detector. However cross section limits derived in this way are not as satisfying or perhaps as reliable as those obtained at the accelerators.

The other major area in which experiments have been performed is in the search for a concentration of fractionally charged quarks in matter. Such searches suffer from the same difficulty as previously mentioned for cosmic ray searches and are further complicated by considerable uncertainties in the exact quark capture process and the subsequent enhancement or degradation of a given material. However, it is possible that these searches, if they are improved and the quark capture process more fully understood, could be more sensitive than the rather more direct cosmic ray experiments. This arises from the relatively long irradiation time of the earth ( $\sim 5 \cdot 10^9$  years) by any quarks produced in cosmic ray interactions.

A full review is given in Chapter 6 of all the quark searches in the different fields and they are comparatively analysed so as to yield the best limits on the quark production cross section for each possible charged state. Particular attention is given to the experiments performed in the cosmic radiation, where the situation is reviewed with respect to four widely differing, yet still plausible, models of quark propagation through the atmosphere which have been proposed and the consequences of which have been calculated in Chapter 5.

### 1.3. The present quark search

As mentioned in the previous section quark searches carried out in the cosmic radiation are particularly sensitive to the mode of quark propagation in the atmosphere. Prior to the present work the majority of searches had been directed towards quarks having an interaction length and a four momentum

transfer in an interaction (equivalent to an inelasticity of  $0.5M_p/M_q$ ) identical to that of a nucleon (apart from the experiment of Jones et al., 1967, which was sensitive to locally produced quarks delayed with respect to an air shower and having an inelasticity greater than 5%.) If however the quark interaction is typified by an inelasticity equivalent to that of a nucleon,  $\sim 0.5$ , then most quarks on reaching sea level would have sub-relativistic velocities, hence rendering the previous searches relatively insensitive. The implications on the quark velocity distribution at sea level are discussed fully in Chapter 5, and the suggestion that they are characterised by such a mode of interaction forms the basis of the present experiment.

The experiment to be described in this thesis stems from a suggestion by Ashton, 1965, that a suitable detection technique to search for sub-relativistic massive particles would be a range-threshold velocity method, which at the same time would give efficient rejection of low energy proton contamination. The principle of the experiment is essentially to impose an upper velocity threshold by means of a water Cerenkov counter and then demand that the particles traverse an absorber of such an amount that only those with mass  $\geq 1.3\text{GeV}/c^2$  and having unit charge are able to penetrate it. Variation of the velocity discrimination level or the amount of absorber gives a system capable of mass discrimination over a mass range of several  $\text{GeV}/c^2$ . It should be noted that the mass discrimination level afforded for unit charged particles is substantially decreased for particles of fractional charge using such a technique.

The detector is basically the scintillation counter-neon flash tube telescope used in the search for relativistic fractional charges (Ashton et al., 1968; Appendix A) which was modified to include further trays of neon flash

tubes, two large area water Cerenkov counters and  $\sim 200 \text{ g. cm}^{-2}$  of iron. The properties of the neon flash tubes and scintillators together with the design and development of the Cerenkov counters are given in Chapter 2. Before inserting the iron absorber into the telescope the mass resolution of such an instrument and the velocity response of the Cerenkov counters were studied using low energy sea level protons to trigger the telescope. The calibration of the telescope and the derivation of the mode of analysis to be used in the following quark search are given in Chapter 3. The quark search itself is discussed in Chapter 4 where several possible quark candidates are considered in detail. Limits on the quark production cross section for each possible charged state of the quark (the experiment being sensitive to integral as well as fractional charges) are evaluated at the end of Chapter 5, subject to the models of propagation discussed in that chapter, and later, in Chapter 6, are compared with the limits derived from other cosmic ray searches employing different techniques.

The observation of two particles characteristic of deuterons is discussed in Chapter 4 and consideration is given, together with other work in this field, to the flux of low energy deuterons at sea level.

#### 1.4. The Glashow U particle.

The possibility of other massive particles in the sea level cosmic rays has been raised by Callan and Glashow, 1968, and the present work can also give some information of relevance to this possibility. The idea stems from the work of Bergeson et al., 1967, on the angular distribution of high energy ( $10^3 - 10^4 \text{ GeV}$ ) cosmic ray muons underground, which suggested results that were in marked disagreement with the generally expected  $\sec \theta$  enhancement if muons are the progeny of pions and kaons. Callan and Glashow have reviewed the possible causes of such an observation and they conclude that

the most plausible interpretation is in terms of a hitherto unknown 'U particle'. It is suggested that this particle is stable, singly charged, massive ( $> 4\text{GeV}/c^2$ ), weakly interacting and is present in the primary radiation to a level of  $10^{-3}$  of the proton flux, as well as its spectrum exhibiting the same energy dependence. They go on to suggest that the particles observed by Bergeson et al. are in fact not muons but U particles, and due to their weak interactions their angular distribution would be almost isotropic, in keeping with the experimental observations.

Such a postulate further stimulates searches for massive particles in the cosmic rays and at the end of Chapter 4 discussion is given to the limits that can be placed on the intensity of such particles from the present experiment, which, while designed primarily to search for sub-relativistic quarks, would also be sensitive to U particles which were moderated to sub-relativistic velocities through ionisation loss in the atmosphere.

#### 1.5. Muons from neutral primaries

In the search for sub-relativistic quarks 27 events were observed to traverse the telescope showing the appearance of a relativistic charged secondary, and in some cases bursts, emerging from what was presumably a neutral primary induced interaction, in the detector beneath the Cerenkov counters. Several events showed single, relativistic, non-interacting secondaries (despite traversing a region of the detector equivalent to more than two nucleon interaction lengths) which perhaps suggested that we were observing a neutrally induced secondary component which was not nuclear active in nature, as would be expected if the source of triggers was neutron interactions yielding pion secondaries.

That such a process of a neutral interaction yielding a non-nuclear active secondary exists at a level above that expected from neutrino interactions has repeatedly been reported by the cosmic ray group at the Catholic University of America. They have suggested the observation of a process of the form:-



Their initial detectors were large volume liquid scintillation tanks which were surrounded by anticoincidence shields and a plot of the rate of occurrence of events (selected by recording the electron from a muon decay) showed the existence of peaks in sidereal time, suggesting that the neutral radiation originated from point sources on the celestial sphere (Cowan et al., 1964; Cowan et al., 1965; Ryan et al., 1966; Buckwalter et al., 1966). With a more elaborate detector, comprising multilayers of scintillator and spark chambers completely surrounded by an anticoincidence shield, they have produced maps of the celestial sphere in the declination range  $-10^{\circ}$  to  $+70^{\circ}$  showing the celestial coordinates of several possible sources (Hesse et al., 1967). However the present author considers that the evidence from which they conclude that their observed particles are in fact directly produced muons, and not muons from the decay of pions produced in neutron interactions, is not particularly convincing.

The interesting nature of some of the neutral induced events in the quark search and the observations of Cowan et al., stimulated us to modify the detector so as to perform a series of controlled experiments to study the secondaries produced in neutral interactions, and hopefully to clarify the uncertainty of whether or not the muons observed by Cowan et al. were directly produced. Chapter 7 is devoted to this series of measurements and a comparison of the present work with that of Cowan et al., together with suggestions of

further work in this field, is given.

## CHAPTER 2.

### THE BASIC PROPERTIES OF THE DETECTORS.

#### 2.1. Introduction.

Before considering the telescope to search for heavy mass particles it seems relevant to first discuss individually the general properties and development of the detectors used. Scintillation counters and Cerenkov counters were used to select the desired particles and gave information of time, velocity and charge of an event. Neon flash-tubes were used essentially to give visual confirmation of the interpretation of the information from the scintillation and Cerenkov counters. In experiments of the present type, where a search is being made at a very low level in the cosmic radiation, visual detectors are essential to give an understanding of background effects.

#### 2.2. The neon flash-tubes.

##### 2.2.1 The flash-tube trays.

The flash-tubes are made from soda glass and are painted black apart from the end windows. They have an average external diameter of 1.75 cm. with a wall thickness of 1 mm. and are filled to a pressure of 60 cm. of mercury with commercial grade neon. Each flash-tube tray comprises four layers of closely stacked tubes, staggered so as to optimise the overall tray efficiency. The useful tray area is slightly larger than  $140 \times 75 \text{ cm}^2$ . Each tray is made of a blockboard frame with the top and bottom surfaces covered with aluminium foil to act as earth electrodes, and the high voltage electrode is a 16 s.w.g. aluminium sheet placed centrally between the four layers of tubes. The electrode gap is 3.55 cm.

### 2.2.2 Efficiency of the neon flash tubes.

The properties of neon flash tubes have been fairly well studied for particles of unit charge (Gardener et al., 1957; Coxell and Wolfendale, 1960; Lloyd, 1960). As the present experiment is designed primarily to search for fractionally charged particles it is important to consider the effect on the efficiency of the tubes for particles giving reduced ionisation.

The efficiency - time delay characteristic of the tubes was measured using the flash tubes in the 'quark telescope' described by Ashton et al., 1968a. Efficiency measurements were made on the tracks produced by muons traversing the telescope for time delays up to 250  $\mu$ s. between the traversal of the particle and application of the high voltage pulse to the flash tube trays. A random flash test was also carried out. A high voltage pulse of 3.4 Kv/cm. was applied across the electrodes and was chosen to optimise between maximum efficiency and minimum random flashing.

A rigorous theoretical treatment has been carried out by Lloyd, 1960, to explain the properties of flash tubes and his treatment gave good agreement with the experimental results of Coxell and Wolfendale, 1960. Lloyd gives the expected efficiency as a function of time delay for a parameter,  $afq$ , where  $a$  is the internal tube radius in cm.,  $f$  is the probability of one electron in the tube initiating a discharge, and  $q$  is the probability of the incident particle producing a free electron/cm. in the tube. The values of  $a$  and  $q$  are determined purely by the dimensions and filling of the tubes. Lloyd has suggested a value of  $f = 1$  in order to fit experimental results for tubes filled to a pressure of 0.6 At., and it is assumed that  $f = 1$  for the present tubes which are filled to 0.79 At. The resulting theoretical value of  $afq$  for the present tubes is 12.9. The measured efficiency-time delay characteristic of the tubes is compared with the predicted curves of Lloyd for values of  $afq$  of 8, 10 and 12, in Figure 2.1, where it can be seen that the measured

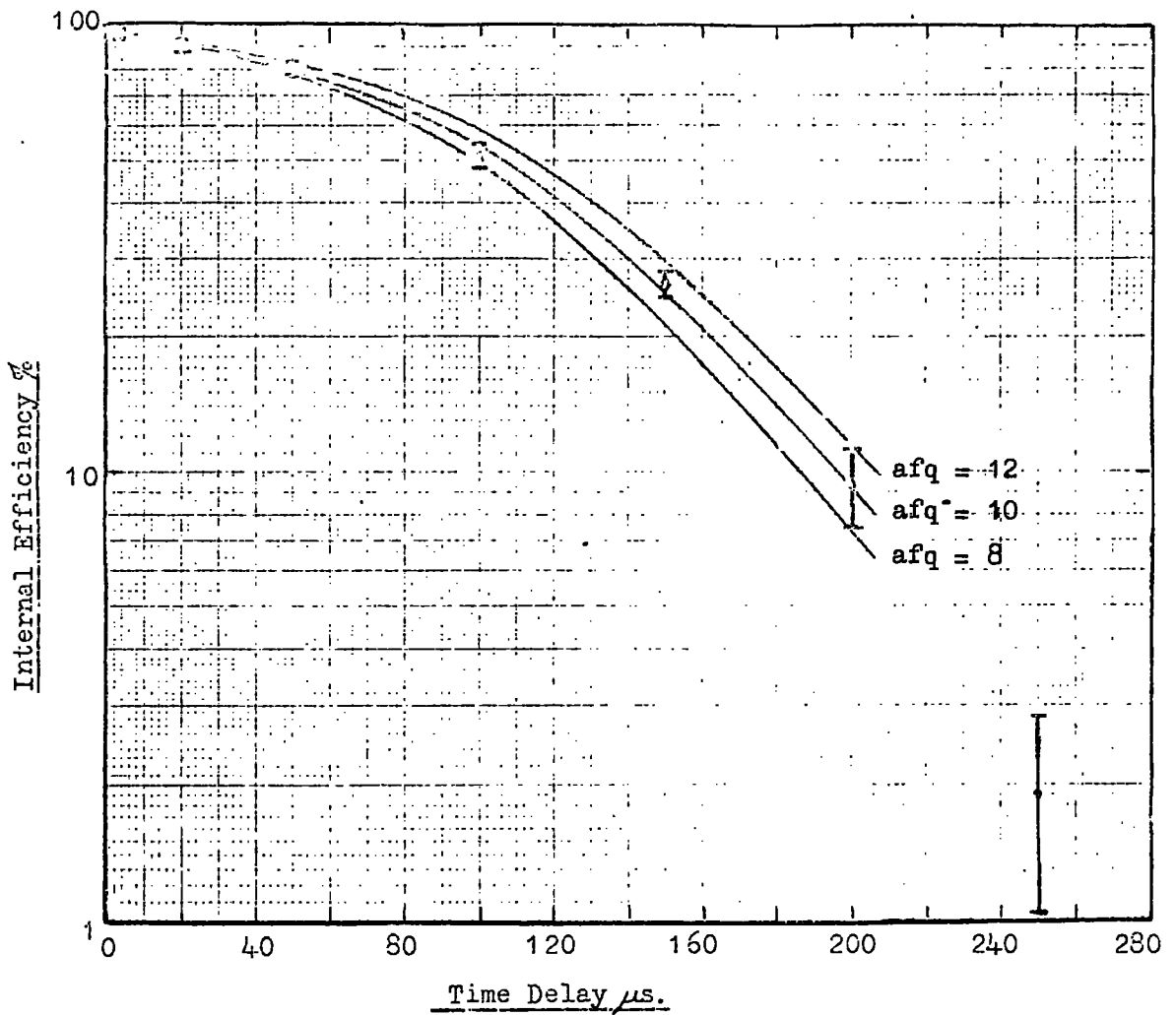


Figure 2.1 The measured internal efficiency-time delay characteristic compared with the theoretical predictions of Lloyd(1960).

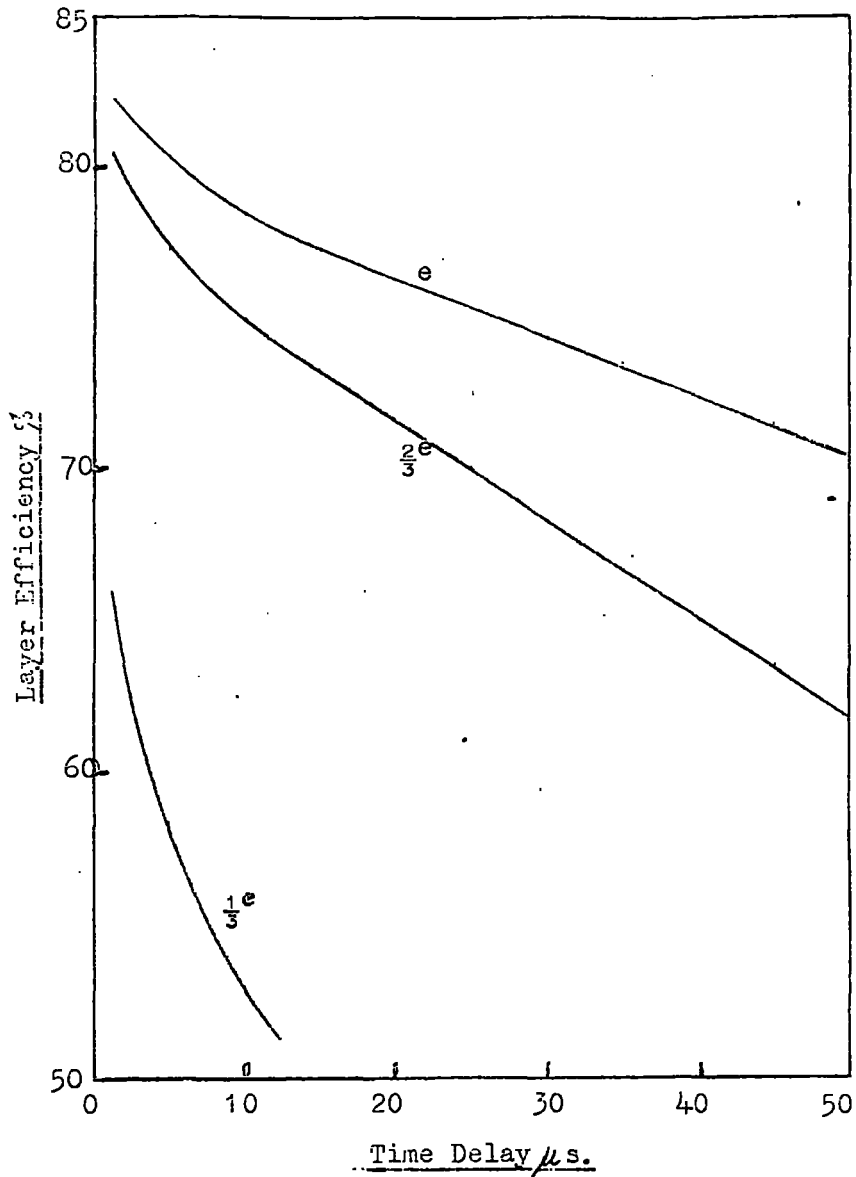


Figure 2.2 Theoretical layer efficiency as a function of time delay for unit and fractional charges.

points are not inconsistent with a value of  $afq$  of approximately 12.

Taking the theoretical value of  $afq = 12.9$  as representative of the tubes for unit charged particles, the corresponding expected values of  $afq$  for particles of  $Z = \frac{2}{3}$  and  $Z = \frac{1}{3}$  are respectively 5.75 and 1.43, since the only parameter that changes is  $q$ , and  $q \propto \frac{Z}{\beta^2}$ . The predicted layer efficiencies for relativistic charge  $e$ ,  $\frac{2}{3}e$  and  $\frac{1}{3}e$  are shown in Figure 2.2 as a function of time delay. While the average number of ion pairs produced in a flash tube by a particle of charge  $\frac{2}{3}e$  and  $\frac{1}{3}e$  are only 8.7 and 2.2 respectively, the predicted efficiencies are still large enough to be easily measurable operating at fairly short time delays. Even if it is assumed that the measured efficiency - delay points fit a value of  $afq = 9$ , which is a severe lower limit to impose, the efficiency even in the worst case, i.e. for particles of  $Z = \frac{1}{3}$ , is only reduced by  $\sim 3\%$  operating at a time delay of  $5 \mu s$ . It can be concluded that neon flash tubes are quite capable of detecting relativistic particles of  $Z = \frac{2}{3}$  and  $Z = \frac{1}{3}$ . As  $afq$  is a function of  $1/\beta^2$  the theoretical efficiencies shown in Figure 2.2 will be increased for sub-relativistic particles.

### 2.3 The Scintillation Counters.

#### 2.3.1 Design of the counters.

The main factor governing the design of the counters was a compromise between large light collection and good linearity over the counter. A diagram of a counter is shown in Figure 2.3. It consists of NE 102 A phosphor of dimensions  $140 \times 75 \times 5 \text{ cm}^3$ , with density  $1.032 \text{ g. cm.}^{-2}$ , a decay time of fluorescence of 3 ns. and a light output of 65% of that of an anthracene crystal of the same geometry. A perspex light guide of dimensions  $75 \times 30 \times 5 \text{ cm.}^3$  is optically cemented to each 75 cm. edge of the phosphor. To each light guide are attached three 2" photomultipliers cemented to the perspex

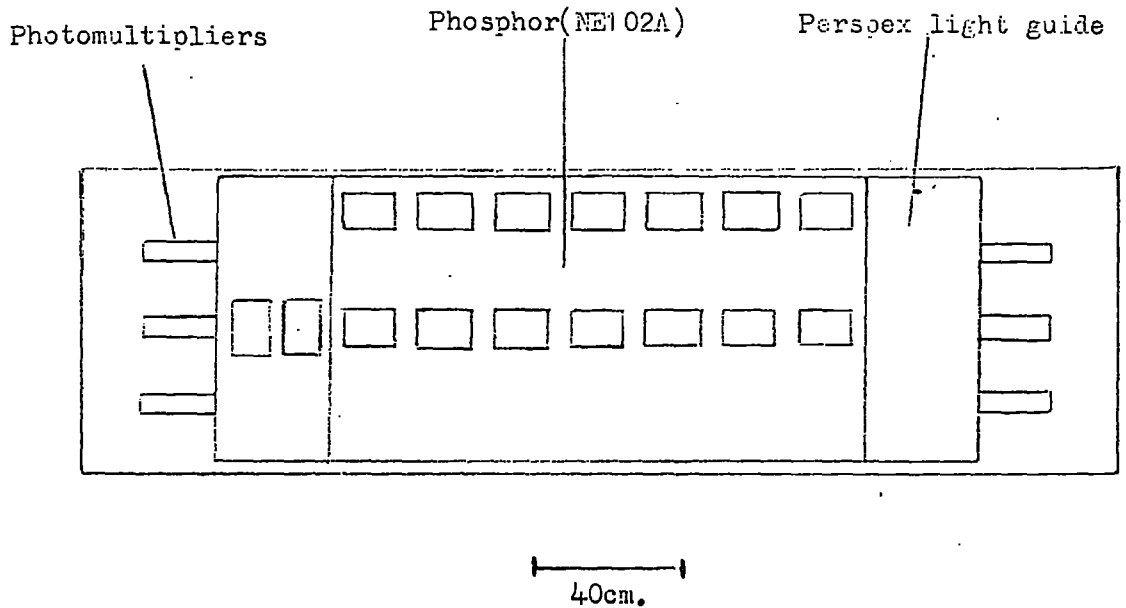


Figure 2.3 Top view of the scintillation counter showing the positions at which the response was measured (small rectangles).

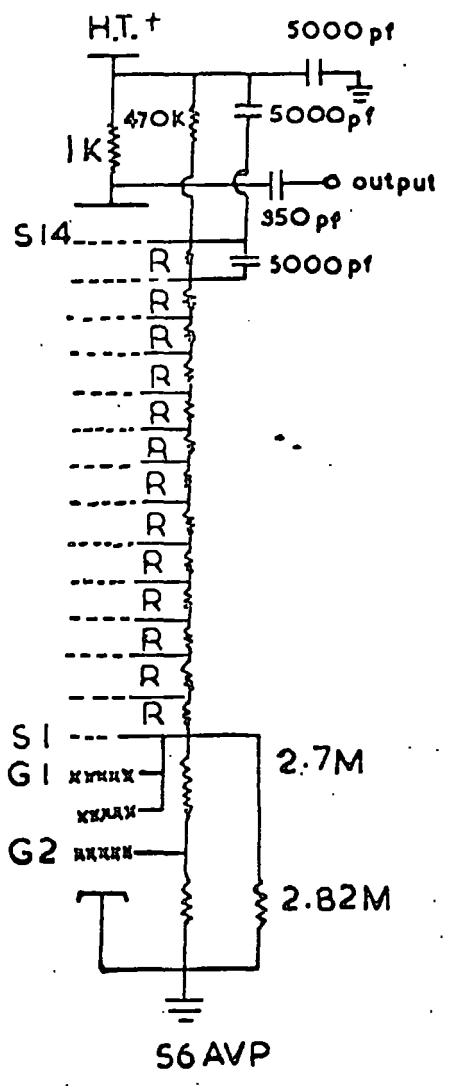
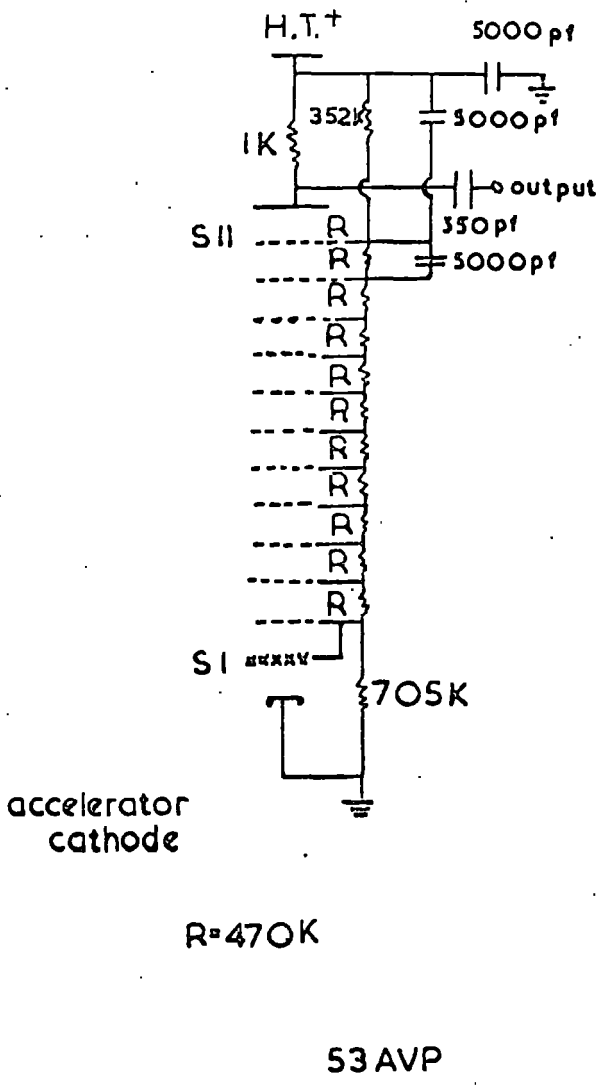


Figure 2.4 The resistance chains used for the 53AVP and 56AVP photomultipliers.

with N.E. 580. The scintillator is mounted in a light tight aluminium box in a manner such as to minimise the area in contact with the phosphor to ensure the most efficient light transmission by means of total internal reflection.

The six photomultipliers attached to each counter comprise one 56 AVP and five Mullard 53 AVP photomultipliers. The resistance chains, shown in Figure 2.4, were chosen for high gain. A positive supply voltage is applied to the photomultipliers and the output, a negative pulse of decay time 100 ns., is taken from the anode. The three outputs from each end are fed into an emitter follower and the outputs from both emitter followers are then added.

### 2.3.2 Linearity of the scintillation counter.

Before the photomultipliers were attached to the light guides they were matched by a method due to Kerns et al., 1959. Each photomultiplier in turn was placed in a light tight box and the output pulse in response to a fixed source of light was measured as a function of supply voltage. The source of light was a spark generated in the arc discharge of a mercury-wetted relay having a decay time of 3 ns., the same as that for the phosphor. Although each tube was found to have a different gain at a given supply voltage, the variation of gain as a function of supply voltage was the same for the same type of photomultiplier and the output pulse height,  $v$ , satisfied the relation

$$v = a V^n$$

where  $a$  is a constant (varying between tubes) and  $V$  is the supply voltage. For the 53 AVP tubes  $n$  was found to be 8 and for the 56 AVP tubes  $n = 14$ . A supply voltage was assigned to each tube so that they all had the same gain.

The linearity of the counter was then studied by measuring the response of the three photomultipliers at one end of the counter as a function of the position in the counter through which the particles pass. This was achieved by selecting muons with two scintillation counters of dimensions  $15 \times 10 \times 2.5$  cm.<sup>3</sup>, and separation 40 cm. forming a coincidence telescope. The coincidence pulse was used to trigger the oscilloscope and the pulse from the main scintillator displayed on the time base. Pulse height distributions were measured along the centre line of the counter and along a line 25 cm. from the centre line in the positions shown in Figure 2.3. Measurements were also made of Cerenkov light produced in the perspex light guide.

The results are shown in Figure 2.5. There is no significant difference between the response along the centre line and the line 25 cm. away, and it can be concluded that there is no response variation across the 75 cm. side of the scintillator. The total response of the counter is the sum of the curve shown in Figure 2.5 and its mirror image about the centre point. The maximum non-uniformity of the counter, expressed as

$$\frac{R_o - R_c}{R_c} \times 100\%$$

where  $R_o$  is the total response at the end of the phosphor and  $R_c$  is the total response at the centre of the phosphor, was found to be 18%. Such a non-linearity is not serious and can be corrected for with knowledge of where the particle traversed the scintillator by use of the scintillators in conjunction with visual detectors.

### 2.3.3. Pulse height distributions for muons traversing the scintillator.

A detailed analysis of the measured and predicted distributions in these scintillators has been reported by Simpson, 1968, and Ashton et al., 1968a, and hence the present discussion will be brief.

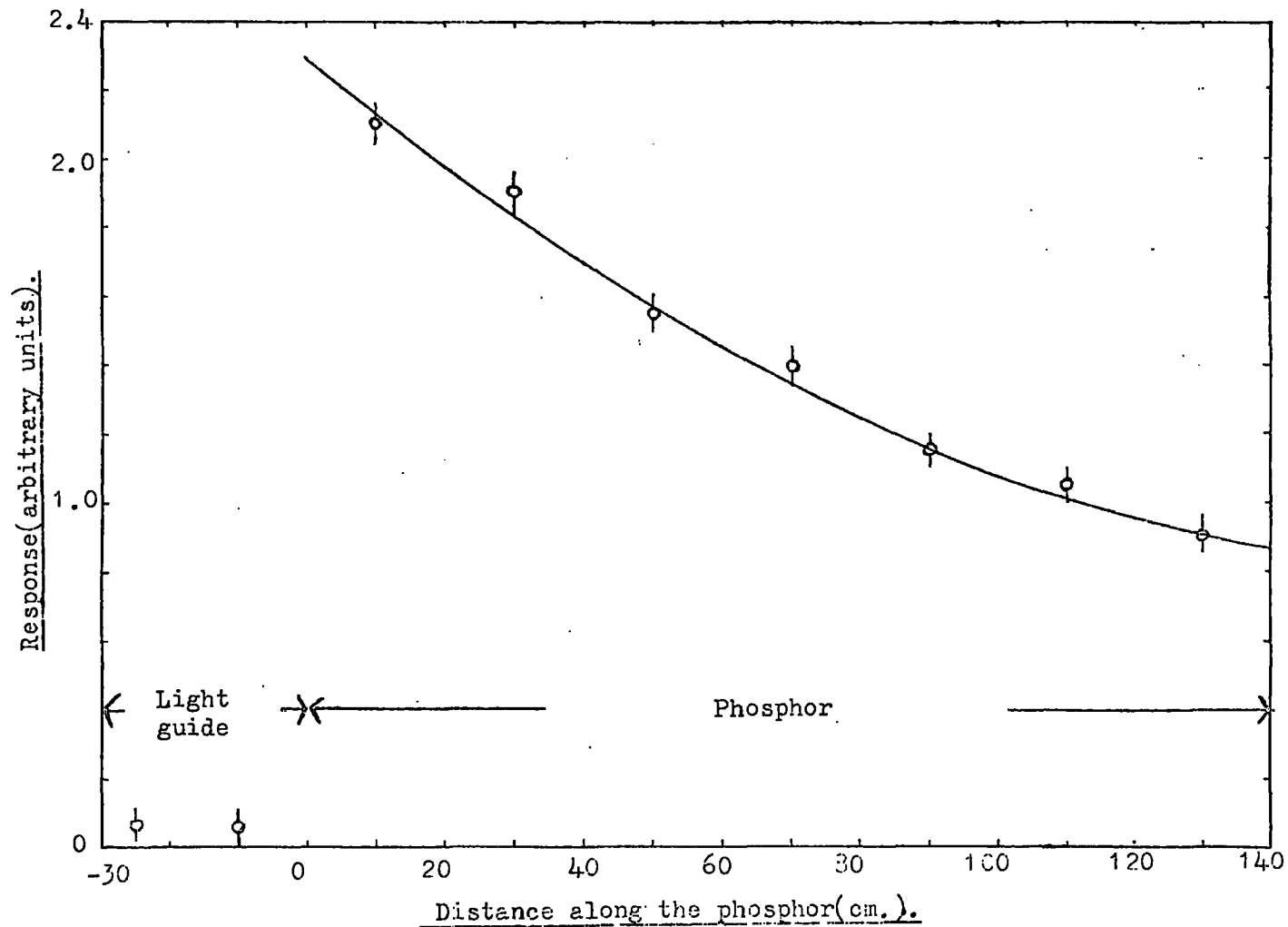


Figure 2.5 Response of one end of the scintillator as a function of the position of the incident particle, also showing the response due to Cerenkov light produced in the perspex light guides.

Muons were selected to traverse within  $\pm 7$  cm. of the centre line of the scintillators in the 'quark telescope' (Ashton et al., 1968a; and Appendix A) by means of a three fold geiger coincidence, where the bottom layer of geiger counters was shielded by  $61 \text{ g. cm.}^{-2}$  of lead to ensure that muons were at minimum ionisation throughout the whole telescope. Such a selection minimised broadening of the distribution due to non-linearity over the scintillators, and the restricted angular range accepted by the geiger telescope made broadening due to path length variations in the scintillators negligible. The pulse height distribution obtained for such a selection is shown in Figure 2.6 and its full width at half height is 25%.

The shape of the distribution is governed by several factors, notably the Landau distribution of energy loss, fluctuations in the number of photoelectrons produced at the photocathode and fluctuations in the photo-electron multiplication process. The relative contributions of these different processes to the full width at half height of the scintillation line are 18%, 12% and 12% respectively. When the fluctuations in the photomultiplier are folded into the Landau distribution of energy loss, the predicted distribution is obtained as shown in Figure 2.6 and can be seen to be in good agreement with the measured distribution.

Two independent methods (Simpson, 1968) give the number of photoelectrons produced at the photocathodes to be 220, where the average fraction of light collected is 0.05, the efficiency of the phosphor is 200 ev/photon, and the conversion efficiency of photons to photoelectrons is 10%.

## 2.4. The Cerenkov Counters.

### 2.4.1 Introduction.

To search for sub-relativistic quarks in the cosmic radiation by a Cerenkov threshold - range technique (Ashton, 1965) it was necessary to

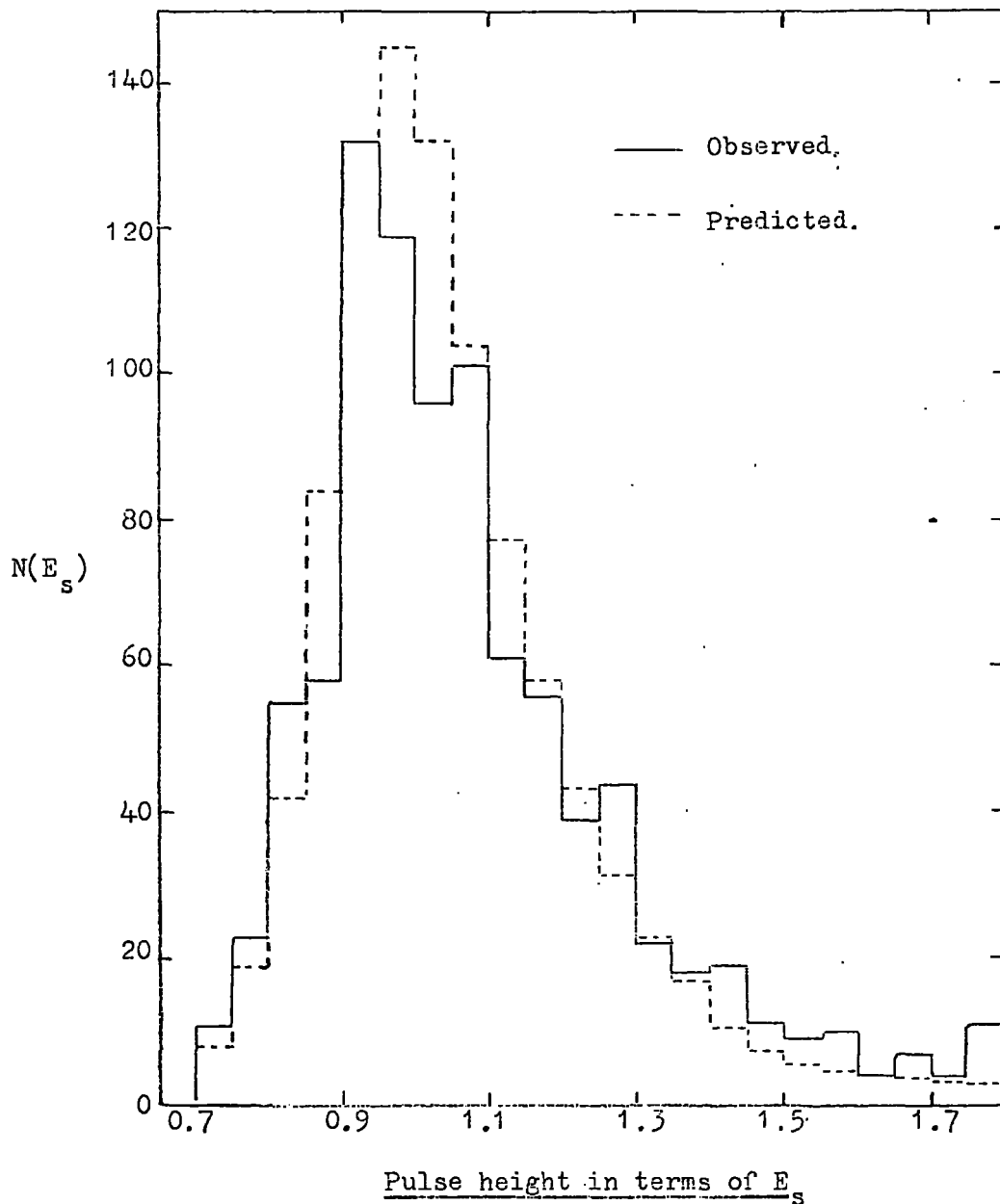


Figure 2.6 Pulse height distribution due to muons traversing a scintillator (where the muons were selected by a geiger coincidence such that they were confined to traverse within  $\pm 7$ cm. of the centre of the scintillator).

construct large area, relatively thin Cerenkov counters which would be efficient even for particles with a velocity close to the Cerenkov threshold. It was thus essential to collect as much of the produced light as possible as well as at the same time preserve a reasonable uniformity over the counter, an important requirement in any large area proportional detector.

#### 2.4.2 Design of the Cerenkov counters.

A diagram of the counter is shown in Figure 2.7. It comprises a perspex box of wall thickness 0.95 cm. with an external cross-section 149.5 x 86.5 cm.<sup>2</sup> and depth 18.5 cm. It was filled to a depth of 16.5 cm. with distilled water and sealed by means of a rubber gasket. The whole box apart from the two viewing ends, 86.5 x 18.5 cm.<sup>2</sup>, was surrounded by high reflectivity silvered foil to further improve the light collection. The Cerenkov light was viewed by eight 5" photomultipliers, EMI 9583 B, four at each end, placed in optical contact with the end of the container (Figure 2.7). The resistance chains, chosen for high gain, are shown in Figure 2.8. The container and attached photomultipliers were supported in a light tight blockboard box such as to give minimum contact between the container and the supports. The pulse from each of the four photomultipliers at one end was fed into an emitter follower and the output from the emitter follower at each end added.

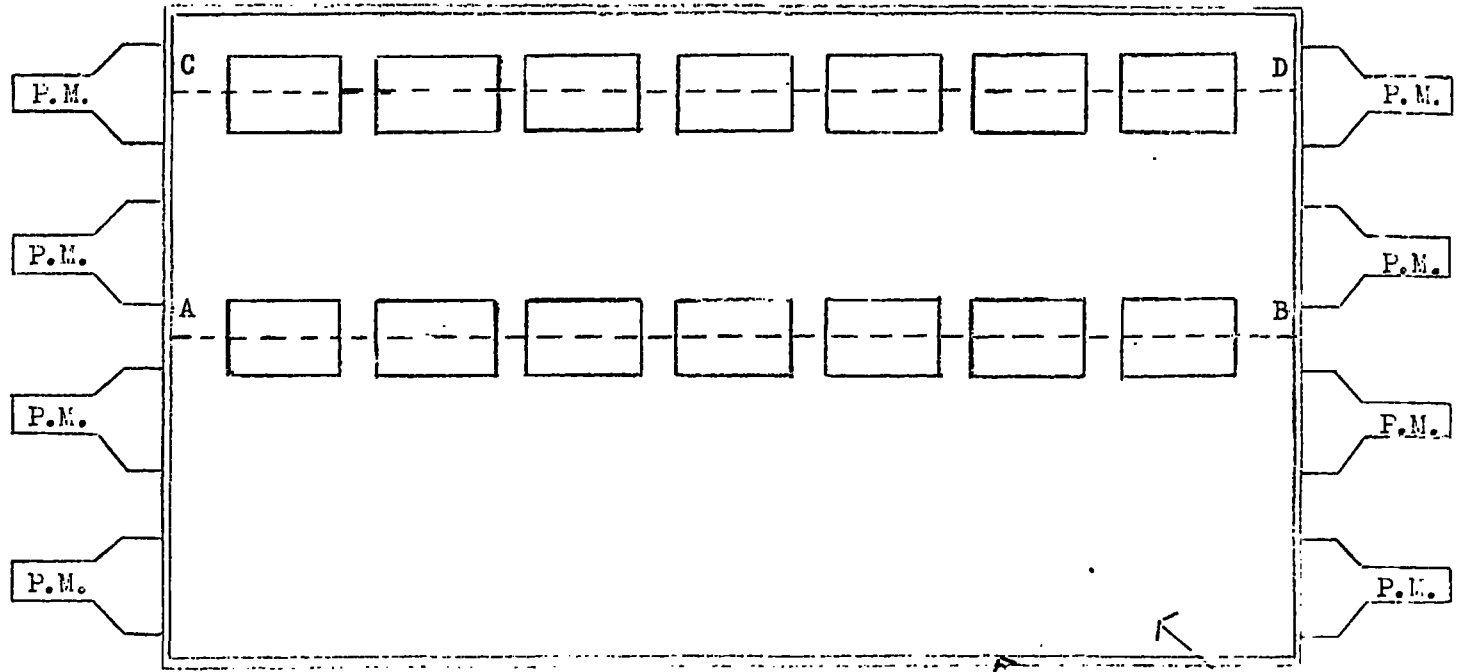
#### 2.4.3 Response of the counter containing pure water,

Before the photomultipliers were attached to the perspex box they were matched in the manner described in Section 2.3.2. As before, the output pulse height,  $v$ , from the photomultiplier satisfied the relation

$$v = a V^n$$

and for these tubes  $n$  was found to be 8.75. The supply voltage for each tube was then chosen to give them all the same gain.

TOP VIEW



Perspex container    \ Water

SIDE VIEW



Figure 2.7 Scale diagram of Cerenkov counter showing the positions at which the response was measured.



The linearity of the counter was measured in the manner described for the scintillators in Section 2.3.2 using a scintillation counter telescope as the triggering source for muons traversing the counter. The response of the four photomultipliers at one end only was measured as a function of position along the lines AB and CD shown in Figure 2.7. The results are shown in Figure 2.9 where it can be seen that the responses along AB and CD are not significantly different for distances greater than 30 cm. away from the photomultipliers, while at nearer distances the response curves begin to diverge. The reason for this divergence is twofold: the absence of light guides which would smooth out such a divergence; and CD lying along the axis of a photomultiplier while AB lies centrally between two photomultiplier axes, giving, for small distances away, a larger solid angle subtended at the photomultipliers by points on CD than on AB.

#### 2.4.4. Inadequacies of a pure water counter of the present geometry.

When a particle with  $\beta = 1$  traverses the counter at normal incidence Cerenkov radiation will be emitted in a cone of half angle  $41.2^\circ$ . Since this angle is smaller than the critical angle at a water-air interface, the light reaching the photomultipliers will have come mainly by virtue of reflections at the silvered surfaces. As the reflectivity of these surfaces can only be of the order of 0.9 such a method of light transmission is inefficient compared with direct transmission or through total internal reflection. The angle of emission of Cerenkov radiation decreases with decreasing  $\beta$  as

$$\theta = \cos^{-1} \left( \frac{1}{\beta n} \right),$$

where  $n$  is the refractive index of the medium, resulting in a decreasing efficiency of light collection with decreasing velocity due to the increasing number of reflections at the silvered surfaces, and the resulting increased path length of the light in reaching the photomultipliers. This effect will

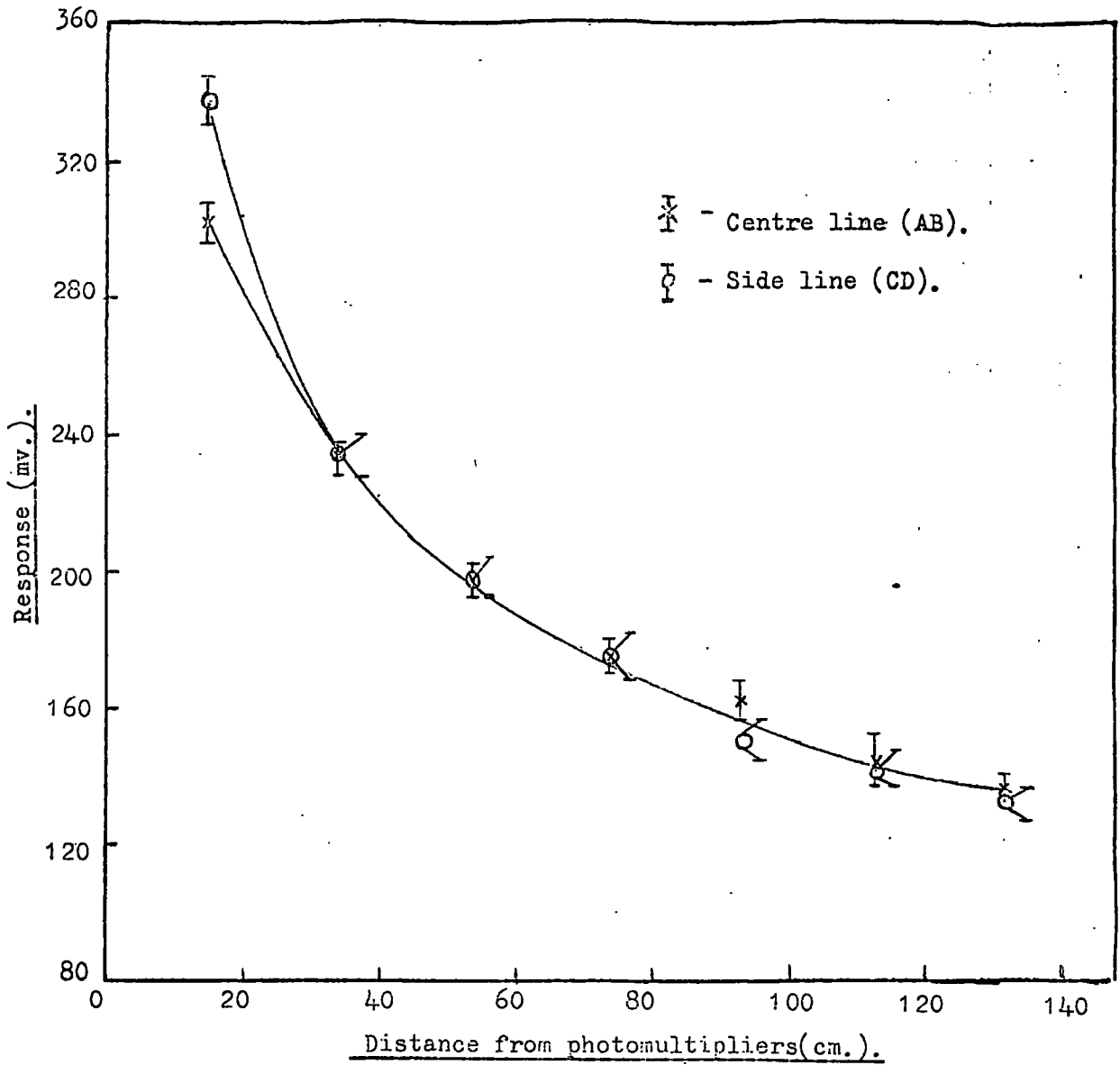


Figure 2.9 Response of one end only as a function of the particle position in the Cerenkov counter containing pure distilled water.

become severe as the particle velocity approaches threshold, and the sharp velocity cut off, an inherent property of a Cerenkov counter, would be smeared out. A pure water counter of the present geometry would obviously not be very efficient for velocity discrimination purposes.

This situation can be improved by the addition of a suitable solute to the water. A survey of various solutes suitable for use in a water Cerenkov counter has been carried out by Heiberg and Marshall, 1956, who concluded that the most efficient was 2- amino - 6,8 - naphthalene disulfonic acid, disodium salt, commonly known as 'amino acid G.' The improvement due to the addition of this solute is twofold. Firstly, it increases the number of photons reaching the photomultipliers by absorption of light of lower wavelengths and re-emission at higher wavelengths which have a good matching to the spectral response of the photomultipliers, as well as having a higher transmission coefficient in water. The enhancement due to this factor can be seen to be large when one considers the differential Cerenkov production spectrum as a function of wavelength falling as  $1/\lambda^2$ . The emission and absorption spectra of this solute have been studied by Saito and Suga, 1959, and are shown in Figure 2.10, as well as the spectral response of the photomultipliers. In Figure 2.11 is shown the attenuation of light in distilled water as a function of wavelength (Pathak, 1967). The second improvement of such a solute is that the majority of light emission is then isotropic (due to absorption and isotropic re-emission coupled with the Cerenkov spectrum falling as  $1/\lambda^2$ ) ensuring that the mode of light transmission to the phototubes is essentially independent of particle velocity.

The effects of adding the solute to the counter are discussed in the next section.

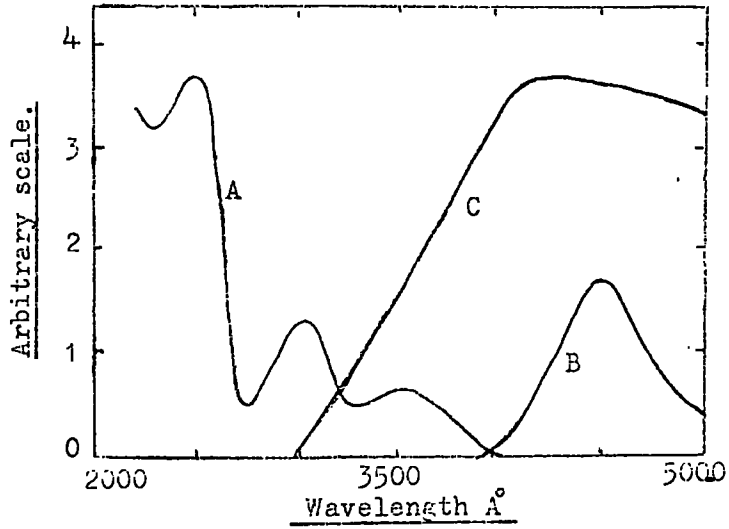


Figure 2.10 The absorption(A) and emission(B) spectra of amino acid G , together with the photocathode sensitivity(C) of the EMI9583B photomultiplier. The vertical scale in each case is arbitrary.

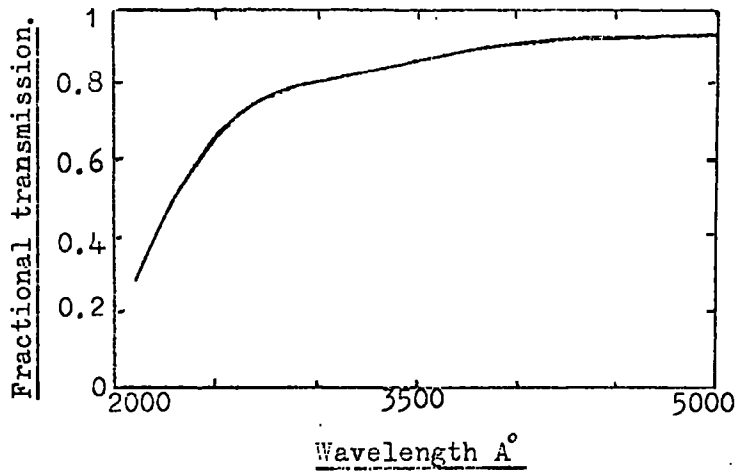


Figure 2.11 The fractional transmission of light through a 10cm. cell of distilled water as a function of wavelength. (Pathak, 1967).

#### 2.4.5 Increased efficiency due to the addition of amino acid G.

The response of one end of the counter was measured at the same positions as before along AB for concentrations of 1,2,4,8 and 16 mg./litre of amino acid G. The response of a second counter, exactly the same as the first, was measured containing pure water and normalised to the first. Solute was then added to this counter to a concentration of 6 mg./litre and the response remeasured.

The response as a function of position along AB of one end only of the counter for various solute concentrations is shown in Figure 2.12. In Figure 2.13 is shown the ratio of the response for a given concentration of solute to the response for a pure water counter as a function of solute concentration for the central and extreme positions measured along AB. Figure 2.14 shows the non-uniformity of the counter as a function of solute concentration. The non-uniformity quoted is arbitrary as the maximum non-uniformity can not be evaluated due to the difficulty in determining the response at the end of the counter in the absence of light guides, and for the present purpose is defined as

$$100 (R_{15} - R_{\text{centre}}) / R_{\text{centre}} \%$$

where  $R_{15}$  refers to the total response (the sum of the response curve for one end and its mirror image) at a distance 15 cm. away from the photomultipliers.

Inspection of the results shows that a gain of 4.6 was achieved in the response at the centre of the tank for a concentration of 16mg./litre of amino acid G. Reference to Figure 2.14 shows that the minimum non-uniformity is achieved at a solute concentration of about 6mg./litre. Increasing the concentration from 6 to 16 mg./litre increases the response by 16% at the expense of reducing the uniformity by a further 36% of the value at 6mg./litre. While the first counter was left containing 16 mg./litre of solute it was

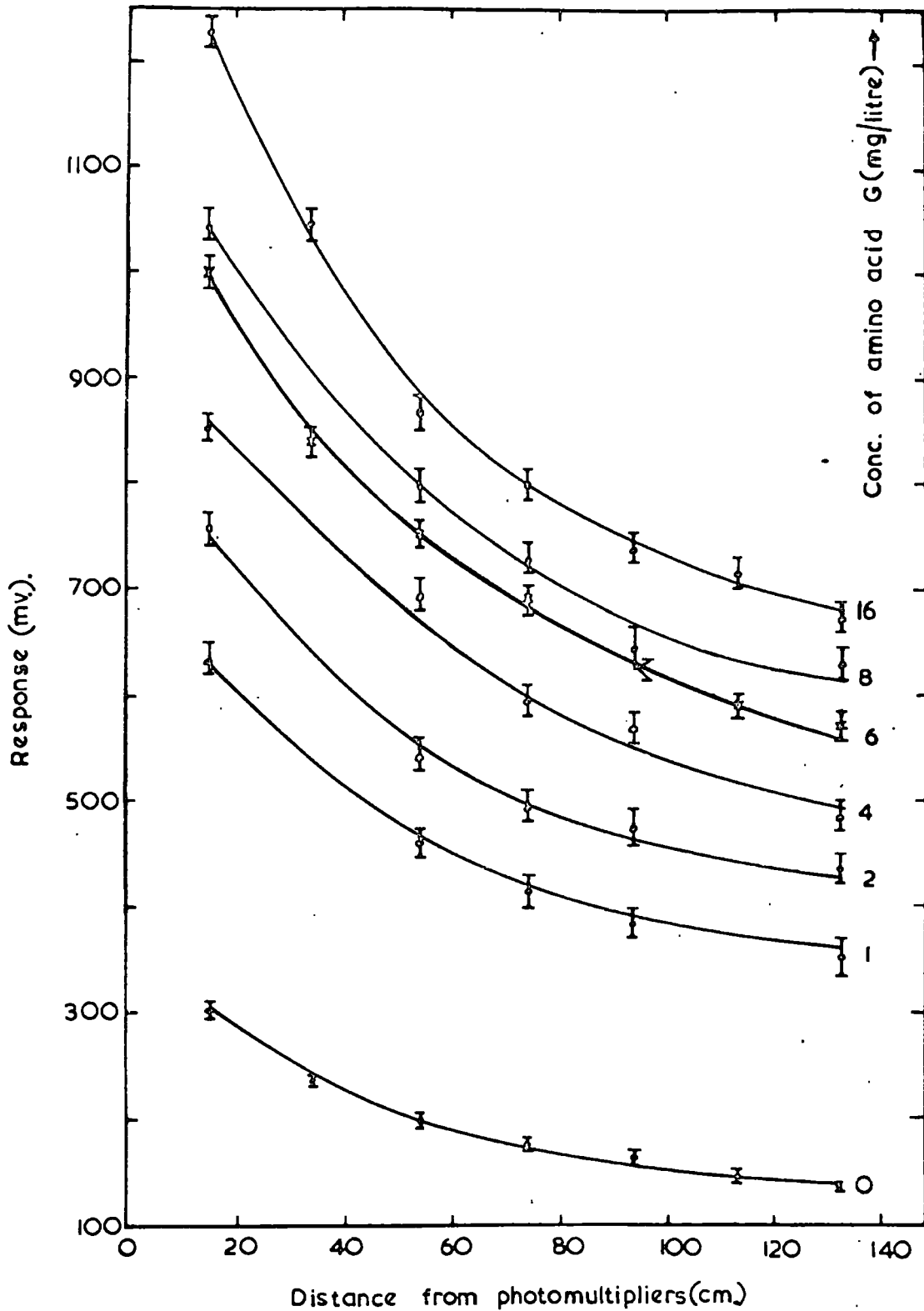


Figure 2.12 Response of one end of the Cerenkov counter as a function of position along the centre line (AB), with the amino acid G concentration as a parameter.

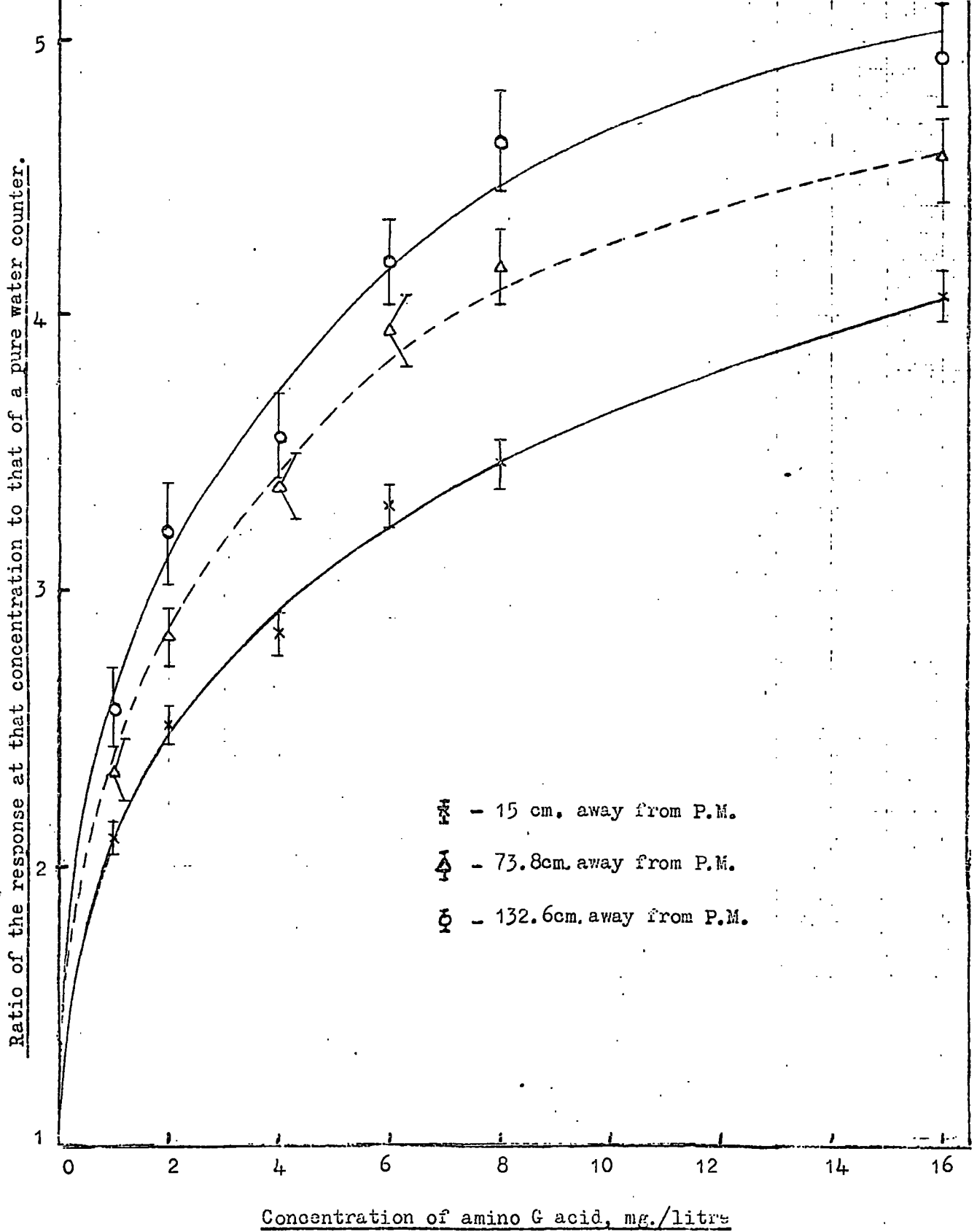


Figure 2.13

The increased response as a function of amino G acid concentration.

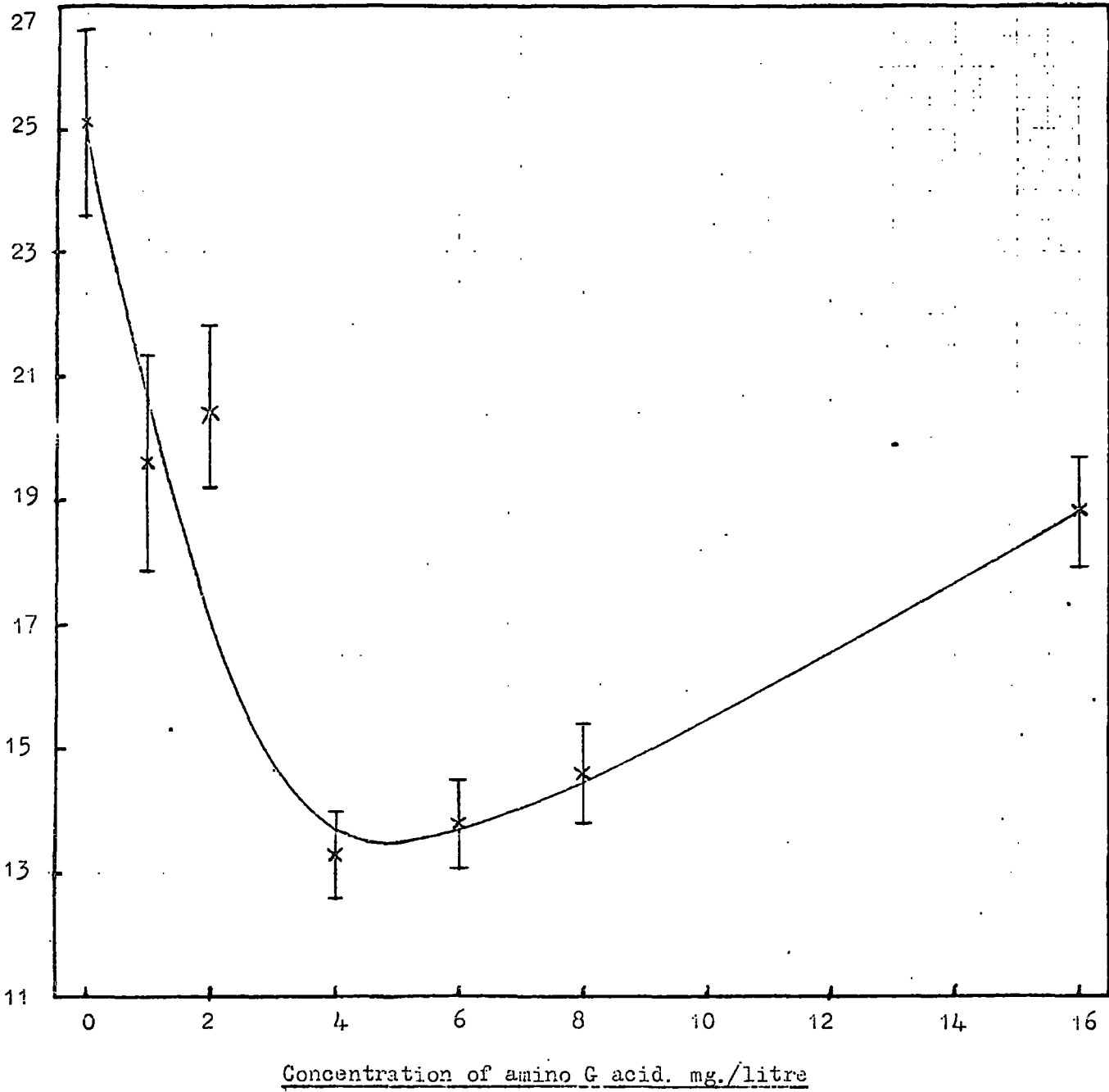


Figure 2.14 Variation of the non-uniformity of the Čerenkov counter as a function of amino G acid concentration.

decided that the extra 16% increase in response was not justifiable at the expense of a worsened uniformity, and the second counter was left containing 6mg./litre of solute.

The response curves for one end of a counter only as a function of position along AB and CD are shown for the counters in their final form in Figures 2.15 and 2.16.

#### 2.4.6 Pulse height distributions for muons traversing the counter.

The Cerenkov tanks were incorporated into a scintillation counter-neon flash tube telescope which is described later in Chapter 3. Muons were selected to traverse within  $\pm 7$  cm. of the centre of the Cerenkov tanks by means of a 3 fold geiger coincidence, as described in Section 2.3.3. The pulse height distributions obtained for each counter are combined and the final distribution is shown in Figure 2.17. Unlike the scintillation counter, where the line shape is governed by the Landau distribution of energy loss with Gaussian distributions superimposed due to photomultiplier fluctuations, the Cerenkov line shape by virtue of the continuity of the produced radiation is purely Gaussian. However due to Cerenkov radiation from knock on electrons the distribution is distorted from Gaussian shape by having a long tail. The full width at half height of the measured distribution is 35% for relativistic particles. This resolution is achievable over the whole counter if corrections are applied for response and track length variations. Such a resolution can be seen to be fairly good in comparison with the value of 25% obtained for the plastic scintillators.

#### 2.4.7 Efficiency of amino acid G as a function of time.

It has been suggested by Saito and Suga, 1959, that the efficiency of the solute degenerates with time, due possibly to the solution dissolving

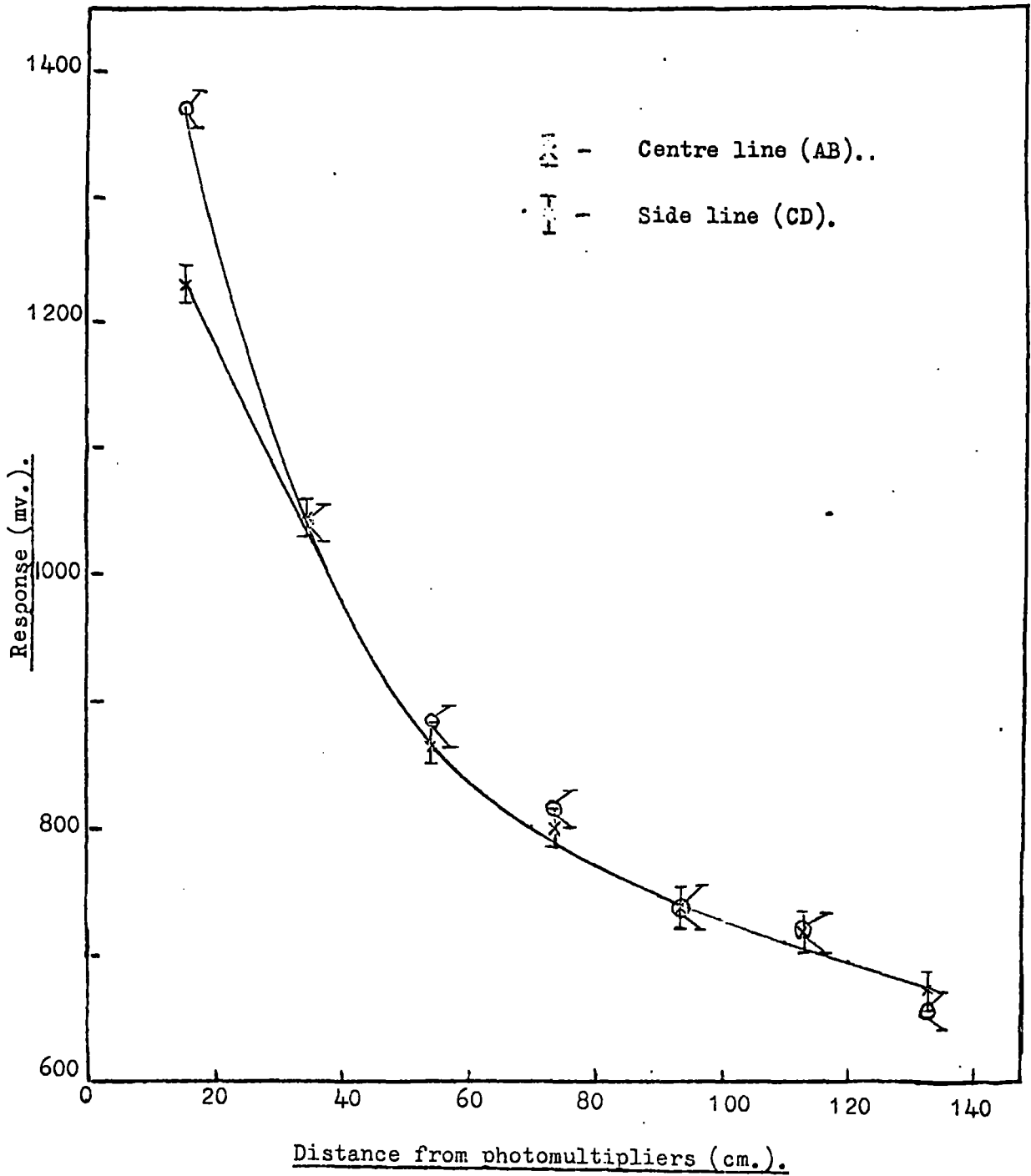


Figure 2.15 The response of one end only of the counter CI in its final form containing 16mg./litre of amino acid G.

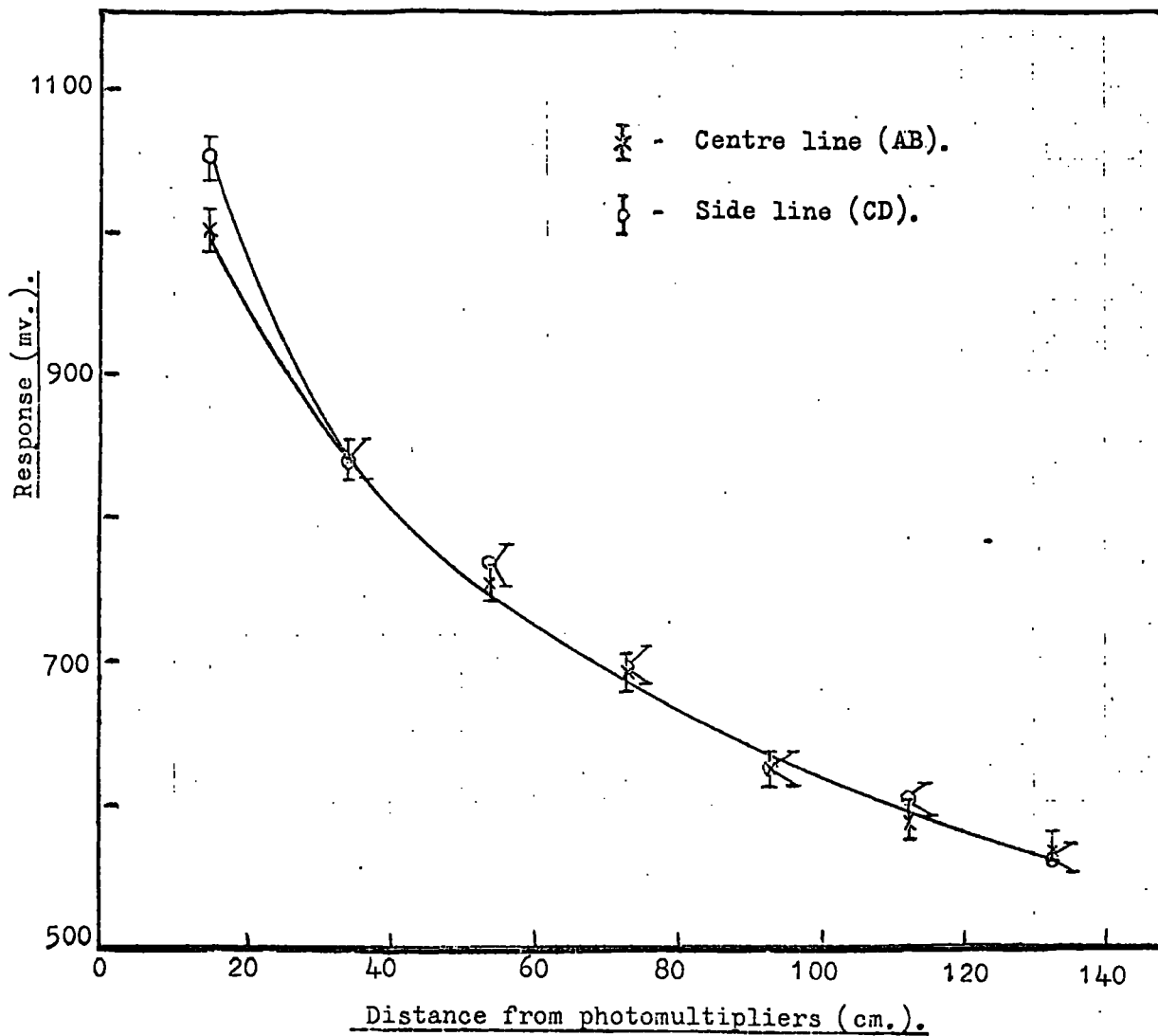


Figure 2.16 The response of one end only of counter CII in its final form containing 6mg./litre of amino acid G.

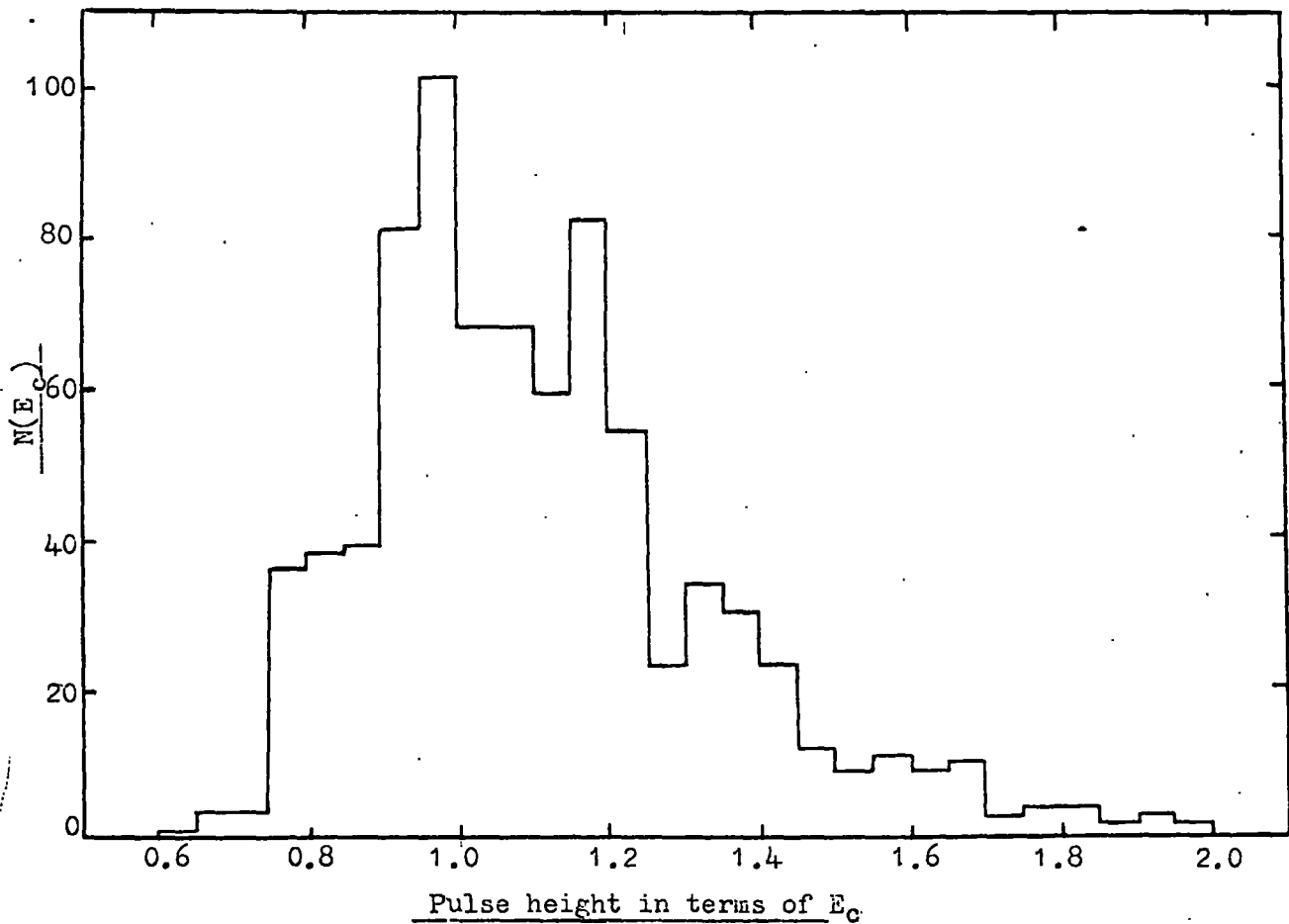


Figure 2.17 Pulse height distribution in the Cerenkov counter produced by muons selected to traverse within  $\pm 7$ cm. of the centre of the counter by means of a geiger telescope.

atmospheric oxygen. However they suggested that its activity would be maintained for months if sealed and kept in a light tight container.

For the duration of the present work the tanks were calibrated periodically by measuring the median pulse height of the distributions obtained for muons traversing the counters, and the results are shown in Figure 2.18. Both counters exhibit the same rate of fall off of efficiency with time of  $\sim 3.5\%$  per month. Although the efficiency has fallen to  $\sim 57\%$  of its original value after a year the response is still, even then, greater than twice that of a pure water counter. It would seem, however, that if such counters were to be used over a period of many years the solute should be replaced at least once a year.

#### 2.4.8 Comparison with results of other workers.

The published results, known to the author, on the use of amino acid G are summarised below in Table 2.1.

Reference	Conc. of amino acid G. mg./litre.	Increased Response	Time variation of solute efficiency
Heiberg et al., 1956	30	1.3	-
Saito et al., 1958	200	4.4	Activity maintained for months is sealed
Barton et al., 1962	100	5	-
Present Work	16	4.6	Fall of $3\frac{1}{2}\%$ per month even when sealed.

It is difficult to compare the various results directly due to the different sizes of tank and geometrical arrangements used in each case. What can be concluded is that a gain of 5 can be achieved by suitable use of the solute, noting that such a gain in the present work was obtained with concentrations  $\sim 10\%$  of those reported by the other workers, and that the solute efficiency falls at a rate of  $3.5\%$  per month even when sealed in a

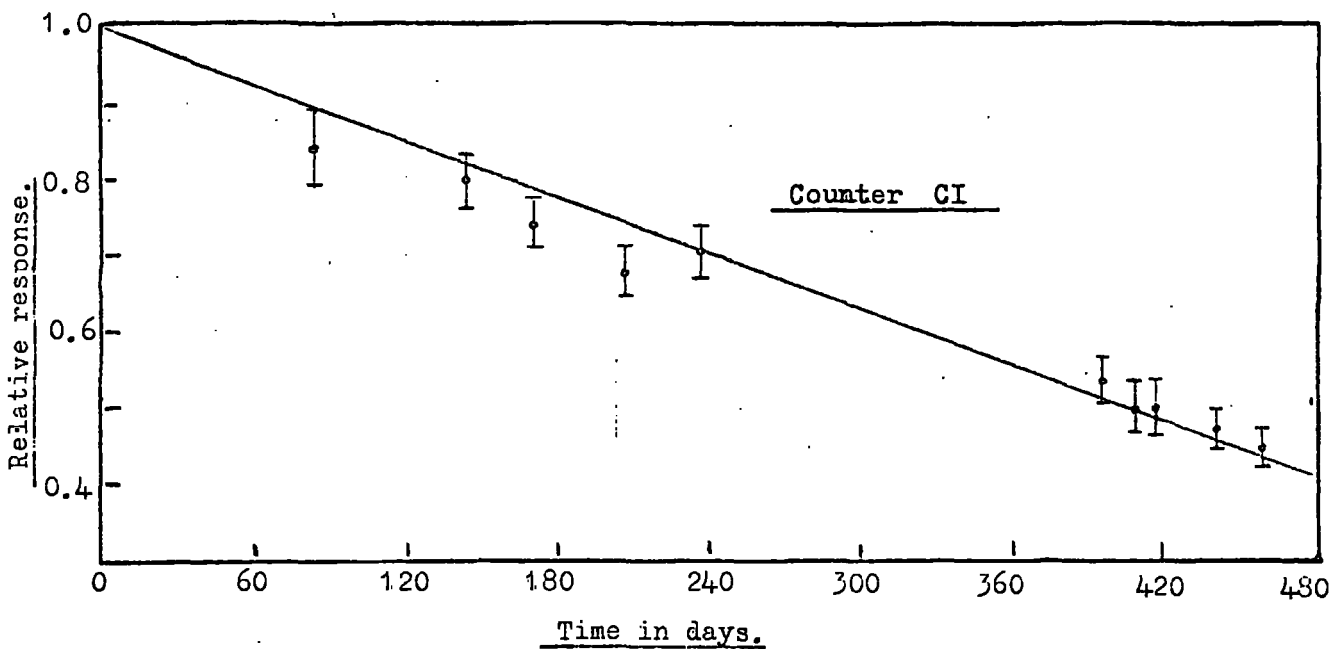
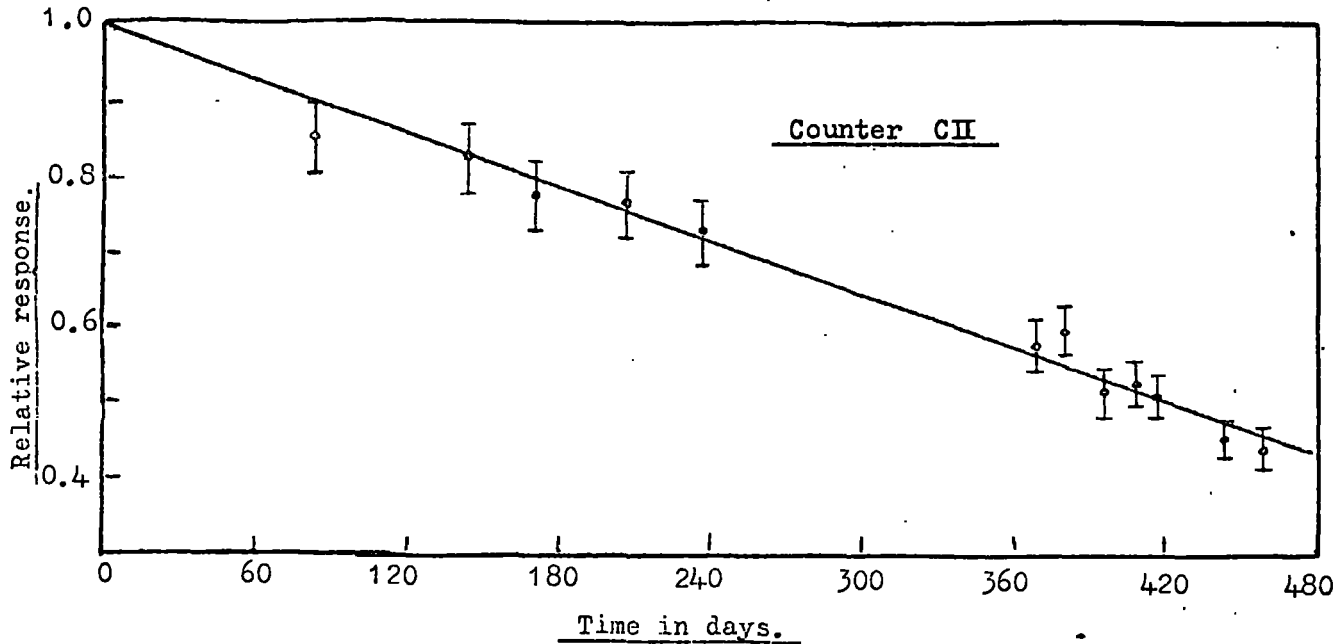


Figure 2.18 The relative response of each Cerenkov counter as a function of time, showing the fall off in efficiency of the amino acid<sup>-</sup>G.

light tight container.

Further discussion of the Cerenkov counters will take place in Chapter 3 with regard to their response as a function of particle velocity, and to possible scintillation effects from the solute.

## CHAPTER 3

### THE PROTON EXPERIMENT - CALIBRATION OF THE DETECTOR

#### 3.1 Introduction

Before proceeding with the main experiment of searching for massive particles in the sea level cosmic radiation the low energy proton flux was used to further calibrate the Cerenkov counters at sub-relativistic velocities, to ensure the absence of scintillation effects from the solute, and also to study the mass resolution attainable with this instrument using a range-velocity method.

#### 3.2. The scintillation counter- Cerenkov counter - neon flash tube telescope.

A scale diagram of the telescope, which was situated under a thin roof at 200 feet above sea level, is shown in Figure 3.1. Basically it is the 'quark telescope' described by Ashton et al., 1968a, with the addition of the two Cerenkov counters and further flash tube trays. It comprises six plastic scintillation counters, A, B, C, D, E and F, two Cerenkov counters, C II and CI, seven trays of flash tubes in the front elevation,  $F_1 - F_7$  and four trays,  $F_a - F_d$ , in the side elevation. There are also three trays of Geiger counters,  $G_1$ ,  $G_2$ , and  $G_3$ , each containing four counters, forming a telescope about the centre of the main telescope where the bottom tray is shielded by  $61 \text{ g. cm.}^{-2}$  of lead.

#### 3.3. Selection, display and recording system.

Three series of measurements P, Q and R were made on the sea level proton flux. The P and Q series selected particles which stopped in the telescope in the regions, E,  $F_7$ ,  $F_d$  and D,  $F_6$ ,  $F_c$  respectively, while the R series selected particles traversing the whole of the telescope. All three series

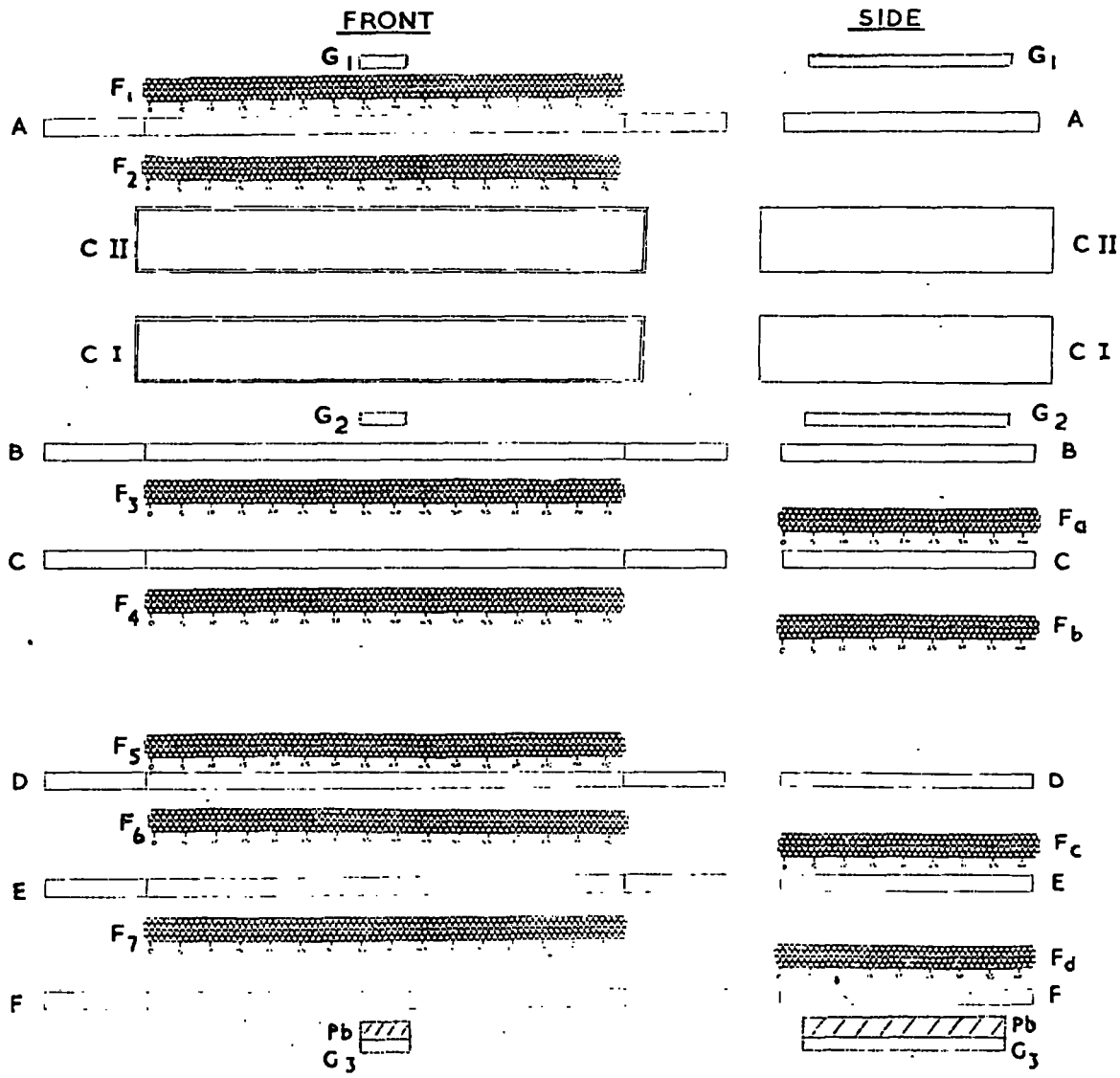


Figure 3.1 The proton telescope: A, B, C, D, E, F are plastic scintillation counters (NE102A); CII, CI are water Cerenkov counters; F<sub>1</sub>-F<sub>7</sub> and F<sub>a</sub>-F<sub>d</sub> are neon flash tube trays; G<sub>1</sub>, G<sub>2</sub>, G<sub>3</sub> are geiger counter trays.

were subject to limiting conditions determined by the discrimination levels on the Gerenkov tanks which were chosen to exclude all known particles having a mass lower than that of the proton (apart from kaons).

Selection of desired particles was carried out by fast electronic logic (Rutherford Series 1500) and that used in the P series is shown in Figure 3.2. A coincidence  $ABCDEF \bar{C} \bar{I}$  was demanded using a resolving time of 55 nanoseconds. To minimise any selection biasing the discriminator levels used on the scintillators were set as liberally as possible. The selection system and discriminator levels used for the three series of measurements are listed in Table 3.1, where 1E is the most probable pulse height produced by a unit charged particle in traversing the counter.

Table 3.1.

	Selection	Discrimination levels in terms of E.							
		A	B	C	D	E	F	CII	CI
P series	$ABCDE \bar{F} \bar{C} \bar{I}$	0.1	0.1	0.1	0.1	0.1	0.05	-	0.3
Q series	$ABCDE \bar{E} \bar{C} \bar{I}$	0.1	0.1	0.1	0.1	0.05	-	-	0.3
R series	$ABCDEF \bar{C} \bar{I} \bar{I} \bar{C} \bar{I}$	0.1	0.1	0.1	0.1	0.1	0.1	0.58	0.58

In the P and Q series CII was left out of the selection system to act as an independent witness of the event.

The display of the pulse from each counter was organised in the following manner. The six scintillation counter pulses were each delayed in increasing steps of 300 ns. and the pulses from the two Gerenkov counters were delayed by  $2.5 \mu\text{s}$  and  $3.0 \mu\text{s}$ . with respect to scintillator A. A further pulse from each Gerenkov counter was taken and amplified by a factor of ten and these two pulses were delayed by  $3.5 \mu\text{s}$  and  $4.0 \mu\text{s}$ . The ten pulses (6 scintillator, 2 direct Gerenkov and 2 amplified) were mixed and displayed on a single time base of a cathode ray oscilloscope (Tektronix 585A) at a sweep speed of  $0.5 \mu\text{s}/\text{cm}$ . The purpose of redisplaying amplified versions of the Gerenkov

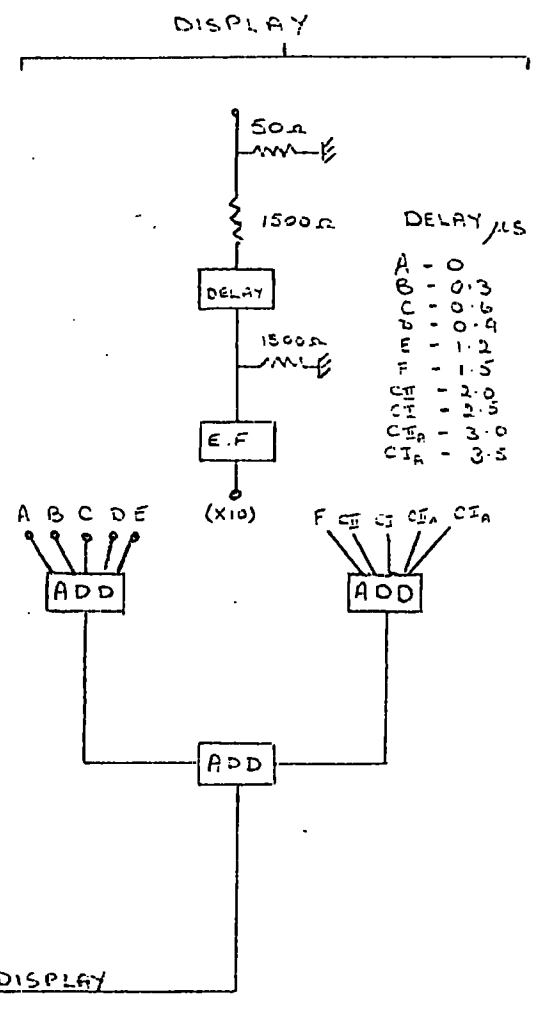
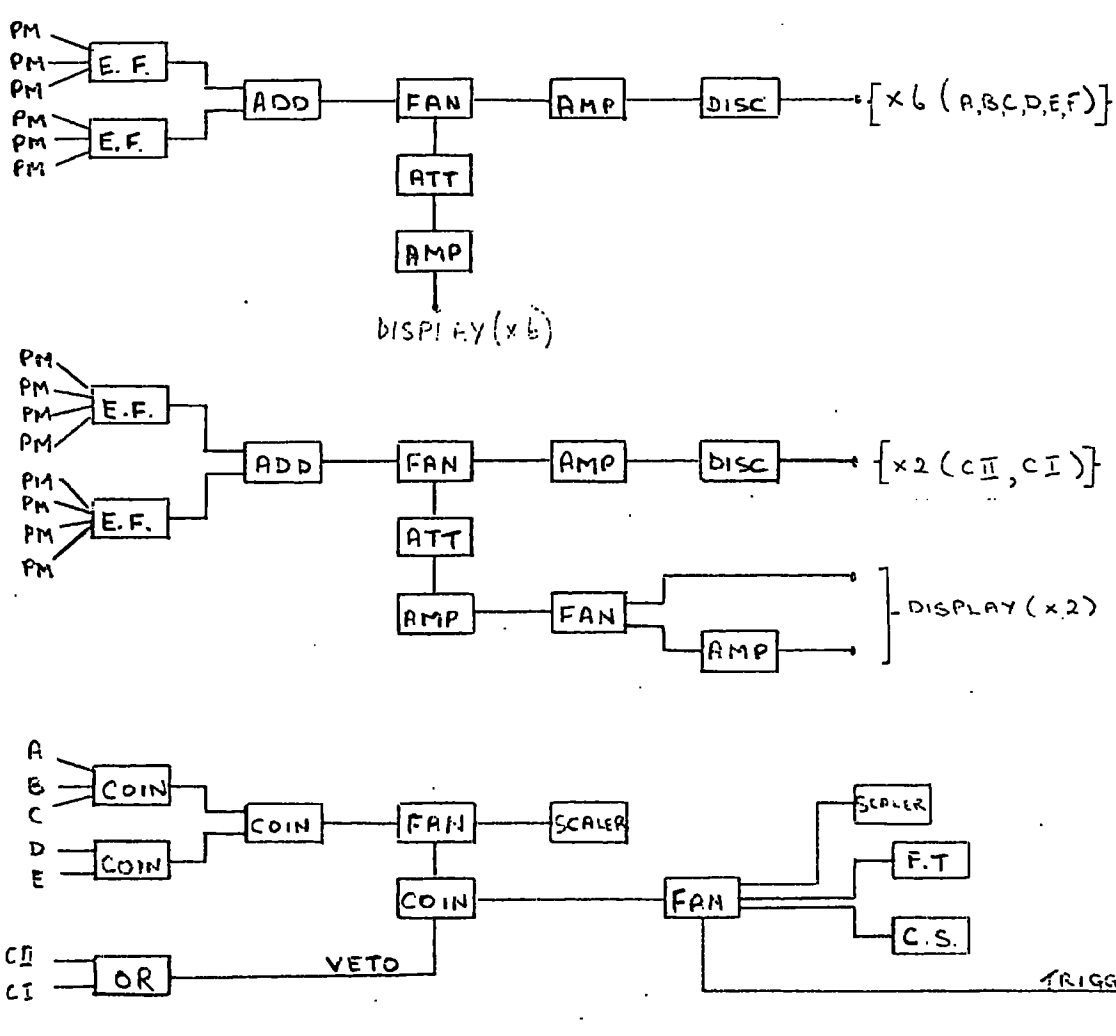


Figure 3.2 The electronic logic used in the P series.

pulses was to enable a greater dynamic range of pulse height to be measured on a single oscilloscope trace.

On an event satisfying the electronic logic the C.R.O. time base was triggered and the ten pulse heights displayed and photographed. After a delay of  $5 \mu s.$ , hence avoiding pick up on the oscilloscope, a high voltage pulse was applied to the electrodes of the flash tube trays and the flashed tubes photographed by two cameras, one viewing the front elevation and the other the side. A cycling system was then triggered which successively paralysed the electronic logic during the cycling time, illuminated fiducial markers on the telescope as well as three clocks (so that the time was recorded on each of the three frames), and advanced the film in each camera in readiness for the next event. Eventstriggering the telescope were analysed by projection of the three films onto scanning tables, correlation being achieved by means of the time on each frame.

During the running of the experiment the display electronics, discrimination levels and oscilloscope gain were checked daily. The most probable pulse height corresponding to the passage of a single charged relativistic particle through each counter was monitored periodically in a manner to be described in Section 3.4.2.

### 3.4. Energy loss in the scintillation counter.

#### 3.4.1. Most probable energy loss as a function of particle velocity.

The average energy loss of a single charged particle is given by Sternheimer, 1953, as

$$\epsilon_{AV.} = \frac{A_0 t}{\beta^2} \left[ B + 0.69 + 2 \ln \frac{B}{\sqrt{1-\beta^2}} + \ln W_{MAX.} - 2\beta^2 - \delta - U \right] \dots \dots \dots 3.1$$

where  $A_0 = 0.3 m_e c^2 \frac{Z}{A}$ ,  $B = \ln \left( \frac{m_e c^2}{I^2(Z)} \right)$ ,  
 $t$  is the thickness of material in  $g. cm.^{-2}$

$$W_{MAX} = 2 m_e c^2 \cdot \frac{p^2 c^2}{\left[ m_e^2 c^4 + M^2 c^4 + 2 m_e c^2 (p^2 c^2 + M^2 c^4)^{\frac{1}{2}} \right]},$$

$$\delta = 4.606 X + C + a (X_1 - X)^m \quad \text{for } X_0 < X < X_1,$$

$$\text{or } \delta = 4.606 X + C \quad \text{for } X > X_1,$$

$$\text{where } X = \log_{10} (p/Mc)$$

and  $a, m, X_0, X_1$  and  $C$  are constants for a given material and are given by Sternheimer, 1956.  $U$  is a shell correction term and can be ignored as negligible in the present treatment. The other symbols have their usual meaning.

Due to the fluctuating nature of the energy loss process allowing large energy transfers the most probable energy loss in a detector is smaller than the average energy loss. The divergence increases rapidly with increasing velocity due to the increasing maximum transferable energy. The problem of most probable energy loss has been treated by Landau, 1944, and more fully by Symon, 1948. Using Symon's treatment the most probable energy loss in a thickness  $t$  g. cm.<sup>-2</sup> is given as

$$\epsilon_p = \frac{A t}{\beta^2} \left[ B + 0.69 + 2 \ln \frac{\beta}{\sqrt{1-\beta^2}} + \ln \frac{A t}{\beta^2} - \beta^2 - \delta + j - u \right] \dots 3.2$$

where  $W_{MAX}$  in equation 3.1 has been replaced by  $\frac{A t}{\beta^2} \exp(j + \beta^2)$ .

This treatment is applicable only for thin absorbers, where the average energy loss in traversing  $t$  g.cm.<sup>-2</sup>,  $\delta E_{AV}$ , is less than  $E_0/10$  where  $E_0$  is the incident energy of the particle. The quantity  $j$  is a function of  $\frac{A t}{\beta^2 W_{MAX}}$

and is given by Symon. For protons equation 3.2 is valid for  $\beta > 0.585$ . As the velocity of the incident particle decreases then the Landau distribution of energy loss approaches Gaussian shape due to the reduced probability of large

energy transfers resulting in  $\epsilon_p \approx \epsilon_{AV}$  for  $\beta < 0.7$ .

Both  $\epsilon_p$  and  $\epsilon_{AV}$  have been evaluated for the scintillators ( $t=5.16\text{g}\cdot\text{cm}^{-2}$ ) as a function of velocity where the constants in equations 3.1 and 3.2 have been given for NE 102A by Crispin and Hayman, 1964, and are:-

$$\begin{aligned} A_0 &= 0.0833 \text{ Mev. g.}^{-1} \text{ cm.}^2, & B &= 18.69, \\ I &= 62.6 \text{ ev.}, & C &= -3.13, & a &= 0.514, \\ m &= 2.595, & X_0 &= 0.044, & X_1 &= 2. \end{aligned}$$

The results are shown in Figure 3.3 as a function of velocity. It can be seen that at  $\beta = 0.585$ , the point where the Symon treatment breaks down, the difference between  $\epsilon_p$  and  $\epsilon_{AV}$  is approximately 0.5%. Due to such a small difference it is justifiable for our present analysis to assume  $\epsilon_p = \epsilon_{AV}$  for  $\beta \leq 0.6$ .

#### 3.4.2 Most probable energy loss recorded by a muon calibration of the scintillators.

To make use of the graph of  $\epsilon_p$  as function of velocity for the scintillators it is necessary to have a normalisation point, which is taken as the value of  $\epsilon_p$  for the particles used to calibrate the scintillators.

Initially the telescope was calibrated by a G calibration which selected particles traversing the telescope satisfying the coincidence requirement  $G_1 \cdot G_2 \cdot G_3$ . The presence of the lead above  $G_3$  ensured a minimum muon momentum required to traverse the telescope, which corresponded to 408 Mev/c and 179 Mev/c at scintillators A and F respectively. The only likely contamination of the muon flux used to calibrate the scintillators is from low energy protons. Using the proton spectrum of Brooke and Wolfendale, 1964(a), and the muon spectrum due to Gardener et al., 1962, the proton contamination is estimated to be less than 0.5%. Such a contamination will have negligible effect on the pulse height distribution obtained.

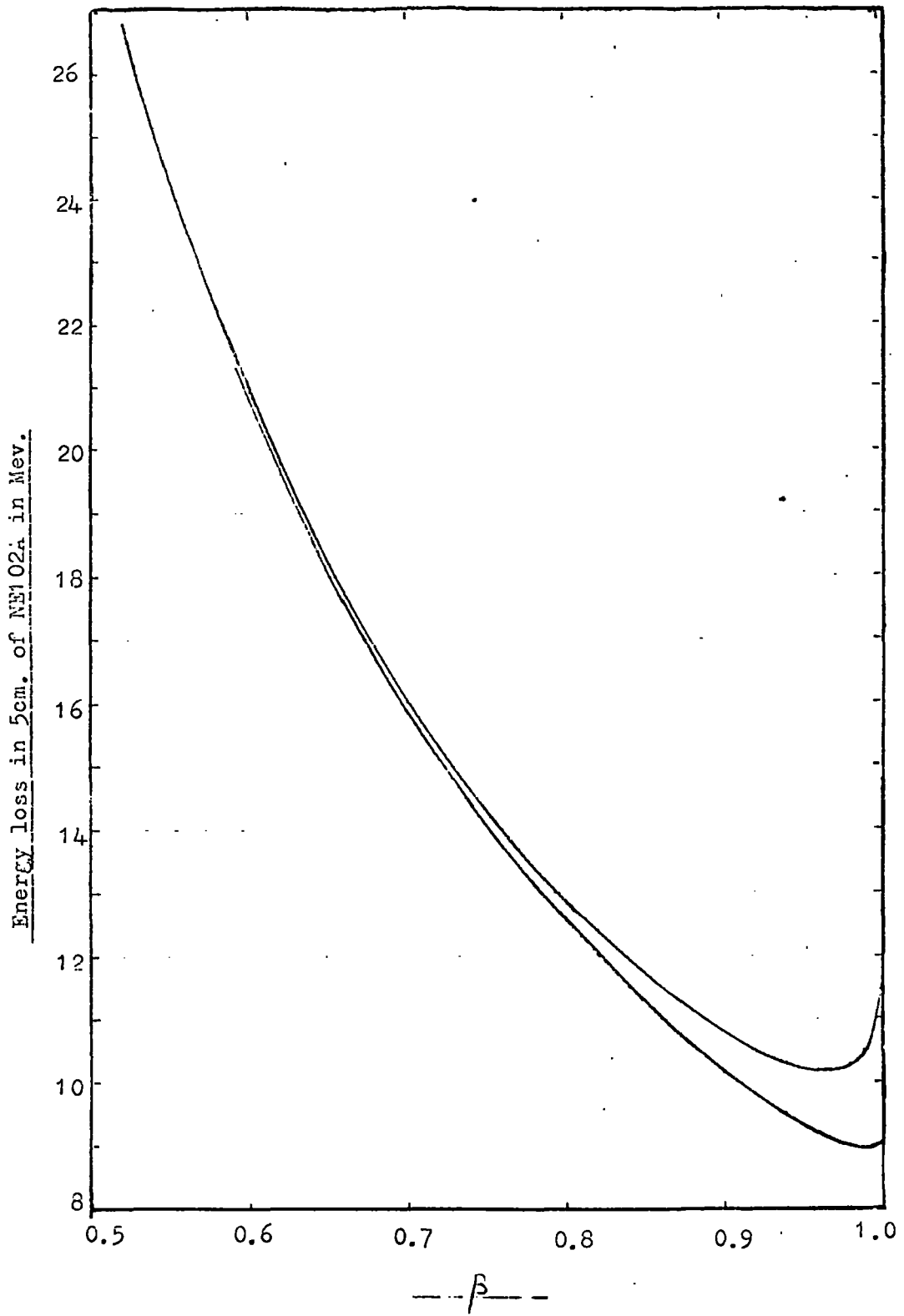


Figure 3.3 The average(upper curve) and most probable(lower curve) energy loss in 5cm. of NE102A as a function of the velocity of the incident particle.

The flux of muons at sea level is not monoenergetic and it is necessary to calculate the spread in values of  $\epsilon_p$  caused by the falling muon spectrum. The muon spectrum in the momentum range 0.4 - 1000Gev/c due to Gardéner et al., 1962, and Hayman and Wolfendale, 1962, was assumed and the expression

$$N(\epsilon_p) d\epsilon_p = \int_{p_1}^{p_2} N_\mu(p) dp$$

was evaluated, where  $p_1$  and  $p_2$  refer to the limits of the incident muon momentum such that the value of  $\epsilon_p$  at scintillator A or F lies between  $\epsilon_p$  and  $\epsilon_p \pm \frac{d\epsilon_p}{2}$ . The muon momentum spectrum used and the variation of  $\epsilon_p$  with muon momentum are shown in Figures 3.4 and 3.5. The distribution of  $\epsilon_p$  at scintillators A and F were considered as being extreme cases, and for both cases the most probable value of the distribution was  $\epsilon_p = 9.04$  Mev, this value pertaining to just over 30% of the distribution in both counters. In scintillator A the whole distribution of values of  $\epsilon_p$  is contained within  $\pm 0.14$  Mev of the most probable, while in F, due to the muon having a reduced momentum after traversing the telescope, only 93% of the distribution lies within these limits with the other 7% lying between 9.18 <  $\epsilon_p$  < 11.1 Mev. The effect of such a spread in the values of  $\epsilon_p$  due to the muon spectrum is to broaden the pulse height distribution in a counter by the order of 1-2%, this being negligible compared with other factors contributing to the width and having no effect on the most probable pulse height observed. When the angular distribution of events selected in a G calibration was considered it was found that the most probable path length in the scintillator was 1.0015 times that for normal incidence. It can be concluded that the most probable pulse height measured in a G calibration corresponds to an energy deposit of 9.055 Mev. It should be noted that this calibration was carried out over an area of the scintillator of uniform minimum response.

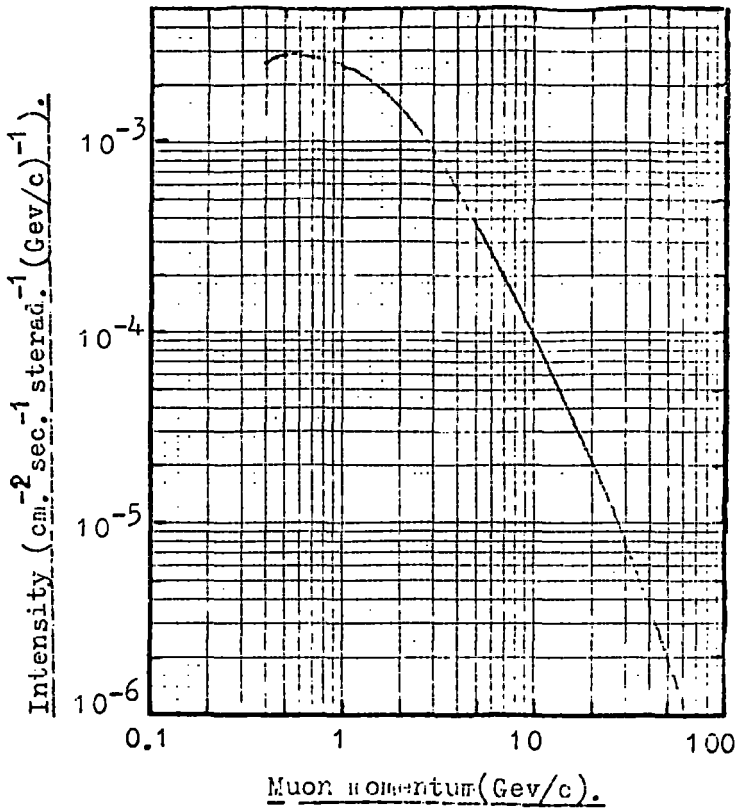


Figure 3.4 The differential muon momentum spectrum at sea level in the vertical direction (Gardner et al., 1962).

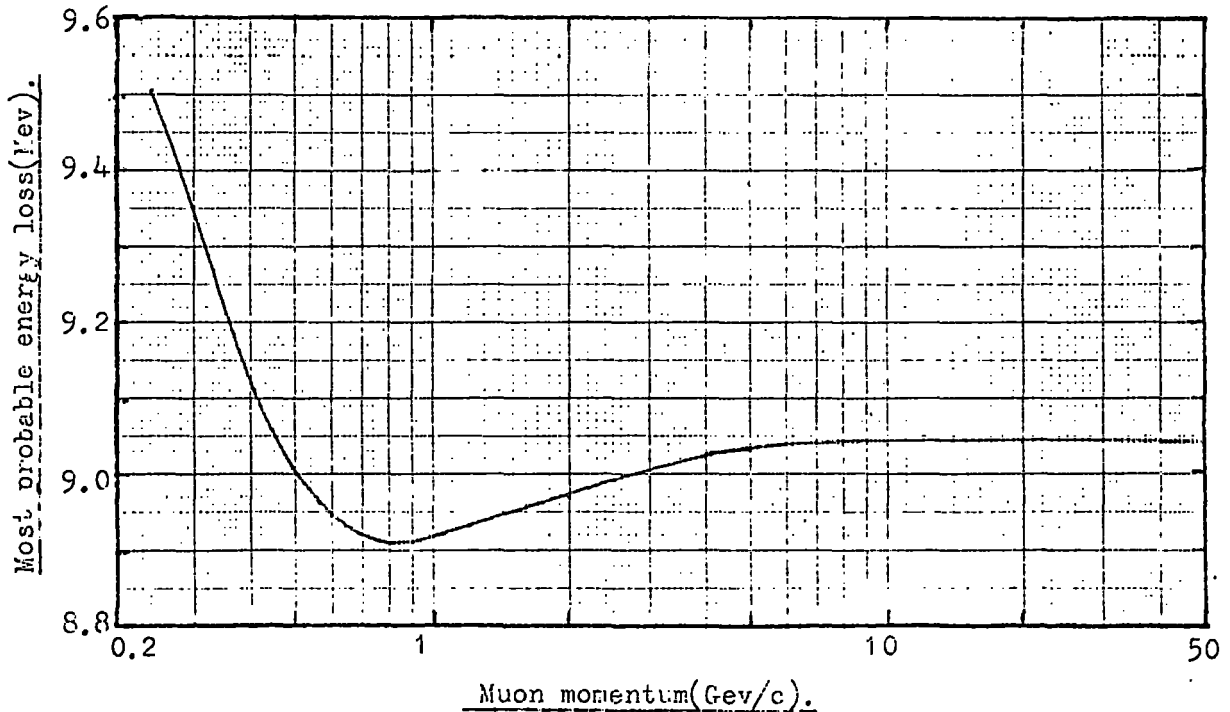


Figure 3.5 The most probable energy loss in 5 cm. of NE102A as a function of muon momentum.

To minimise alteration to the display electronics during the running of the experiment later calibrations of the scintillators were carried out using a C calibration. In this case muons were selected to traverse the telescope by demanding a scintillator coincidence ABCDEF. The pulse height distribution obtained from this calibration is broader and peaked at a higher value than that of a G calibration due to non-uniformity and increased track length effects. A relationship was found between the most probable pulse height,  $V_p$ , from a C calibration and that from a G calibration and is given by

$$V_p(G) = (0.935 \pm 0.02) \cdot V_p(C)$$

Hence 0.935 times the most probable pulse height from a C calibration corresponds to an energy deposit of 9.055 Mev.

It is thus possible to evaluate the velocity of a particle traversing a scintillator by measuring the output pulse from the scintillator, correcting it for non-uniformity and normal incidence, comparing it with the most probable pulse height from a G calibration, hence finding the corresponding energy loss and then the velocity from Figure 3.3.

### 3.5. Expected velocity response of the Cerenkov counter.

#### 3.5.1. Cerenkov light from the water.

A detailed review of the subject of Cerenkov radiation has been given by Jelley, 1958. The number of Cerenkov photons,  $N$ , emitted by a particle of unit charge and velocity,  $\beta$ , in a spectral range defined by the wavelengths  $\lambda_1$  and  $\lambda_2$  in a medium of refractive index,  $n$ , and thickness,  $l$ , is given by

$$N = 2\pi\alpha l \left( \frac{1}{\lambda_2} - \frac{1}{\lambda_1} \right) \left( 1 - \frac{1}{\beta^2 n^2} \right)$$

where  $\alpha$  is the fine structure constant.

Reference to Figure 2.10 shows that the majority of useful light will come in the wavelength interval  $2000 - 4000\text{\AA}$  when account is taken of the absorption and emission spectra of the solute, the spectral response of the photo-multiplier and a Cerenkov spectrum as a function of wavelength falling as  $1/\lambda^2$ . As  $dN/d\lambda$  is proportional to  $1/\lambda^2$  the median wavelength in the assumed useful spectral band of  $2000 - 4000\text{\AA}$  is  $2666\text{\AA}$ . The effect of not considering radiation greater than  $4000\text{\AA}$  is reasonable in that the transmission of this component is much less efficient than transmission of the re-emitted isotropic component between  $2000$  and  $4000\text{\AA}$ , (see section 2.4.4) in particular for  $\beta < 1$ . The median value of  $2666\text{\AA}$  taken here is reasonable under the assumptions made, although a more accurate value would be obtained by weighting the Cerenkov spectrum with the absorption efficiency of the solute. At such a wavelength the refractive index of water is given by Pathak, 1967, as 1.39. Hence the number of photons produced in 16.5 cm. of water in the spectral band  $2000 - 4000\text{\AA}$  is given as

$$N = 1.893 \cdot 10^4 \cdot \left[ 1 - \frac{1}{1.93 \beta^2} \right]$$

### 3.5.2 Cerenkov light from the perspex box.

Although the majority of Cerenkov radiation produced will come from the water there will also be a contribution from the perspex container. Due to the refractive index of perspex being larger than that of water the effect of this contribution will be most severe near the velocity threshold for water, and will have the effect of rounding off any sharp velocity cut off.

In estimating the contribution it is assumed that the Cerenkov light produced in the perspex box is only useful if it is transmitted into the water and then wavelength shifted, using the same reasoning as in Section 3.5.1.

The spectral band assumed to contribute is taken as  $3300 - 4000\text{\AA}$ , the two limits being the wavelength at which the transmission in perspex falls to zero (Jelley, 1958) and at which the solute absorption curve falls to zero. Taking a median  $\lambda$  of  $3640\text{\AA}$  this corresponds to a refractive index in perspex of 1.523. The contributions from the top and bottom of the box will be treated separately.

A section through the centre of the tank is shown in Figure 3.6, and the contribution from the top of the box will be considered first. If a particle of  $\beta > 0.87$  traverses the lid of the box then, as the emission angle of the Cerenkov radiation is greater than the critical angle at a perspex air interface, the light will be trapped in the lid by total internal reflection. For velocities less than 0.87c the Cerenkov light is refracted into the water and the contribution, where the effect of path length variation due to a varying Cerenkov angle with velocity has been ignored, and normal incidence assumed, is,

$$\int_{l_1}^{l_2} N_p e^{-l/X} dl = [N_p \times e^{-l/X}]_0^{l_2}$$

where

$$N_p = 2\pi\alpha \left( \frac{1}{\lambda_2} - \frac{1}{\lambda_1} \right) \left( 1 - \frac{1}{\beta^2 n^2} \right) \quad \text{and is the}$$

number of photons produced in 1 cm. of perspex between the wavelengths  $3300 - 4000\text{\AA}$ , and  $X$  is the attenuation length in perspex for  $\lambda = 3640\text{\AA}$  and is equal to 3.02 cm.

The contribution from the lid of the box,  $C_L$ , then becomes:-

$$\begin{aligned} \beta > 0.87; & \quad C_L = 0 \\ \beta < 0.87; & \quad C_L = 2.37 \cdot 10^2 (1 - 1/\beta^2 n^2) \end{aligned}$$

At the bottom of the box, for  $0.87 < \beta \leq 1$ , the radiation will be totally internally reflected at the lower perspex-air interface and will then be

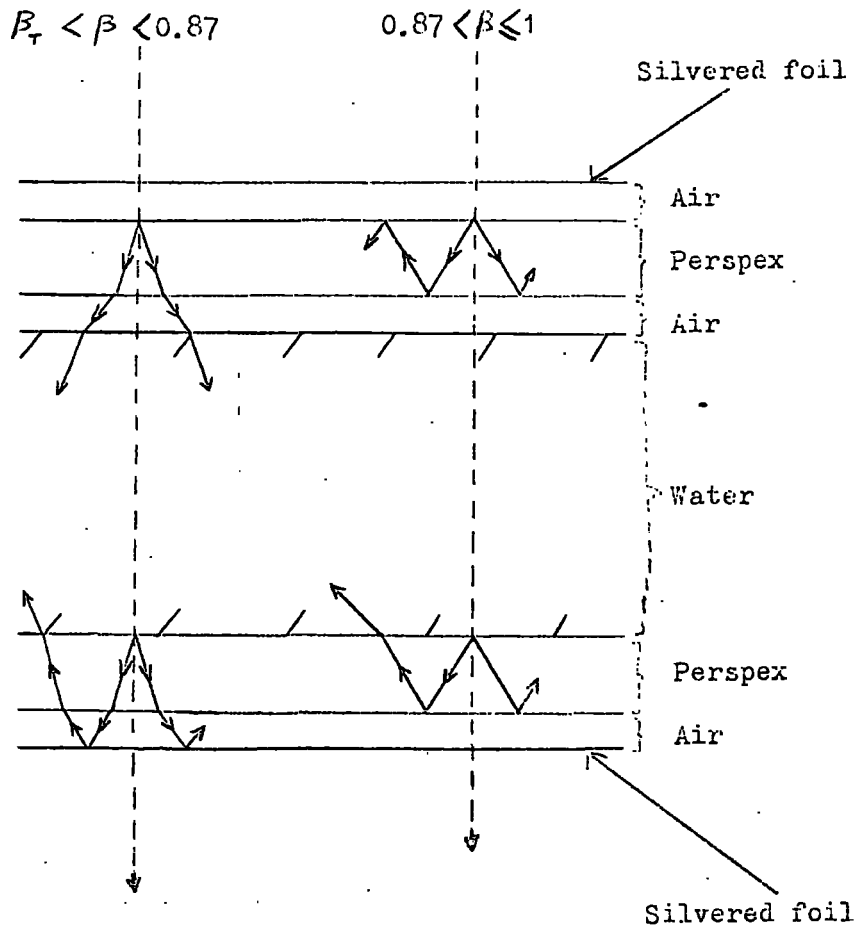


Figure 3.6

Vertical section (not to scale) through the lid and base of the Cerenkov counter, showing the transmission of light from the perspex into the water for limiting cases of  $\beta$ .

refracted into the water on meeting the perspex-water boundary. The contribution  $C_B$ , for  $0.87 < \beta \leq 1$ , becomes

$$C_B = \exp\left(\frac{-0.375}{x}\right) \cdot \int_{l_1}^{l_2} N_p e^{-l/x} dl = 1.4 \cdot 10^2 (1 - 1/\beta^2 n^2)$$

For  $\beta < 0.87$  the light will be refracted at the perspex-air interface, reflected at the silvered surface, which is assumed to have a reflectivity of 0.9, and transmitted back into the water. This contribution is:-

$$C_B = 0.9 \exp\left(\frac{-0.375}{x}\right) \cdot \int_{l_1}^{l_2} N_p e^{-l/x} dl = 1.26 \cdot 10^2 (1 - 1/\beta^2 n^2)$$

Hence the total contribution from the perspex container is

$$\begin{aligned} & 1.4 \cdot 10^2 (1 - 1/\beta^2 n^2) \text{ for } 0.87 < \beta \leq 1 \\ \text{and} & 3.63 \cdot 10^2 (1 - 1/\beta^2 n^2) \text{ for } \beta < 0.87 \end{aligned}$$

This treatment is satisfactory in that it will predict the true shape of the Cerenkov response as a function of velocity for the perspex box. However its absolute comparison with the contribution from the water is probably only accurate within a factor of 2 or 3, due to the assumptions made regarding the spectral ranges of the Cerenkov radiation considered for both the water and perspex.

### 3.5.3 Cerenkov light from knock on electrons.

In the absence of knock on electrons the pulse height distribution from the Cerenkov counter would be Gaussian. The effect of Cerenkov radiation from knock on electrons is to place a long tail on the upper side of the distribution.

The contribution from knock on electrons can be expressed as:-

$$\iint_{x E'} \psi(E, E') dE' dx N(E') \text{ ----- 3.3}$$

where

$$\psi(E, E') dE' dx = \frac{2C m_e c^2 z^2}{\beta^2} \left[ 1 - \frac{\beta^2 E'}{E_m} + \frac{1}{2} \left( \frac{E'}{E + Mc^2} \right)^2 \right] dE' dx$$

and is the probability of producing a knock on electron of energy between  $E^1$  and  $E^1 + dE^1$  in a region of  $dx$  g. cm.<sup>-2</sup> where the symbols have their usual meaning, and where  $N(E^1)$  is the number of Cerenkov photons produced in water in the spectral range 2000 - 4000Å<sup>0</sup> by an electron of energy  $E^1$ , before falling below the Cerenkov velocity threshold for water, which corresponds to an electron kinetic energy of 0.23 Mev. The limits of integration are  $0 < x < 16.5$ , and  $E_T^1 < E^1 < E_m^1$  where  $E_T^1 = 0.23$  Mev.  $N(E^1)$  was evaluated as  $N(E^1) = \int_{+} N(E(r)) dr$ , where  $N(E(r))$  is the number of photons emitted in a distance  $dr$  by an electron of energy  $E$ , where  $E$  is a function of  $r$ . The integration limits of  $r$  are the initial range and the range at which the electron velocity falls beneath the Cerenkov threshold. The range energy relationship used for electrons in water was due to Pathak, 1967.

For  $\beta < 0.9$  the knock on electron contribution is essentially independent of the incident particle mass, as then  $E_m^1 = \frac{2m_e c^2 \beta^2}{1 - \beta^2}$ .

Calculations of the knock on electron contribution have been carried out for  $\beta < 0.9$ . Beyond this no further evaluations were made apart from that for  $\beta = 1$ . For normalisation purposes this contribution has been evaluated for incident muons of momentum 2 Gev/c, this being the median muon momentum triggering the telescope in a G calibration. Corrections were applied for knock on electrons having a range greater than the thickness of the counter.

The resulting contributions from these three sources, water, perspex and knock on electrons, are shown in Figure 3.7 and they are summed to give the total response of the counter as a function of the velocity of the

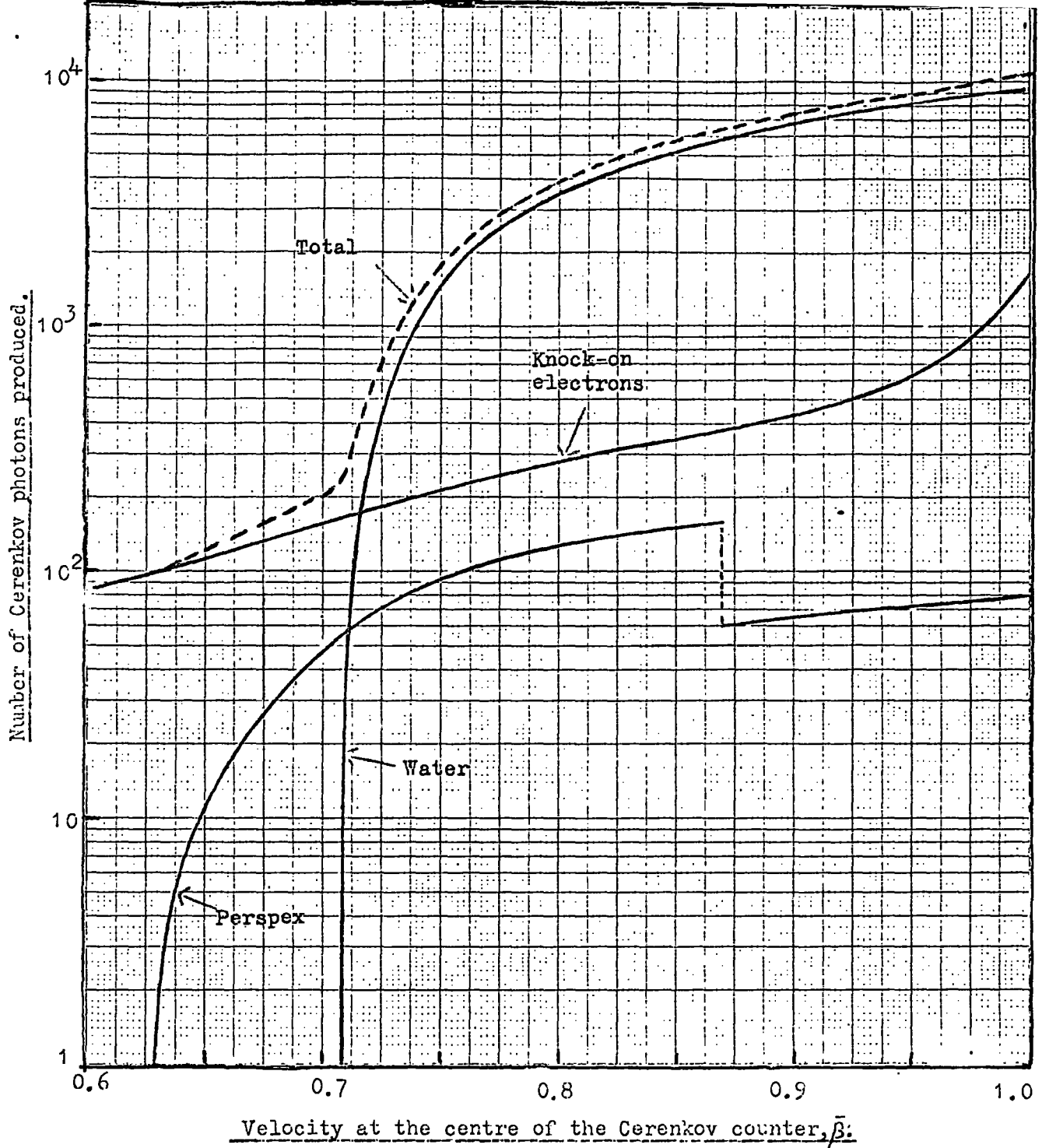


Figure 3.7 The theoretical velocity response of the Cerenkov counters showing the relative contributions from the water, perspex and knock on electrons as well as the sum of all three. The curves were evaluated for protons having a velocity,  $\bar{\beta}$ , at the centre of the counter and hence they would be slightly different in the threshold region for other particles.

incident particle. The shape of the response curve is accurate as far as the contributions from the water and knock on electrons are concerned, but as mentioned in Section 3.5.2 the contribution from the perspex, while in itself being correct in shape, may be out by a factor of 2 or 3 in its absolute value when in comparison with the other two contributions.

3.5.4 Median pulse height recorded by a muon calibration of the Cerenkov counters

The Cerenkov counters were calibrated in the same manner as described for the scintillators in Section 3.4.2. In the absence of any theory of most probable Cerenkov response as a function of velocity, the median pulse height of the distribution obtained for the counters in a G calibration is taken to be equal to the response shown in Figure 3.7 for  $\beta = 1$  (this corresponding to the response for muons of momentum 2 Gev/c, the median momentum in a G calibration). As the counters were normally calibrated under a C calibration a conversion factor was found as

$$\text{Median}_G = (0.83 \pm 0.02) \text{Median}_C$$

Hence the velocity of a particle traversing the Cerenkov counter can be found by measuring the pulse height in the counter, normalising for non-uniformity and normal incidence, expressing the normalised pulse height as a ratio of the median pulse height in a G calibration and finding the velocity from Figure 3.7.

Experimental measurements of the velocity response of the counters are presented later in Section 3.9.1 and are compared with the present theoretical predictions.

3.6 Normalisation of the telescope material for ionisation purposes.

For convenience the telescope materials were normalised to g. cm.<sup>-2</sup> water equivalent. Range-energy calculations have been carried out by several workers, notably Sternheimer, 1960, and Serre, 1967. Serre has tabulated range-

energy relations for protons in a variety of media and where they covered media in the telescope her values were used. For materials not treated by Serre an interpolation formula due to Sternheimer, 1960, was used. This is given as

$$R(E_p, I) = R(2\text{Mev}, I) + \frac{A}{2Z} \cdot \bar{\Phi}_{AL}(E_p) \cdot [1 + J_1 \chi + J_2 \chi^2 + J_3 \chi^3]$$

where  $R(E_p, I)$  is the range of a proton of kinetic energy  $E_p$  in a material of ionisation potential  $I$ ;  $R(2\text{Mev}, I)$  is the range of a proton of kinetic energy 2 Mev in a material of ionisation potential  $I$ . This is to be determined experimentally and is negligible in the present work.  $\bar{\Phi}_{AL}(E_p)$  is the range of a proton of kinetic energy  $E_p$  in aluminium;  $J_1, J_2, J_3$  are constants for a given  $E_p$  and are tabulated by Sternheimer; and  $\chi = \log_{10} \left( \frac{I}{I_{AL}} \right)$ .

Range energy relationships were calculated for all the materials in the telescope using Sternheimer's interpolation formula, and where comparison could be made with the results of Serre agreement was found within less than 1% over ranges of several hundreds of  $\text{g. cm.}^{-2}$  of material. The materials were normalised to  $\text{g. cm.}^{-2}$  of water as follows:-

$$\text{Normalisation factor} = \frac{[R_p(600 \text{ Mev}) - R_p(120 \text{ Mev})]_{\text{water}}}{[R_p(600 \text{ Mev}) - R_p(120 \text{ Mev})]_{\text{material}}}$$

where  $R_p(600 \text{ Mev})$  is the range of a proton of kinetic energy 600 Mev. The normalisation factor is fairly insensitive to the choice of energy limits, which in the present case were chosen as being representative of the limits within which the proton energy would be for the most part in traversing the telescope. In Table 3.2. are listed the various materials in the telescope, their constants and normalisation factors.

Table 3.2

Material	Density	$\bar{z}$	$\bar{A}$	I	Normalisation Factor
Water	1.0	3.31	5.97	74.12	1.0
Glass	2.5	10.61	21.33	138*	0.826**
NE 102A	1.032	3.65	6.83	62.6	0.986**
Perspex	1.2	3.56	6.58	69.09	0.969**
Aluminium	2.7	13	27	166	0.784
Wood	<del>0.54</del> 0.71	4.68	7.74	63.6*	1.097**

\* These values of I have been found using  $I = 13 \bar{z}$ . The others have been given by Sternheimer.

\*\* These normalisation factors have been found from the interpolation formula of Sternheimer and the others from the results of Serre.

The telescope was reduced to its constituent parts and normalised so that the range in  $\text{g. cm.}^{-2}$  of water from the top of the telescope to any point in it could be evaluated.

### 3.7. Selection criteria and analysis of events.

#### 3.7.1 Initial selection of events from the film.

The three frames (two of the flash tubes and one of the oscilloscope) were correlated by reference to the time on each frame. The flash tube photographs were projected onto scanning tables on which the location of every tube had been recorded (this was achieved by photographing all the flashed tubes when the trays were pulsed in the presence of a radioactive source). Alignment of the frame on the scanning table was carried out by superposition of both sets of fiducial markers. The criterion for selection of an event was that a track should be observed in both flash tube views, the definition of a track being that its trajectory should pass through at

least one flashed tube in each flash tube tray traversed. It should be noted that both scattered and unscattered tracks were accepted. For each event selected under the flash tube criterion the corresponding oscilloscope frame was measured. The frame was projected onto a scanning table on which the oscilloscope graticule had been drawn and the pulse height from each counter measured. Where possible the amplified versions of the Cerenkov pulses were measured (to minimise measuring errors) and only when these were saturated were the direct pulses measured.

Further criteria, which depended on the film series being considered, were then imposed on the selected tracks. For all three series of measurements it was demanded that the track should pass through at least half of scintillator A. In the P series, where the tracks were required to stop in the region E,  $F_7$ ,  $F_d$ , the projections of their trajectories were demanded to pass through at least half of scintillator F. (This condition was required to remove events which may not have stopped in the selected region and which, even if they had not stopped, would have missed scintillator F, hence giving no anti-coincidence signal). In the Q series, where particles stopped in the region D,  $F_6$ ,  $F_c$ , the projections of their trajectories were required to pass through at least half of scintillator E. (for the same reasons as above). In the R series the condition was that the track should traverse the whole telescope. Imposing these conditions the acceptance of the telescope is defined by scintillators A and F for the P and R series, and by scintillators A and E for the Q series.

For each event satisfying the initial selection criterion the coordinate of the track in each flash tube tray traversed was recorded in units of flash tube separation to the nearest half unit. For events also satisfying the latter selection criterion (P and Q series only) the position at which the track was observed to stop was noted (this was recorded as either being

in the scintillator or as being the last flashed tube observed on the trajectory).

### 3.7.2 The basic data

A summary of the basic data is given in Table 3.3.

Table 3.3

	P series	Q series	R series
Electronic Selection	ABCDEF $\bar{C}\bar{I}$	ABCDE $\bar{C}\bar{I}$	ABCDEF $\bar{C}\bar{I}\bar{I}\bar{C}\bar{I}$
Running time (hours)	36.07	27.07	28.26
Total number of triggers	2144(59.5)	2799(103.5)	1860(63.6)
Number of angled tracks plus accompaniment	509 (14.1)	520 (19.2)	375 (13.3)
Total number of tracks satisfying initial selection	768 (21.3)	1022 (37.8)	1252 (39.2)
Number scattered	221 (6.1)	359 (13.3)	386 (12.1)
Number stopping in defined acceptance	553 (15.4)	668 (24.7)	-
Mean atmospheric pressure mb.	1009.3	1012.7	1004.9

The numbers in brackets after the number of events refer to the rate of that type of event in units of  $\text{hr.}^{-1}$ .

The difference between the total number of triggers and the sum of the types of triggers listed in Table 3.3. is accounted for predominantly by weak electron-photon showers triggering the telescope. One interesting feature of the above table is the number of triggers generated by angled tracks (that is those entering the telescope below the Cerenkov counters) which are accompanied presumably by an electron component which gives a signal in scintillator A and no signal in the Cerenkov counters, hence satisfying the electronic selection. The rate of such triggers,  $\sim 15 \text{ hr}^{-1}$ , while causing no more trouble than film wastage in the present experiment

would have serious implications if the telescope in its present form was used to search at low levels in the cosmic radiation, in that besides causing enormous film wastage rare events would have to be sorted from tens of thousands of angled tracks. Obviously the telescope would require redesign before such a search could be undertaken. A further point to note is that 30% of the tracks are rejected in the P and Q series due to their projection missing scintillator F and E respectively (however this is a necessary condition to ensure that the particle has stopped).

### 3.7.3 Initial analysis of events.

For each track selected under the initial criterion the coordinates of its trajectory at every flash tube tray and the pulse in each of the six scintillators and two Cerenkov counters were fed into a computer (IBM 360/67). Careful measurements of the geometrical constants of the telescope were made using flash tube zero in tray  $F_1$ , and flash tube zero in tray  $F_a$  as the zero reference levels in the front and side elevations respectively. The trajectory of the particle was reconstructed by the computer and the projected zenith angles,  $\theta_f$  and  $\theta_s$ , in both elevations were calculated as well as the scattering angles if a scatter had occurred. The true zenith angle,  $\theta_T$ , given as

$$\theta_T = \tan^{-1} \left[ \tan^2 \theta_f + \tan^2 \theta_s \right]^{\frac{1}{2}}$$

was evaluated and the coordinates of the particle at each scintillator and Cerenkov counter were calculated and converted into the individual reference system of that particular counter.

The output pulse height from each counter was converted to the equivalent pulse height at the input to the emitter follower by calibration curves of the display electronics and was normalised by expressing it as, in the case of the scintillators, a function of the most probable pulse height obtained for that counter for a G calibration (which is equal to  $1E_s$ ) and in

the case of the Cerenkov counters as a function of the median pulse height obtained in that counter for a G calibration (which is equal to  $1E_c$ ). The normalised pulse heights were further corrected for normal incidence, by multiplying by  $\cos \theta_T$ , and also for non-uniformity of the counter by means of the response curves shown in Figure 3.8 (a,b,c) and the coordinates of the particle at each counter. The curves in Figure 3.8 are essentially those shown in Figures 2.5, 2.15 and 2.16, where the response of one end of the counter has been summed with its mirror image to give the total response.

With the pulse heights corrected and normalised they can be used to ascertain the velocity of the incident particle at each scintillator and Cerenkov tank with reference to Figures 3.3 and 3.7 respectively, where  $1E_s$  and  $1E_c$  refer to the case of  $\beta = 1$ .

#### 3.7.4 Mass determination of an event

Knowledge of the velocity of a particle and its residual range, or the velocity at two points separated by a known amount of absorber enables its mass to be determined. Reference to equation 3.1. shows that the average energy loss is independent of the mass of the particle for  $\beta < 0.9$  (the only mass dependent term being  $W_{\max}$ , and then only slightly for  $\beta > 0.9$ ). The average rate of energy loss can then be written as

$$\left(\frac{dE}{dx}\right)_{av} = -z^2 A(\beta) \quad \text{where } A(\beta) \text{ is given by:-}$$

$$A(\beta) = \frac{A_0}{\beta^2} \left[ B + 0.69 + 21 \ln \frac{\beta}{\sqrt{1-\beta^2}} + \ln W_{\max} - 2\beta^2 - \delta - U \right]$$

Writing  $E = (\gamma - 1) Mc^2$  then

$$dE = Mc^2 \beta (1 - \beta^2)^{-3/2} d\beta.$$

Substituting for  $dE$  in the previous equation one can write

$$\int_0^R dx = \int_0^\beta \frac{\beta}{(1-\beta^2)^{3/2}} \cdot \frac{Mc^2}{z^2} \cdot \frac{1}{A(\beta)} \cdot d\beta = \frac{Mc^2}{z^2} \cdot f(\beta)$$

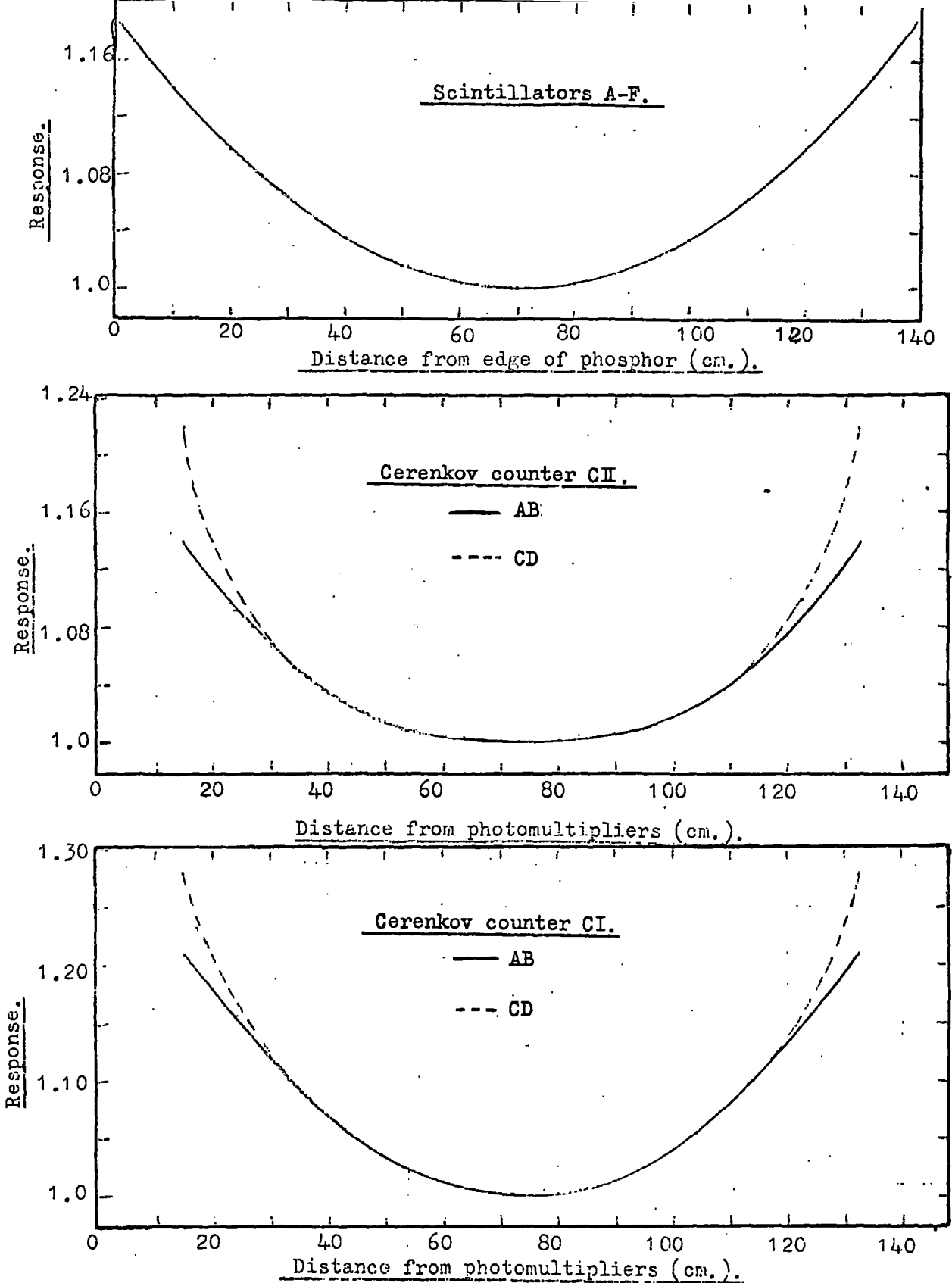


Figure 3.8 The response curves for the scintillators and Cerenkov counters, where the contributions from the photomultipliers at both ends have been summed, and the response normalised to that at the centre of each counter.

where

$$f(\beta) = \int_0^\beta \frac{\beta}{(1-\beta^2)^{3/2}} \cdot \frac{1}{A(\beta)} \cdot d\beta$$

and is independent of the particle mass for  $\beta < 0.9$ .

Thus  $R = \frac{Mc^2}{z^2} \cdot f(\beta)$ , and knowledge of  $R$ , the residual range, and the velocity,  $\beta$ , allows the particle mass to be determined.

It is not necessary to calculate  $f(\beta)$  as a function of  $\beta$  as it can be evaluated from range-energy tables as

$$f(\beta) = \frac{R z^2}{Mc^2}$$

For the present work it was derived from range-energy tables (Serre, 1967) for protons in water (the telescope having been previously normalised to  $\text{g.cm.}^{-2}$  of water, Section 3.6). Having already expressed the scintillator pulses in terms of  $E_s$  and corrected for non-uniformity and normal incidence, the velocity and hence the value of  $f(\beta)$  at a given scintillator can be found. In Figure 3.9 is shown the variation of  $f(\beta)$  as function of  $E_s$  (this being more convenient than expressing it as a function of velocity).

Assigning an arbitrary range scale to the telescope, where  $R_A = 0$  and  $(R_A - R_i)$  is the amount of absorber in  $\text{g. cm}^{-2}$  of water between scintillator A and scintillator i, an equation of the following form can be written for the situation at each scintillator:-

$$R_i = M \cdot f(\beta)_i + C$$

where  $C$  is a constant and is the residual range of the particle in  $\text{g. cm.}^{-2}$  of water from scintillator A, and  $z^2$  has been taken as unity. If a particle is observed to stop a further equation can be written as then  $f(\beta) = 0$  and  $R_s = C$ . The values of  $R_i$  for normal incidence have been found from the normalisation of the telescope in Section 3.6 and for a given event have to be corrected for inclined trajectories by multiplying by  $\sec \theta_T$ .

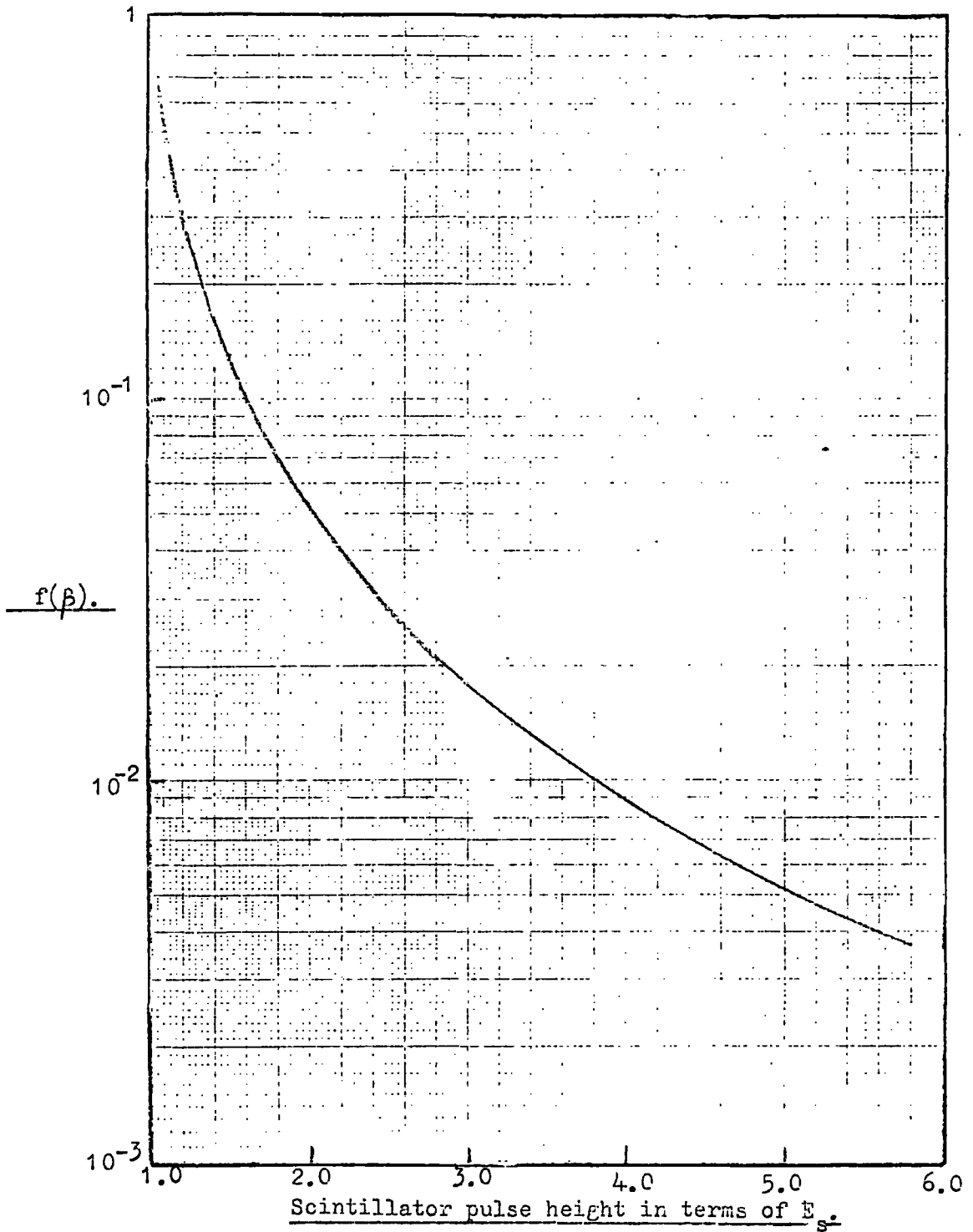


Figure 3.9 The variation of the function  $f(\beta)$  with the pulse height in a scintillator (the pulse height being expressed in terms of the most probable pulse height produced by muons traversing the scintillator in a G calibration).

A least squares fit can be applied to the available equations where each equation has been given a weight,  $W_i$ , and the values of M and C are given by:-

$$M = \frac{[w].[w.f(\beta).R] - [w.f(\beta)][w.R]}{[w].[w.f(\beta).f(\beta)] - [w.f(\beta)][w.f(\beta)]},$$

and 
$$C = \frac{[w.R].[w.f(\beta).f(\beta)] - [w.f(\beta)][w.f(\beta).R]}{[w].[w.f(\beta).f(\beta)] - [w.f(\beta)][w.f(\beta)]}.$$

where  $[w] \equiv \sum w_i$ ; etc..

A measure of the internal consistency of the equations can be obtained by the errors on M and C which are given by:-

$$\frac{\alpha_M^2}{[w]} = \frac{\alpha_C^2}{[w.f(\beta).f(\beta)]} = \frac{\alpha^2}{[w].[w.f(\beta).f(\beta)] - [w.f(\beta)][w.f(\beta)]}$$

where  $\alpha^2 = \frac{[wdd]}{(N-2)}$  where N is the total number of equations used and

$$d_i = R_i - \bar{M}.f(\beta)_i - \bar{C}$$

where  $\bar{M}$  and  $\bar{C}$  are the respective values calculated from the least squares fit.

### 3.7.5 Weighting of the equations.

In the absence of any systematic errors the random errors in the following parameters govern the weight to be attached to each equation: the most probable pulse height,  $E_s$ , from a G calibration; the pulse heights measured from the scanning table; the inherent width of the scintillation line (comprising the width due to the Landau effect and fluctuations in the photomultipliers); and the response corrections. The errors in the values of  $R_i$  are negligible. The error in the normalised and corrected pulse height,  $V_N$ , for each scintillator is hence given by:-

$$\frac{\alpha_{V_N}}{V_N} = \left[ \left( \frac{\alpha_v}{V_{out}} \right)^2 + \left( \frac{\alpha_{E_s}}{E_s} \right)^2 + \left( \frac{\alpha_{Resp}}{Resp} \right)^2 + \left( \frac{\alpha_n}{n} \right)^2 + \left( \frac{\alpha_L}{L} \right)^2 \right]^{1/2}$$

where  $\frac{\alpha_v}{V_{out}} = \frac{1.2}{V_{out}}$  and is the fractional error in the measured pulse from the scintillator ( $V_{out}$  measured in m.v.);

$\frac{\alpha_{E_s}}{E_s} = 0.037$  and is the fractional error in the most probable pulse

height obtained in a G calibration;

$\frac{\alpha_{Resp}}{Resp} = 0.014$  and is the fractional error in estimating the response correction;

$\frac{\alpha_n}{n} = \frac{0.087}{\sqrt{V_N}}$  and is the fractional error due to fluctuations in the photo-electron collection and multiplication processes;

and  $\frac{\alpha_L}{L}$  is half width at half height of the scintillation line due to the Landau process (Akimov, 1965) and is shown as a function of  $V_N$  in Figure 3.10.

The corresponding error in  $f(\beta)$  for the calculated error in  $V_N$  was found from Figure 3.9 and each equation was weighted accordingly as

$$w_i = \left( \frac{1}{\alpha_{f(\beta)_i}} \right)^2$$

The weighting of the equation representing the particle when it had stopped is somewhat different. Such a telescope, unlike for example a cloud chamber, lacks continuous visual sensitivity, and location of the stopping point is somewhat imprecise. In order to weight such an equation it was necessary to determine the precision with which the stopping point could be located.

If a particle entered a scintillator in the stopping region and no further tubes were observed on the projection of its trajectory it was assumed to have stopped in that scintillator. An estimate of the stopping position was made by normalising the pulse height distribution of all events appearing to stop in that scintillator to an assumed uniform stopping distribution across the scintillator, hence obtaining a relationship between pulse height and where the particle stopped in that scintillator (this is only approximate as some events appearing to stop in the scintillator may well have traversed the whole scintillator and stopped in the next flash tube frame). A sample of the particles appearing to stop in the scintillator were taken and assumed to be protons. From the value of  $f(\beta)$  evaluated for the preceding scintillator to that where the particle appeared to stop, the value of the residual range

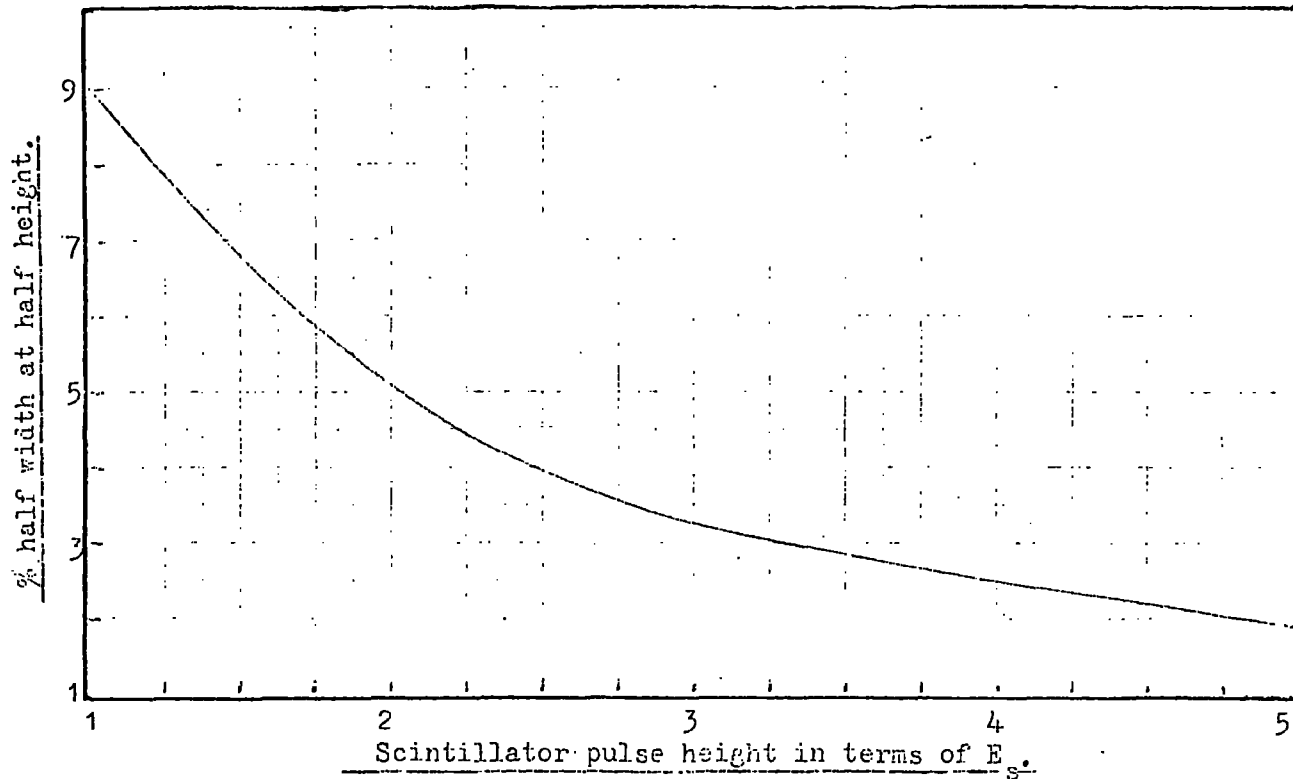


Figure 3.10 The percentage half width at half height of the scintillation line, due to the Landau process, for 5cm. of NE102A as a function of scintillator pulse height (the variation with pulse height has been derived from the variation with velocity (Akimov, 1965) assuming an unique pulse height for a given velocity).

from that scintillator was calculated and compared with that measured using the normalisation described previously. A standard deviation measuring error of  $\pm 1.5 \text{ g. cm.}^{-2}$  of water was obtained for locating the stopping position by the present method, when the distribution of the differences between the measured and calculated residual ranges was corrected for broadening due to errors in the value of  $f(\beta)$ .

For particles stopping in the flash tube trays the recorded stopping position was taken as the mean position between the last flashed tube observed and the next tube which would have flashed on the projection of the particle trajectory. A standard deviation measuring error of  $\pm 2.0 \text{ g. cm.}^{-2}$  of water was obtained when a sample of events stopping in the flash tube trays was treated in the same way as the sample stopping in the scintillator.

The corresponding errors in  $f(\beta)$  for these errors in determining the stopping position are given by

$$\alpha_{f(\beta)} = \frac{\alpha_R}{M},$$

and for the present work  $M$  was assumed to be  $938 \text{ Mev}/c^2$ , as protons represent by far the majority of events (known particles (kaons apart) of mass lower than that of the proton not being able to satisfy the selection criteria). For stopping particles with mass larger than that of the proton the effect is to reduce the weight assigned to the equation representing where the particle stopped by a factor  $(M/M_p)^2$ . However this has negligible effect on the resulting calculated mass of the particle. The weights to be applied to the equations representing stopping in the scintillators and the flash tube trays are  $3.9 \cdot 10^5$  and  $2.2 \cdot 10^5$  respectively.

For each event the mass and residual range from scintillator A were calculated, as well as the respective errors on these quantities. In the case

of events stopping in a scintillator the equation representing that scintillator was not used in the least squares fit due to saturation effects in the phosphor at high levels of ionisation (the constant proportionality between the light output and energy loss in the phosphor breaking down for protons of energy less than ~50 Mev.). In all other cases all available equations were used apart from where the level of ionisation in A was higher than that in B, when the equation due to scintillator A was then ignored (this was to avoid biases caused by events being accompanied at the top of the telescope).

3.7.6 A more precise estimate of the residual range.

As one of the main purposes of performing the experiment was to measure the velocity response of the Cerenkov counters it was desirable to obtain the best possible estimate of the velocity of the particle in the telescope. The method so far evolved for determining the mass and residual range of the particle is sufficient in itself to determine the velocity of the particle anywhere in the telescope. However, a more precise estimate can be made if all the events are assumed to be protons (which is almost true) as then the number of unknowns is reduced to only one, the residual range. Taking the mass as  $938 \text{ Mev}/c^2$  the residual range from scintillator A is given by

$$\frac{\sum_i w_i (R_i + Mf(\beta)_i)}{\sum w_i} ,$$

where the values of  $R_i$ ,  $f(\beta)_i$  and  $w_i$  are those evaluated in the previous sections, and the summation is carried out over all values of  $R_i$  and  $f(\beta)_i$  which were valid in the least squares fit. From this calculated residual range from scintillator A, and the assumed mass, the incident residual range, velocity, energy and momentum were evaluated, as well as the velocity of the particle at the centre of each scintillator and each Cerenkov counter traversed.

Hence for every event the following information was calculated; the projected and true zenith angles, the scattering angle if a scatter occurred, the mass and residual range, and then assuming the events to be protons, the incident velocity, energy and momentum, and the velocity at each of the scintillation and Cerenkov counters, where in each case the velocity was correlated with the normalised pulse height for that counter.

The results of the analysis are reviewed in the following sections.

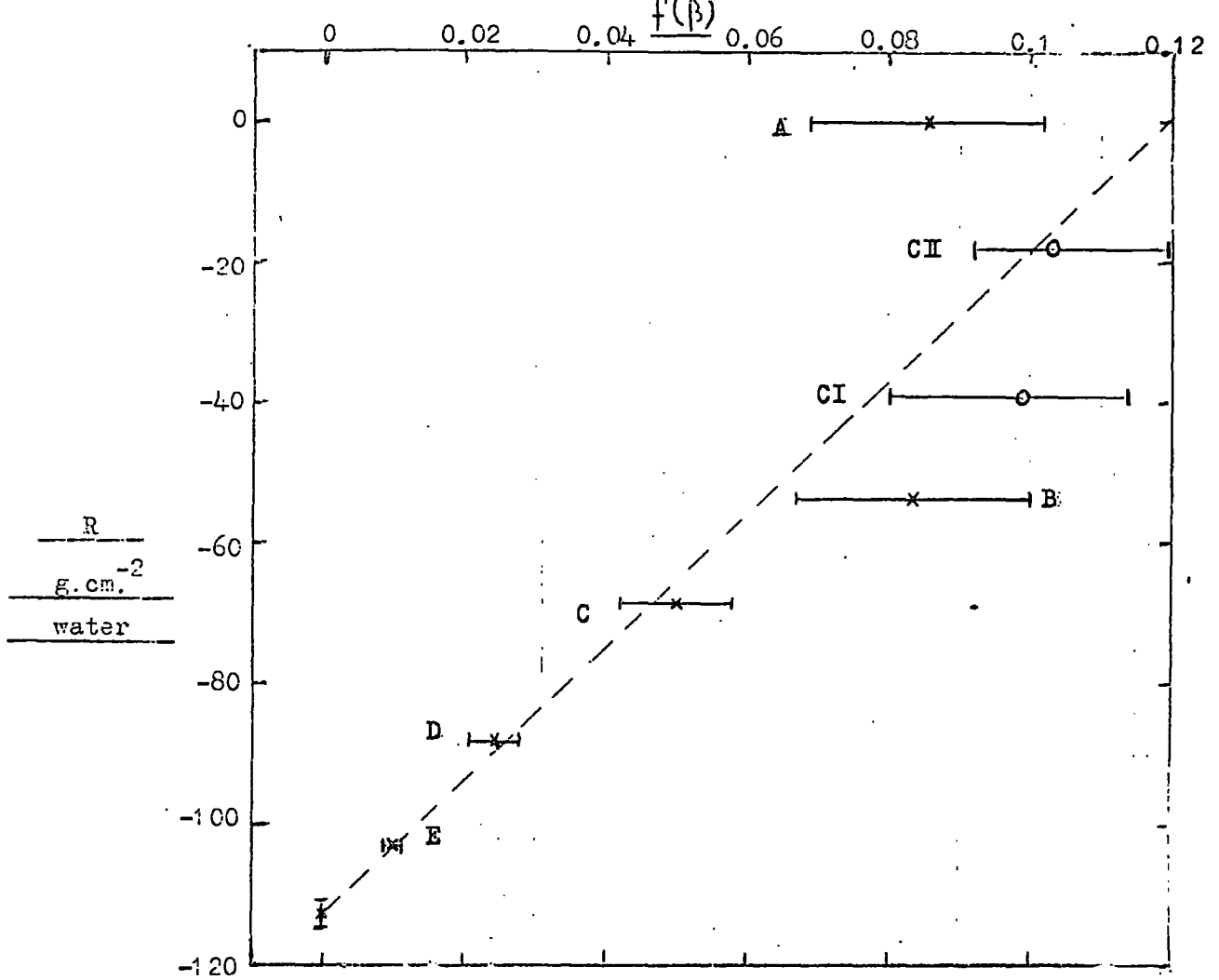
### 3.8. Experimental mass distributions obtained from the P,Q and R series.

In obtaining the mass distribution for each of the film series a further criterion was invoked to simplify the analysis. The elements in the telescope were supported in a framework by L shaped steel girders which overlapped the phosphor by 8 cm. at both edges of the 75cm. side along the whole length of 140 cm. To preserve uniformity in the analysis those particles selected were constrained to have traversed the telescope without passing through a single supporting girder. This further criterion reduced the acceptance of the telescope to the aperture defined between the two limiting scintillators of now reduced useful area  $59 \times 140 \text{ cm}^2$ , and resulted in reducing the useful events to 66% of the total.

A diagram of a typical event in the P series is shown in Figure 3.11 together with its  $R - f(\beta)$  plot and the least squares fit to the mass and residual range. It can be seen that the lower the scintillator is in the telescope the greater is its contribution in determining the mass. This is due to the nature of the curve shown in Figure 3.9 of normalised pulse height,  $V_N$ , in a scintillator against  $f(\beta)$  which gives, for a constant fractional error in  $V_N$ , a decreasing error in  $f(\beta)$  and hence an increasing weight as  $V_N$  increases.

Figure 3.11

Event 29/52.



P9/52	A	CII	CI	B	C	D	E	F
$V_N$	1.71	0.11	0.076	1.72	2.04	2.65	3.79	0
$\beta$	0.71	0.735	0.728	0.71	0.64	0.55	0.45	-

Figure 3.11 A typical event selected in the P series. The event itself is shown opposite and the particle appears to stop in the second layer of the flash tube tray F<sub>d</sub>. Above in the table the normalised pulse heights in each counter are given together with their corresponding velocities. The R-f( $\beta$ ) plot is shown above and the resulting mass after applying a least squares fit is  $910 \pm 70 \text{ Mev}/c^2$ . It should be noted that the least squares fit was not applied over the points CII and CI, these being included later from the results of the present experiment on the velocity response of the Cerenkov counters.

For convenience the results of the P and Q series have been combined and the resulting distributions are shown in Figure 3.12 for scattered and unscattered particles separately. For the unscattered sample the resolution obtained was a full width at half height of  $350 \text{ Mev}/c^2$ , and for the scattered sample a value of  $550 \text{ Mev}/c^2$ . The scattered sample as well as being broader is also more distorted towards lower mass values, and there are two factors contributing to this shift. The first is the effect of interactions in a scintillator giving an increased energy deposit which has the effect of moving  $f(\beta)$  for that scintillator to a lower value as well as increasing its relative weight. The combination of such a biased value of  $f(\beta)$  and the normal values of  $f(\beta)$  for the other scintillators leads in the majority of cases to a reduced mass and only rarely to an increase. The second effect is due to a charge exchange in the stopping region, or to unobserved scatterings out of the defined geometry. Several events were seen where the ionisation level in each of the scintillators suggested that the particle should still have a significant residual range beyond the point at which it was observed to stop. As  $M = R/f(\beta)$  the reduction in R due to a charge exchange or unobserved scattering has a large effect in reducing the mass estimate. While both effects contribute to the scattered sample only the latter, with a small contribution in the stopping region from the former, contributes to the unscattered sample. It is obvious that an improved mass resolution would be obtained if measurements were being made on a weakly interacting sample of particles.

One further interesting feature of the distributions is the presence of a long tail on the high mass side. The proximity of the deuteron mass to this region suggests their possible presence in the sample and discussion will be given to this in Section 3.12. Apart from a possible 1 or 2%

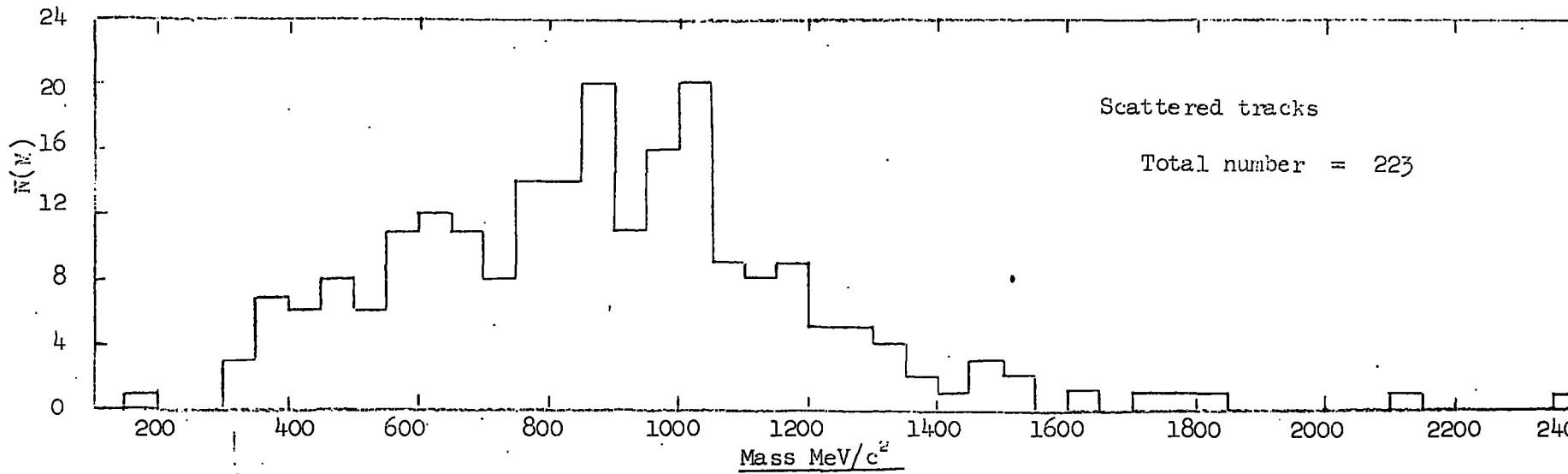
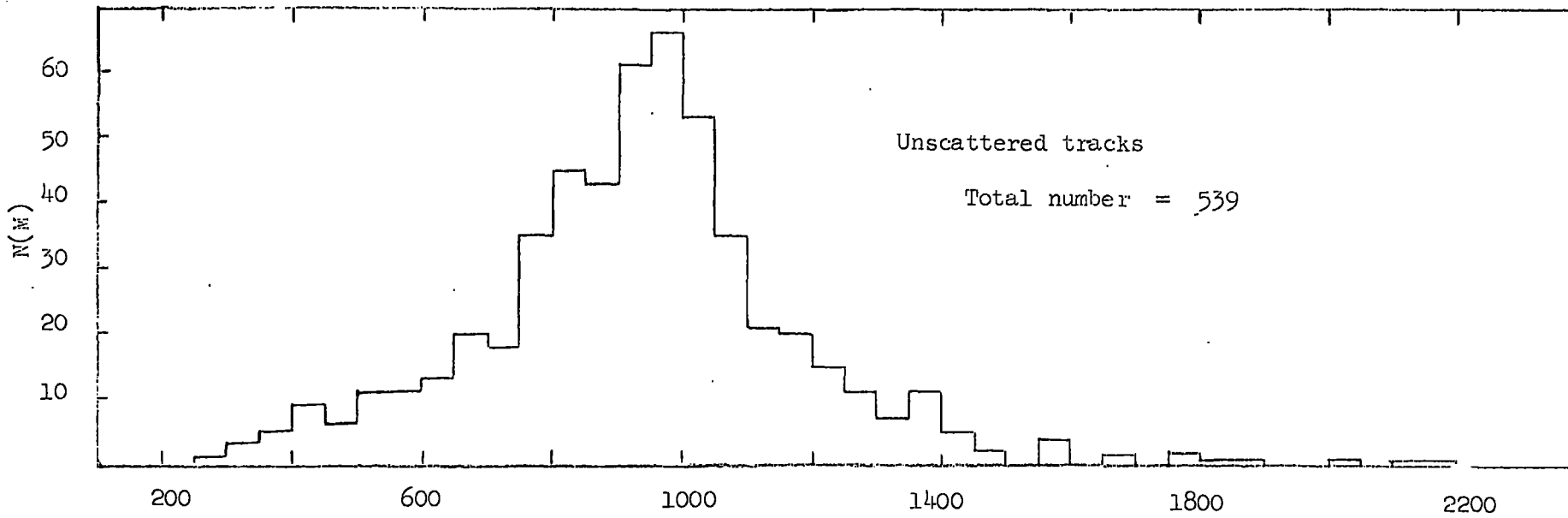


Figure 3.12. Mass distribution of particles selected in the P and Q series.

of particles in the tail being deuterons the rest of the distribution is consistent with all the particles being protons.

The mass distribution for the R series for both scattered and unscattered particles together is shown in Figure 3.13, where it can be seen that the whole distribution is shifted to lower masses and is centred about a mass of  $\sim 750 \text{ Mev}/c^2$ . Such a shift, as well as the disconcerting occurrence of negative masses, can be reconciled when the events are subdivided with respect to their calculated incident velocity. They were divided into three regions of incident velocity;  $0.77 < \beta_i < 0.79$ ,  $0.79 < \beta_i < 0.81$ , and  $0.81 < \beta_i < 0.87$ . The mass distribution for each interval is shown in Figure 3.14 and each is compared with the expected mass distribution for protons of incident velocity 0.78, 0.8 and 0.83c respectively. The expected distributions were obtained from a Monte Carlo calculation by assigning the expected pulse height to each scintillator, corresponding to a proton of a given incident velocity, and then imposing Gaussian errors, which were representative of the experimental conditions (Section 3.75), on each of these values. The mass was then determined in the same manner as for real particles and 500 trials were carried out for each incident velocity.

The comparison between the observed and expected distributions while being far from perfect shows the basic trend of the mass distribution being shifted to lower values as the incident velocity increases. For the case of  $0.77 < \beta_i < 0.79$  the disagreement is most pronounced and is due to several factors; the Monte Carlo calculation takes no account of scatterings or interactions and is also idealised in that it contains only random errors, whereas in the experimental situation systematic errors are possible, e.g. in the normalisation of the scintillator output pulse to the most probable pulse height obtained in a scintillator calibration; the experimental

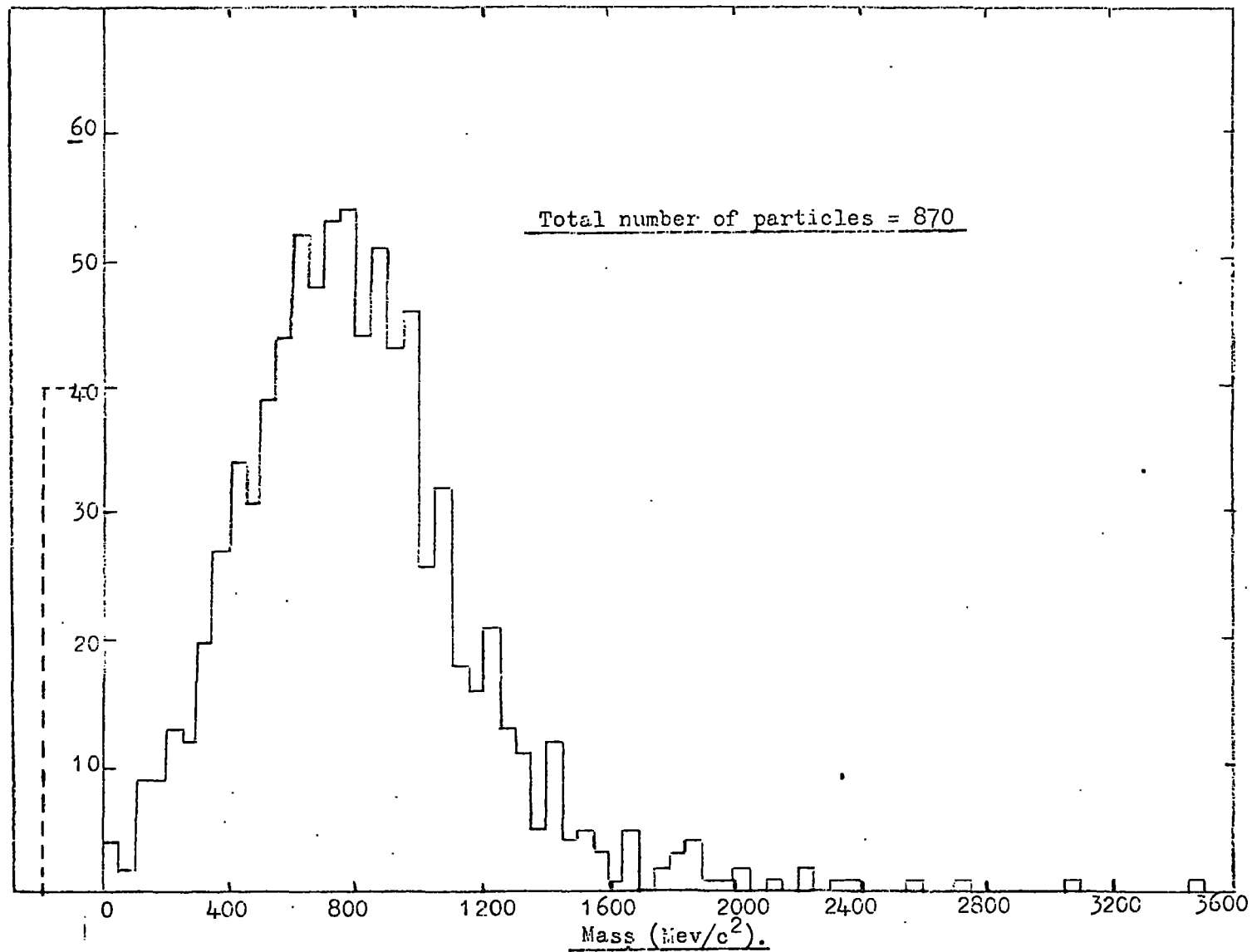


Figure 3.13 Mass distribution of both scattered and unscattered particles selected in the R series.

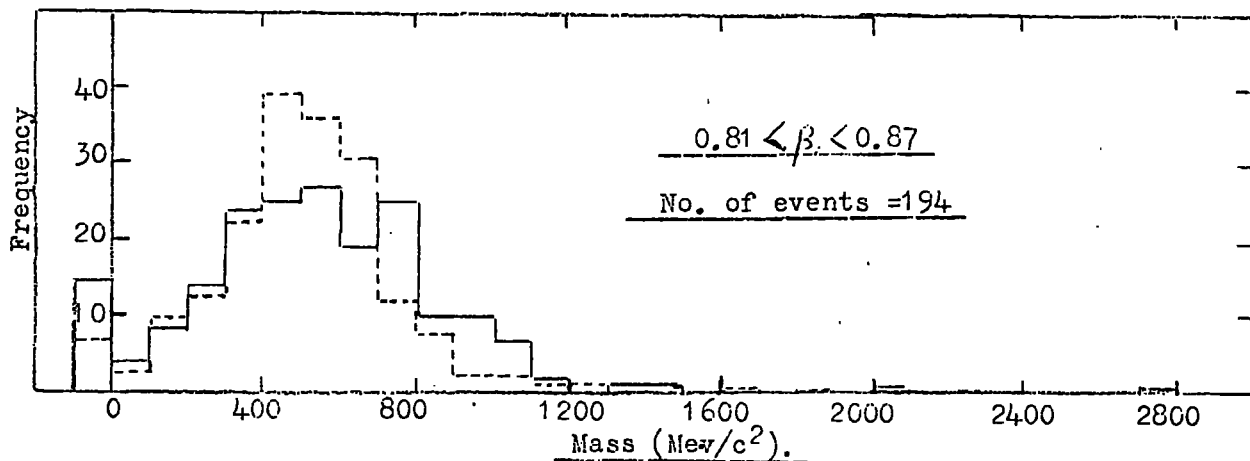
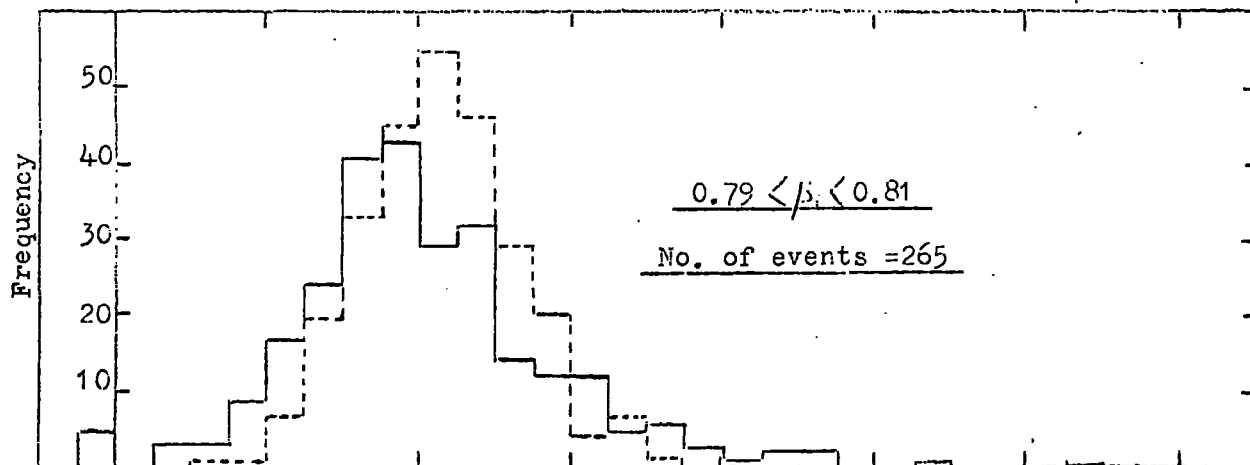
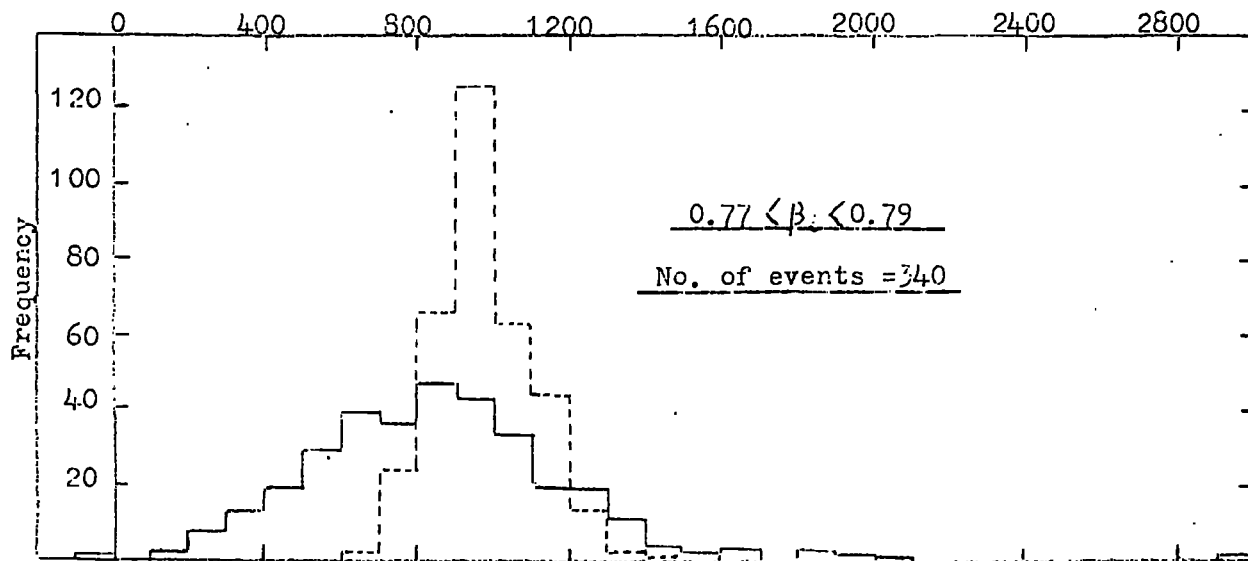


Figure 3.14 The events selected in the R series subdivided into incident velocity cells. The full line is the experimental observations and the dotted the theoretical distribution.

distribution is broadened due to interactions and due to particles of  $\beta_i > 0.79$  being contained in that velocity cell due to errors in measurement.

The shift to lower mass values is caused by a breakdown in the analysis procedure when the change in the ionisation level of the particle in traversing the whole telescope is comparable with the error in its measurement at each scintillator. Further Monte Carlo calculations show that with the telescope in its present form reliable mass estimates can be achieved only when  $\beta_i < 0.71$  for  $M = 2M_p$ , and when  $\beta_i < 0.56$  for  $M = 5M_p$ . Hence use of such a detector in searching for massive particles is somewhat limited in mass resolution in that for a given mass there is a corresponding incident velocity above which no exact mass can be estimated, and for those cases only a minimum mass can be attributed to the particles.

### 3.9. Measurements on the Cerenkov counters.

#### 3.9.1. The measured velocity response.

Only those unscattered particles traversing the revised acceptance of the telescope were used in this analysis. Under the assumption that all the particles were protons the velocity of each particle was evaluated at the centre of each Cerenkov counter, in the manner described in Section 3.7.6, and was correlated with the normalised pulse height in that counter. The selection of particles was further restricted by the rejection of those particles which had passed within 10 cm. of either end of the tank because of the uncertainties in the response correction beyond this region. The data were sorted according to velocity into cells of  $0.01c$  for  $\beta < 0.73$  and cells of  $0.005c$  for  $\beta > 0.73$ . For each velocity interval the mean and standard deviation of the data were evaluated and those cases where the pulse height was  $>3\sigma$  from the mean were rejected. The mean, median and standard error on the mean were calculated on the remaining data. The purpose of using the median as opposed to the mean, and the rejection of values which were greater than  $3\sigma$  from

the mean was to minimise the effect of events which had been scattered into the wrong velocity cells. Also the median was more appropriate in that each pulse height had already been normalised to the median pulse height obtained for particles of  $\beta = 1$ .

The pulse height distributions obtained for several of the velocity cells are shown in Figure 3.15 and the broadest distribution obtained is that for  $0.72 < \beta < 0.73$  and is due to this interval being in the region of the velocity threshold for the counter. The experimental velocity response is shown in Figure 3.16 where the points are the medians of the obtained distributions and the errors quoted are the standard errors on the mean, which are taken as representative of the errors on the median. The points are compared with the predicted response as evaluated in Section 3.5 and the agreement can be seen to be good. The only region of poor agreement is for  $0.67 < \beta < 0.71$  where the points are consistently  $2\sigma$  above that expected. Such a discrepancy can be readily accounted for by dispersion effects, which become important near the velocity threshold, and by an increased contribution from the perspex container relative to that from the water (as discussed in Section 3.5.2). An increase by a factor of 3 in the relative contribution from the perspex container, which is not unreasonable, would result in a good fit over this region without effecting the goodness of fit elsewhere.

It can be concluded that the experimental results are in good agreement with the theoretical Cerenkov yield as a function of velocity. Similar agreement has been obtained in this velocity region by Millar and Hincks, (1957), who studied muons traversing a plexiglass radiator, and by Belcher, 1953, who studied the faint luminescence observed from aqueous solutions of radioactive isotopes.

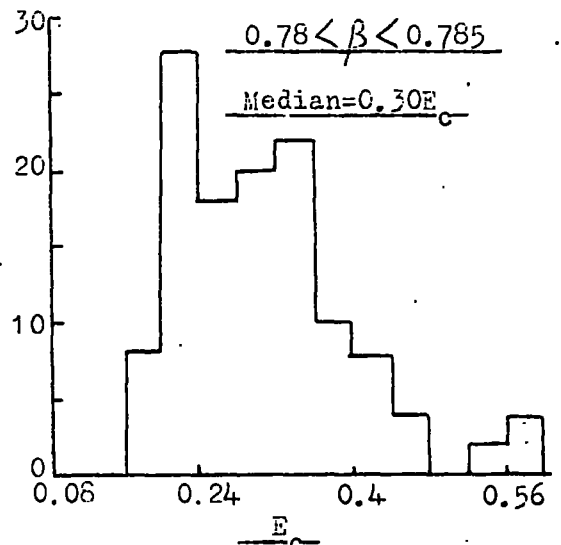
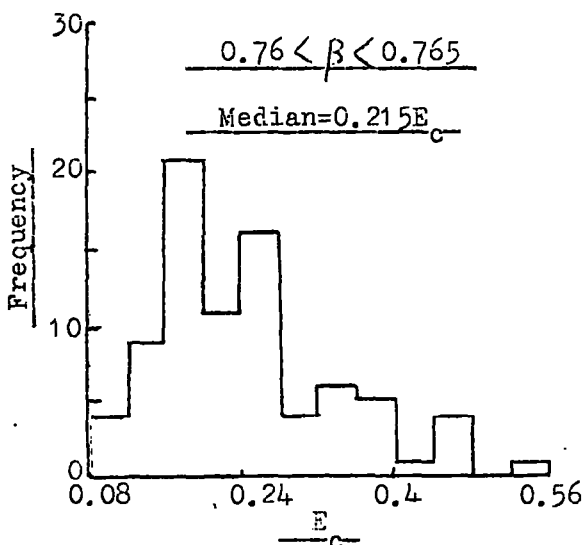
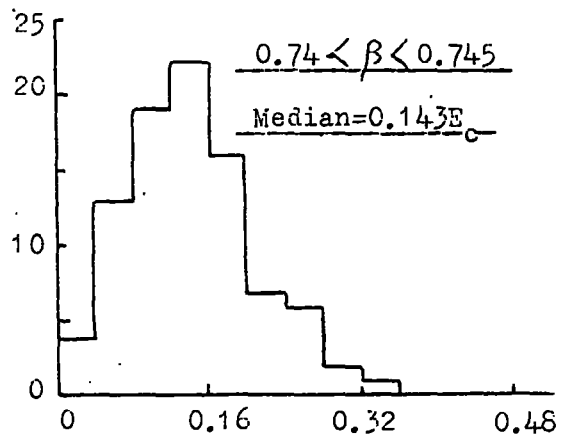
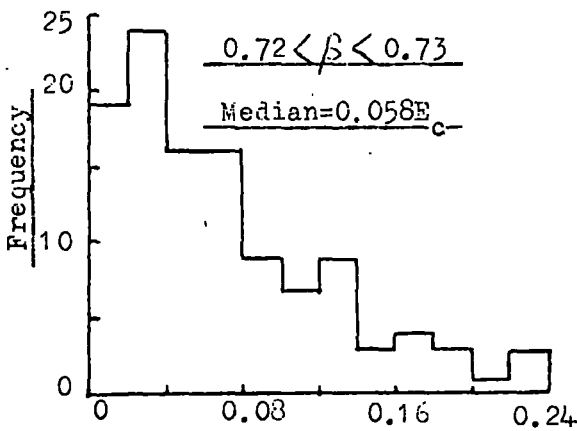
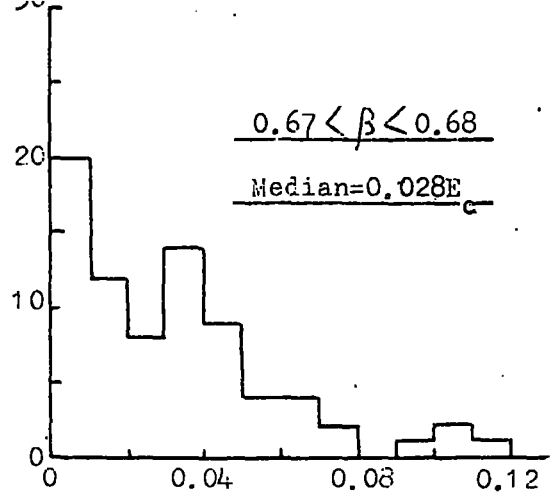
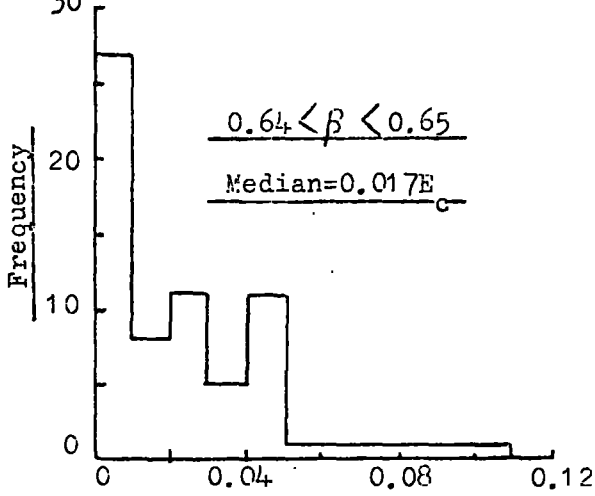


Figure 3.15 Cerenkov pulse height distributions for various velocity cells, the velocity referring to that at the centre of the counter. The pulse heights are normalised in terms of  $E_c$ , where this is the median pulse height produced in a G calibration.

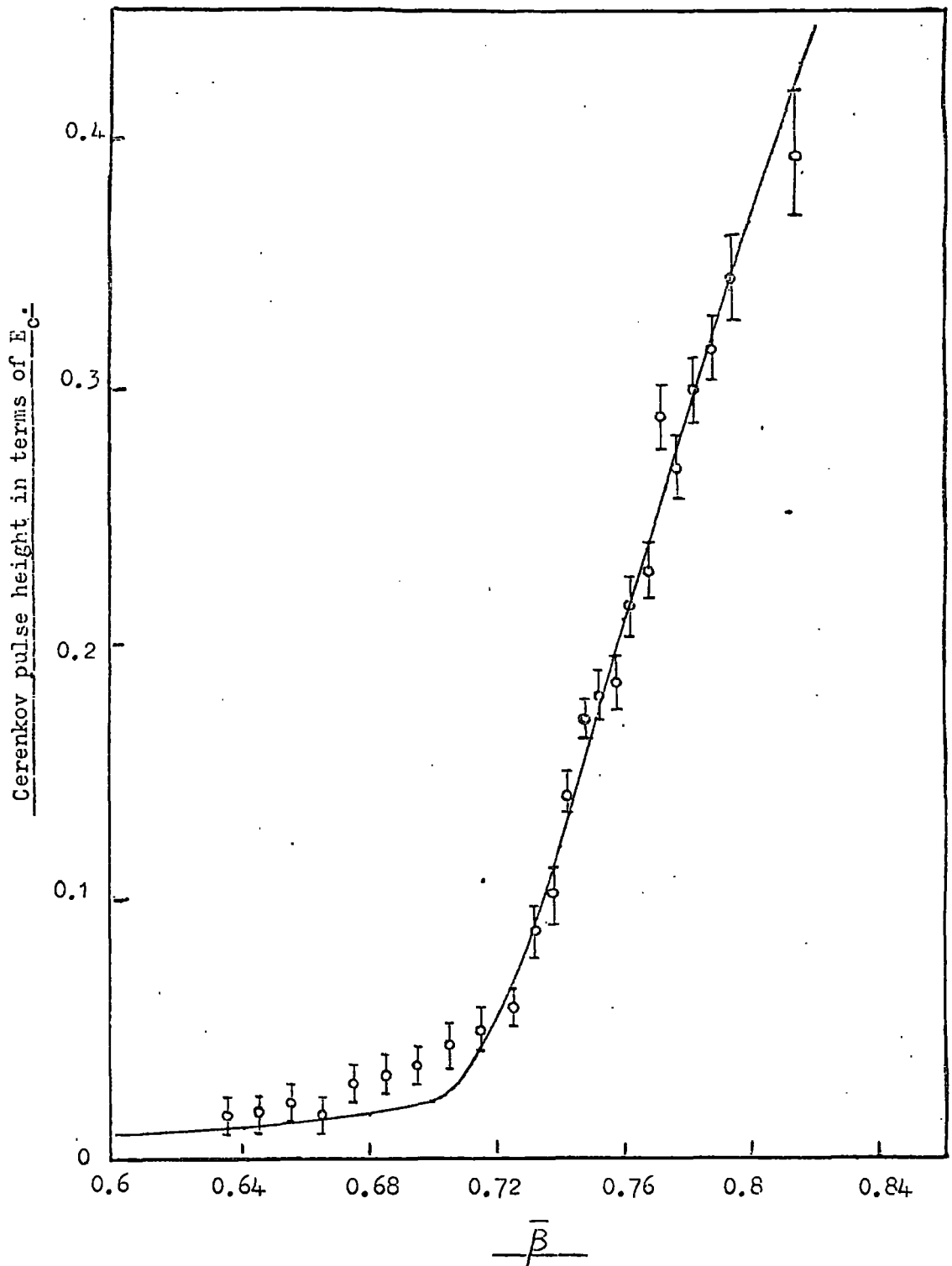


Figure 3.16 The measured Cerenkov response as a function of proton velocity compared with the theoretical response derived in Figure 3.7.  $\bar{\beta}$  refers to the velocity at the centre of the Cerenkov counter.

Having established the measured velocity response of the counters they themselves can now be used in a mass estimate together with the scintillators. For a given pulse height in a counter the velocity of the particle can be evaluated (Figure 3.16) together with its corresponding value of  $f(\beta)$ . (Section 3.7.4). Hence two further points can be included in the  $R - f(\beta)$  plot for a given particle and the least squares fit can be applied over a further two equations, thus giving a greater precision in the fit.

### 3.9.2 Scintillation light from the solute.

Saito and Suga, 1958, measured the scintillation light produced when an intense source of  $^{210}\text{Po}$ , free from its parent activity, was added to the solute and found that the amount of direct scintillation light was less than a few percent of the total light from the solution. The presence of scintillation light in the present experiment can best be considered at the lowest velocities measured in Figure 3.16. The measured points are consistent with the response expected from a knock on electron contribution and suggest that if scintillation light is produced it is present at a level of less than 1% of the Cerenkov light produced by a relativistic particle. Such a contribution, even if it exists, would have a negligible effect being only of the same order as background radiation from knock on electrons. Hence the counter with the addition of amino acid G, while giving an increased response over a pure water counter, still maintains its property of velocity discrimination.

## 3.10 The proton spectrum at low energies.

### 3.10.1 The telescope acceptance functions.

The differential aperture of a cubical detector of dimensions  $X, Y (> X)$ , and  $Z$  as a function of the true zenith angle,  $\theta$ , has been obtained for a

primary flux of the form  $I = I_0 \cos^n \theta$  incident on the XY plane following a method due to Osborne, 1966, and is given by

$$\left(\frac{d\Omega}{d\theta}\right)_n = 4 \sin \theta \cos^{n+1} \theta \int_{\psi_1}^{\psi_2} (XY - XZ \tan \theta \sin \phi - YZ \tan \theta \cos \phi + Z^{-2} \tan^2 \theta \sin \phi \cos \phi) d\phi$$

where  $\phi$  is the azimuth angle measured from the X axis. The limits of  $\phi$  depend on  $\theta$  in the following manner.

$\theta$	$\phi_2$	$\phi_1$
$0 \leq \theta \leq \tan^{-1}(X/Z)$	$\pi/2$	0
$\tan^{-1}(X/Z) \leq \theta \leq \tan^{-1}(Y/Z)$	$\pi/2$	$\cos^{-1}(X \cot \theta / Z)$
$\tan^{-1}(Y/Z) \leq \theta \leq \tan^{-1}\left(\frac{\sqrt{X^2 + Y^2}}{Z}\right)$	$\sin^{-1}(Y \cot \theta / Z)$	$\cos^{-1}(X \cot \theta / Z)$

For the present work particles were accepted only if they had traversed the telescope without passing through any supporting girders and this criterion defines the values of X and Y, which are 59 cm. and 140 cm. respectively. The value of Z depends on the film series and for the P and R series  $Z = 253.1 \text{ cm.}$ , and for the Q series  $Z = 221.4 \text{ cm.}$  For each value of Z the differential aperture was calculated for values of n from 0 to 14.

### 3.10.2 Angular distribution of accepted particles.

To avoid biasing of the data, due to the scattered particles possibly imposing some distortion on the true angular distribution of the incident flux, only the unscattered particles were considered. The distributions of projected angle in both front and side elevations of the telescope were considered for all three series of measurements and in each case a symmetrical distribution about zero angle was obtained, the mean values of the distributions always falling between  $\pm 1^\circ$ . This demonstrates the accuracy of the geometrical constants adopted for the telescope, and also shows that the detection efficiency of the telescope is uniform throughout.

The distributions of true zenith angle were obtained for each series and compared with the expected distributions as a function of the exponent  $n$  as calculated in Section 3.10.1. A minimum  $\chi^2$  test was employed to obtain the best fit and this yielded values of  $n$  of  $10.0 \pm 3.5$ ,  $6.5 \pm 3.2$  and  $8.5 \pm 2.6$  for the P, Q and R series respectively. The measured and expected distribution for the value of  $n$  giving the best fit are shown in Figure 3.17. The resulting weighted mean value of  $n$  of  $8.3 \pm 0.6$  is not inconsistent with a value of 8 commonly accepted for the higher energy nucleon component of the sea level cosmic radiation.

### 3.10.3 The observed rates of stopping protons

All the stopping particles in the defined acceptance for both the P and Q series are assumed to be protons. That this is a reasonable assumption can be seen by reference to Figure 3.18 where the Cerenkov pulse height as a function of the residual range from the Cerenkov counter is shown for a range of mass values, and the selection bands for each film series are shown in the same terms of reference. The only likely contamination is from deuterons, (assuming the contribution from kaons to be negligible), and discussion in Section 3.8 suggests that they may be present to a maximum level of 2% but in the present analysis their possible presence is ignored.

The basic information for both series is given in Table 3.4.

Table 3.4

Film Series	Number of particles (N)	Running Time (T) in hours	Aperture (A) cm <sup>2</sup> st.	Accepted momentum band ( $\Delta p$ ) Mev/c	Mean Momentum Mev/c	Mean Pressure m. bars.
P	353	36.07	$7.9 \cdot 10^2$	52.7	1087.3	1009.3
Q	409	27.07	$9.6 \cdot 10^2$	57	1032.5	1012.7

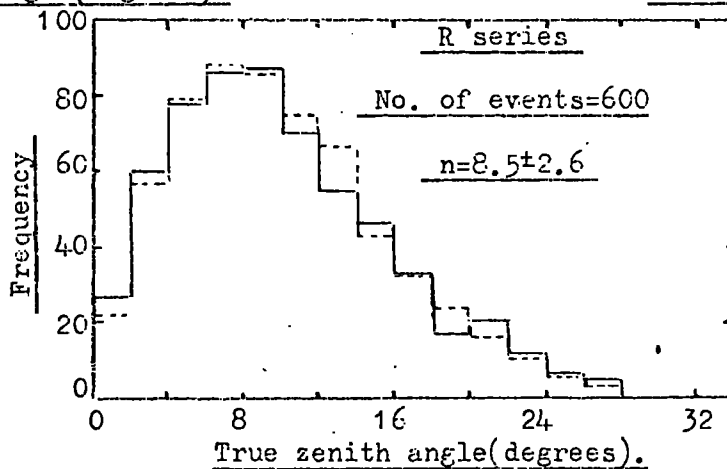
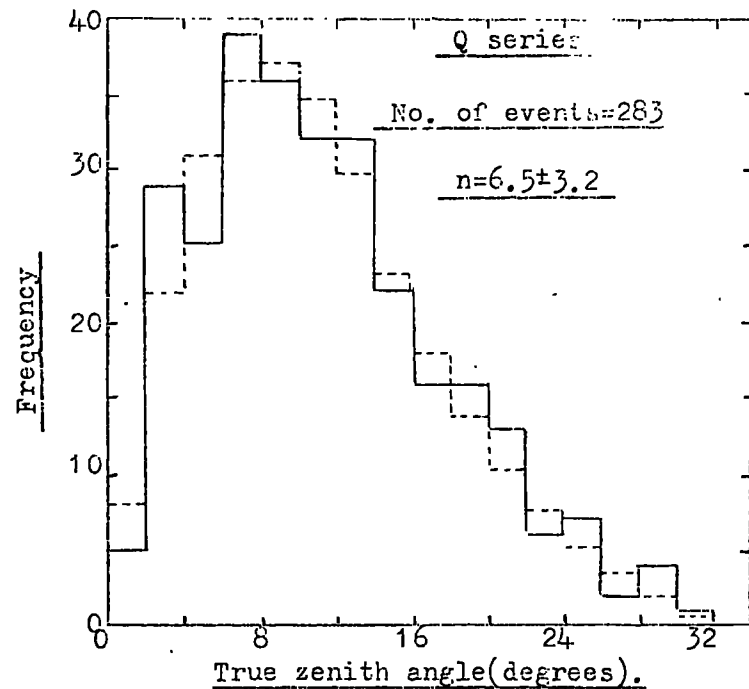
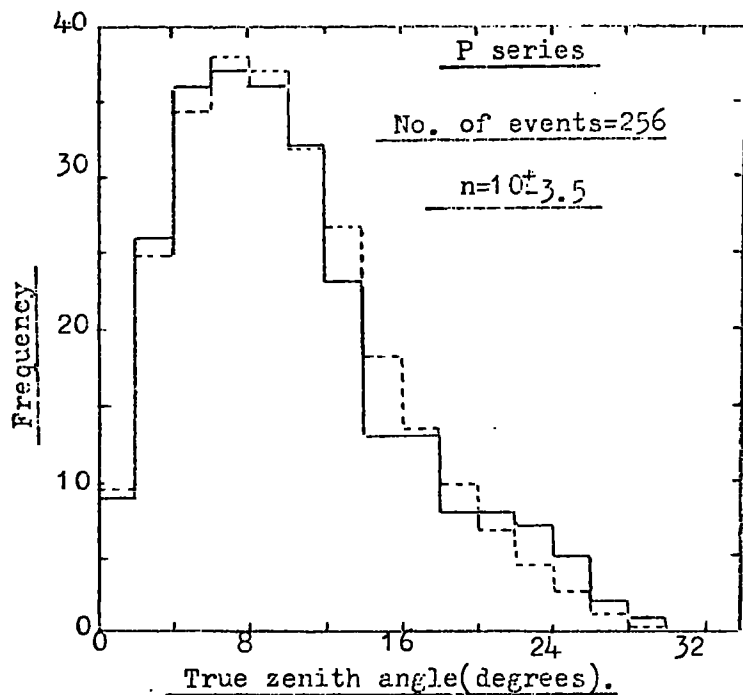
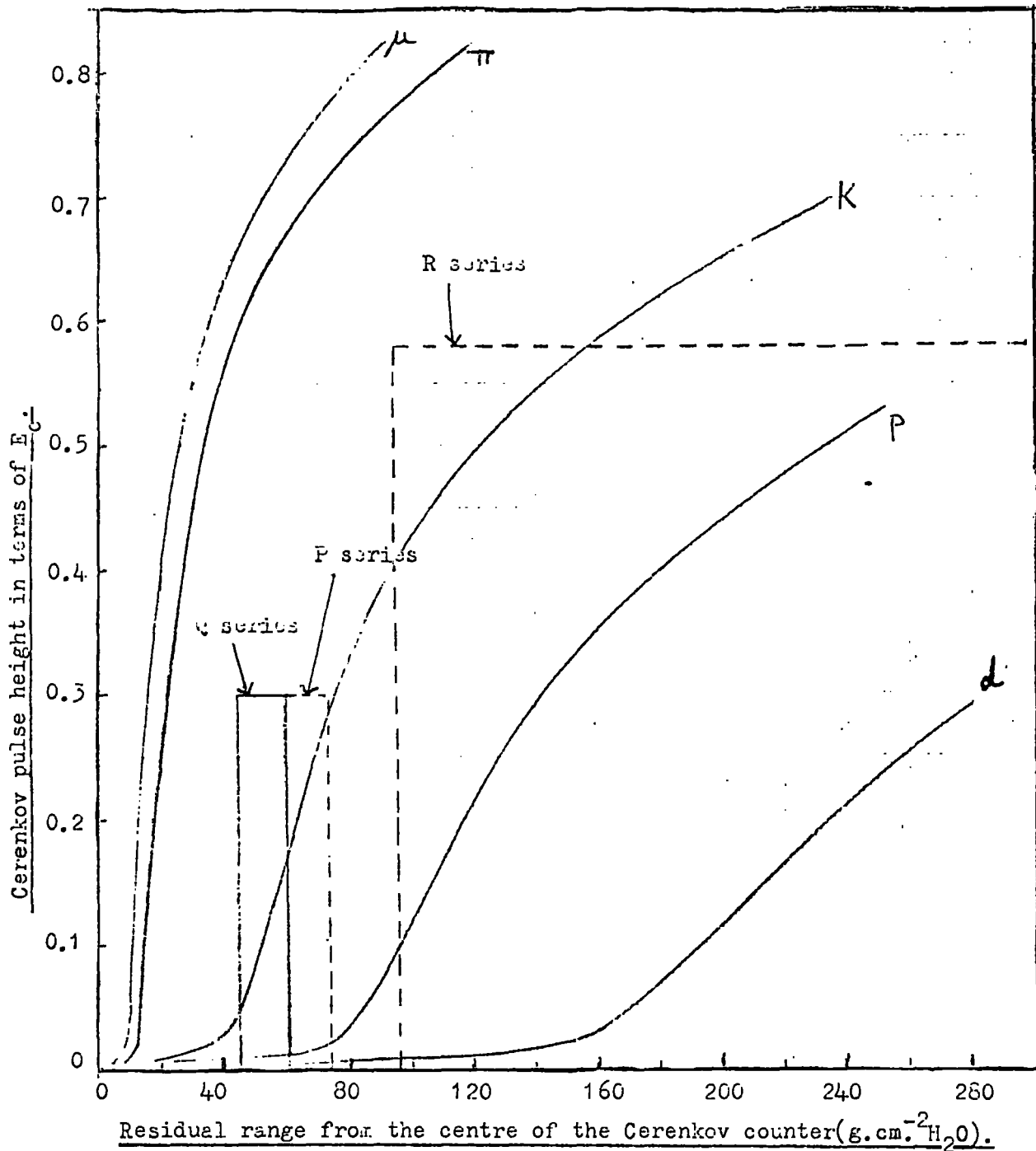


Figure 3.17 The true zenith angle distributions of unscattered particles accepted in each film series. The full line is the experimental data and the dashed line the angular distribution corresponding to the exponent of the radiation derived from a minimum  $\chi^2$  test.



**Figure 3.18** Cerenkov pulse height as a function of residual range for particles of different mass, showing the acceptance criteria used in the three series of measurements.

The quoted aperture is for an assumed value of  $n = 8$  and the momentum bands refer to normal incidence. The observed rate of protons is then given by

$$N(p)dp = \frac{N}{3600. A. T. \Delta p} \text{ cm.}^{-2} \text{ sec.}^{-1} \text{ sterad.}^{-1} (\text{Mev/c})^{-1}$$

Analysis of the variation of observed rate with atmospheric pressure during each run yields a pressure coefficient of  $1.3 \pm 0.5\%$ /mbar. which is not inconsistent with the accepted value of  $0.72\%$ /mbar for the nucleon component, and the latter value was used to normalise the observed rates to an atmospheric pressure of 1000 mbar. The resulting observed rates are  $(6.98 \pm 0.38) \cdot 10^{-8}$  and  $(8.37 \pm 0.43) \cdot 10^{-8} \text{ cm.}^{-2} \text{ sec.}^{-1} \text{ sterad.}^{-1} (\text{Mev/c})^{-1}$  for mean momenta of 1087 and 1033 Mev/c respectively. No corrections have been applied for range straggling or for the increased accepted momentum bands for inclined particles, these effects being small compared with the statistical errors quoted on the observed rates.

#### 3.10.4 Correction of the observed rates due to proton interactions in the telescope.

Due to the strongly interacting nature of protons those observed to stop in the telescope do not comprise totally of particles incident in the defined momentum bands. The non-interacting component in the accepted momentum band will be observed together with protons of higher momentum which interact in the telescope, lose a certain fraction of their energy, and then stop in the selected region. Applying a correction for such effects is quite complex in that it requires accurate values of cross sections and inelasticity distributions for nucleon-nuclei interactions, and is further complicated by the rapidly changing energy of the proton between entering and stopping in the telescope. In the absence of the complete basic information required only an approximate estimate of the effect in the present experiment has been made.

Fairly precise measurements of the total neutron-nucleus cross-section for a variety of nuclei, ranging from deuterium to uranium, have been made by Nedzel, 1953, for a neutron energy of 410 Mev (the average incident proton energy in the P and Q series was 440 Mev). The total and inelastic cross sections for nucleon-nuclei collisions for various nuclei have been reviewed by Chen et al., 1955, and for nucleon-carbon collisions by Batty, 1961, as a function of the incident nucleon energy for energies less than 1.5 Gev. The results show negligible difference between proton-nuclei and neutron-nuclei cross sections, which is as expected from charge symmetry considerations, and also that while the total cross sections rise fairly quickly for nucleon energies below 150 Mev the inelastic cross sections remain essentially constant down to the lowest energy (95 Mev) considered by the above workers.

For the present analysis the elastic part of the cross section can be ignored as such interactions involve only small energy transfers having negligible effect. That this is so is fortunate in that the remaining inelastic cross section is energy independent over the range encountered in the present experiment, hence alleviating problems of a varying cross section as the proton traversed the telescope. The total and inelastic interaction lengths have been determined from the results of the above workers for nucleons of energy 410 Mev incident on various nuclei from the relationship  $\lambda = \frac{A}{N\sigma}$ , where A is the atomic weight of the nucleus, N is Avagadro's number and  $\sigma$  the measured cross section. The resulting interaction lengths are shown in Figure 3.19 as a function of atomic weight. The number of inelastic interaction lengths in each of the various detecting elements in the telescope was evaluated using Figure 3.19 and the mean values of A given in Table 3.2 for the telescope materials, and the results are given in Table 3.5.

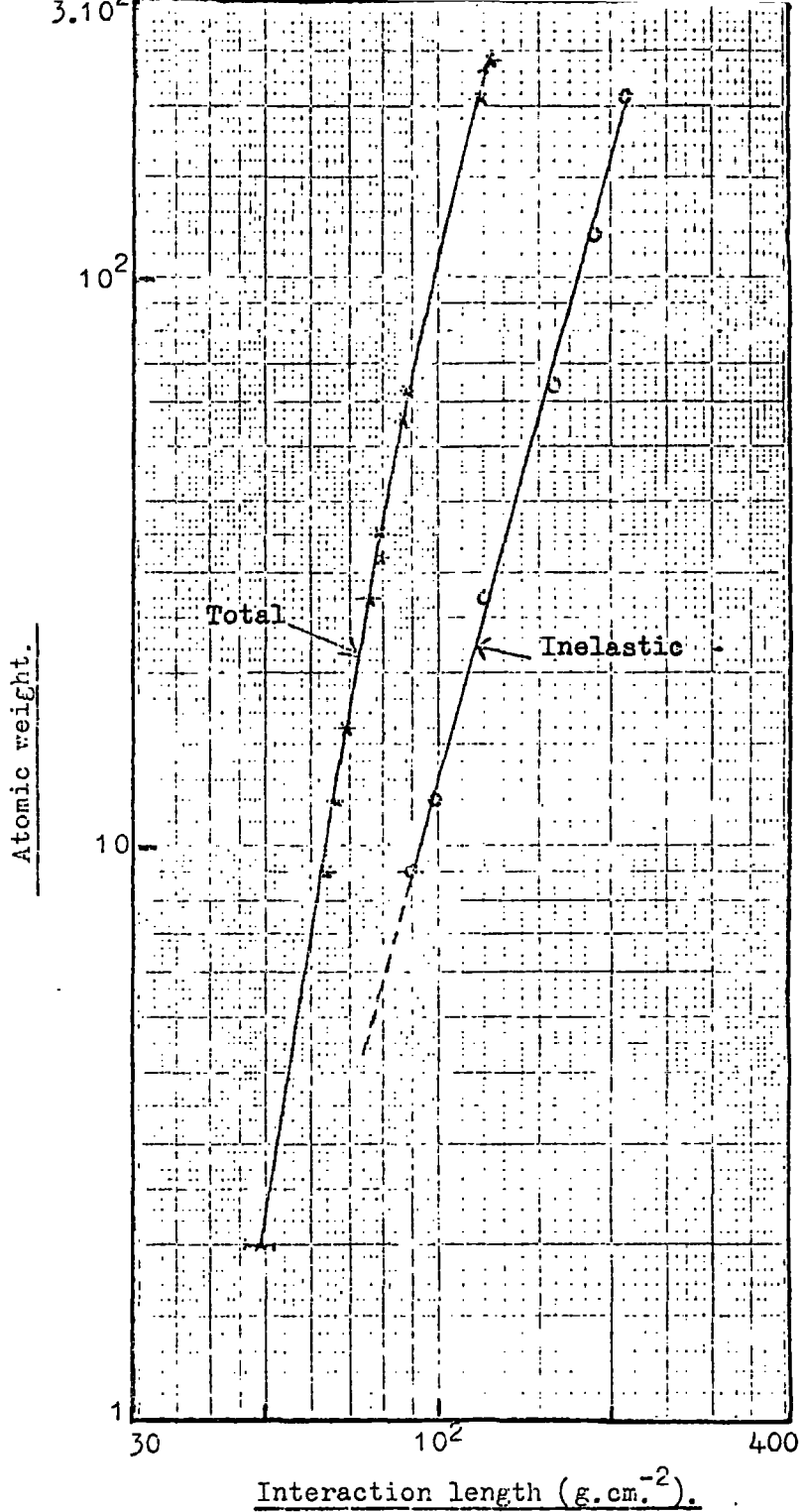


Figure 3.19

Total and inelastic nucleon interaction lengths in various nuclei as a function of atomic weight.(Chen et al.,1955).

Table 3.5

Detector	No. of $\lambda$ in.
Scintillator; A, B, C, D, E, F	0.069
Cerenkov counter: CII, CI	0.262
Flash Tubes; F <sub>1</sub> , F <sub>2</sub>	0.057
Flash Tubes; F <sub>5</sub>	0.052
Flash Tubes; F <sub>3a</sub> , F <sub>4b</sub> , F <sub>6c</sub> , F <sub>7d</sub>	0.097

To estimate the ratio of the observed to the expected number of stopping protons the shape of the low momentum proton spectrum is required and that measured by Brooke and Wolfendale, 1964(a), has been used. The ratio  $N_o/N_e$  can be approximated to

$$\frac{N_o}{N_e} = e^{-l/\lambda} + \alpha + \delta$$

where  $N_e = \int_{p_1}^{p_2} N(p) dp$  where  $p_1$  and  $p_2$  are the limits of incident momentum for non-interacting protons stopping in the selected region;  $e^{-l/\lambda}$  is the fractional contribution from non-interacting protons

incident in the defined momentum bands;

$$\alpha = \int_{p_1}^{p_T} [N(p) dp (e^{-x_1/\lambda} - e^{-x_2/\lambda}) e^{-(l-x)/\lambda}] / N_e$$

and is the contribution from interacting protons of incident momentum between the limits  $p_1$  and  $p_T$ , where  $p_T$  is the momentum corresponding to the Cerenkov discrimination level;

$x_1$  and  $x_2$  are functions of momentum and inelasticity,  $K$ , and define the region in which a proton of incident momentum  $p$  can interact with an inelasticity  $K$  such that it will then stop in the selected region. The values of  $x$  can range from 0 to  $l + \Delta l$ , where  $l$  is the number of interaction lengths to the stopping region, and  $\Delta l$  is the number of

interaction lengths in that region;  $\bar{x} = (x_1 + x_2)/2$ ;

and  $\lambda$  is the nucleon inelastic interaction length;

$$\delta = \int_{p_T}^{\infty} [N(p) dp (e^{-x_3/\lambda} - e^{-x_4/\lambda}) e^{-(\ell - \bar{x})/\lambda}] / N_e$$

and is the contribution from protons of incident momentum  $> p_T$  which interact before traversing 0.3 of counter CI (corresponding to the discrimination level in CI) and then stop in the selected region;

$x_3$  and  $x_4$  again are functions of  $p$  and  $K$  and define the limits of the possible interaction region. Their range of values lies between 0 and  $0.56\lambda$ .

For the P and Q series respectively the values of the parameters were:-

$$p_1 = 1061 \text{ and } 1004 \text{ Mev/c}; p_2 = 1113.6 \text{ and } 1061 \text{ Mev/c}; \ell = 1.25 \text{ and } 1.09\lambda;$$

$$p_T = 1330 \text{ Mev/c}; \Delta\ell = 0.165\lambda.$$

No information is known to the author on inelasticity distributions for proton interactions with nuclei in the relevant energy range, and in its absence the value of  $N_0/N_e$  has been evaluated for both the P and Q series assuming a fixed inelasticity,  $K$ , for values of  $K$  from 0.3 to 0.7. The variation of  $N_0/N_e$  is shown in Figure 3.20 as a function of  $K$  for each series.

The evaluation of these correction factors is obviously approximate in the absence of accurate inelasticity distributions, and to take these uncertainties into account the observed rates were corrected using a value of  $K = 0.5$ , the statistical errors on the rates being broadened assuming the error in the correction factor to be the limits for  $K = 0.7$  and  $0.3$ . The resulting rates are  $(1.03^{+0.13}_{-0.12}) \cdot 10^{-7}$  and  $(9.9^{+1.2}_{-0.5}) \cdot 10^{-8} \text{ cm.}^{-2} \text{ sec.}^{-1} \text{ sterad.}^{-1}$  (Mev/c) $^{-1}$  at mean proton momenta of 1087 and 1032.5 Mev/c respectively.

### 3.10.5 Comparison with other workers.

Several measurements of the proton intensity in the present momentum range have been carried out and a summary of such measurements is shown in

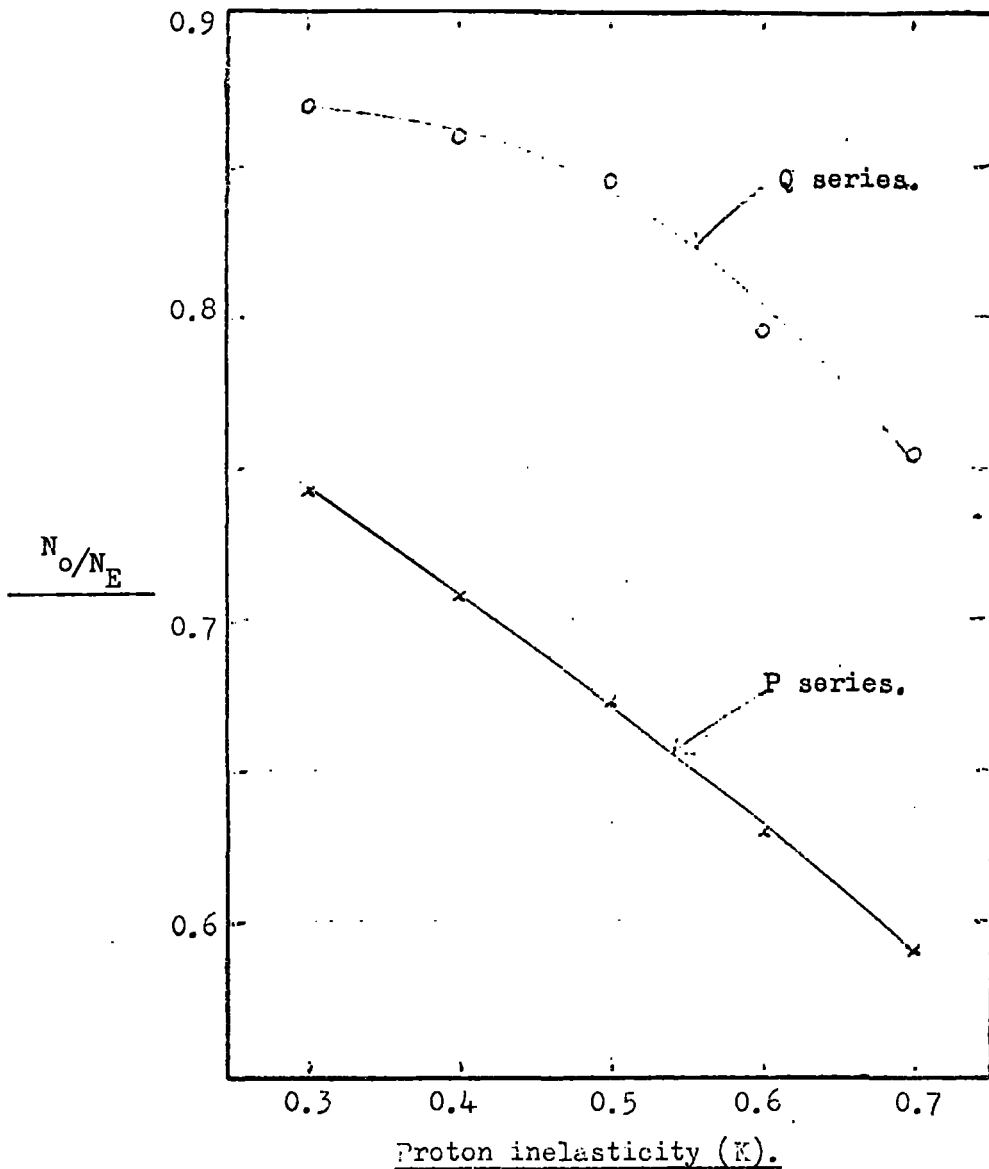


Figure 3.20 The ratio of the observed number of protons to the expected number (ignoring interactions) as a function of the proton inelasticity.

Figure 3.21 together with the present results where the rates before and after correction are shown. Agreement can be seen to be fairly good and in fact would be improved by an increase in the quoted errors on some of the other points, due to uncertainties in the correction factors used to take into account proton interactions (this applies particularly to those measurements made by a range-velocity technique, as in the present experiment, and not to the measurements where momentum was measured). Such agreement further substantiates the fact that the Cerenkov counters containing amino acid G still retain their role of velocity discrimination and that the method of analysis, relying on the most probable energy loss in the scintillator and normalisation of the telescope material, is valid.

### 3.11 Response of the scintillators as a function of velocity.

As described in Section 3.7.6 the velocity of each incident particle, assumed to be a proton, was calculated at the centre of each scintillator, and correlated with the pulse height in that scintillator. This information for unscattered particles only in the P and Q series was considered and pulse height distributions were obtained for a range of velocity intervals from which the most probable pulse height as a function of velocity was derived. The experimental points are shown in Figure 3.22 and are compared with the expected curve calculated in Section 3.4. Agreement can be seen to be good and this further shows the validity of the calculated most probable energy loss as a function of velocity.

### 3.12 Estimate of the deuteron intensity at sea level.

#### 3.12.1 Extraction of deuterons from the tail of the mass distributions.

For this analysis only the unscattered mass distribution for the P and Q series (Figure 3.12) was considered. Each particle yielding a mass value of  $>1500 \text{ Mev}/c^2$  was carefully reanalysed. It was assumed that the particle

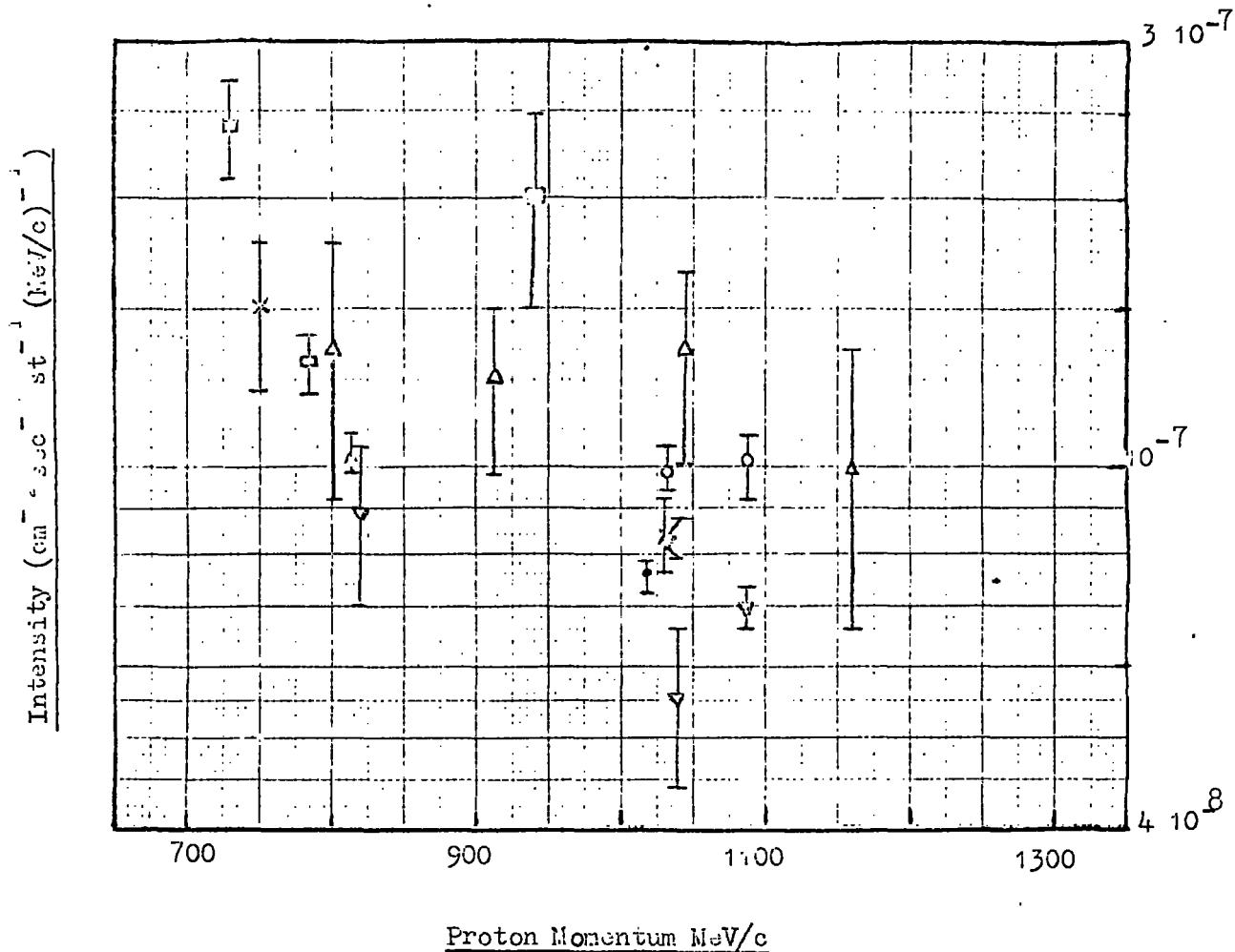


Figure 3.21

Proton Spectrum

- ▼ Present work uncorrected
- Present work corrected
- × Brooke, G. et al., 1964 a
- McDiarmid, I.B., 1959
- △ Ballam, J. et al., 1954
- ◇ Baccalini, C. et al., 1955
- ▽ Mylori, M.G. et al., 1951
- ▣ Goldwasser, E.L. et al., 1951
- ▤ York, C.M., 1952

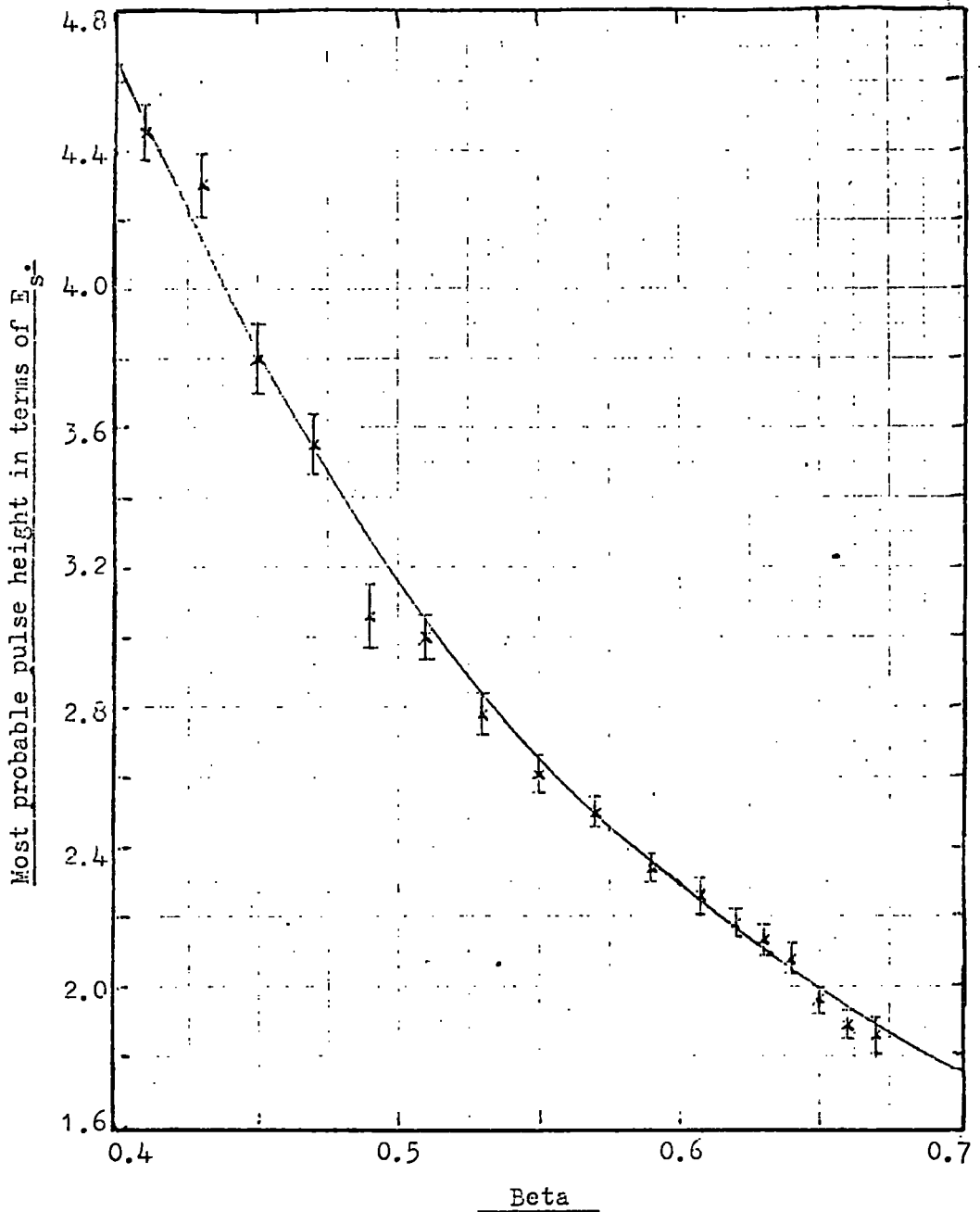


Figure 3.22 The measured most probable pulse height recorded by the scintillators as a function of the proton velocity, compared with the expected variation derived in Section 3.4.1.

had stopped at the observed point, and the expected pulse heights in each scintillator were calculated assuming the stopping particle to be a proton or a deuteron. The expected error on each pulse height was evaluated (Section 3.7.5) and the particle was accepted as being a deuteron if the following conditions were satisfied:  $(V_e - V_o)_p$  in each scintillator (apart from scintillator A which was ignored due to possible accompaniment) was greater than  $1.96 \sigma_e$ ,  $2.3 \sigma_e$ , and  $3.1 \sigma_e$ , for particles stopping in the regions  $F_{7d}$ ,  $EF_{6c}$  and D respectively, where  $V_e$  is the expected pulse height,  $V_o$  is the observed pulse height and the suffix refers to the expected pulse height for a proton or a deuteron, resulting in the probability of the particle being a proton being  $< 10^{-6}$ ;

$(V_e - V_o)_d$  in each scintillator was within  $\pm 2 \sigma_e$  with a resulting average efficiency of accepting a deuteron of 0.94.

In all 13 particles were analysed and of these 6 satisfied the imposed criteria, and the residual range  $-f(\beta)$  plot for each is shown in Figure 3.23, together with its corresponding least squares fit mass. Assuming the deuteron mass distribution to follow the same shape as that obtained for protons, the efficiency for accepting deuterons in a mass band  $> 1.5 \text{ GeV}/c^2$  is 0.8, and taking account of the acceptance efficiency of 0.94 imposed by the previous selection criteria the corrected number of deuterons in the sample becomes 7.6.

The incident momentum band, for normal incidence, over which deuterons would be accepted was 1565-1725  $\text{MeV}/c$ , and the mean telescope aperture was  $8.6 \cdot 10^2 \text{ cm}^2 \text{ sterad.}$ , assuming a  $\cos^8 \theta$  zenith angle dependence for the incident flux, the effective running time being 31.6 hours. The observed rate of deuterons was  $(4.83^{+2.98}_{-1.98}) \cdot 10^{-10} \text{ cm.}^{-2} \text{ sec.}^{-1} \text{ sterad.}^{-1} (\text{MeV}/c)^{-1}$  at a mean momentum of 1.65  $\text{GeV}/c$ . Taking a value of  $3.1 \cdot 10^{-8} \text{ cm.}^{-2} \text{ sec.}^{-1} \text{ sterad.}^{-1}$

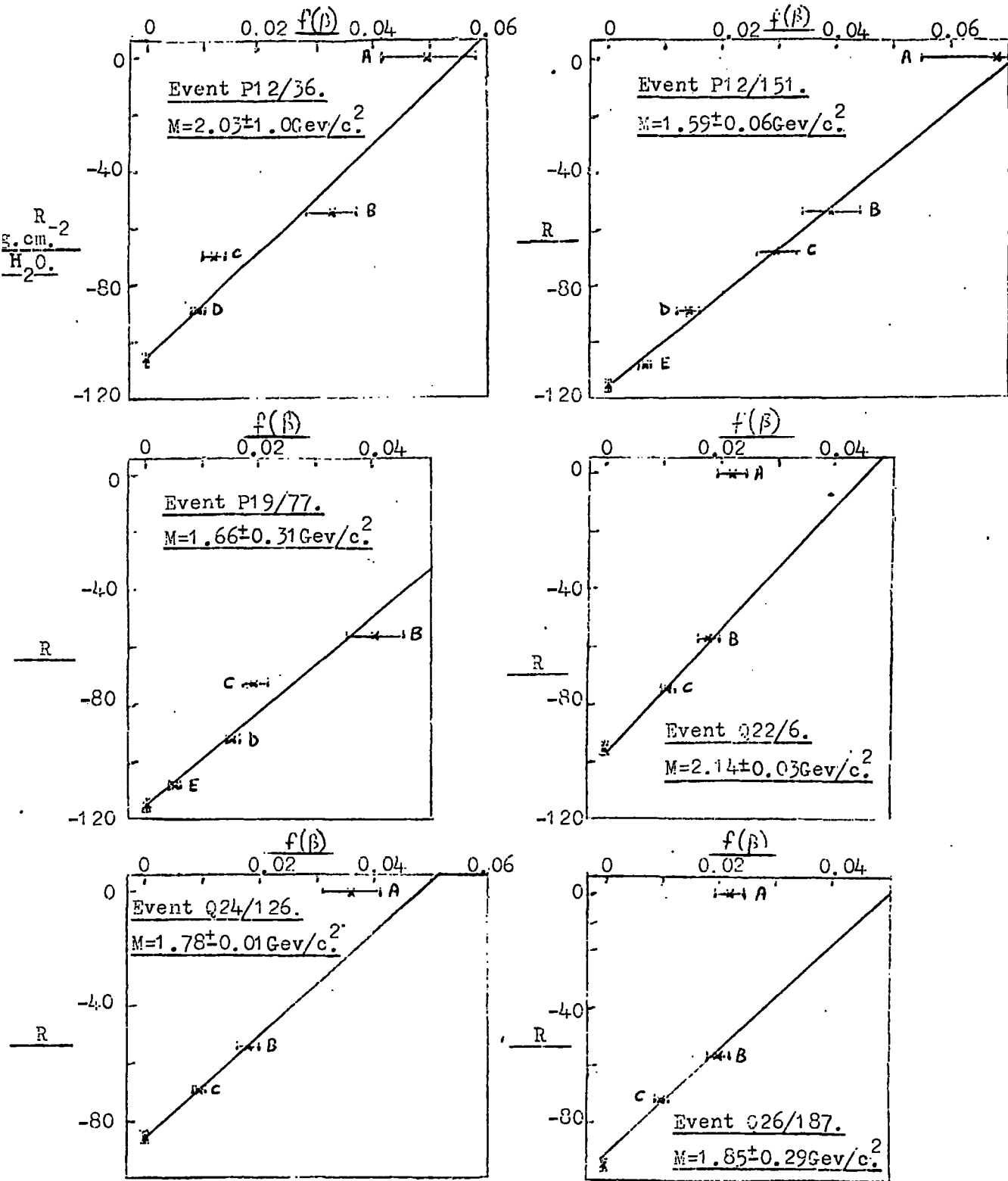


Figure 3.23

The  $R-f(\beta)$  plots for the six events extracted from the tail of the mass distribution for unscattered particles selected in the P and Q series (Figure 3.12). The mass of each event is shown and it should be noted that in some cases scintillator A has been omitted from the least squares fit.

$(\text{Mev}/c)^{-1}$  for the proton flux at the same momentum (Brooke and Wolfendale, 1964a) the observed d/p ratio at 1.65 Gev/c was  $(1.56^{+0.97}_{-0.64})\%$ .

### 3.12.2 Correction of the deuteron intensity for interactions in the telescope.

Deuterons being nuclear active would be attenuated in traversing the telescope, and only those not interacting would have been accepted in the present experiment. Unlike the case of protons, where there is a contribution at the stopping region from interacting protons of higher momentum, no such contribution is possible from higher momentum deuterons as, because of their small binding energy, their identity would be lost in any inelastic interaction and they would not be present in the interaction products. There is of course the possibility of contamination from higher momentum deuterons interacting in the stopping region (without the interaction being observed) where the interaction products do not leave that region. However it is unlikely that such cases would be accepted as being deuterons, as the reduced range of the deuteron due to its interaction would have the effect of reducing the mass estimate below  $1.5 \text{ Gev}/c^2$ , the level above which deuterons were extracted from the mass distribution.

In the absence of deuteron-nuclei cross sections recourse was taken to a consideration of nucleon-nucleon and nucleon-deuterium cross sections. A summary of such cross sections has been given by Longo, 1968, to evaluate the Glauber shadow correction for nucleon-deuterium interactions. He has determined  $\delta\sigma$  in the momentum range 3-27 Gev/c from the available data where

$$\delta\sigma = \sigma_{pp} + \sigma_{np} - \begin{cases} \sigma_{pd} \\ \sigma_t \\ \sigma_{nd} \end{cases}$$

and where all the np cross sections have been measured directly using neutron beams, and not by subtraction methods commonly employed where the Glauber correction is assumed. The work of Marshall et al., 1953, and Nedzel, 1954,

with neutrons and protons of momentum 0.97 Gev/c incident on hydrogen and deuterium allows a further value of  $\delta\sigma$  to be evaluated at a lower momentum than considered by Longo. The values of  $\delta\sigma$  as well as  $\sigma_{pd}$  are listed in Table 3.6 as a function of momentum together with the references from which they were derived. Further in Figure 3.24  $\delta\sigma$  is plotted as a function of the incident nucleon momentum.

Reference to Figure 3.24 shows that at low momenta ( $\sim 1\text{Gev}/c$ ) the Glauber correction is very small and hence in this momentum region

$$\sigma_{pd} \approx \sigma_{np} + \sigma_{pp}$$

to within the order of 2%. The present work is concerned with incident deuterons of mean momentum 1.65 Gev/c, which is equivalent to protons of momentum 0.83 Gev/c incident on deuterium, and at such a momentum  $\delta\sigma \approx 0$  which suggests that for the present work the deuteron can be considered as two individual nucleons acting independently. Under such an assumption deuteron-nuclei interaction lengths can be evaluated from Figure 3.19 as being 0.5 times the corresponding nucleon-nucleus interaction length. Only the inelastic interaction lengths have been considered as elastic interactions can be ignored as resulting in negligible energy transfers and small angle scatterings.

The resulting mean number of deuteron inelastic interaction lengths from the top of the telescope to the stopping region is 2.18, and estimating an error of 5% in this value the corrected intensity of deuterons incident on the telescope is  $(4.21_{-2.38}^{+2.95}) \cdot 10^{-9} \text{ cm.}^{-2} \text{ sec.}^{-1} \text{ sterad.}^{-1} (\text{Mev}/c)^{-1}$  and the incident d/p ratio is  $13.6_{-7.7}^{+9.5}\%$  at a mean momentum of 1.65 Gev/c.

This observed deuteron intensity will be discussed further at the end of Chapter 4 and compared with other measurements of deuterons in the cosmic radiation.

Table 3.6.

Nucleon Momentum Gev/c	$\int \sigma$ mb.	Derived from	$\sigma_{nd}$ (or $\sigma_{pd}$ ) mb	Derived from
0.97	$0.2 \pm 3.2$	6,7	$57.5 \pm 2.8$	6,7
3.0	$1.3 \pm 1.4$	1,8	-	8
6.5	$3.0 \pm 1.7$	1,4	$77.4 \pm 1.3$	3
14.6	$4.3 \pm 1.9$	2,5	$72.2 \pm 1.5$	5
17.8	$3.9 \pm 1.7$	2,3,5	$72.8 \pm 1.3$	3
21.6	$5.0 \pm 1.5$	2,3,5	$71.6 \pm 1.3$	3
27.0	$8.0 \pm 0.9$	2,5	$69.7 \pm 0.7$	5

Key to references:-

- 1) Bugg et al., 1966
- 2) Foley et al., 1967
- 3) Galbraith et al., 1965
- 4) Khachaturyan et al., 1963
- 5) Longo, 1968
- 6) Marshall et al., 1953
- 7) Nedzel, 1954
- 8) Palevsky et al., 1964

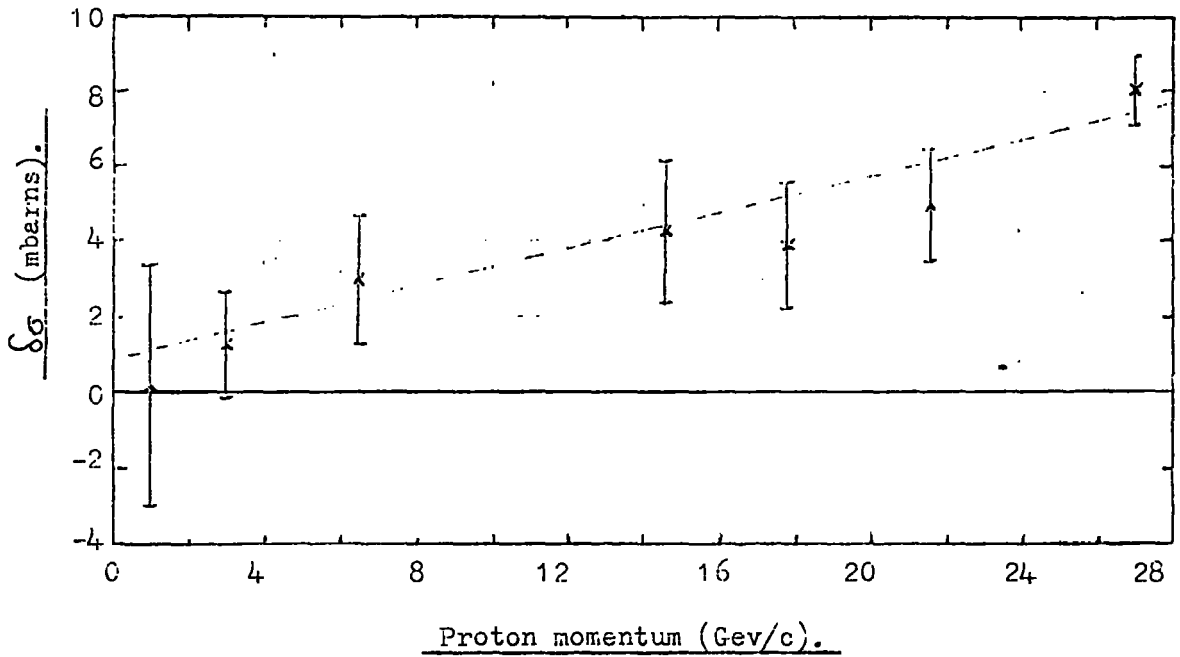


Figure 3.24

The Glauber shadow correction as a function of the incident nucleon momentum where

$$\Delta\sigma = \sigma_{pp} + \sigma_{np} - \begin{cases} \sigma_{nd} \\ \text{or} \\ \sigma_{pd} \end{cases}$$

### 3.13 Summary

Use of the low energy sea level proton flux has enabled a study to be made of various properties of the detectors in the telescope and has tested the validity of the analysis evolved to determine the mass of an incident particle.

The measured velocity response of the Cerenkov counters has been shown to be in good agreement with that expected and establishes that the addition of amino acid G, while destroying the directional property of the Cerenkov radiation, does not affect the property of velocity discrimination. Further, no evidence was found for the existence of scintillation light from the solute.

The mass distributions obtained and the agreement found between the measured intensities of protons and those of other workers show the validity of the various aspects of the analysis, the following in particular: the determination of the velocity of a particle from the pulse height from a scintillator (comprising the relationship between energy loss in the scintillator and velocity; the normalisation to the most probable energy loss recorded in a G calibration; and the correction for the variation of response over the scintillator); the weight attached to each equation; the normalisation of the telescope material to water equivalent; and the method of mass determination employed. The limits of such a telescope in mass evaluation have also been exposed; for a given mass there corresponds a velocity, which depends on the amount of material in the telescope, above which only a minimum mass can be attached to the incident particle.

In conclusion it is considered that the properties and limitations of the telescope are well understood, and that such a telescope can be used with confidence as a mass discriminator to search for heavy mass

particles in the cosmic radiation and enable a reliable mass estimate to be assigned to any such particles observed.

CHAPTER 4THE HEAVY MASS SEARCH4.1. Introduction

Since the concept of quarks was introduced (Gell Mann, 1964; Zweig, 1964) many experiments have been performed to search for them; the main areas in which the search has taken place are at the accelerators, in the cosmic radiation, and in various types of matter, and as yet none has proved successful.

Initially the searches carried out in the cosmic radiation all used scintillation counter telescopes which accepted only relativistic fractionally charged particles. The lack of success in such searches has many possible explanations; a very small production cross section, a very high mass, a non fractional charge, or a large cross section for interaction with matter combined with a large inelasticity. Because of the many uncertainties in the quark properties different methods of detection were invoked and recently searches have been made for massive particles of any charge by looking for delayed particles in air showers (Bjornboe et al., 1968; Jones et al., 1967) and for massive sub-relativistic particles using a magnetic spectrometer inclined at  $75^\circ$  to the zenith (Kasha et al., 1968c). Calculations of Adair and Price, 1966, using a plausible model of the quark interaction with matter, suggested that such an inclination was the optimum to look for quarks in the velocity range 0.5-0.75c.

The present experiment was undertaken to search for sub-relativistic massive particles of any charge in the cosmic radiation in the vertical direction by a method suggested by Ashton, 1965, as reasonable modifications of the quark interaction properties yield results that show that even in the

vertical direction most quarks would be reduced to sub-relativistic velocities (this problem will be treated in detail in Chapter 5). The method employed to search for such particles was to construct a telescope capable of mass discrimination and the following relationship shows how this can readily be achieved:-

$$R(M, z, \beta) = \frac{M}{M_p} \cdot \left( \frac{z_p}{z} \right)^2 \cdot R_p(M_p, z_p, \beta)$$

where  $R(M, z, \beta)$  is the residual range of a particle of mass,  $M$ , charge,  $z$ , and velocity,  $\beta$ , where the suffix  $p$  refers to a proton. Hence if a demand of  $\beta < \beta_T$  is placed on incident particles and then a further demand that they must traverse at least an amount of material  $R_T$ , then the only particles selected would be those satisfying  $\frac{M}{M_p} \cdot \left( \frac{z_p}{z} \right)^2 > \frac{R_T}{R_p(M_p, z_p, \beta_T)}$ .

Such a detector can be easily constructed by the inclusion of a suitable quantity of absorber and obtaining a velocity selection from Cerenkov counters.

Further interest was stimulated in the present search by the suggestion of Callan and Glashow, 1968, of the existence of  $U$  particles to explain the unusual muon angular distributions observed by Bergeson et al., 1967, as they postulated that such particles would have a mass of several  $\text{Gev}/c^2$ , be weakly interacting and be present to a level of  $10^{-3}$  of the primary proton flux. Such a flux of massive weakly interacting particles would be readily detectable in the present experiment.

#### 4.2. The heavy mass telescope.

The telescope, a scale diagram of which is shown in Figure 4.1, is essentially a modified version of that used in the 'proton experiment'. The primary factor governing its design was to adjust the minimum mass threshold to reject particles of mass less than or equal to that of the proton, hence eliminating the problems of looking for rare events in a large proton background. This was achieved by the inclusion of  $184\text{g}\cdot\text{cm}^{-2}$  of steel in the

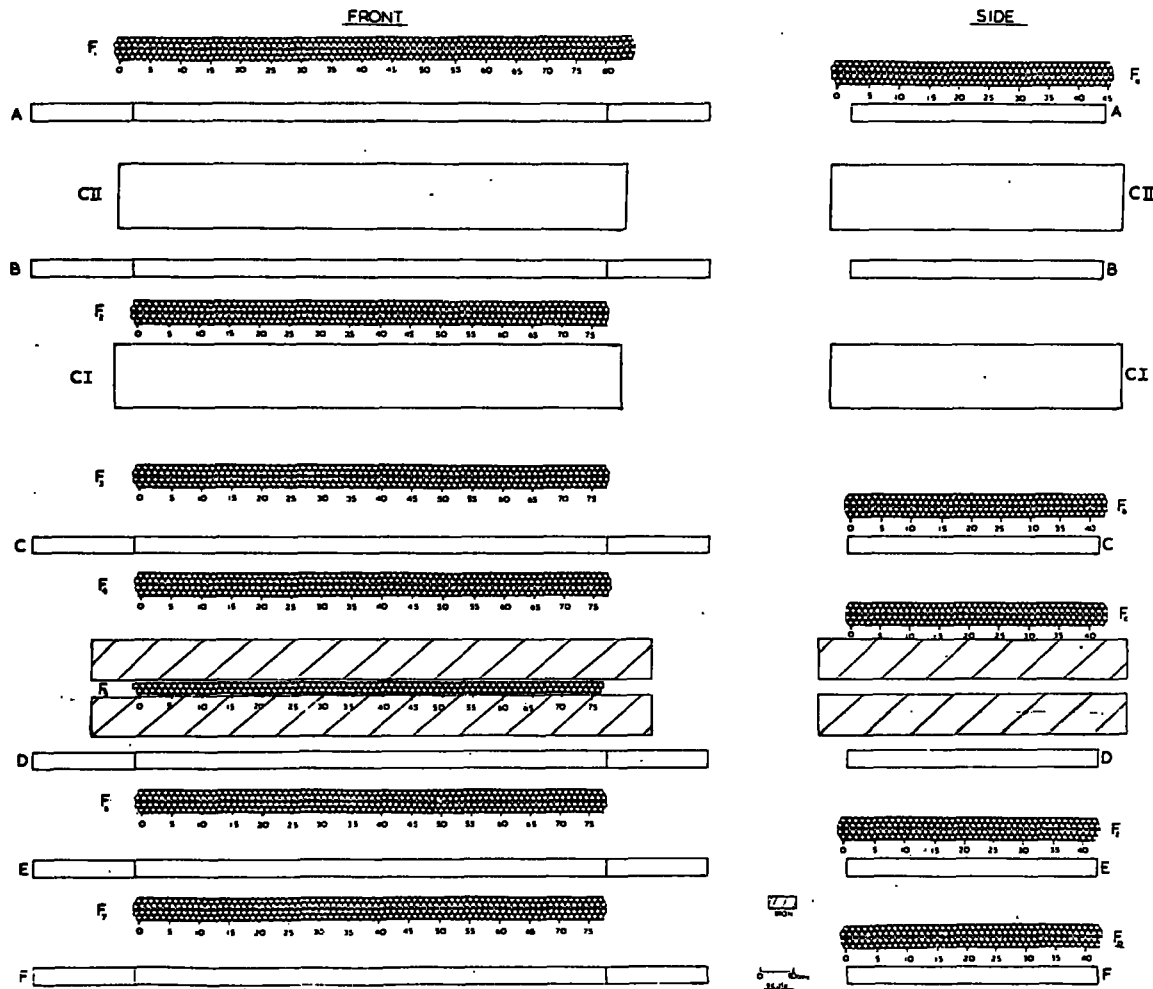


**Figure 4.1.** The 'heavy mass' telescope. A-F are plastic scintillators (NE102A); CII, CI are water Cerenkov counters; F<sub>1</sub>-F<sub>7</sub>, F<sub>a</sub>-F<sub>e</sub> are neon flash tube trays and the hatched area is steel.

telescope as shown with two layers of flash tubes sandwiched between it. Suitable choice of the velocity discrimination level at the Cerenkov counters enabled a mass threshold to be obtained which was sufficiently larger than  $M_p$  to avoid proton contamination due to fluctuations in the Cerenkov pulse height for a particle of a given velocity. The other major reconstruction was to place one of the scintillators between the two Cerenkov counters for the purpose of reducing the rate of angled tracks triggering the telescope (a rate of  $13 \text{ hr.}^{-1}$  was observed in the proton experiment). The effectiveness of this redesign can be understood by the following considerations: if the selection of the angled tracks is caused by a coincident random pulse elsewhere, the inclusion of a further scintillator above the angled track will reduce such triggers by a factor  $1.5N\tau$  where  $N$  is the total counting rate from the scintillator, and  $\tau$  the resolving time of the coincidence circuitry, the reduction factor being  $\sim 10^{-5}$ ; if the effect is due to an accompanying particle then this particle has now to traverse at least one Cerenkov counter and such events will be rejected except for sub-relativistic accompanying particles.

The only other modification was the addition of two further flash tube trays, one in each elevation, to improve track definition.

#### 4.3. Selection, display and recording system.

A block diagram of the electronic logic used is shown in Figure 4.2 and events were selected by an  $ABCDEF\overline{C}\overline{I}\overline{I}\overline{C}\overline{I}$  coincidence with a resolving time of 55 ns. Because of the finite sensitive time of the flash tubes ( $200 \mu\text{s}$ . to fall to an efficiency of 10%) it was possible to observe a spurious track in them due to the traversal of a particle through the telescope in the sensitive time of the flash tubes prior to an event satisfying the electronic logic. To avoid ambiguities of having pulse heights in the counters correlated with a spurious track from a previous particle a coincidence arrangement

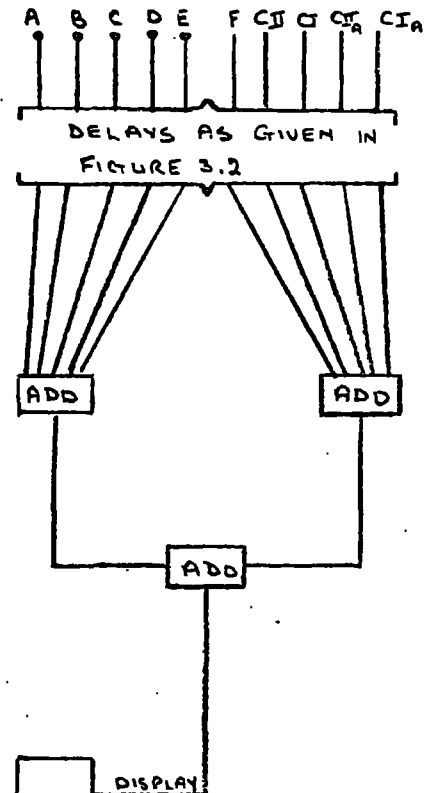
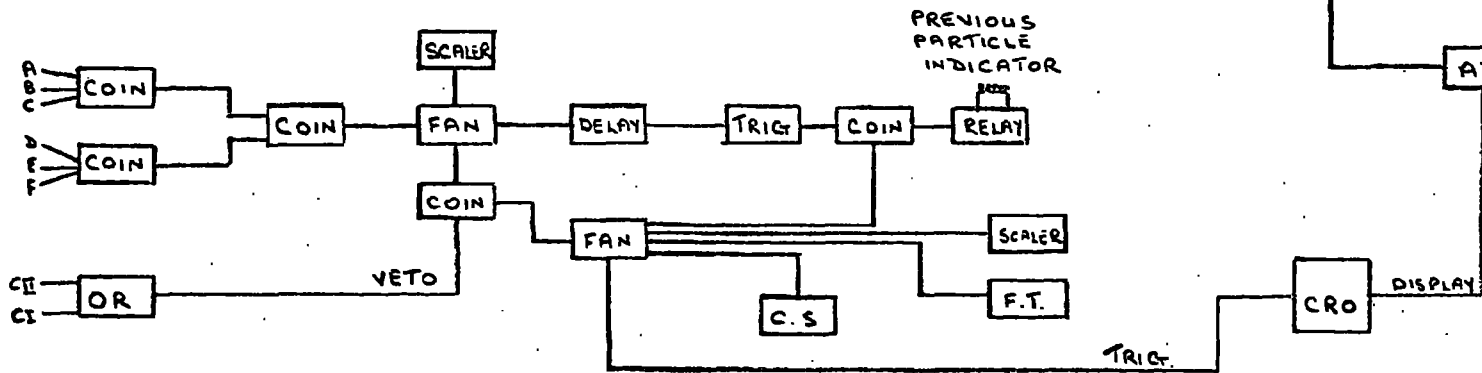
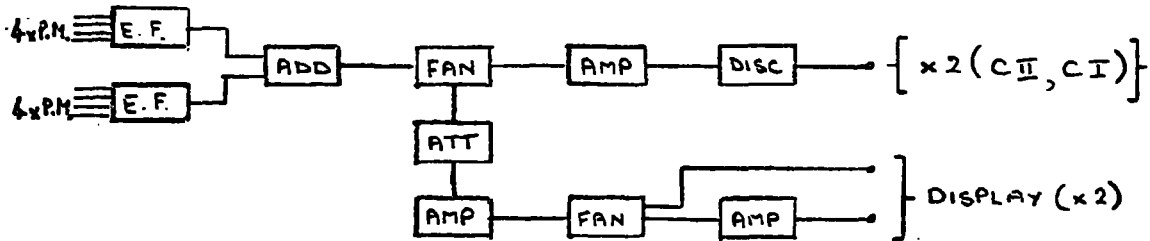
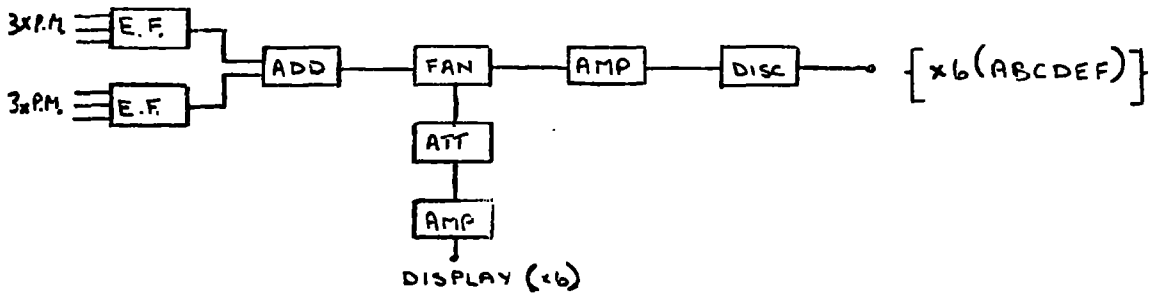


Figure 4.2 The electronic logic used in the heavy mass search.

of  $(ABCDEF) + (ABCDEF\overline{CI}\overline{CI})$  was used with a resolving time of  $200\mu s.$  If such a coincidence occurred with the selection of an event it was indicated by the illumination of a marker bulb on the telescope.

The discrimination levels used on each counter throughout the experiment are given in Table 4.1. in terms of  $E_s$  for the scintillators and  $E_c$  for the Cerenkov counters.

Table 4.1.

Counter	A	B	C	D	E	F	CII	CI
Disc. level	0.15	0.15	0.15	0.15	0.15	0.1	0.37	0.32

The display of the pulse heights from each counter was identical to that described in Section 3.3 for the proton experiment. On an event satisfying the electronic selection the following sequence of events took place: the electronic logic was paralysed; the pulse height from each counter was displayed and photographed; after a delay of  $5\mu s.$  a high voltage pulse was applied to the flash tubes and the flashed tubes photographed by two cameras, one viewing each elevation; fiducial markers were illuminated on the telescope and the time was recorded by each camera; the film in each camera was advanced one frame in readiness for the next event and the paralysis removed from the electronic logic. If an ABCDEF coincidence had occurred in the  $200\mu s.$  prior to the event the illuminated marker bulb was recorded by the camera viewing the front elevation. Information regarding each selected event was obtained by projection of the three frames onto scanning tables as described in Chapter 3.

Throughout the run daily checks were made on the discrimination levels, display electronics and C.R.O. gain. The scintillation and Cerenkov counters were calibrated periodically by selecting muons to traverse the telescope with an ABCDEF coincidence.

#### 4.4. The basic data

The basic data are summarised in Table 4.2.

Table 4.2.

Useful running time (hours)	1040.4
Mean pressure (mbars)	1007.5
ABCDEF rate, hr. <sup>-1</sup>	3.81 10 <sup>4</sup>
Veto rate, hr. <sup>-1</sup> (CII + CI)	4.16 10 <sup>6</sup>
ABCDEF $\overline{\text{CII}}$ $\overline{\text{CI}}$ rate, hr. <sup>-1</sup>	2.12
Total number of triggers	2200
No. of angled triggers	1810
No. of weak showers	359
No. requiring further analysis	31

The classification of the triggers was as follows: 'angled triggers', comprising tracks, bursts or showers traversing counters C-F but missing the region A-CI; 'weak showers' were those cases where only occasional flashed tubes were observed in the telescope which bore little or no relationship to each other; events requiring further analysis were those where a particle was observed to traverse the whole telescope or those where a track or burst was observed to traverse only part of the telescope but its projection traversed the remainder of the telescope.

Of the 31 events requiring further analysis only four showed a track through the whole telescope, that being the selection criterion for accepting events from the film as being possible heavy mass candidates (a track being defined as at least one flashed tube in each flash tube tray, apart from F<sub>5</sub>, lying on the trajectory of the particle). Three of these tracks were scattered and the other showed an interaction from which two charged prongs

emerged; the events will be considered in detail in the next section.

The remaining 27 events all showed a track, shower or burst commencing below CI in the telescope and all had the appearance of being neutrally induced. Such triggers have been assumed to be initiated by neutrons and no further discussion will be given to them until Chapter 7, where a controlled experiment was performed to study charged particle production from neutral primaries.

#### 4.5. Analysis of the heavy mass candidates.

##### 4.5.1. Mass determination of the events.

The method of mass determination was essentially that expounded in Section 3.7.4, with the addition of two further points on the  $R - f(\beta)$  plot, obtained from the Cerenkov counter information, over which the least squares fit was applied. Such information was available, having established the experimental velocity response of the counters which was found to be in good agreement with that expected. The value of  $f(\beta)$  was evaluated from the value of  $\beta$  corresponding to the pulse height in the counter (Figure 3.16), and the error in  $f(\beta)$ , and hence the weight to be attached to its value, was determined from the error in  $\beta$  derived from the standard error on a single pulse height obtained from the Cerenkov pulse height distributions as a function of velocity (Section 3.9.1).

So far the mass analysis has been directed towards particles of unit charge only. As the present experiment was also designed to accept fractionally charged particles the mode of analysis has to be modified to consider such possibilities. As the pulse height in each counter is expressed as a ratio of the most probable (median in the case of the Cerenkov counters) pulse height obtained in a G calibration (where muons having unit charge are the particles used in the calibration) then if the incident particle is assumed to be of

charge  $z = \frac{2}{3}$  or  $\frac{1}{3}$  then these pulse heights must be multiplied by  $1/z^2$ , that is 2.25 and 9 respectively, before the value,  $\beta$ , and hence  $f(\beta)$  are assigned to the particular counter. The slope of the  $R - f(\beta)$  plot then gives  $M/z^2$  from which the mass can be obtained from prior definition of  $z$ .

Hence for each heavy mass candidate the mass analysis must be carried out over the three possibilities of  $z = 1, \frac{2}{3}$  and  $\frac{1}{3}$ , where the values of  $f(\beta)$  in each case are determined from the direct pulse heights, the pulse heights increased by a factor of 2.25 and by a factor of 9 respectively.

#### 4.5.2 Individual analysis of the possible candidates.

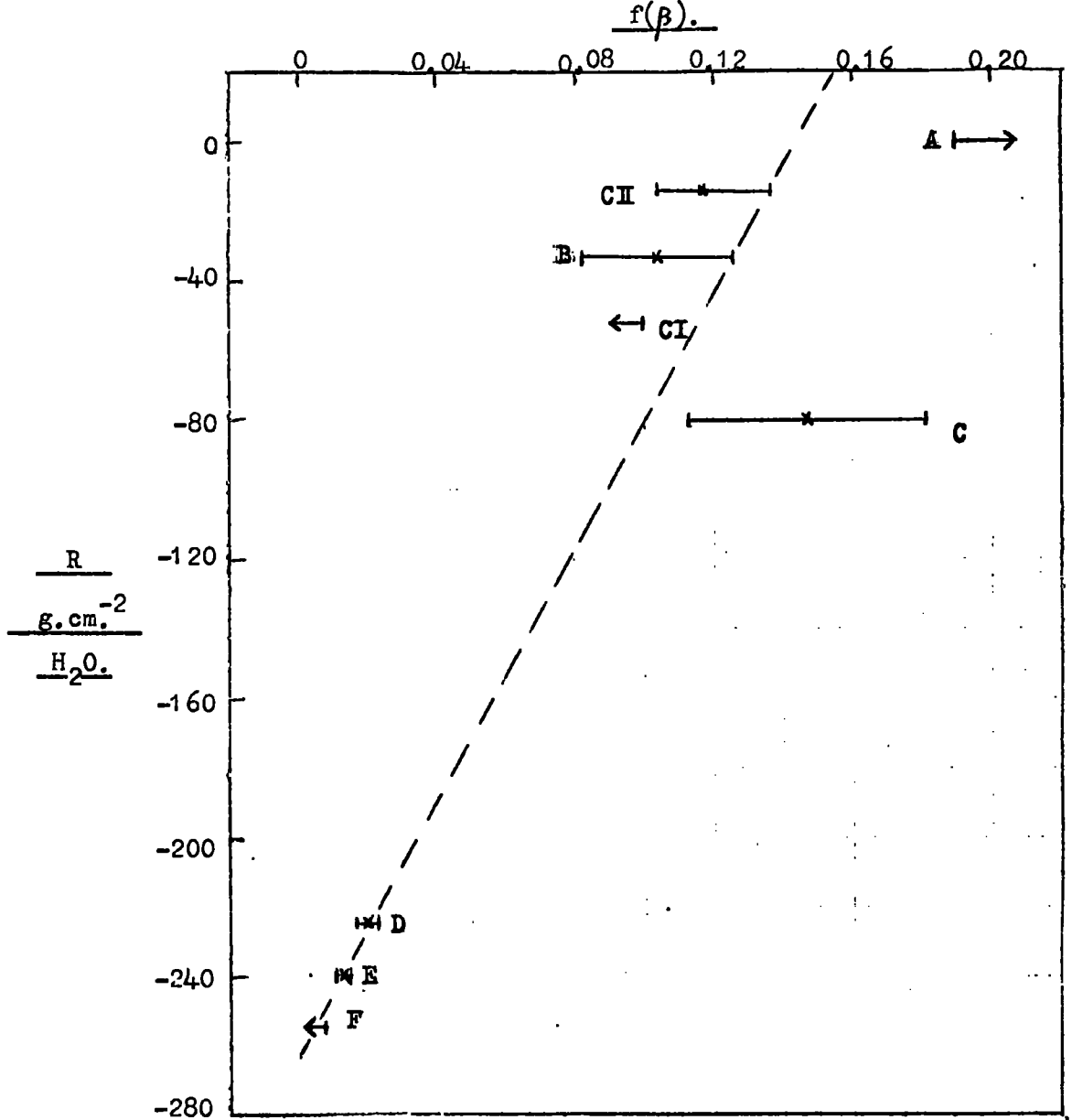
##### 4.5.2 (a) Event H8/18

The trajectory of the particle through the telescope and its corresponding  $R - f(\beta)$  plot, assuming it to have unit charge, are shown in Figure 4.3. The incident zenith angle is  $3.7^\circ$  and the particle is scattered through an angle of  $4.7^\circ$  in the steel. In the  $R - f(\beta)$  plot the  $f(\beta)$  value recorded for CI is the upper  $1\sigma$  level only as a zero pulse height was observed in that counter. Also the pulse from scintillator F was saturated and only an upper limit for the corresponding value of  $f(\beta)$  is shown. Because of this the L.S.F (least squares fit) was only applied over the points corresponding to A, CII, B, C, D and E and the resulting mass was  $1890 \pm 540 \text{ Mev}/c^2$ .

When the possibility of sub-integral charge was considered the  $f(\beta)$  values for every scintillator were found to fall below  $2 \cdot 10^{-2}$  and  $10^{-3}$  for  $z = \frac{2}{3}$  and  $\frac{1}{3}$  respectively, while  $f(\beta)$  for the Cerenkov counters increased to 0.2 and  $> 1$ . The apparent inconsistency of the values of  $f(\beta)$  rules out the possibility of the particle having sub-integral charge.

The particle then is consistent with having unit charge and its mass is  $1890 \pm 540 \text{ Mev}/c^2$ .

Figure A.5    Event HQ/10.



EE/18	A	CII	B	CI	C	D	E	F
$V_N$	1.25	0.17	1.61	0	1.45	2.88	3.43	> 4.26
$\beta$	0.85	0.75	0.74	< 0.72	0.78	0.53	0.48	< 0.42

Figure 4.3 Event H8/18. The trajectory of the particle through the telescope is shown opposite and the pulse height recorded by each counter and the corresponding  $\beta$  values, assuming unit charge, are given above in the table. The  $R$ - $f(\beta)$  plot is given above and the resulting mass estimate is  $1.89 \pm 0.5 \text{ Gev}/c^2$ .

#### 4.5.2 (b) Event H32/99

The trajectory of the particle and its  $R-f(\beta)$  plot assuming unit charge are shown in Figure 4.4. The incident zenith angle is  $14.5^\circ$  and the particle is scattered in the region of  $F_7$  through an angle of  $\sim 15^\circ$ . The L.S.F. was applied over all  $f(\beta)$  values and the resulting mass obtained was  $2490 \pm 550$  Mev/c<sup>2</sup>.

Consideration of the particle being fractionally charged led to the same conclusions as for event H8/18, as again large inconsistencies were obtained for the  $f(\beta)$  values from the scintillators and Cerenkov counters. Hence the particle is consistent with having unit charge and having the mass value quoted above.

#### 4.5.2(c) Event H9/64

Figure 4.5 shows the trajectory of the particle and its  $R-f(\beta)$  plot assuming unit charge. The incident zenith angle is  $6.5^\circ$  and a scattering of  $25^\circ$  occurs in scintillator D. A notable feature of the trajectory is the absence of any flashed tubes in tray  $F_5$ . Measurements of the probability of two, one or zero tubes flashing in  $F_5$ , when muons were selected to traverse the telescope by an ABCDEF coincidence, showed that the probability of observing zero flashed tubes was 4.3%. It would appear that, with a high probability, this particle was neutrally charged in the steel around  $F_5$  and the presence of a large angle scatter in D suggests that this was the location where it became charged again. The possibility of the particle being neutral during part of its traversal of the telescope invalidates the interpretation of the  $R-f(\beta)$  plot as a whole, and further the possibility of it being partially neutral while traversing D casts doubts on the validity of the  $f(\beta)$  value obtained from D. The values of  $f(\beta)$  for the

Figure A.8 Front 11/2/99.

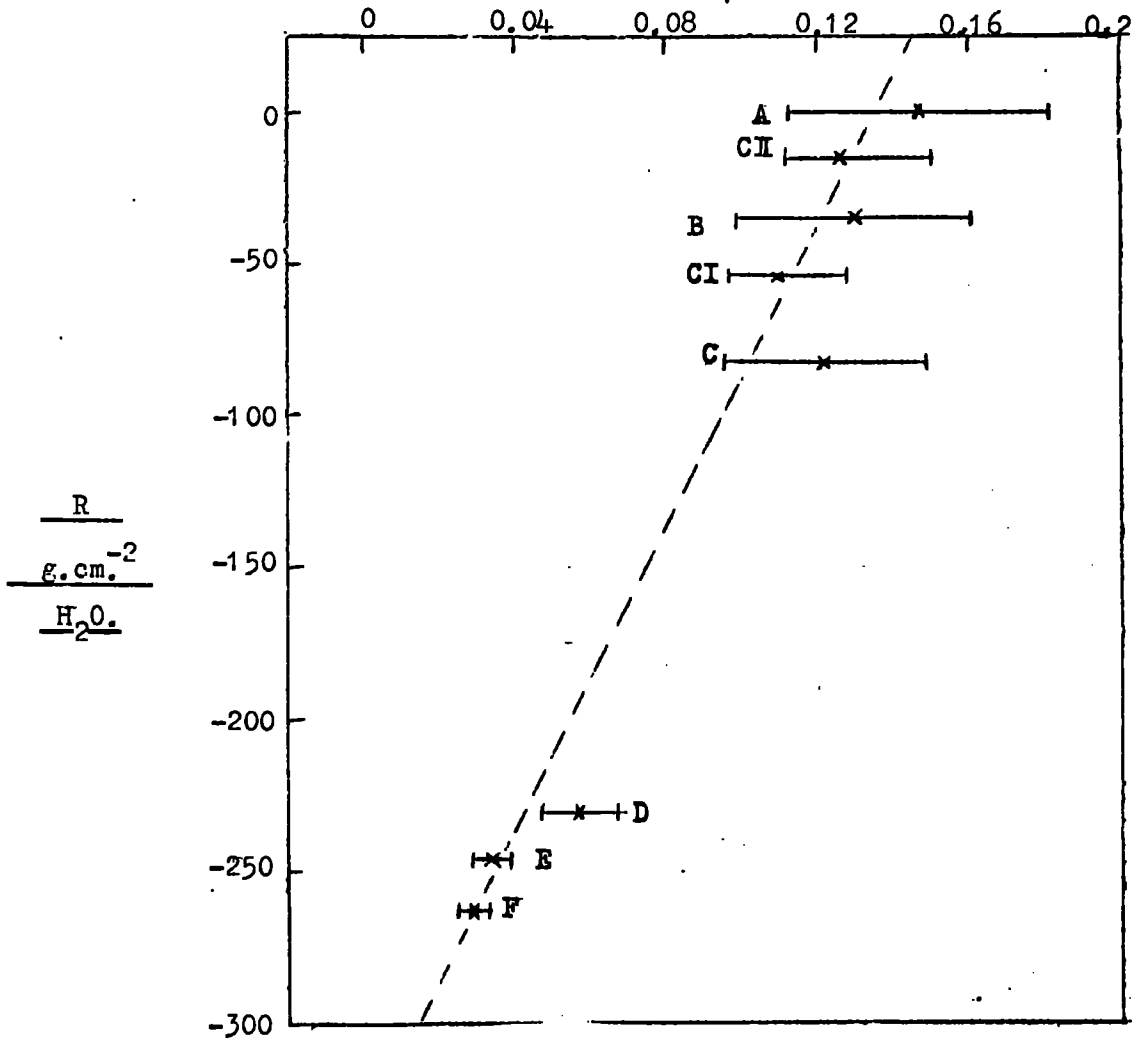
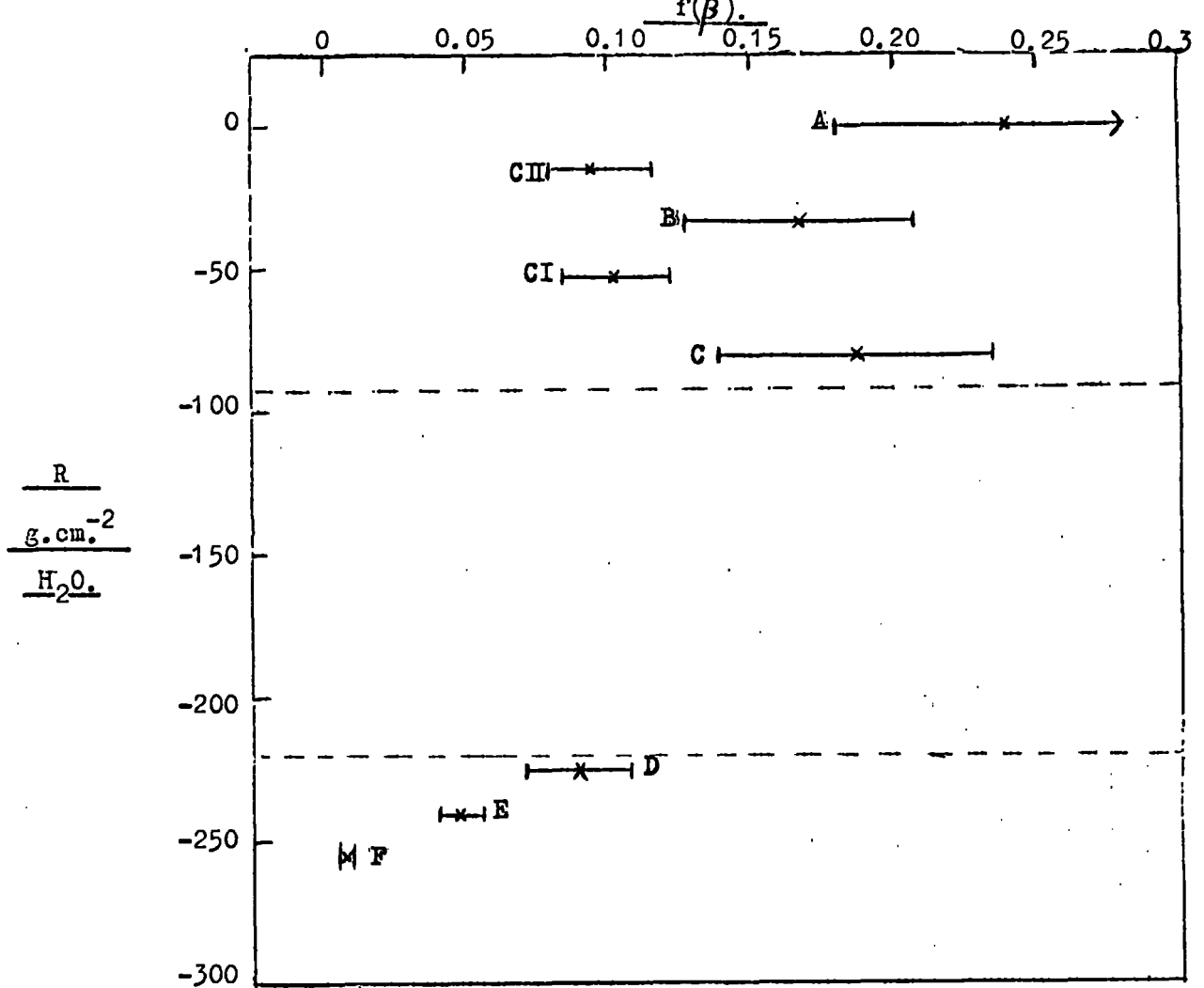


Figure 4.4

Event H32/99. The trajectory of the particle through the telescope is shown opposite and the pulse height recorded by each counter and the corresponding  $\beta$  values, assuming unit charge, are given above in the table. The  $R$ - $f(\beta)$  plot is shown above and the resulting mass estimate gives  $2.49 \pm 0.5 \text{ Gev}/c^2$

Figure A.5

Event H9/6a.



H9/46	A	CI	B	CI	C	D	E	F
$V_N$	1.26	0.06	1.40	0.10	1.36	1.69	2.07	4.14
$\beta$	0.85	0.72	0.80	0.74	0.81	0.72	0.64	0.43

Figure 4.5 Event H9/64. The particle trajectory is shown opposite and it can be seen to be apparently neutral while traversing  $F_5$ . The pulse height recorded by each counter and the corresponding  $\beta$  values, assuming unit charge, are given in the table above. The  $R-f(\beta)$  plot is shown above, but no least squares fit has been applied due to the particle being neutral during part of its traversal. The dashed lines in the figure show the location of the iron absorber in the telescope.

counters A-C are too imprecise to be useful, but a coarse mass estimate can be made of the particle after the scatter by considering only scintillators E and F, and a value of  $420 \text{ Mev}/c^2$  was obtained.

Perhaps the simplest and hence most appealing explanation of this event is that the incident particle is a proton suffering a double charge exchange in traversing the steel and scintillator D of the form:-



An estimate of the expected number of such events will be considered.

The number of protons incident on the telescope during the experiment suffering a double charge exchange in  $l$  charge exchange mean free paths can be written as:

$$\int_x^l \int_p A \Omega t N(p) dp (1 - e^{-(l-x)/\lambda_c}) \cdot \frac{dx}{\lambda_c},$$

where  $A \Omega$  is the aperture of the telescope in  $\text{cm}^2 \text{sterad.}$ ,

$t$  is the running time of the experiment in seconds,

$N(p)dp$  is the incident sea level differential momentum spectrum of protons in units of  $\text{cm}^{-2} \text{sec.}^{-1} \text{sterad.}^{-1} (\text{Mev}/c)^{-1}$ ,

$\lambda_c$  is the mean free path for charge exchange,

$l$  is the number of  $\lambda_c$  in which the charge exchanges can occur,

$x$  is expressed in units of  $\lambda_c$  and is the location of the first charge exchange,

and where the attenuation of the proton flux in reaching the charge exchange region has been ignored.

The work of Bernardini et al., 1952, with 410 Mev protons incident on emulsion showed that 0.059 of all inelastic interactions observed were charge exchanges of the incident proton, where the proton track disappeared in the presence of a short nuclear recoil. Assuming this fraction of all inelastic interactions to be nucleus independent the effective number of mean

free paths for charge exchange in the relevant region of the telescope (that is in the steel and in D) is  $0.088 \lambda_c$ , where the total inelastic interaction mean free paths were obtained in the same manner as in Section 3.10.4. Taking  $A\Omega = 1.25 \cdot 10^3 \text{ cm.}^2 \text{ sterad.}$  and  $t = 3.75 \cdot 10^6$  seconds, the expected number of events of this type is  $1.8 \cdot 10^7 N(\bar{p}) dp$ , where  $\bar{p}$  is the mean momentum in the contributing momentum band.

An attempt to estimate the effective momentum band can be made by considering the mean case of the proton charge exchanging at  $0.25\ell$  and  $0.75\ell$ . Assuming a negligible energy loss in the charge exchange process the minimum incident proton momentum required would be  $1340 \text{ Mev}/c$ . Although the velocity of the proton with this momentum would be above the Cerenkov velocity discrimination level, there will still be a source of protons available as fluctuations in the location of the charge exchanges will allow protons of lower momenta to contribute, as well as a contribution coming from protons of higher momenta due to fluctuations in the output pulse from the Cerenkov counter for a given particle velocity. An absolute estimate of the effective momentum band is obviously very complex; however when the proton flux of  $4.7 \cdot 10^{-8} \text{ cm.}^{-2} \text{ sec.}^{-1} \text{ sterad.}^{-1} (\text{Mev}/c)^{-1}$  at  $1340 \text{ Mev}/c$  (Brooke and Wolfendale, 1964(a)) is considered the expected rate of such events becomes  $\sim 1$  for a value of  $\Delta p$  even as small as  $1 \text{ Mev}/c$ . Hence the rate expected for protons undergoing a double charge exchange is of the same order as that observed, and it can be concluded that the interpretation is valid.

The error in the mass estimate of the particle emerging from the steel is such that the particle is not inconsistent with being a pion or a proton. If in fact the second interaction was not a charge exchange but an interaction of the form  $n + N \rightarrow N + N + \pi$  the previous argument is little affected, as the

mean free path for pion production, at the typical energies experienced here, is of the same order as that adopted for charge exchange.

It should be noted that no satisfactory explanation of this event is possible under the hypothesis of fractional charge due to the large inconsistency then obtained between the  $f(\beta)$  values for the scintillators and Cerenkov counters as in the case of the previous events.

#### 4.5.2(d) Event H40/6

The flash tube information concerning the event is shown in Figure 4.6 and the pulse height information from each counter is given in Table 4.3, in terms of  $E_s$  for the scintillators and  $E_c$  for the Cerenkov counters. Also shown in the table are the corresponding velocity estimates of the particle, assuming unit charge, at each counter where such an estimate was possible. There are two notable features of the event, the first being an interaction in the region of CII, the flash tube resolution not being sufficient to locate the exact interaction point, and the second being a further interaction just below scintillator C.

Consideration of the observed range of the secondary particle produced in the first interaction can be used to establish a lower limit to the energy transferred to it. The minimum range that can be attributed to the particle is 21 g. cm.<sup>-2</sup> water equivalent, where in deriving the minimum range it was assumed that the particle stopped at its last observed point (that is in  $F_2$ ) and that in the side elevation, where its trajectory was not observed, it was normally incident. The corresponding energy transferred is  $>185$  Mev if the particle is a proton and  $>220$  Mev if it is a pion. The possibility of the particle being an electron can be ignored, the maximum transferable energy to an electron from a particle of incident velocity  $\sim 0.76c$  being only 1.35 Mev. Possible supporting evidence that the particle is in fact a pion comes

Figure A.6 Event H/O/6.

Table 4.3

Counter	Pulse height in terms of $E_s$ or $E_c$	Velocity Estimate
A	1.51	0.76c
CII	0.21	0.76c
B	5.22*	-
CI	0	< 0.72c
C	1.24	0.85c
D	2.91	-
E	2.60	-
F	2.58	-

\* Pulse height in B is not normalised for response and track length corrections.

Table 4.4

Prong	Assumed particle	Assumed level of ionisation in terms of $I_{MIN}$	Energy required at production Mev	Total energy required by both prongs Mev.
a	p	1.35	1150	1970
b	p	1.35	820	
a	p	1.7	850	2150
b	p	1.0	1300	
a	p	1.0	1550	2130
b	p	1.7	580	
a	p	1.7	850	1235
b	$\pi$	1.0	385	
a	$\pi$	1.0	665	1245
b	p	1.7	580	

from the observation of an extra pulse on the oscilloscope display. The width of this pulse signifies that it originated from one of the Cerenkov counters ( $\tau_c \sim 200 \text{ ns.}$  where as  $\tau_s \sim 100 \text{ ns.}$ ) but it is impossible to be certain as to which counter or which version, direct or amplified, it comes from. However, the high level of ionisation in scintillator B is suggestive of the particle rapidly slowing down, and it seems a reasonable assumption that the extra pulse is from CI and is due to an electron from a stopping pion undergoing a  $\pi \rightarrow \mu \rightarrow e$  decay. The time delay of the pulse was  $0.8 \mu\text{s.}$  or  $1.8 \mu\text{s.}$  depending upon whether it was the direct or amplified version, and such a delay is not inconsistent with that expected for a  $\pi \rightarrow \mu \rightarrow e$  decay. It can thus be concluded that the most probable interpretation of this interaction is the production of a pion with an energy transfer of  $> 220 \text{ Mev.}$

Observation of the second interaction shows the emergence of two prongs whose trajectories cannot be projected back to intersect at the same level in both elevations. However one of the prongs appears to have been produced via a neutral mode (concluded by the absence of flashed tubes on the trajectory in  $F_5$ , the probability of observing no flashed tubes for the traversal of a charged particle being only 4%) and if this is so it is not unreasonable that both prongs do not converge back to the interaction point. In order to conserve momentum in this interaction a further neutral particle must have been produced or the nucleus involved in the interaction must have taken a sizeable recoil energy (this is necessary as the two visible prongs in both elevations are scattered in the same direction with respect to the direction of the incident particle).

It is relevant in trying to interpret the event as a whole to estimate the energy present in the two emerging prongs so as to place a lower limit on the available energy before the interaction. Such an estimate is complicated by the presence of two particles and by a lack of knowledge of their identity.

Various postulates as to their identity and their relative contributions to the energy deposited in each scintillator have been made with regard to establishing the minimum energy carried away from the interaction. In the ensuing discussion the two observed prongs are labelled in the following manner: 'a' refers to the prong that emerges from scintillator C and is observed to be charged in traversing the remainder of the telescope; 'b' refers to the prong appearing to be produced via a neutral mode.

Obviously the smaller the assumed mass of the prongs the smaller is the energy they are required to carry in order to penetrate the telescope. Hence in evaluating the minimum energy present consideration will be given only to the observed particles being protons or pions (the most common nuclear active particles having the smallest masses). The first possibility considered is that both particles are pions. However an explanation in these terms can be shown to be impossible with reference to Table 4.4 where it can be seen that the level of ionisation over all three counters, D, E and F, is relatively constant at an average value of  $2.7 I_{\min}$ . Taking both pions to be contributing equally to the level of ionisation, that is  $1.35 I_{\min}$  each, then neither would be able to penetrate from D to F, a range of  $35.2 \text{ g. cm.}^{-2}$  of water, as the residual range of a pion ionising at such a level in D is only  $25 \text{ g. cm.}^{-2}$  of water. Variation of the relative contributions of each pion to the observed ionisation does not help, in that while it would allow one of them to penetrate from D to F the residual range of the other would be further reduced. Hence an estimate in terms of both particles being pions is not feasible.

A summary of other possibilities, that is both particles being protons, or one a proton and the other a pion, for varying contributions to the ionisation level is given in Table 4.4, and in each case the minimum energy

of the two particles after the interaction at C is listed. The energy carried by 'a' immediately after the interaction is evaluated by finding its energy on leaving the telescope (using its assumed mass and assuming that the attributed ionisation level pertains on leaving the telescope) and increasing this for the energy lost in traversing the telescope from C-F, a range of  $173 \text{ g. cm.}^{-2}$  of water. Similarly for 'b' its ionisation level is assumed to pertain on leaving the telescope and its corresponding energy at production can be evaluated ('b' assumed to have been produced at the end of the steel, a range of  $35.2 \text{ g. cm.}^{-2}$  of water from the end of the telescope, this then establishing the minimum energy that 'b' could possibly have). It should be further noted that when an ionisation level of  $I_{\min}$  was assigned to a particle in Table 4.4 then its velocity on leaving the telescope was taken as  $0.9c$  (corresponding to  $1.13 I_{\min}$ ) to ensure that a realistic estimate of the minimum energy present was being calculated.

It can be concluded from Table 4.4 that the minimum energy of the incident particle before the interaction at C must have been  $> 1200 \text{ Mev}$ . That this is a severe lower limit can be realised by considering first that the identity of the particles has been chosen to represent the lowest possible energy carried from the interaction; second that no account has been taken of any energy loss in creating 'b' from a neutral mode, and also that 'b' was assumed to be produced at the lowest possible level in the telescope; third that no account has been taken of the necessary extra energy released in the interaction that is required to conserve momentum. Hence this lower limit of  $1200 \text{ Mev}$  can be used with confidence as being representative of the incident particle before the second interaction, at the same time realising that it would be substantially increased, as can be seen from Table 4.4, if the identity of the emerging

particles is changed and consideration is given to the other effects discussed.

Having established the incident velocity of the particle, the minimum energy transferred in the initial interaction and the minimum energy of the particle prior to its second interaction, various attempts at an explanation have been tried in terms of the following particles having initiated the event :-

(i) Proton: The event being initiated by a proton can immediately be discounted as the incident kinetic energy of  $510 \pm 90$  Mev, corresponding to the measured velocity, is insufficient to enable the proton to penetrate the telescope let alone after suffering two interactions.

(ii) Deuteron: The incident kinetic energy if the particle were a deuteron would be  $1020 \pm 180$  Mev. Taking account of the energy transfer of  $> 220$  Mev in the first interaction and allowing for energy loss due to ionisation in traversing the telescope, the remaining kinetic energy of the deuteron prior to the second interaction would be  $< 700$  Mev, where the value quoted refers to the upper  $1\sigma$  level of the energy at that point. As the observed interaction products require a minimum energy of 1200 Mev no satisfactory explanation of the event can be obtained under the assumption of the incident particle being a deuteron.

(iii) Antiproton: Such a possibility is immediately more favourable in that there is the order of 2 Gev more energy available on an annihilation. Considering an antiproton incident with a kinetic energy of  $510 \pm 90$  Mev and allowing for the observed energy transfer in the interaction in CII, and for energy loss due to ionisation it would stop and annihilate approximately  $10 \text{ g. cm}^{-2}$  of water before reaching scintillator C. However there is no supporting evidence for such an annihilation occurring before C. The possibility of an annihilation having occurred in CII can be discounted due to the absence of a prompt Cerenkov pulse from CI, as such a pulse would have been expected from the

relativistic annihilation products. Even if the evidence against the antiproton reaching C is ignored it would still be very difficult to explain the second interaction in terms of a  $p\bar{p}$  annihilation. There are two contradictory factors against such an interpretation, the first being the absence of any visible prongs in the backward direction and secondly the appearance of one prong originating from a neutral mode ( in terms of an annihilation this neutral particle cannot be a neutron and hence strange particles must be invoked to be present, with a resulting decrease in the probability of the interaction in fact being an annihilation). The weight of evidence would suggest that an interpretation in terms of an antiproton is extremely unlikely.

(iv) Decay of a baryon: Such explanations can be disregarded on two counts; first the minimum observed decay time would be of the order of 3 ns, that is the time taken for the particle to reach C from the top of the telescope, which is some thirty times larger than typical heavier baryon half lives of  $10^{-10}$  secs; secondly there would be insufficient energy available in the decay to create the observed forward prongs and at the same time conserve momentum.

It would appear that no satisfactory explanation of the event is forthcoming in terms of the conventional particles. However before proceeding to discuss the event in terms of hypothetical particles consideration will be given to the possibility of the event being spurious. Due to the relatively long sensitive time of the flash tubes (see figure 2.1) and despite the incorporation of the previous particle indicator (Section 4.3) there is still a finite probability that part of the flash tube information is not correlated with the actual event triggering the electronic logic. Under the hypothesis of part of the flash tube information being spurious two different

interpretations can be made of the event and the probability of each has been evaluated.

It can be assumed that the electronic logic was triggered by a neutron incident at the top of the telescope, producing knock-on protons in A and C, interacting in CII and producing a pion, and finally interacting in the steel below  $F_5$  and giving rise to prong 'b'. The remaining track, which traverses the whole telescope, must then be assumed to be spurious, and while the fact that the previous particle indicator was not triggered establishes that a particle could not have traversed the telescope in the  $200\mu s$ . prior to the neutron, it would still be possible for it to have traversed the telescope after the neutron, but before the high voltage pulse was applied to the flash tubes. The time available for this to occur without the presence of a late particle being detected by a further pulse train appearing on the oscilloscope sweep is  $2\mu s$ . The track can be seen to suffer a single large angle scatter of  $17^\circ$  which is incompatible with the particle being a muon, and it must be concluded to be nuclear active. Taking the flux of nuclear active particles through the telescope to be  $< 10^{-1}$  sec., and as the total number of neutrally (presumably neutrons) induced events observed in the experiment was 27, the probability of observing a spurious event of this type in the whole experiment is  $< 5 \cdot 10^{-6}$ .

The interpretation of course can be reversed and the complete track can be assumed to be the real cause of the electronic logic trigger, while 'b' can be assumed to be spurious, caused by a neutron interacting in the steel. The time available for the occurrence of such a spurious prong as 'b' is the  $200\mu s$ . prior to the real event (the reason that there is  $200\mu s$ . available is because 'b' would not have triggered the previous particle indicator as it

would only have yielded a DEF coincidence). Taking account of the sea level neutron flux and the probability of an interaction in the steel below  $F_5$ , the expected occurrence of such prongs in the telescope is  $<10^{-2}$  sec. Having observed only three penetrating particle tracks in the total running time, the probability of observing a track accompanied by such a spurious prong in the whole experiment is  $<6.10^{-6}$ .

It can thus be concluded that the probability of observing such a spurious event during the whole experiment is small,  $<10^{-5}$ , and this probability would be further reduced if account was taken of obtaining such close proximity of the observed prongs and also of the scattering of the track in the same region in which a further prong appears. With such a low probability of the event being spurious it seems justifiable to evolve an interpretation of the event in terms of a heavy mass particle.

A plausible explanation would be that the incident particle was massive ( $M \gg M_p$ ), and suffered an interaction in CII with an energy transfer of  $>220$  Mev (the absence of any scattering of the incident particle in this interaction adds further weight to it being massive). It then suffered a further interaction just below C, being scattered through an angle of  $17^\circ$  as well as producing a neutral particle which later interacted producing a charged prong 'b'. If it is accepted that there are two particles traversing D-F then the maximum level of ionisation that can be attributed to the primary particle in this region is  $1.7 I_{\min}$ , where prong 'b' has been assigned the lowest possible level of  $1.0 I_{\min}$ . Hence the maximum change in the ionisation level of the primary particle in traversing the whole telescope, equivalent to  $266.8 \text{ g. cm.}^{-2}$  of water, is only from  $1.5 I_{\min}$  to  $1.7 I_{\min}$ , despite suffering two interactions. A severe lower mass estimate can be evaluated for the incident particle by considering the minimum energy it would have required to have produced the

observed interactions and its incident level of ionisation. Assuming it to have unit charge its incident velocity was  $0.76c$  and its incident kinetic energy must have been  $> 1750$  Mev, this value being derived from the previous analysis assuming the interaction products to be conventional particles. From these two values a strict lower mass of  $3.3 \text{ Gev}/c^2$  can be placed on the incident particle.

An interpretation in terms of a massive fractionally charged particle is not particularly appealing in that if a value of  $z = \frac{2}{3}$  is assumed the velocity of the particle predicted by A is  $0.48c$  while that from CII is  $0.83c$ , the inconsistency becoming greater if a value of  $z = \frac{1}{3}$  is assumed. This divergence can be reconciled if the pulse from CII is considered to have come from the assumed pion produced in the interaction in that counter. Under this assumption mass values of  $> 12.5 \text{ Gev}/c^2$  and  $> 70 \text{ Gev}/c^2$  have been evaluated for assumed charges of  $\frac{2}{3}$  and  $\frac{1}{3}$  respectively. However the value of  $z = 1$  is more favourable in requiring fewer assumptions.

#### 4.5.2 (e) Summary.

Two of the events, H8/18 and H32/99 have been shown to be consistent with having unit charge and masses of  $1.89 \pm 0.54$  and  $2.49 \pm 0.55 \text{ Gev}/c^2$  respectively. While it cannot be completely ruled out that these two particles are integrally charged quarks of mass  $\sim 2 \text{ Gev}/c^2$ , a more likely interpretation is that they are both deuterons, in view of the proximity of their masses to that of the deuteron. That this interpretation is valid will be shown later, when the measured rate of these events is compared with measurements of deuterons in the cosmic radiation made by other workers.

Event H9/64 has been adequately explained by the incident particle being a proton suffering a double charge exchange in the telescope and hence requires no further discussion as it is not relevant to the present search.

No satisfactory explanation of event H40/6 has been obtained in terms of the conventional particles and as the probability of observing such a spurious event in the whole experiment was  $< 10^{-5}$  resort was made to postulating a hypothetical heavy mass particle to obtain a plausible interpretation. It has been shown that the most likely cause of the event was an incident particle having unit charge and a mass greater than  $3.3 \text{ GeV}/c^2$ ; however the possibility of the event being initiated by a fractionally charged particle cannot be totally disregarded. While this event obviously constitutes evidence for the presence of heavy mass particles (quarks?) whether unit or fractionally charged, it is not sufficient in itself (based on only one observation) to enable a categorical conclusion to be drawn as to their existence, particularly in light of the extremely small but still finite probability of the event being partially spurious. However in determining any flux limits from the present experiment account must be taken of this one anomalous observation.

#### 4.6. The incident momentum bands accepted by the telescope.

The lower limits of momentum imposed on incident particles of charge 1,  $\frac{2}{3}$ , and  $\frac{1}{3}$  are determined by the amount of material in the telescope, and are such that particles of that momentum can just traverse the whole telescope. For particles of charge 1 and  $\frac{2}{3}$  the upper momentum limits are determined from the velocity discrimination levels imposed by the Cerenkov counters (CII discriminates at velocities of  $0.8c$  and  $0.95c$  for  $z = 1$  and  $\frac{2}{3}$  respectively, while CI discriminates at  $0.79c$  and  $0.92c$  for  $z = 1$  and  $\frac{2}{3}$  respectively). In most cases the discrimination level of CI determines the limit but for particles with mass near to the smallest mass able to traverse the telescope, where the rate of change of velocity is greatest, then CII takes over. For particles of  $z = \frac{1}{3}$  the upper momentum cut off is determined by the

discrimination level on scintillator A ( in this case the Cerenkov counters afford no veto as even for a relativistic charge  $\frac{2}{3}$  particle the response from the counters would be only  $0.1E_c$  compared with their discrimination levels of  $\sim 0.3E_c$  ) which is  $0.15E_s$  and corresponds to a velocity cut off of  $0.81c$  for  $z = \frac{1}{3}$ .

The limiting incident momentum bands have been evaluated subject to the above conditions as a function of mass for particles having  $z = 1, \frac{2}{3}$  and  $\frac{1}{3}$  and are shown in Figure 4.7. For completeness Figure 4.8 shows the corresponding incident velocity bands accepted by the telescope.

#### 4.7. Aperture of the telescope.

The aperture, defined by scintillators A and F of area  $140 \times 75 \text{ cm.}^2$  and separation  $253.1 \text{ cm.}$ , has been evaluated according to the expression given in Section 3.10.1 and is given in Figure 4.9 as a function of the angular exponent of the incident radiation. No account has been taken of the non-uniformity introduced by the supporting steel girders as was done in the 'proton experiment'.

#### 4.8. Limits on the intensity of quarks.

Only one anomalous event, H40/6, has been observed whose interpretation requires the existence of particles with mass greater than those of the conventional particles. For reasons previously discussed this one event cannot be used to establish an absolute rate of such particles and can only be used to impose upper limits on the flux based on this one observation. Taking the aperture of the telescope to be that corresponding to a value of  $n = 8$  (assuming the nucleon angular distribution to pertain for quarks) the derived upper limits at the 90% confidence level are given in Table 4.5 and apply over the accepted momentum bands given in Figure 4.7.

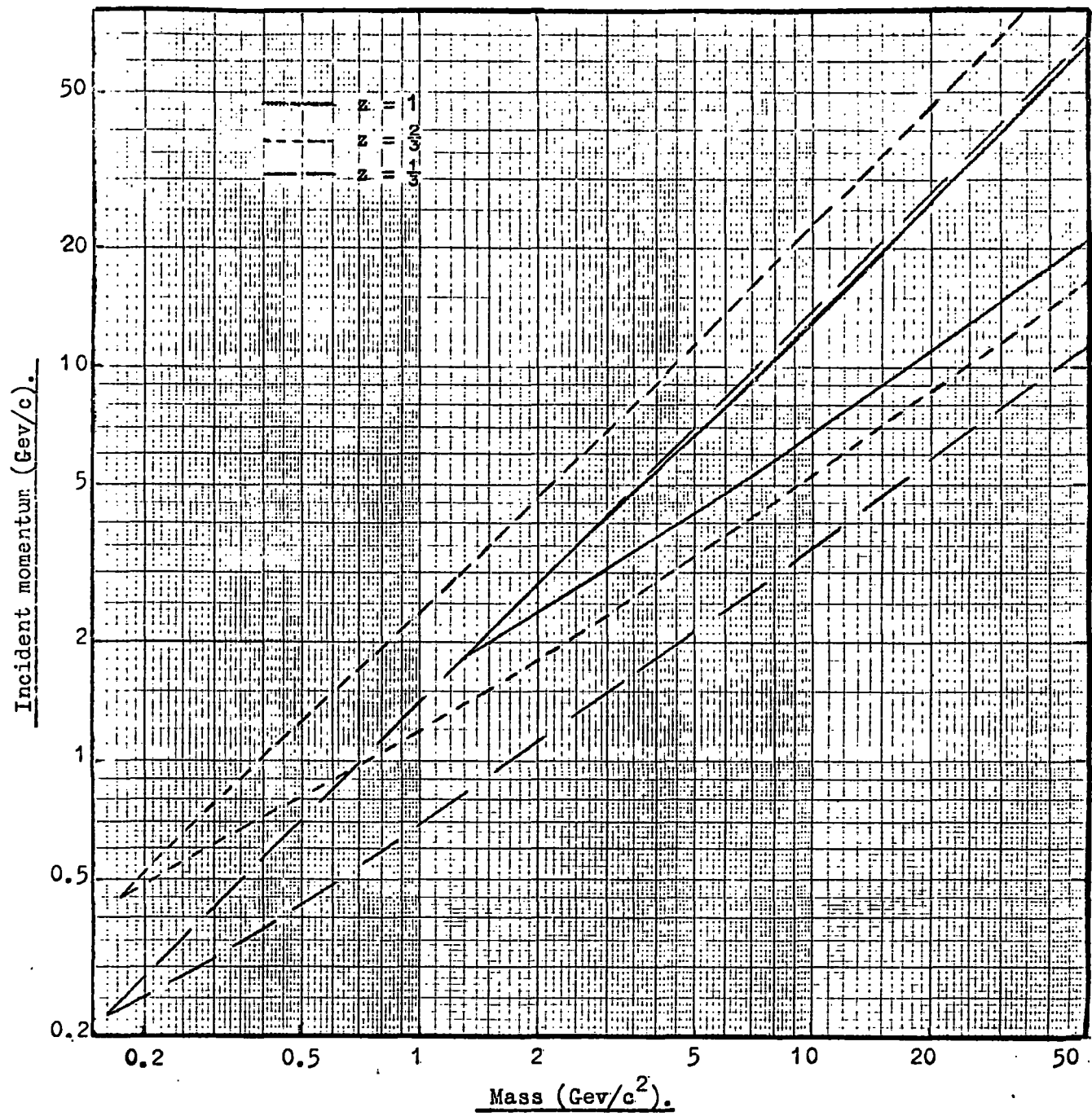


**Figure 4.7** The incident momentum bands, as a function of the particle mass, accepted by the telescope for charges of  $z = 1$ ,  $\frac{2}{3}$ , and  $\frac{1}{3}e$ .

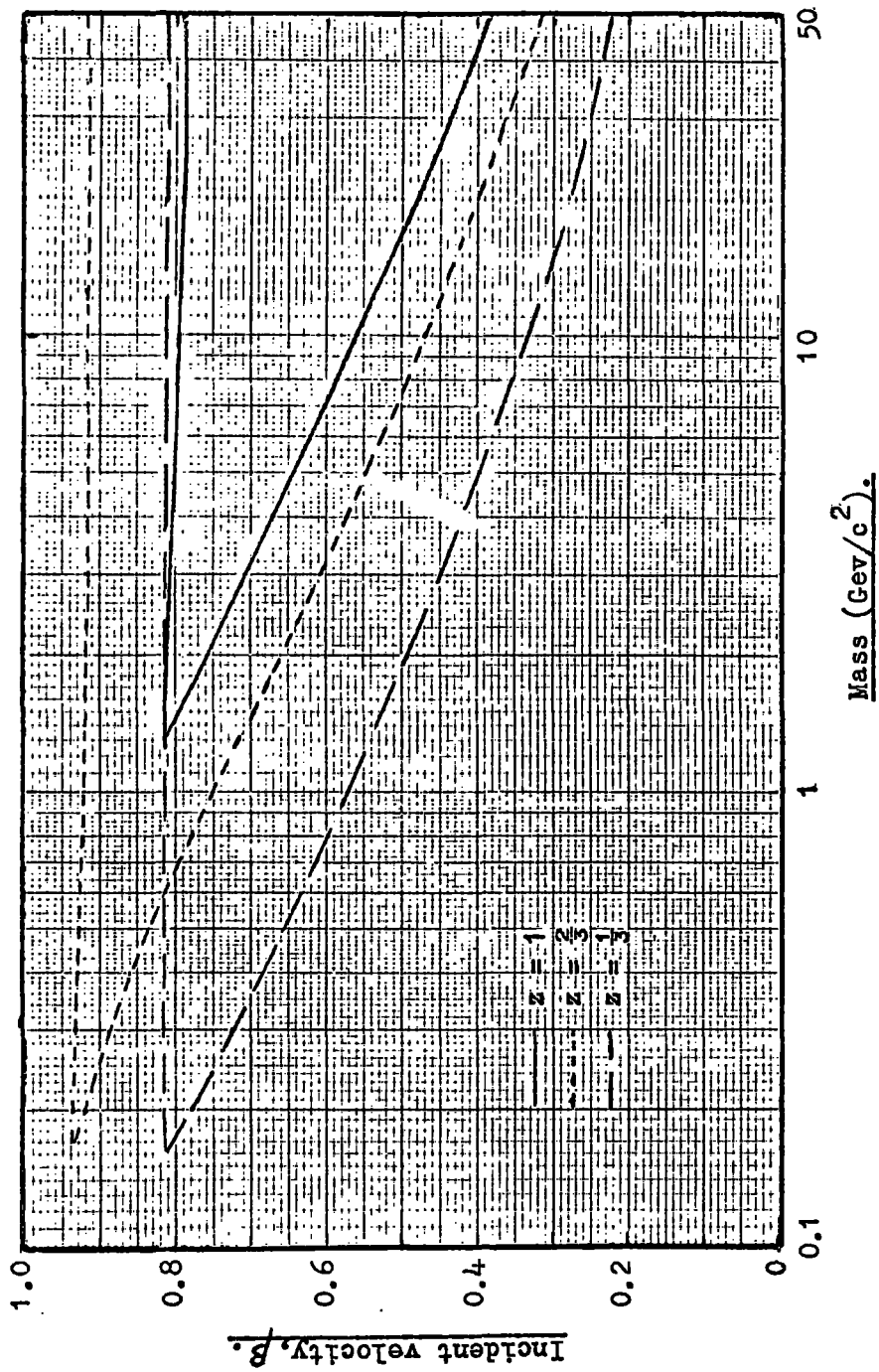


**Figure 4.8** The incident velocity bands, as a function of the particle mass, accepted by the telescope for charges of  $z = 1, \frac{2}{3},$  and  $\frac{1}{3}e$ .

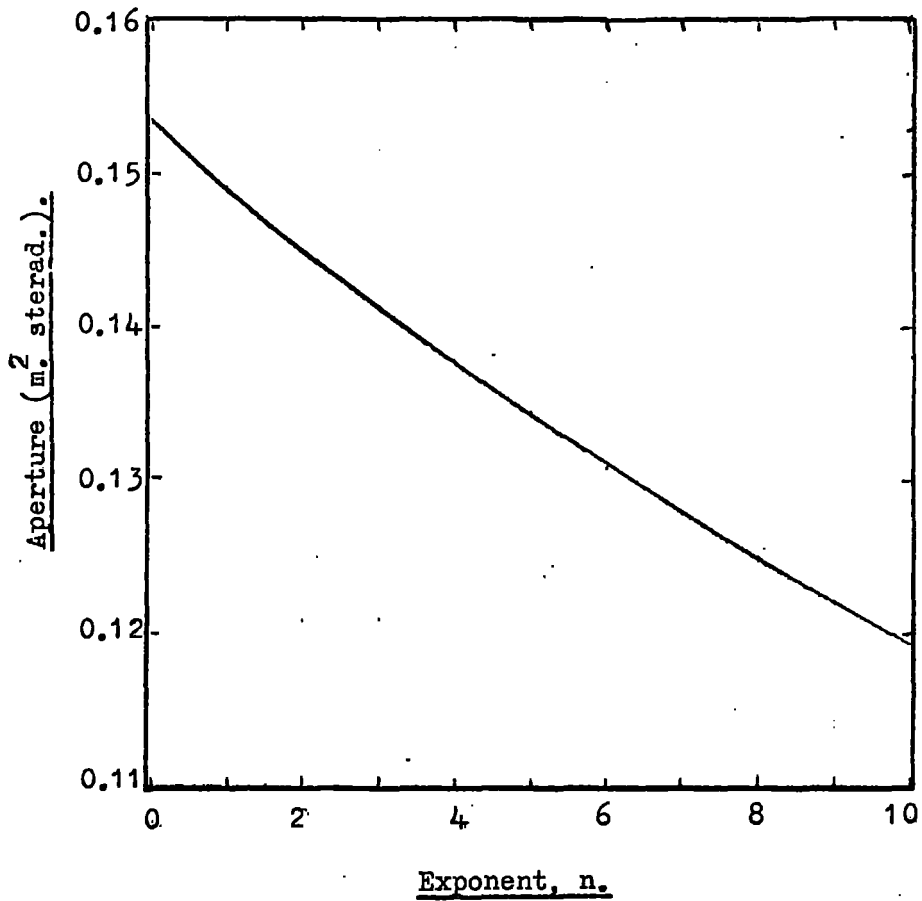


Figure 4.9 The 'heavy mass telescope' aperture as a function of the angular exponent of the incident radiation.

Table 4.5

Upper intensity limit at 90% confidence level cm. <sup>-2</sup> sec. <sup>-1</sup> sterad <sup>-1</sup> .	Mass Gev/c <sup>2</sup>	Charge
6.4 10 <sup>-10</sup>	< 3.3	1
	< 12.5	$\frac{2}{3}$
	< 70	$\frac{1}{3}$
1.01 10 <sup>-9</sup>	> 3.3	1
	> 12.5	$\frac{2}{3}$
	> 70	$\frac{1}{3}$

If account is taken of quark interactions in the telescope then the quoted upper limits should be increased. In Table 4.6. a breakdown is given of the materials in the telescope together with the corresponding number of nucleon inelastic interaction lengths of each material, which have been derived from Figure 3.19

Table 4.6

Material	Mean atomic weight	No. g. cm <sup>-2</sup>	No. of nucleon inelastic int. lengths.
Aluminium	27	11.7	0.096
Glass	21.3	40.7	0.356
Wood	7.74	16.6	0.191
Phosphor	6.83	31.0	0.369
Perspex	6.58	5.3	0.064
Water	5.97	33.0	0.408
Steel	56	200.9	1.340

Assuming the quark-nuclei interaction to be identical to the nucleon-nuclei interaction then the telescope contains 2.82 quark inelastic interaction lengths. If the most pessimistic assumption is made that all interacting quarks are lost then the quoted limits should be raised by a factor of 17 at the most.

Further consideration is given to these intensity limits and to the effect of interactions in Section 5.6, where limits are derived on the quark production cross section subject to specific models, proposed in Chapter 5, of the quark propagation in the atmosphere.

#### 4.9. The deuteron intensity at sea level.

##### 4.9.1. The observed intensity

Taking the two events H8/18 and H32/99 as both being due to deuterons the observed flux is  $(1.3^{+1.7}_{-0.8})10^{-12}$  cm.<sup>-2</sup> sec.<sup>-1</sup> sterad.<sup>-1</sup> (Mev/c)<sup>-1</sup> at a mean incident deuteron momentum of 2.45 Gev/c, where the aperture was taken as  $1.25 \cdot 10^3$  cm<sup>2</sup> sterad. for an assumed angular exponent of  $n = 8$ , the running time as  $3.74 \cdot 10^6$  sec. and the accepted incident momentum band as 2.28 - 2.61 Gev/c. To enable the true incident flux to be evaluated corrections have to be applied for fluctuations in the Cerenkov pulse height at a given velocity and for deuteron interactions in the telescope.

##### 4.9.2 Corrections to the observed intensity.

In the absence of fluctuations in the recorded Cerenkov pulse only deuterons in the momentum limits prescribed above would be accepted. However the finite width of the Cerenkov pulse height distribution corresponding to a fixed incident velocity will cause some loss of deuterons incident in the defined momentum band, by upward fluctuations in pulse height, as well as allowing particles of higher momentum, whose pulse heights fluctuate downwards, to be accepted.

The probabilities  $f_1(p)$  and  $f_2(p)$  of a deuteron traversing CI or CII respectively without producing a Cerenkov pulse greater than the discrimination level in that counter have been evaluated as a function of the incident deuteron momentum,  $p$ , and are shown in Figure 4.10. In evaluating  $f_1(p)$  and  $f_2(p)$  the Cerenkov pulse height distributions at given velocities were assumed to be Gaussian ( a reasonable assumption at velocities encountered here, the only non-Gaussian component being small and coming from knock-on electrons) and the standard deviation of each distribution was obtained as a function of velocity from the analysis in Section 3.9, where the velocity response of the counters was measured (typically  $\sigma = 0.09E_c$  for  $\beta = 0.78$ ). The probability,  $f(p)$ , of a deuteron of momentum  $p$  traversing both counters without producing a veto was also evaluated as  $f = f_1 f_2$  and its momentum dependence is also shown in Figure 4.10. Hence the following relationship can be written between the observed flux,  $N_o$ , and the flux,  $N_i$ , incident within the defined momentum band:

$$\frac{N_i}{N_o} = \frac{\int_{2.28}^{2.61} N_d(p) dp}{\int_{2.28}^{\infty} f(p) \cdot N_d(p) dp} = C$$

where  $N_d(p)dp$  is the incident sea level deuteron differential momentum spectrum, and  $C$  is the correction factor by which the observed flux must be multiplied to obtain the incident flux. Assuming the deuteron spectrum to have the same momentum dependence as the sea level proton spectrum measured by Brooke and Wolfendale, 1964(a), the correction factor  $C$  has been evaluated to be 1.42. However this value is fairly insensitive to the shape of the deuteron spectrum as assumptions of a flat spectrum (momentum independent) or a spectrum with an exponent twice that of the proton spectrum only alter  $C$  by the order of 1.5%

The other correction factor to be applied is to take account of deuteron interactions in the telescope. As discussed in Section 3.12.2 a deuteron

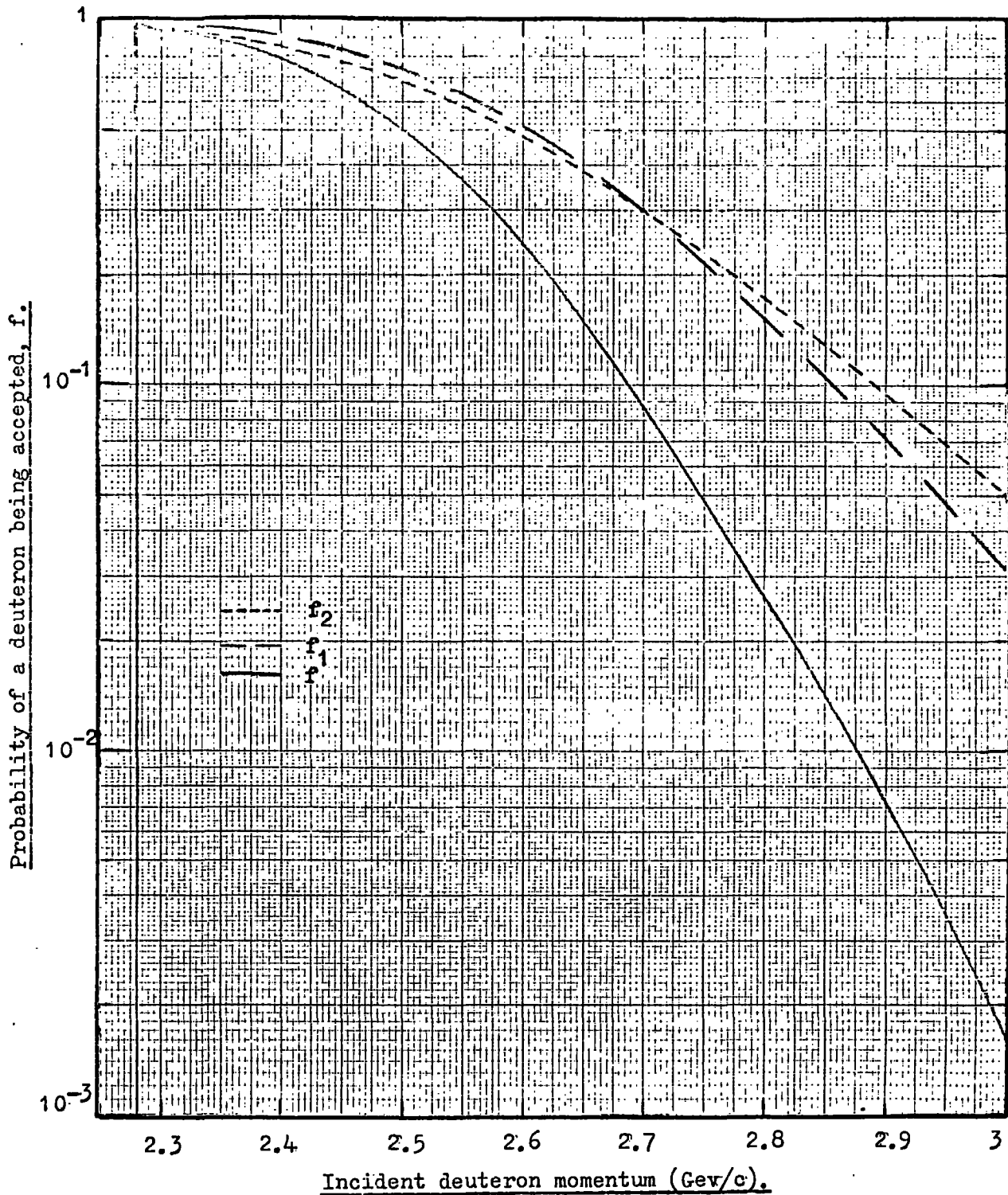


Figure 4.10

The probability of an incident deuteron, as a function of its momentum, being accepted by the Cerenkov counter CII, ( $f_2$ ), by the Cerenkov counter CI, ( $f_1$ ), or by both counters, ( $f$ ).

suffering an inelastic interaction will lose its identity and even if the interaction products succeed in traversing the remainder of the telescope the resulting mass value obtained would not be representative of a deuteron. Hence all deuterons having an inelastic interaction in the telescope will be lost; however those experiencing elastic interactions will not be affected, such interactions resulting in small energy transfers.

The evaluation of the number of deuteron inelastic interaction lengths in the telescope follows the method adopted in Section 3.12.2, where it was shown that for interaction purposes the deuteron could be considered as two individual nucleons (that such an argument still pertains here can be realised by considering that the p-d momentum corresponding to 2.45 Gev/c deuterons is 1.22 Gev/c, and reference to Figure 3.24 shows that at this momentum  $\delta\sigma$  is only of the order of 1 mb). Under this assumption the number of deuteron inelastic interaction lengths in the telescope is 5.64, being twice the nucleon number of 2.82 derived from Table 4.6.

Correcting for interactions and for fluctuations in the Cerenkov pulse heights the true incident intensity becomes

$$N_i = N_0 C e^{5.64} = 4.8 \begin{matrix} +6.8 \\ -3.3 \end{matrix} \cdot 10^{-10} \text{ cm.}^{-2} \text{ sec.}^{-1} \text{ sterad.}^{-1} (\text{Mev/c})^{-1}$$

where the statistical error has been broadened to include an assumed 5% error in the number of interaction lengths in the telescope and a 1.5% error due to the uncertainty in the shape of the deuteron momentum spectrum. Comparing this intensity with that of sea level protons of the same momentum (Brooke and Wolfendale, 1964(a)), a d/p ratio of  $3.4 \begin{matrix} +4.8 \\ -2.4 \end{matrix} \%$  is obtained at a mean momentum of 2.45 Gev/c. The present result and that obtained in Chapter 3 are tabulated below and are also compared with the proton spectrum of Brooke and Wolfendale in Figure 4.11.

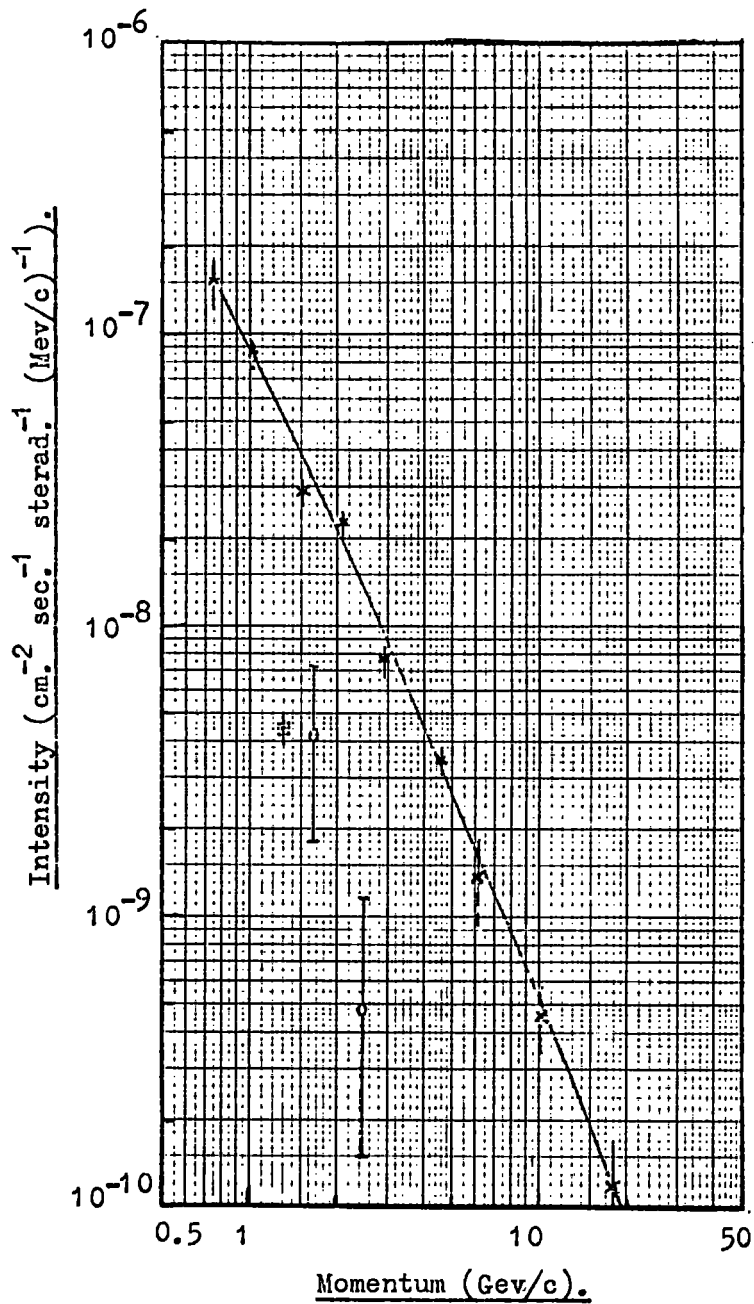


Figure 4.11

The measured sea level deuteron intensities (open circles) compared with the proton spectrum due to Brooke and Wolfendale, 1964a, (crosses). The measurement due to Badalian, 1959, (full square) is included for completeness and was derived assuming the same d/p ratio to pertain at sea level as at 3200m. above sea level, the location of the latter measurement.

Momentum Gev/c	Deuteron intensity $\text{cm.}^{-2}\text{sec.}^{-1}\text{sterad.}^{-1}(\text{Mev/c})^{-1}$	d/p%
1.65	$(4.2^{+3.0}_{-2.4}) \cdot 10^{-9}$	$14^{+10}_{-8}$
2.45	$(4.8^{+6.8}_{-3.3}) \cdot 10^{-10}$	$3.4^{+4.8}_{-2.3}$

While the measurements are statistically very weak they are suggestive of a deuteron spectrum falling more rapidly with momentum than the proton spectrum.

#### 4.9.3 Comparison with measurements of other workers.

No other measurements of the sea level deuteron intensity in the present momentum range are known to the author. The work of Kasha et al., 1968(a), using a scintillation counter hodoscope to search for quarks of charge  $4e/3$  should have been sensitive to low momentum deuterons; however their lack of observation of any low energy protons (discussed in more detail in Chapter 6) casts doubts on their quoted discrimination levels for their scintillators, and this invalidates an analysis of their experiment in terms of deuterons.

The only other work on deuterons of similar momentum to the present work has been carried out by a Russian group at Mt. Aragats (3200m. above sea level) in particular by Badalian, 1959. Although these measurements were made at an atmospheric depth of  $710 \text{ g. cm.}^{-2}$ , compared with the present work under  $1000 \text{ g. cm.}^{-2}$  of a atmosphere, the results can be directly compared by expressing them in terms of a deuteron to proton ratio in the same momentum band rather than as an absolute deuteron intensity. This arises from the shape of the nucleon momentum spectrum (nucleons being the primaries responsible for deuteron production) being, in the lower regions of the atmosphere, essentially independent of atmospheric depth (Schopper, 1967) for nucleon momenta greater than  $1 \text{ Gev/c}$  (that is to

say that the number of deuterons produced is directly proportional to the number of nucleons at that level and hence the d/p ratio is insensitive to atmospheric depth). In the experiment of Badalian deuterons were identified by two multiplate cloud chambers, one placed above, and the other below a magnetic spectrometer, and the observed incident d/p ratio was  $8.6 \pm 1.0\%$  at a mean momentum of 1.3 Gev/c, a value with which the present results are not inconsistent.

A more interesting problem is to consider the production mechanisms responsible for the relatively high observed deuteron intensities. Detailed consideration is given to deuteron production in reactions such as  $NN \rightarrow d\pi$  in Appendix B, and it is shown that the present observations suggest intensities which are at least a factor of 10 greater than would be expected on the basis of the cross sections for such processes which have been measured at the proton accelerators. It can be concluded therefore that the observed deuterons have not (apart from a small fraction) been produced in such a manner. An analysis of deuteron production through direct and indirect 'pick up' has been carried out by Badalian (indirect 'pick up' being the most important for momenta presently considered, this cross section for deuteron production varying with the incident nucleon energy as  $\sim E_N^{-2}$  (Bransden, 1952) whereas the cross section for direct 'pick up' varies as  $\sim E_N^{-6}$  (Heidman, 1950)) and he has evolved a momentum spectrum of produced deuterons of the form

$$N_d(p) dp \propto p^{-3.14 \pm 0.44} dp$$

for  $p_d > 1\text{Gev}/c$ . The rates and momenta of deuterons observed to be produced within the upper cloud chamber in his experiment were in good agreement with the absolute intensities and momentum dependence predicted by his spectrum, and such an agreement confirms that the dominant mechanism for deuteron production at these momenta is direct and indirect 'pick up'. Further support

for such a spectrum can be obtained from the work of Alikhanov et al., 1960, also working at Mt. Aragats, who found the incident deuteron differential momentum spectrum to vary as  $p_d^{-3}$  for  $p_d > 0.8 \text{ GeV}/c$ .

The incident  $d/p$  ratio measured by Badalian has been transformed into a deuteron intensity at sea level by direct comparison with the sea level proton spectrum of Brooke and Wolfendale and is shown together with the present results in Figure 4.11. The results can be further compared by resort to the calculated deuteron production spectrum due to Badalian. Writing the differential proton momentum spectrum as  $N_p(p) dp \cong b p^{-2.5}$  for  $p_p > 1 \text{ GeV}/c$  then

$$\frac{d/p}{N_p(p)dp} = \frac{N_d(p)dp}{N_p(p)dp} = c p^{-0.64 \pm 0.44}$$

Normalising the  $d/p$  ratio to the measurement of Badalian, (this being statistically the most precise) the present results, at higher momenta than that of Badalian, can be compared with the predicted  $d/p$  fall off with momentum. This comparison is shown in Figure 4.12 where it can be seen that the present work is not inconsistent with the fall off with momentum predicted on the basis of the observed deuterons being produced through direct and indirect 'pick up'.

This apparent agreement adds further weight to the conclusion that the two events found in the heavy mass search were in fact deuterons, and not perhaps integrally charged quarks of mass  $\sim 2\text{GeV}/c^2$ .

In conclusion the deuterons observed in both the 'proton experiment' and the heavy mass search are consistent with having been produced via locally occurring 'pick up' processes (their intensities being too large to have been produced via reactions such as  $NN \rightarrow d\pi$ ) since, due to the fairly short interaction length of the deuteron and the fact that its identity

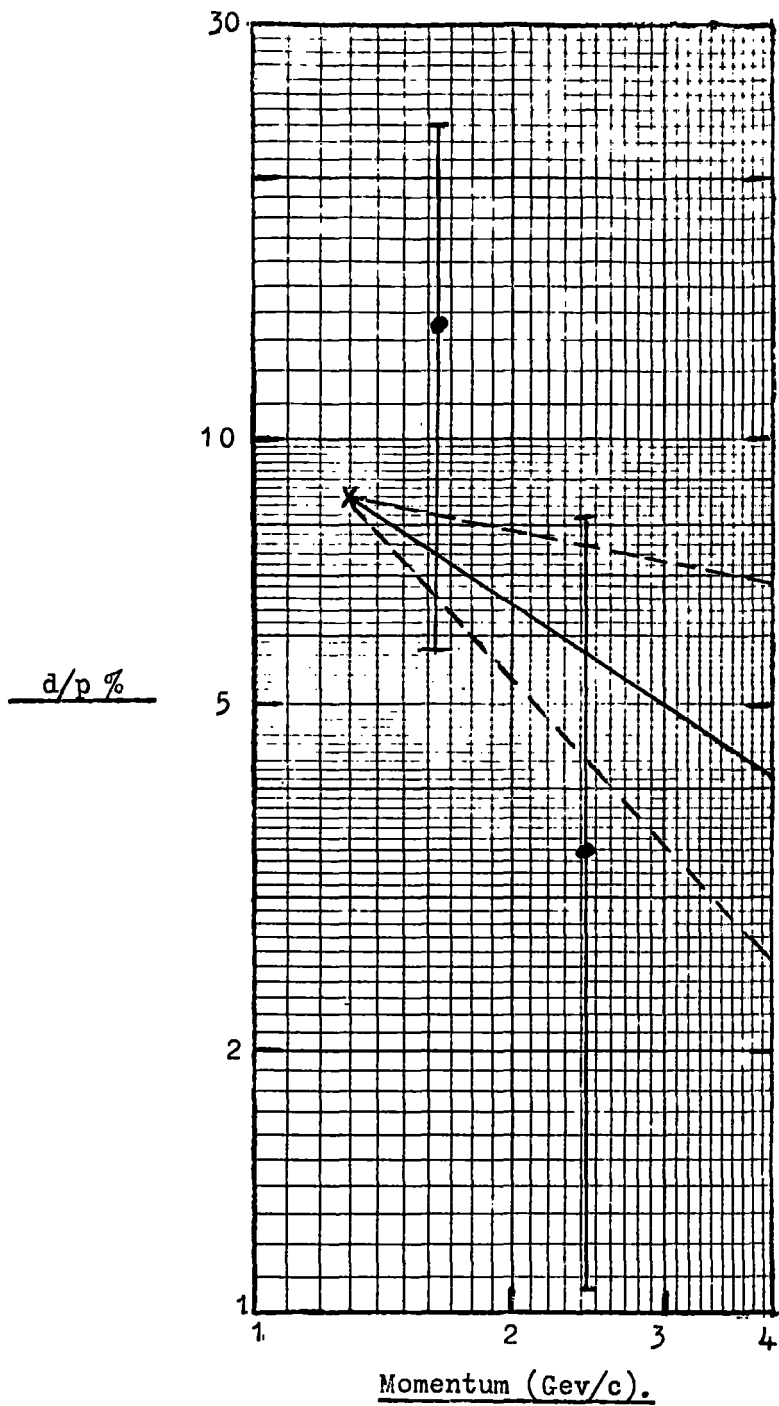


Figure 4.12 The measured  $d/p$  ratio compared with its calculated momentum dependence (Badalian, 1959). The  $d/p$  variation has been normalised to the measurement of Badalian at 1.3 GeV/c and the predicted momentum dependence varies as  $p^{-0.64 \pm 0.44}$ .

will be lost in any inelastic interaction, the mean height of production above the detector of those observed is only  $\sim 60 \text{ g. cm}^{-2}$  of air (see Appendix B).

#### 4.10 The Glashow U particle.

##### 4.10.1 Introduction

The observation by Bergeson et al., 1967, of an angular distribution of cosmic ray muons underground, in the energy range  $10^3 - 10^4 \text{ Gev}$ , which strongly contradicted the expected  $\sec \theta$  enhancement expected if the muons were the progeny of pions and kaons, has led Callan and Glashow, 1968, to propose the existence of an hitherto unknown U particle to explain the observed effect. They suggested that the particles observed by Bergeson et al. were in fact not muons but U particles to which they assigned the following properties: they are stable, singly charged, massive ( $> 4 \text{ Gev}/c^2$  otherwise they would have been detected at the accelerators) and have weak interactions with matter; further they comprise part of the primary radiation and are present to a level of  $10^{-3}$  of the primary proton flux.

Hence at energies greater than  $10^3 \text{ Gev}$  the flux of U particles would be greater than that of muons and as they are present in the primary radiation their angular distribution underground will be essentially isotropic, in keeping with the observation of Bergeson et al., While to explain the effect, the presence of the U particles need only commence at primary energies above  $10^3 \text{ Gev}$ , Callan and Gashow go on to suggest that the fraction of U particles,  $10^{-3}$ , in the primary radiation will be energy independent (this extension over all energies is necessary if the proposal is to be plausible, in that the U particles will be accelerated in the galaxy by the same mechanisms accelerating protons, and hence should exhibit the same energy dependence

as the primary proton spectrum).

If such an intensity of U particles exists in the primary radiation with the above listed properties they would have been readily detected by the present experiment.

#### 4.10.2 Limits on the intensity of U particles.

Of the heavy mass candidates discussed in Section 4.5.2 none can be interpreted in terms of a U particle; two of them are consistent with being deuterons while the third, by suffering two interactions in the telescope, contradicts the hypothesis of the U particle being weakly interacting. On the basis of having observed no events upper limits can be placed on the flux of U particles in the primary radiation.

The momentum bands accepted by the telescope as a function of mass for  $z=1$  are given in Figure 4.7. These limits have been transformed to give the accepted momentum bands as a function of mass at the top of the atmosphere using range-energy tables for protons in air (Serre, 1967) and the following relationships;

$$R_M (M, \alpha) = \frac{M}{M_p} \cdot R_{M_p} \left( M_p, \frac{\alpha \cdot M_p}{M} \right);$$

$$\text{and } \alpha_M (M, R) = \frac{M_p}{M} \cdot \alpha_{M_p} \left( M_p, \frac{RM}{M_p} \right);$$

where  $R_M(M, \alpha)$  is the range of a particle of mass M and momentum  $\alpha$ ,

$\alpha_M(M, R)$  is the momentum of a particle of mass M and residual range R,

and  $M_p$  is the mass of the proton.

The calculated momentum limits at the top of the atmosphere which would be accepted by the telescope at sea level are given in Figure 4.13.

Geomagnetic effects have been considered and the fraction of the total primary radiation reaching the top of the atmosphere as a function of momentum for  $z=1$  is shown in Figure 4.14 for a latitude of  $54.8^\circ\text{N}$ , the location of the

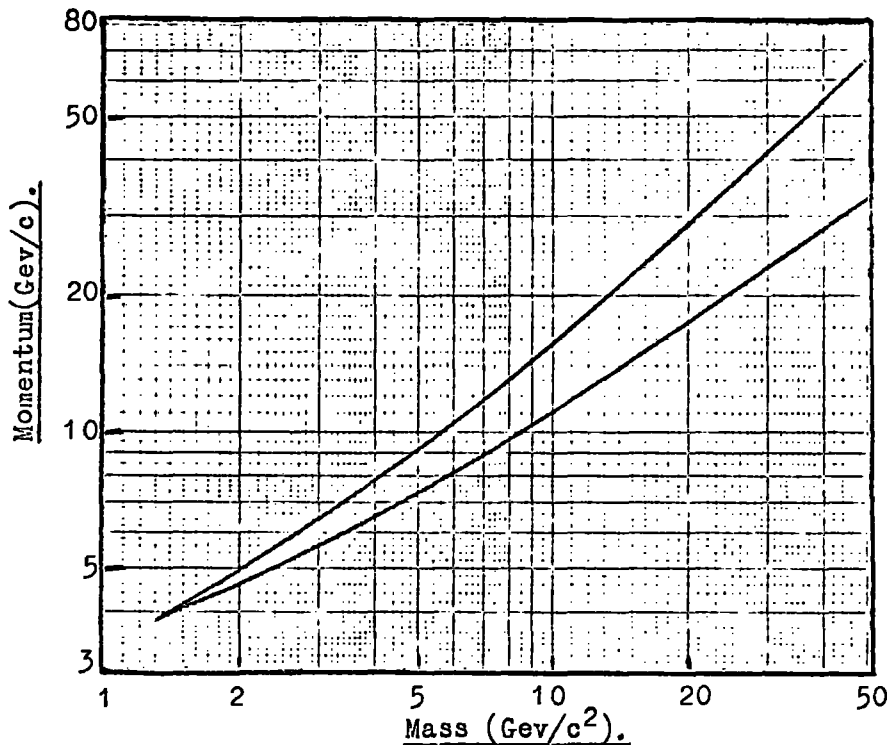


Figure 4.13

The momentum bands for unit charged particles, as a function of their mass, at the top of the atmosphere that would be accepted at sea level by the 'heavy mass telescope' (applying only to weakly interacting particles which lose energy through ionisation only in traversing the atmosphere).

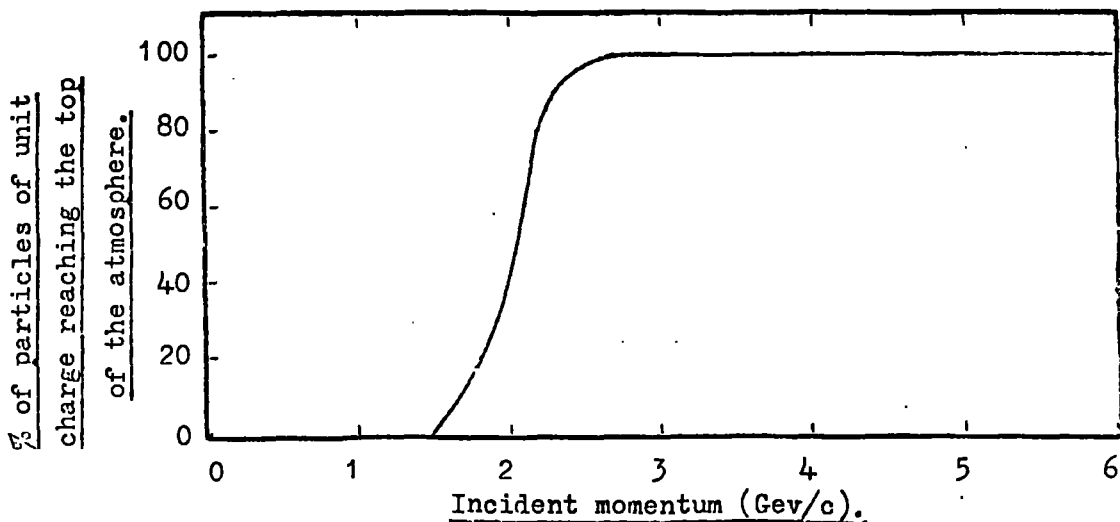


Figure 4.14

The effect of the earth's magnetic field on unit charged particles, arriving vertically at the top of the atmosphere at a latitude 54.8° N., as a function of their momentum.

present experiment. The curve was derived from calculations of Lemaitre et al., 1933, and consideration of Figures 4.13 and 4.14 shows that at the momenta accepted by the telescope no reduction in flux would be expected from geomagnetic effects.

The upper limit of the observed intensity of U particles at the 95% confidence limit is  $< 5.23 \cdot 10^{-10} \text{ cm}^{-2} \text{ sec}^{-1} \text{ sterad}^{-1}$ , where the telescope aperture has been taken as  $1.53 \cdot 10^3 \text{ cm}^2$  sterad. for a value of  $n = 0$ , that is an assumed isotropic flux. Assuming no attenuation of the U flux in traversing the atmosphere (since they are weakly interacting) this intensity limit has been compared with the primary proton intensity incident at the top of the atmosphere within the same momentum bands available for U detection.

A primary proton spectrum due to Brooke and Wolfendale, 1964 (b), of the form

$$N (>E_p) = 0.87 E_p^{-1.58} \text{ cm}^{-2} \text{ sec}^{-1} \text{ sterad}^{-1}$$

was assumed and the upper limit of the U/p ratio at the 95% confidence level is shown in Figure 4.15 as a function of the U mass. It can be seen that the upper limit to the U/p ratio varies from  $\sim 4 \cdot 10^{-8}$  for  $M_u = 2 \text{ Gev}/c^2$  to  $\sim 2 \cdot 10^{-7}$  for  $M_u = 50 \text{ Gev}/c^2$ . The present results are completely inconsistent with a U/p ratio of  $10^{-3}$  pertaining in the primary radiation.

Confirmation of the present results comes from a value of U/p of  $\sim 10^{-5}$  obtained by Ashton et al., 1968(b), from preliminary results of the 'proton experiment' previously discussed, and from a value of  $\sim 10^{-5}$  obtained by Kasha et al., 1968b, using a spectrometer elevated at  $75^\circ$  to the zenith which accepted heavy mass particles in the velocity range  $0.5 - 0.75c$ .

It would appear that U particles are not present in the primary radiation to the level suggested by Callan and Glashow, at least in the momentum bands shown in Figure 4.13. While the present results or those of Ashton et al.,

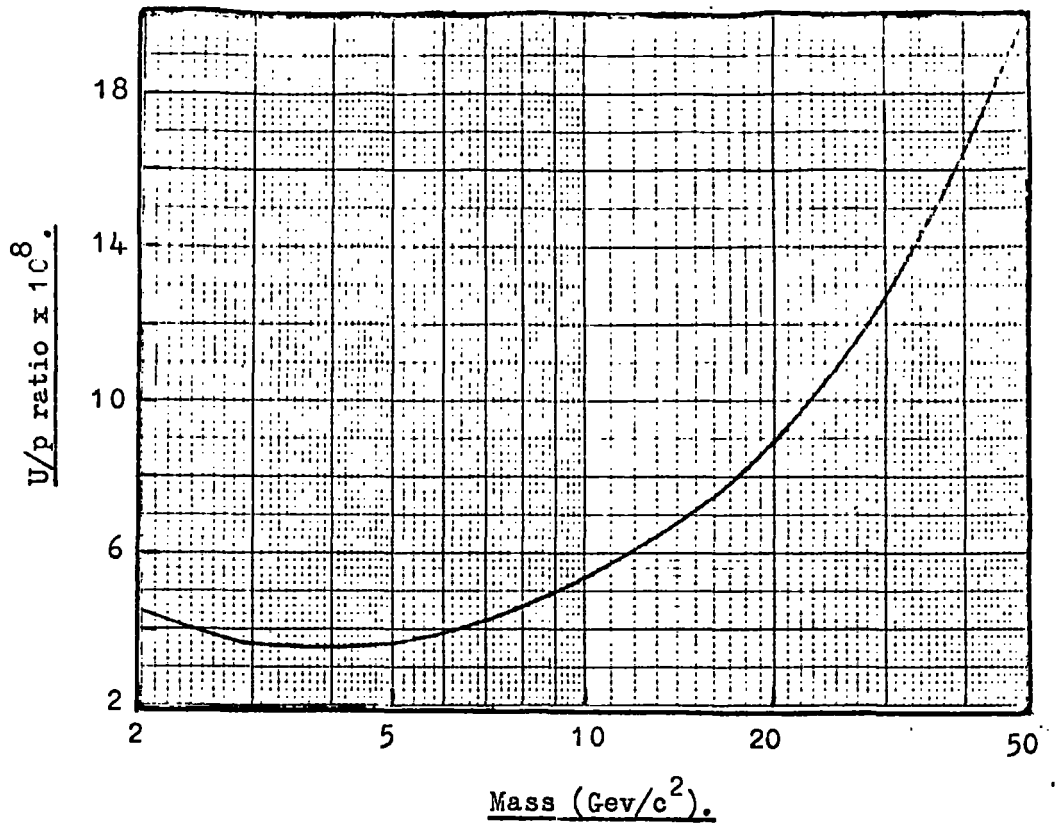


Figure 4.15 The limits at the 95% confidence level on the U/p ratio pertaining at the top of the atmosphere, in the momentum bands given in Figure 4.13, as a function of the U particle mass.

or Kasha et al., cannot disprove the existence of U particles at much higher energies they do show that the hypothesis of Callan and Glashow becomes much less plausible in that it must demand a primary U spectrum significantly different in shape from that of the primary proton spectrum.

#### 4.10.3 Further evidence against the U particle.

A detailed account of further evidence against the existence of the U particle has been given by Ashton et al., 1968(b), and only the evidence at the highest energies will be discussed here, having already established their non-existence at low energies.

The energy loss of a U particle, by virtue of its large mass, by bremsstrahlung and pair production will be considerably reduced compared with the corresponding energy loss of a muon, and since the proposal of Callan and Glashow requires that most particles below 2000 m.w.e (m. water equivalent) are U particles an analysis of the electromagnetic interactions of particles observed at such depths should yield some evidence as to the mass of the penetrating particles. Such an analysis of the secondary particles accompanying penetrating particles down to depths of 7500 m.w.e has been carried out by Menon et al., 1967, who have made a rough estimate of the mean energy underground by comparing the degree of accompaniment with observations at sea level using a magnetic spectrograph to select particles of known energy (Kelly et al., 1967). That the particles detected by the spectrograph are muons is concluded from the observed frequency of accompaniment being in agreement with that expected for muons being the initiating particles, and from the experiment of Ashton et al., 1967(a), who find agreement between the measured energy spectrum and that derived from observations of electromagnetic bursts produced in local absorbers, where in the transition from burst size to

particle energy the incident particles were assumed to be muons. The mean energies evaluated by Menon et al., are close to those expected on the basis of the particles being muons down to the greatest depth, 7500 m.w.e., where the corresponding sea level energy is at least  $10^4$  Gev.

Hence even at such high energies there appears to be no evidence for U particles and it is concluded that the hypothesis of Callan and Glashow is unable to explain the observation of Bergeson et al. In conclusion it is perhaps pertinent to note that a recent experiment performed by Krishnaswamy et al., 1968, on the angular distribution of underground muons ( $E_\mu > 5.10^2$  Gev) at the Kolar Gold Fields has found no deviation from the normally expected  $\sec \theta$  enhancement.

#### 4.11 Summary.

The present search for sub-relativistic massive particles in the cosmic radiation at sea level in the vertical direction, while yielding only upper limits on the intensity of quarks, and U particles, has given some information on the intensity of low energy deuterons. The techniques employed which formed the basis of the search have proved particularly successful in rejecting sub-relativistic particles of mass lower than  $\sim 1.3$  Gev/ $c^2$  as well as discriminating against  $\sim 4.10^7$  relativistic muons which would have traversed the telescope during its operation.

The analysis of the experiment with respect to U particles has shown that if they are present in the primary radiation then their spectrum is either not continuous or that they are present at a level less than  $\sim 10^{-7}$  of the proton flux. Such an intensity would be insufficient to explain the observations of Bergeson et al., and since the particle was invoked purely for this purpose its existence even at very low levels must be

extremely doubtful.

Of the three heavy mass candidates observed two have been found to be consistent with having masses of  $\sim 2\text{Gev}/c^2$  and having unit charge. Their interpretation as deuterons has been substantiated by the agreement of their observed intensity with other measurements in the same momentum region, and this agreement allows a conclusion to be drawn that the deuteron intensity in the sea level cosmic radiation in the momentum range 1- 3  $\text{Gev}/c$  is a few percent of the proton intensity in the same momentum band, and that the deuteron momentum spectrum is falling somewhat more steeply than the proton spectrum with increasing momentum. Further, the observed rates have been shown to be consistent with deuteron production occurring through 'pick up' processes and to be at least an order of magnitude greater than would be expected for production via the reactions  $NN \rightarrow d\pi$ .

The remaining event H40/6 would appear to be difficult to explain in terms of the conventional particles and a more plausible interpretation has been suggested in terms of a massive ( $M > 3.3.\text{Gev}/c^2$ ) unit charged particle. However the finite but small probability ( $< 10^{-5}$ ) of observing such a spurious event, due to the relatively long sensitive time of the flash tubes, does not allow a definite conclusion to be made and this one observation, while suggesting the possible existence of massive unit charged particles, has been used only to place upper limits on the intensity of such particles. The implications of this limiting intensity on the quark production cross section are discussed fully in Chapter 5 where cross section limits are derived subject to specific models of quark propagation in the atmosphere.



## CHAPTER 5

### PROPAGATION OF QUARKS IN THE ATMOSPHERE

#### 5.1. Introduction

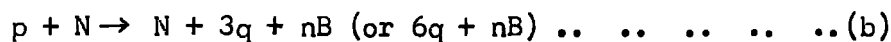
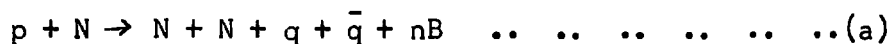
The negative results as to the existence of quarks obtained at the accelerators have led to searches in the cosmic radiation where the energy spectrum of incident protons is effectively continuous, this eliminating the problem of a maximum attainable quark mass experienced at the accelerators. However due to the rapidly falling proton spectrum the flux of quarks produced may be too small to be detectable by detectors of the size presently used, particularly if the quark mass is very high. Because of this, searches have been extended to look for quarks in various materials thus utilising the relatively long irradiation time of the earth by the cosmic radiation (of the order of  $5 \cdot 10^9$  years).

While many searches have been made for quarks in these areas little consideration has been given to the sensitivity of each individual experiment to the mode of propagation of quarks in the atmosphere. To compare the relative merits of each type of experiment performed and to assess the most likely areas for further quark searches it is necessary to adopt a model of quark production and propagation in the atmosphere. Such a model has been proposed by Adair and Price, 1966, and while little improvement can be made to their model of production, due to the uncertainties involved in particle production at very high energies, further consideration can be given to the unique propagation model they have used by invoking widely differing, yet at the same time plausible, properties of the quark interaction with matter.

The purpose of the present work is to evaluate the velocity dependence of the quarks at various levels from their point of production, and to determine the rate at which they stop for various plausible assumptions as to their interaction properties. Further it is intended to use these calculations to establish limits on the quark production cross section from the flux limits of quarks obtained from the present work and from other experiments.

## 5.2 Quark production in the atmosphere.

The most likely reactions leading to quark production are as follows:-



where  $q$  refers to a quark,  $B$  to a boson (mainly pions) and  $n$  is an integer ( $n = 0, 1, 2 \dots$  etc).

It is impossible in the light of present knowledge to ascertain which reaction, either (a) involving the production of quark-antiquark pairs or (b) resulting in nucleon dissociation, will have the higher cross section, but in the present treatment production via reaction (a) will be given the greatest consideration, since if both reactions were to have the same cross section it can be realised that (a) would be more important when account is taken of the rapidly falling proton spectrum, and of the threshold production energy for (a) being about half (or one ninth) that for (b) (for  $M_q \gg M_p$ ). The threshold proton energy for production via reaction (a) is given by  $E_{pT}$ , where

$$E_{pT} = 2 \left[ \left( \frac{M_q}{M_p} + 1 \right)^2 - 1 \right] \cdot M_p c^2 \quad \dots \dots \dots (5.1)$$

disregarding Fermi motion of the target nucleon.

Typically for the production of a particle in a given channel the cross section rises from threshold as the phase space for that channel increases, reaches a maximum and then declines again as further new channels become

available, the phase space for these new channels increasing faster than that for the initial channel. However the probability of producing that particular particle does not necessarily decrease, as some of the new channels opened up are channels in which that particular particle can be produced. In general the total cross section from all channels tends to rise rapidly from threshold and then at a few times threshold energy tends to rise only slowly. A calculation of quark production via reaction (a) has been carried out by Takahashi (private communication) based on the Fermi statistical model and the cross section evolved exhibits the above discussed features. However whether quark production can be expressed in these terms is a matter for conjecture and for this reason, as well as the present work being concerned with determining the shape of the quark velocity distribution, the cross section for quark production adopted here is assumed to be constant at all energies above threshold. Such an assumption has been shown to be reasonable by Adair and Price who adopted a cross section of the form

$$\sigma_q = \sigma_0 (E/3E_T - 0.33)^2 \quad \text{for} \quad E_T < E < 4E_T$$

and

$$\sigma_q = \sigma_0 \quad \text{for} \quad E \gg 4E_T$$

where  $\sigma_0 = \pi a^2$  and  $a = \hbar/M_q c$

by using an analogy with antiproton production, but finally expressed their results in terms of a constant cross section above threshold as they found that the velocity dependence of the quark flux was insensitive to a constant or such a varying cross section apart from a scaling factor of approximately three.

Taking a constant cross section the quark production spectrum can be obtained using the relatively simple model proposed by Ashton, 1965. In the absence of any firm understanding of the mode of quark production this model is as appealing as any other. It is assumed that at production quarks have

relatively low kinetic energies in the centre of mass system (C.M). The validity of this assumption can be shown by considering that most quark production will come from near threshold, due to the rapidly falling proton spectrum, where the remaining energy after creation of the  $q\bar{q}$  pair available as kinetic energy will be small. Hence the kinetic energy of the quarks,  $E_q$ , in the laboratory system can be written approximately as

$$E_q = (\gamma_c - 1) M_q c^2$$

where  $\gamma_c$  is the Lorentz factor of the C.M. system. As

$$\gamma_c = \left( \frac{\gamma_L + 1}{2} \right)^{\frac{1}{2}}$$

for nucleon-nucleon collisions, where  $\gamma_L$  is the Lorentz factor of the incident proton then  $E_q$  can be written as

$$E_q = \left[ \left( \frac{E_p}{2M_p c^2} + 1 \right)^{\frac{1}{2}} - 1 \right] \cdot M_q c^2 \quad \dots \dots \dots (5.2)$$

Taking a differential primary proton spectrum of the form

$$N(E_p) dE_p = A E_p^{-\gamma} dE_p \quad \text{m}^{-2} \text{ day}^{-1} \text{ sterad}^{-1} \text{ Gev}^{-1} \dots \dots (5.3)$$

where  $A = 1.19 \cdot 10^9$  and  $\gamma = 2.58$  (Brooke and Wolfendale, 1964(b)),

and integrating Equation 5.3 and substituting for  $E_p$  from Equation 5.2, the integral quark production spectrum can be written as

$$N(> E_q) = \frac{2fA}{(\gamma-1)} \left\{ 2M_p c^2 \left[ \left( \frac{E_q}{M_q} + 1 \right)^2 - 1 \right] \right\}^{-(\gamma-1)} \text{m}^{-2} \text{ day}^{-1} \text{ sterad}^{-1} \dots \dots (5.4)$$

where the minimum quark production energy,  $E_{q_{\min}}$ , is given from Equations

5.1 and 5.2 as

$$E_{q_{\min}} = \frac{M_q^2 c^4}{M_p c^2} \quad \dots \dots \dots (5.5)$$

and where  $2f$  quarks are assumed to be produced in each interaction where the

factor 2 takes account of a  $q\bar{q}$  pair being produced and  $f$  is the probability of a proton-nucleon interaction yielding a quark pair.

So far Equation 5.4 only includes quarks produced by primary protons. However there will also be a contribution from the ensuing generations of nucleons due to the nucleon retaining approximately half of its energy after an interaction. The  $n^{\text{th}}$  generation nucleon spectrum can be written as

$$N_n(E_p) dE_p = \frac{A}{(1-K_p)^n} \cdot \left( \frac{E_p}{(1-K_p)^n} \right)^{-\gamma} dE_p \text{ m}^{-2} \text{ day}^{-1} \text{ sterad}^{-1} \text{ Gev}^{-1}$$

where  $K_p$  is the proton inelasticity which is taken as 0.5 (Brooke and Wolfendale 1964(b)) and hence the quark production spectrum from the  $n^{\text{th}}$  generation nucleons can be written as

$$N_n(>E_q) = (1 - K_p)^{n(\gamma-1)} \cdot N_o(>E_q) \dots \dots \dots (5.6)$$

where  $N_o(>E_q)$  is the quark production spectrum initiated by the primary protons.

Quark production through succeeding generations of nucleons is quite important, constituting  $\sim 50\%$  of that from the primary protons. Its importance increases further if a high quark-nucleon cross section pertains, as quarks produced by later generations of nucleons have less atmosphere to traverse and hence have a greater probability of reaching sea level. The total quark production spectrum can thus be written as

$$N_T(>E_q) = N_o(>E_q) \cdot \sum_{n=0}^{\infty} (1-K_p)^{n(\gamma-1)} \dots \dots \dots (5.7)$$

In the proceeding calculations this spectrum has been used with a value of  $f = 1$ . This corresponds to quark production in every nucleon-nucleon interaction above threshold and is equivalent to assuming a 30 mb. cross section (the nucleon-nucleon cross section) for quark production. While this is certainly most unlikely to be representative of quark production the results

obtained can be normalised to take account of any prescribed cross section.

### 5.3 Quark interactions with matter.

The degradation of the quark energy in traversing the atmosphere will be due mainly to nuclear interactions, and hence the important parameters affecting quark propagation are the quark-nucleon cross section and the quark inelasticity in such an interaction. Before discussing the various values to be assigned to these quantities in the present work it is relevant first to consider the values adopted by Adair and Price.

Their argument stems from considering the nature of the quark-nucleon and nucleon-nucleon interaction to be identical and they describe these interactions in terms of fireball production, following Cocconi, 1962. The two interacting particles are assumed to continue after the interaction with only a small change,  $q \sim 0.5 \text{Gev}/c$ , in their four momentum but with their fields largely stripped, and in recreating their fields mesons are radiated. The two meson clouds are excited by the interaction leading to fireball production from which mesons and particle-antiparticle pairs are radiated. If this mechanism dominates quark interactions then the excitation energy of the fireballs will be about the same for both quarks and nucleons of the same velocity; this is essentially the result if the mean four momentum transfer is the same in both cases. Under such an assumption the proportion of energy lost by a quark in the production of fireballs in an interaction is not large and tends to vary inversely with mass. This fractional energy loss can be expressed approximately as

$$\frac{\Delta E_q}{E_q} \approx \frac{q}{M_q}$$

and for a quark mass of  $10 \text{Gev}/c^2$  the energy loss would be only  $\sim 5\%$  per collision if the mean four momentum transfer is of the order of  $0.5 \text{Gev}/c$ .

To estimate the division of energy loss between the two processes, namely fireball production and the radiation of mesons in recreating the meson field, they have considered the high energy cosmic ray muon flux (which is assumed to come primarily from pions from isobar decay) and conclude that not more than 25% of the incident nucleon energy in a nucleon-nucleon interaction can go into fireball production, leaving approximately 25% of the energy for reconstitution of the nucleon fields. Neglecting transverse components the four momentum transfer is completely determined by the incident and final energies of the nucleon, and hence depends only on the value of inelasticity. Taking an inelasticity of 0.5 this corresponds to  $q \sim 500 \text{ Mev}/c$  and the mean four momentum transfer involved in fireball production is then of the order of  $250 \text{ Mev}/c$ . Returning to the quark interaction it is then assumed that the meson radiation involved in recreating its meson field is similar to that in the nucleon case, but that the proportional energy radiated is smaller by a factor of approximately  $M_p/M_q$ . This assumption would appear to be the weakest in the argument as the quark is not a nucleon and its field may be radically different. However a model of this sort would suggest that the quark nucleon interaction can be characterised by a mean four momentum transfer of the order of  $250 - 500 \text{ Mev}/c$ .

The quark-nucleon cross section used by Adair and Price is  $30 \text{ mb.}$ , equivalent to  $\sim 80 \text{ g. cm.}^{-2}$  of air, and is identical to the nucleon-nucleon cross section. Such a value is derived from considering that in the dynamic theories the three quarks forming the nucleon are together not coupled with excessive strength to the pion, and it is concluded that it is unlikely that any single one is. The enormous quark couplings are then attributed to very short range forces which would not affect total cross sections by much, and the meson cloud about the quark is assumed to be similar to that about

the nucleon. Thus the propagation model of Adair and Price is characterised by a quark-nucleon cross section and a mean four momentum transfer almost identical with those experienced in nucleon-nucleon interactions.

While such an interpretation of quark interactions is certainly plausible and perhaps the most likely in terms of the present understanding of the established particles, it is not unreasonable to assume quite different interaction properties which remain equally plausible when one considers how little is known regarding the quark. From this point of view it is useful to assume some extreme alternatives to those proposed above and to investigate their effect on the propagation. Such alternatives to be considered in the present work are:- that the quark-nucleon cross section is one third that of the nucleon-nucleon cross section, which is equivalent to assuming a quark mean free path of  $240 \text{ g. cm.}^{-2}$  of air (this is based on the simple assumption that the nucleon-nucleon interaction is in fact made up of the sum of three individual quark-nucleon interactions); that the quark interaction cannot be described in terms of fireball production and that its inelasticity is the same as that of a nucleon, namely 0.5 (such an inelasticity could still perhaps pertain even in terms of fireball production if it is assumed that the energy loss in recreating the meson field of the quark is large). These suggested values of cross section and inelasticity, together with those adopted by Adair and Price, will be used to determine various plausible velocity distributions of quarks in the atmosphere.

In each assumed model the assigned value of inelasticity will be used to degrade the quark energy at each interaction, providing that the quark energy is greater than the pion production threshold,  $E_q(\pi)$ , which is

$$E_q(\pi) = M_\pi c^2 \left[ 1 + \frac{M_q}{M_p} + \frac{M_\pi}{2M_p} \right] \dots \dots \dots 5.8$$

where no account has been taken of the Fermi motion of the nucleon in the air nucleus. Below this energy quarks will then lose energy in nuclear collisions by elastic scattering, and assuming qN elastic scattering to be isotropic in the C.M. the average energy lost per collision is

$$\frac{1}{2} \left[ 1 - \left( \frac{M_q - M_p}{M_q + M_p} \right)^2 \right] \cdot E_q \quad \dots \dots \dots 5.9$$

While it is expected, by drawing an analogy with nucleons, that the elastic scattering cross section at low energies will increase rapidly above the value assigned for inelastic interactions, no account will be taken of this and a constant cross section assumed throughout. This assumption is reasonable as the energy loss due to this process is small and becomes negligible for  $M_q \gg M_p$ .

The only other process through which the quark will lose energy is ionisation (bremsstrahlung and pair production being negligible due to the large mass of the quark) and this is taken account of throughout the calculations. The charge of the quark is taken as  $\frac{2}{3}e$ , this being the mean of the three possible charged states of  $1, \frac{2}{3}$  or  $\frac{1}{3}$  in the various representations. The energy loss due to ionisation as a function of quark velocity was derived by scaling down by  $4/9$  the tabulated data due to Serre, 1967, of proton energy loss in air.

#### 5.4. Method of calculation.

The velocity distributions of quarks and the rate at which they stop have been calculated under four assumptions as to the quark interaction with matter, for quark masses of 5, 10, 20 and 50  $\text{Gev}/c^2$ . (the considered values of the quark mean free path in air being 80 or 240  $\text{g. cm.}^{-2}$  of air, and quark inelasticities of 0.5 or  $0.5 \frac{M_p}{M_q}$ ). Further calculations were carried out for intermediate masses where the shape of the velocity distribution

was changing rapidly with mass. Monte Carlo techniques were used throughout to represent the point of quark production and its ensuing propagation through the atmosphere, as well as to determine the quark energy at production.

The mode of calculation was as follows. An incident proton was chosen and a path length to its first interaction in  $\text{g. cm.}^{-2}$  of air was chosen at random, according to a procedure which established probabilities appropriate to the accepted proton mean free path of  $80 \text{ g. cm.}^{-2}$  of air. At this interaction point a quark was assumed to be produced and its energy was chosen such that the energy distribution of all such assigned energies throughout the calculation corresponded to the quark production spectrum given in Equation 5.4. The quark was then followed through a series of collisions, the path lengths between each again chosen at random according to a procedure which established probabilities appropriate to the quark mean free path being used at that time. The energy loss due to ionisation was continuously subtracted and at each collision the quark energy was degraded by  $K_q E_q$ , where  $K_q$  is the relevant quark inelasticity, while  $E_q$  was greater than the pion production threshold. When  $E_q$  fell below this value the energy lost in the interaction is given by Equation 5.9, and this was taken into account. The velocity of the quark was noted as it passed prescribed levels and it was followed until it finally stopped, the stopping point being noted. The whole procedure was then repeated beginning with another proton, following the produced quark until it stopped, and then beginning with another proton.

To take account of quark production from succeeding nucleon generations the whole procedure was repeated for contributions from the first ten generations of nucleons. In evaluating each contribution the procedure is identical with

before apart from the incident proton being allowed to traverse  $(n+1)$  mean free paths (for the contribution from the  $n^{\text{th}}$  generation), where each path length was chosen at random as before, before quark production was allowed. Finally the contributions from all generations were summed and the velocity distributions of quarks at prescribed levels and the rate at which they stopped were obtained.

### 5.5. Results of the calculations.

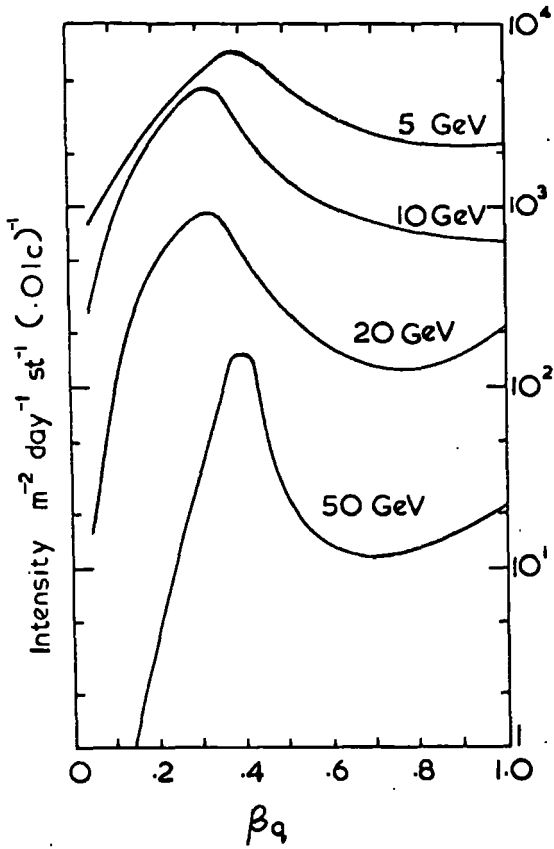
Due to the extent of the calculations only a representative sample of the results can be presented. It should be noted at the outset that the absolute rates evaluated refer to an assumed nucleon-nucleon cross section of 30 mb. for quark production. While this is hardly likely to represent the true situation the results can be directly normalised to take account of any assumed cross section. Further, while the calculations have been performed for quarks of charge  $\frac{2}{3}e$ , the uncertainties in the models used make the calculations almost equally valid for charges of  $e$  and  $\frac{1}{3}e$ .

Figure 5.1. shows the differential velocity distributions of quarks, in the vertical direction, at sea level. For the models where the quark inelasticity was taken as  $0.5M_p/M_q$  the results are given in tabular form since in these cases all quarks have velocities very close to  $c$  at sea level. Figures 5.2 and 5.3 show the intensity of quarks having velocities in the range  $0 < \beta_q < 0.75$ , and Figure 5.4 and 5.5 the intensity of quarks with velocities of  $\beta_q > 0.75$  as a function of the amount of air, in  $\text{g. cm.}^{-2}$ , traversed. However the results are essentially insensitive to the medium considered in light of the uncertainties in other parameters in the models. Finally the rate at which quarks stop is shown in Figures 5.6 and 5.7

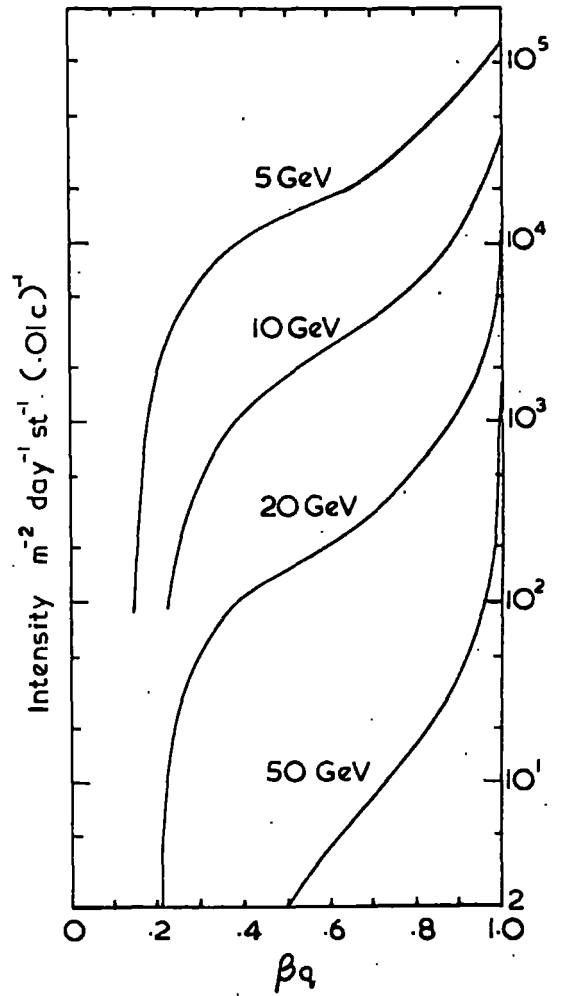
### 5.6. Limits on the quark production cross section imposed by the present work.

The velocity distributions of quarks at sea level, given in Figure 5.1,

(i)



(ii)



(iii)

MASS (GeV/c <sup>2</sup> )	Sea level intensity m <sup>2</sup> day <sup>-1</sup> sterad <sup>-1</sup> with velocity > β	Minimum β at sea level	
		L=80 g cm <sup>2</sup>	L=240 g cm <sup>2</sup>
5	2.5 10 <sup>6</sup>	0.8	0.96
10	3.68 10 <sup>5</sup>	0.9	0.99
20	4.71 10 <sup>4</sup>	0.99	0.99
50	2.78 10 <sup>3</sup>	0.99	0.99

Figure 5.1

The velocity distributions of quarks at sea level for production via  $NN \rightarrow NNq\bar{q}$ .

(i)  $K_q = 0.5$ ;  $\lambda_q = 80 \text{ g} \cdot \text{cm}^{-2}$

(ii)  $K_q = 0.5$ ;  $\lambda_q = 240 \text{ g} \cdot \text{cm}^{-2}$

(iii)  $K_q = 0.5 M_p / M_q$ ;  $\lambda_q = 80 \text{ or } 240 \text{ g} \cdot \text{cm}^{-2}$

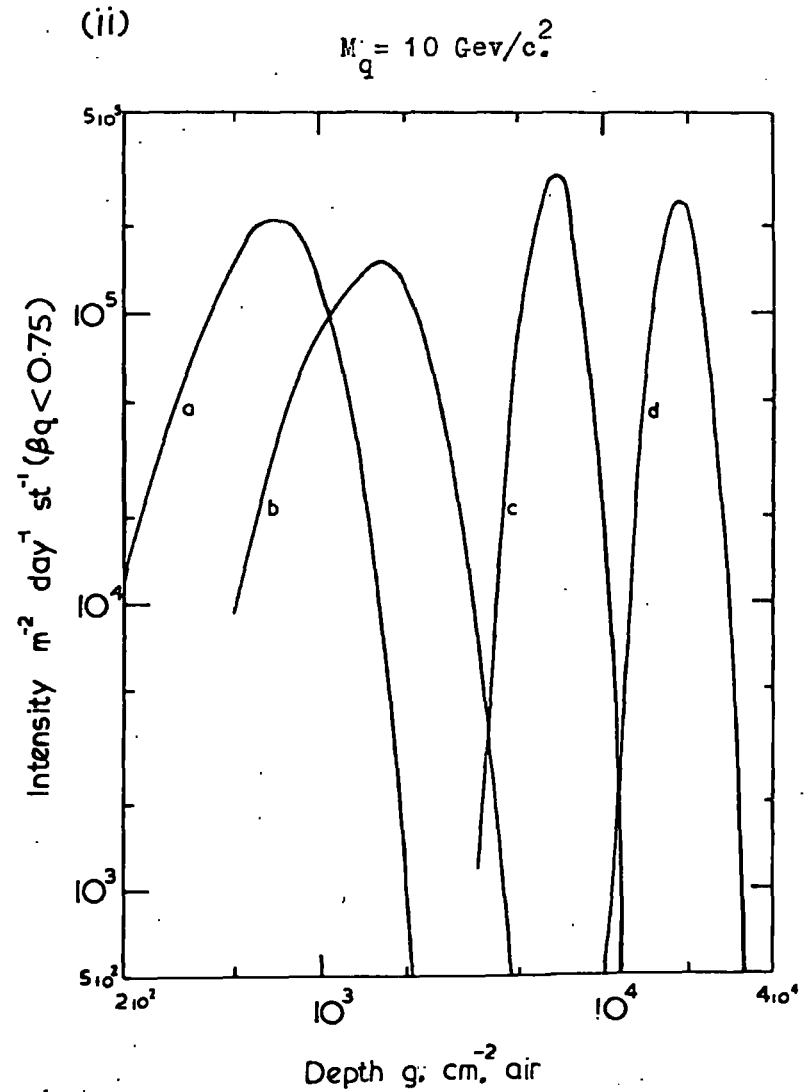
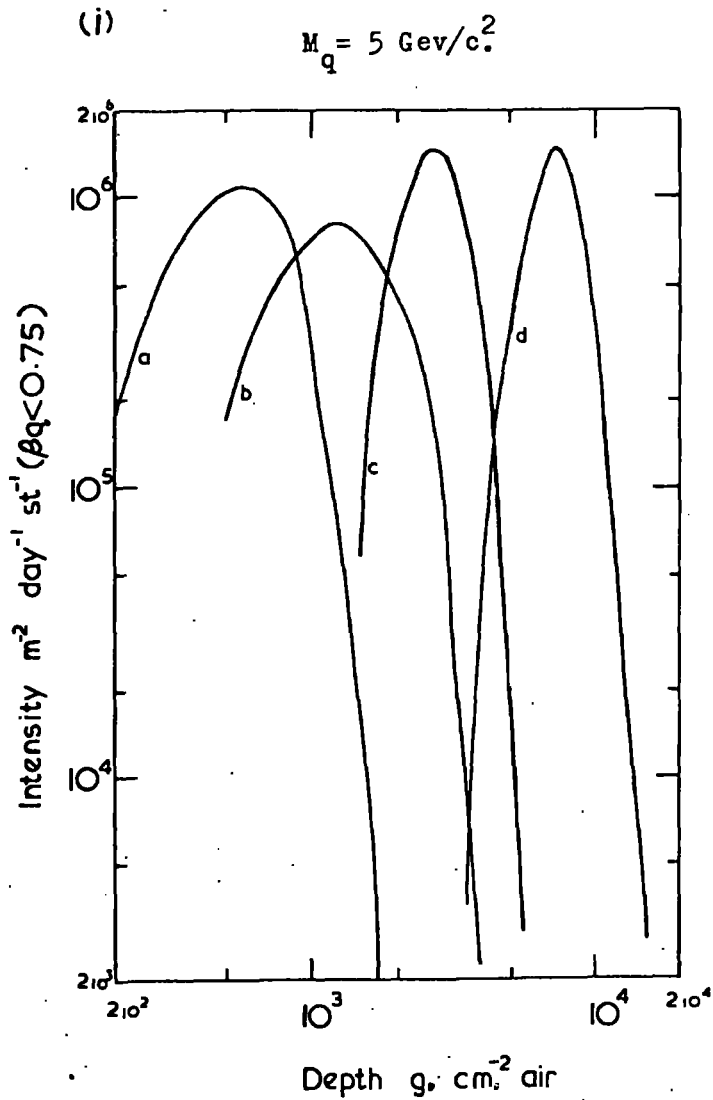


**Figure 5.2** The intensity of quarks with  $\beta_q < 0.75$  as a function of the amount of matter traversed.

(a)  $K_q = 0.5$ ;  $\lambda_q = 80 g \cdot \text{cm}^{-2}$     (b)  $K_q = 0.5$ ;  $\lambda_q = 240 g \cdot \text{cm}^{-2}$     (c)  $K_q = 0.5 M_p / M_q$ ;  $\lambda_q = 80 g \cdot \text{cm}^{-2}$

(d)  $K_q = 0.5 M_p / M_q$ ;  $\lambda_q = 240 g \cdot \text{cm}^{-2}$

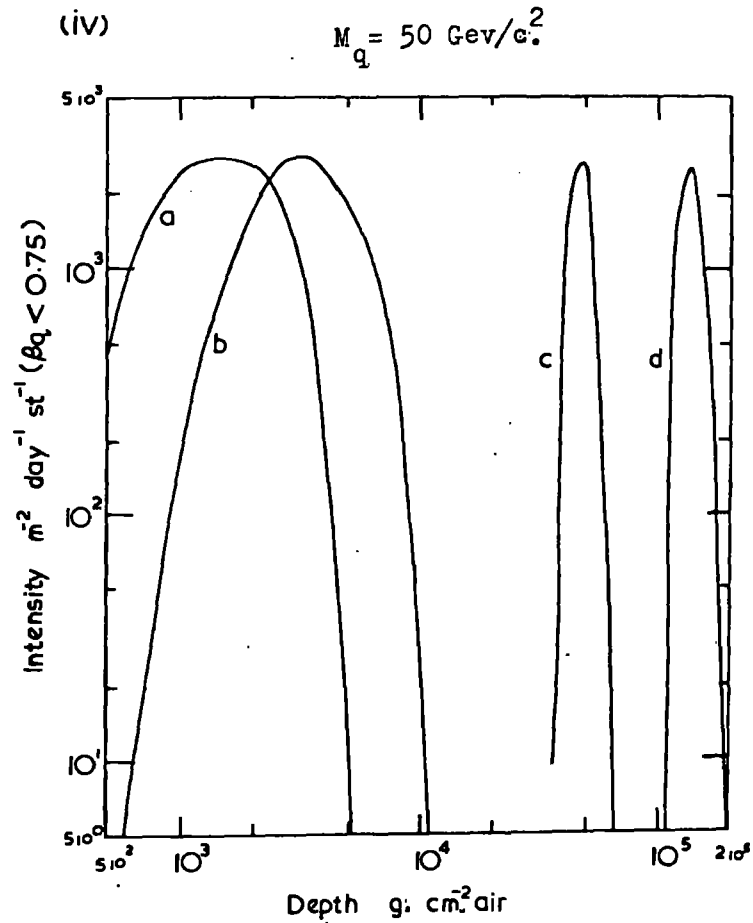
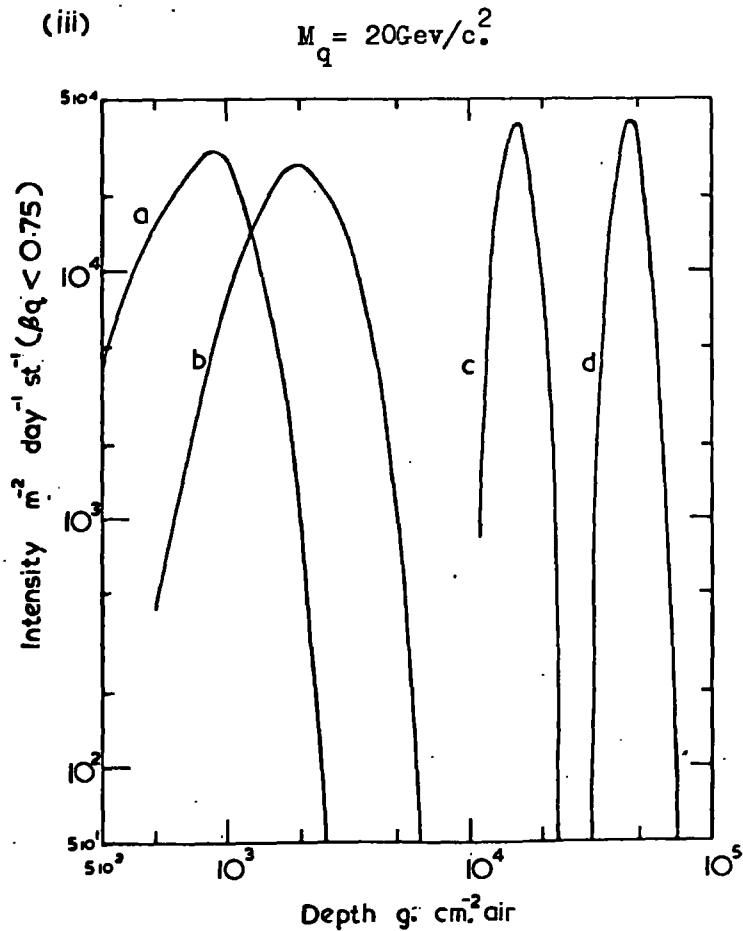


Figure 5.3 The intensity of quarks with  $\beta_q < 0.75$  as a function of the amount of matter traversed.

(a)  $K_q = 0.5$ ;  $\lambda_q = 80 \text{ g} \cdot \text{cm}^{-2}$     (b)  $K_q = 0.5$ ;  $\lambda_q = 240 \text{ g} \cdot \text{cm}^{-2}$     (c)  $K_q = 0.5 M_p / M_q$ ;  $\lambda_q = 80 \text{ g} \cdot \text{cm}^{-2}$

(d)  $K_q = 0.5 M_p / M_q$ ;  $\lambda_q = 240 \text{ g} \cdot \text{cm}^{-2}$

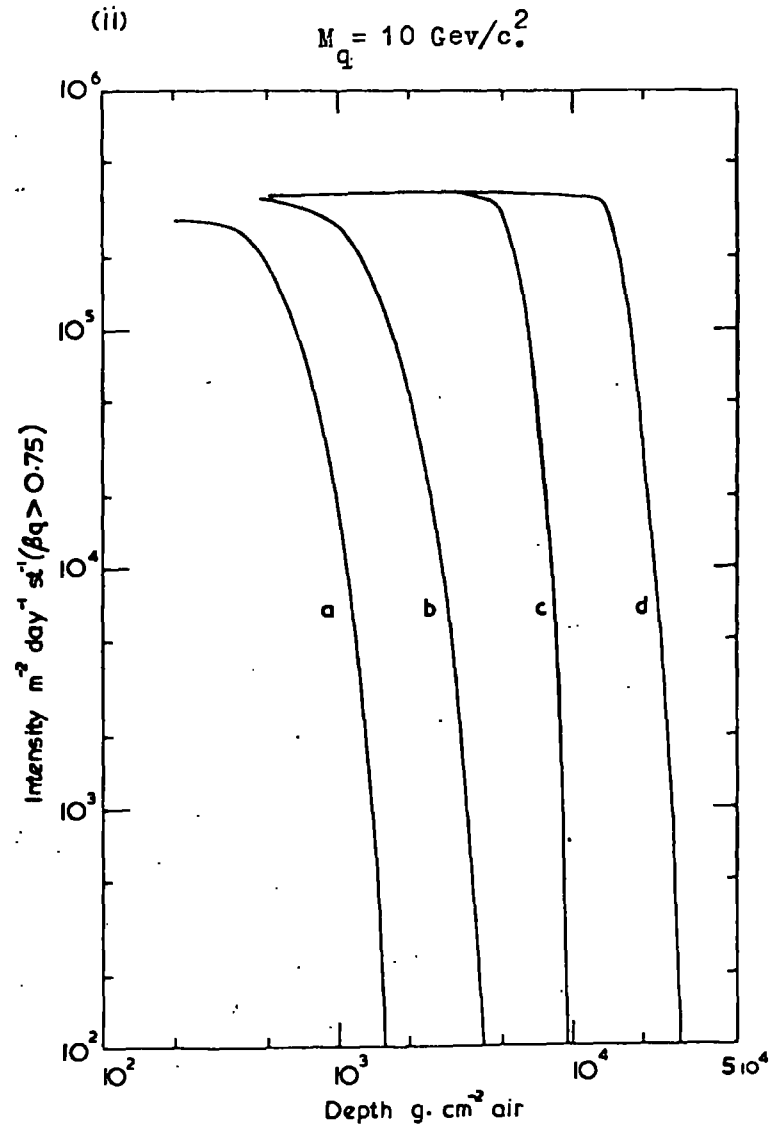
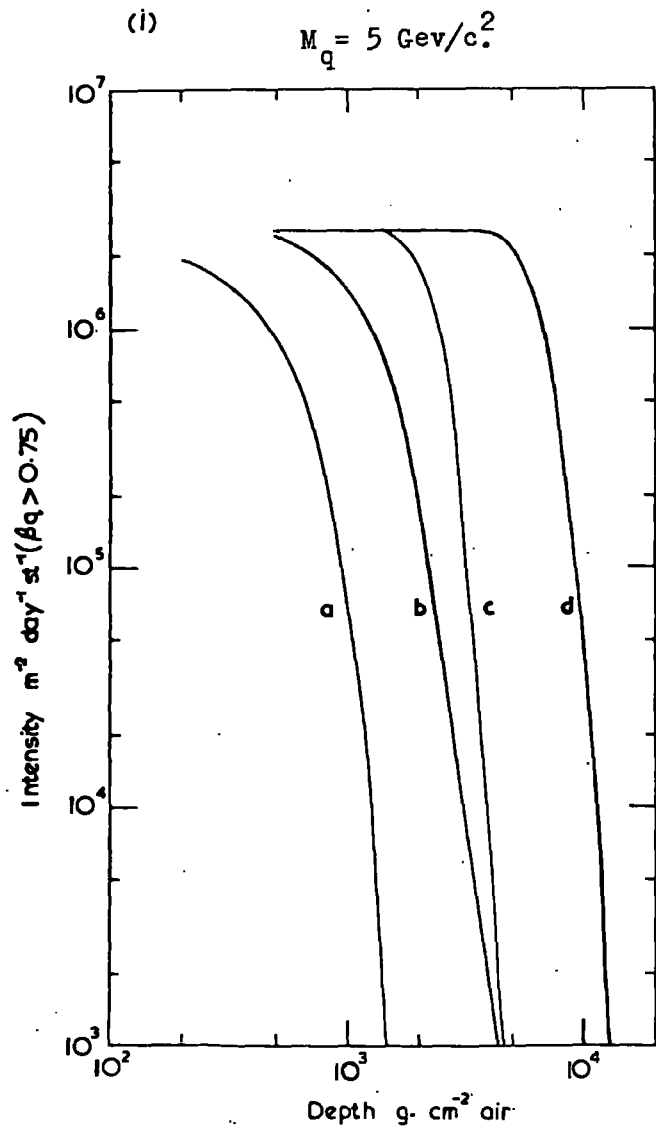
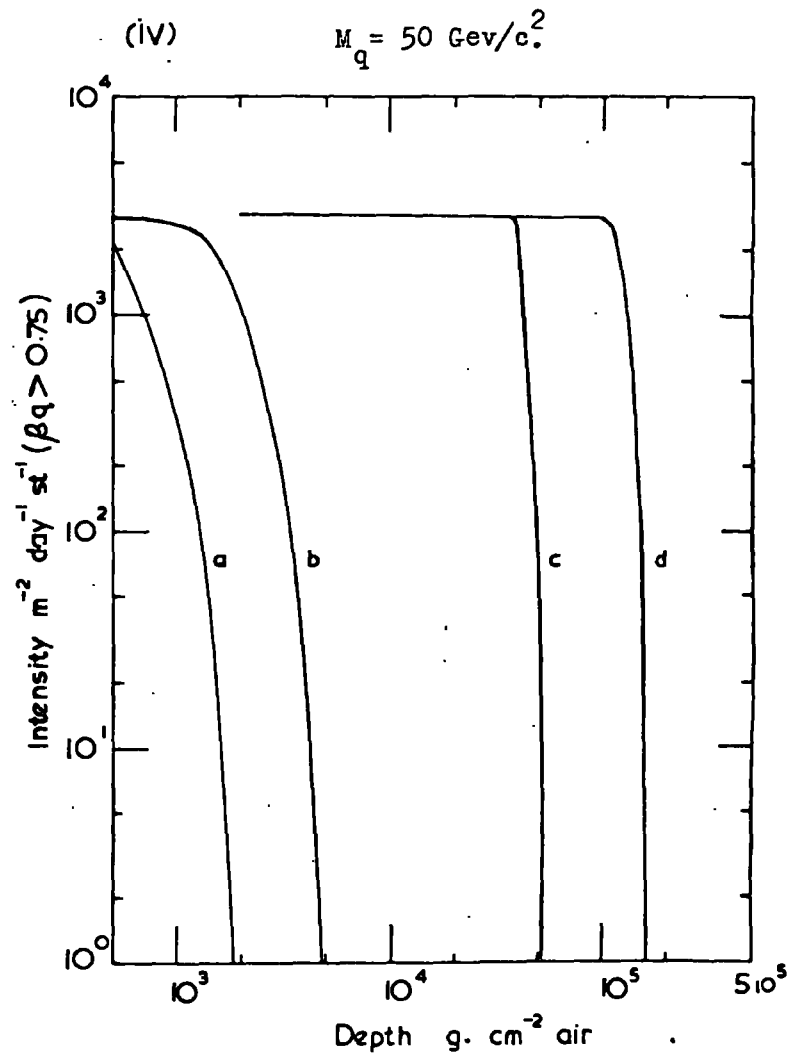
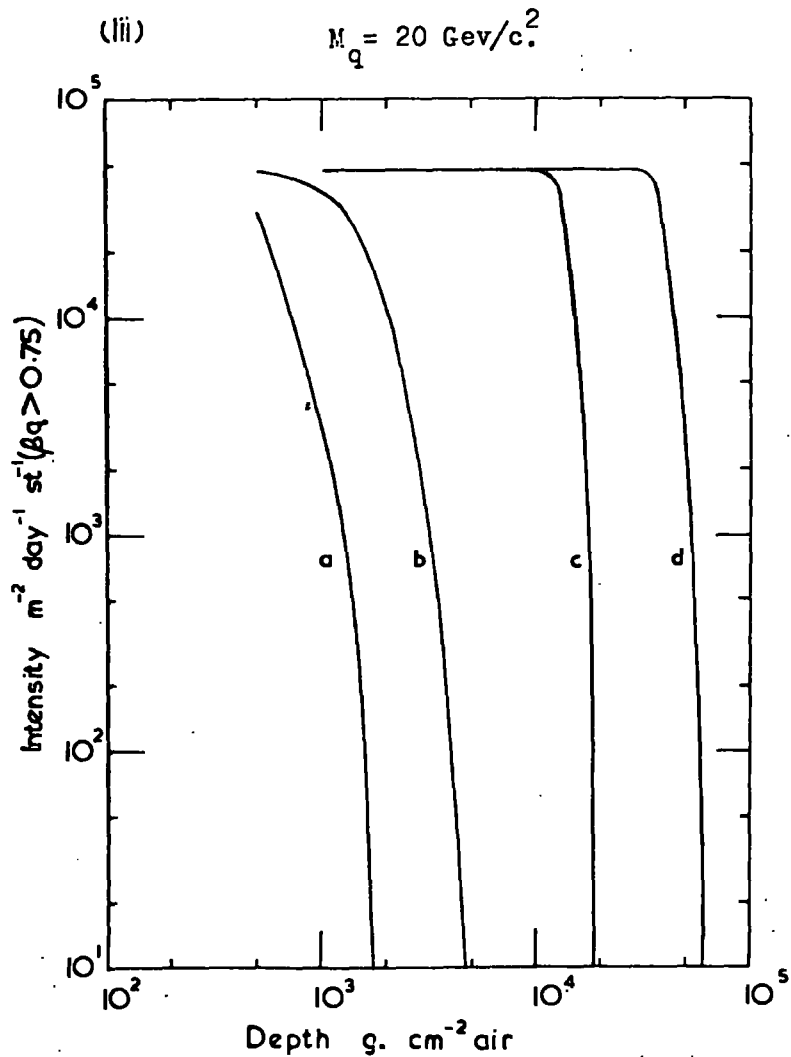


Figure 5.4 The intensity of quarks with  $\beta_q > 0.75$  as a function of the amount of matter traversed.  
 (a)  $K_q = 0.5$ ;  $\lambda_q = 80 \text{ g. cm}^{-2}$       (b)  $K_q = 0.5$ ;  $\lambda_q = 240 \text{ g. cm}^{-2}$       (c)  $K_q = 0.5 M_p / M_q$ ;  $\lambda_q = 80 \text{ g. cm}^{-2}$   
 (d)  $K_q = 0.5 M_p / M_q$ ;  $\lambda_q = 240 \text{ g. cm}^{-2}$



**Figure 5.5** The intensity of quarks with  $\beta_q > 0.75$  as a function of the amount of matter traversed.  
 (a)  $K_q = 0.5$ ;  $\lambda_q = 80 \text{ g. cm}^{-2}$       (b)  $K_q = 0.5$ ;  $\lambda_q = 240 \text{ g. cm}^{-2}$       (c)  $K_q = 0.5 M_p / M_q$ ;  $\lambda_q = 80 \text{ g. cm}^{-2}$   
 (d)  $K_q = 0.5 M_p / M_q$ ;  $\lambda_q = 240 \text{ g. cm}^{-2}$

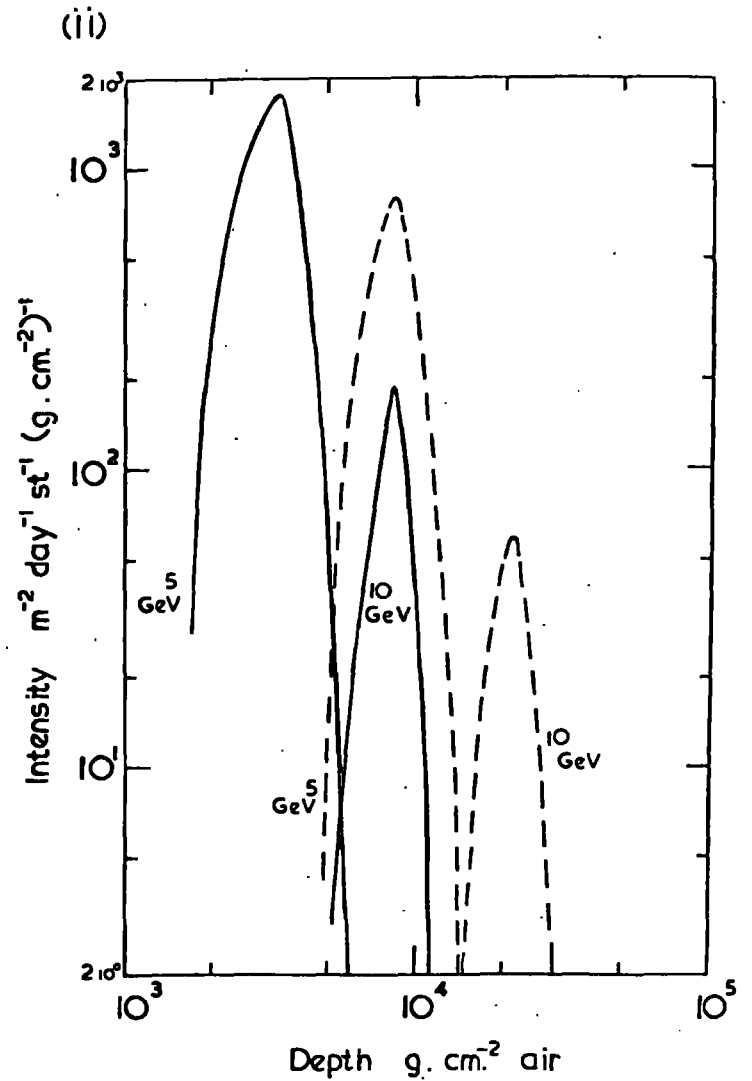
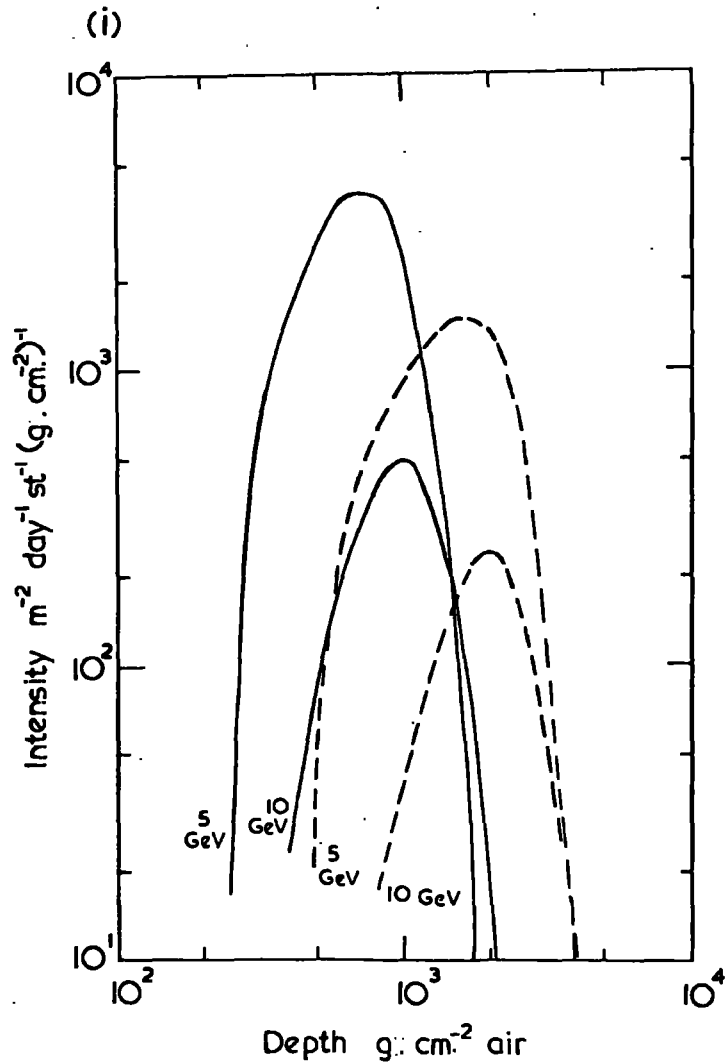


Figure 5.6 The stopping distributions of quarks.

(i)  $K_q = 0.5$ ;      (ii)  $K_q = 0.5 M_p / M_q$

$\lambda_q = 80 \text{g} \cdot \text{cm}^{-2}$  — full line;

$\lambda_q = 240 \text{g} \cdot \text{cm}^{-2}$  ----- dashed line.

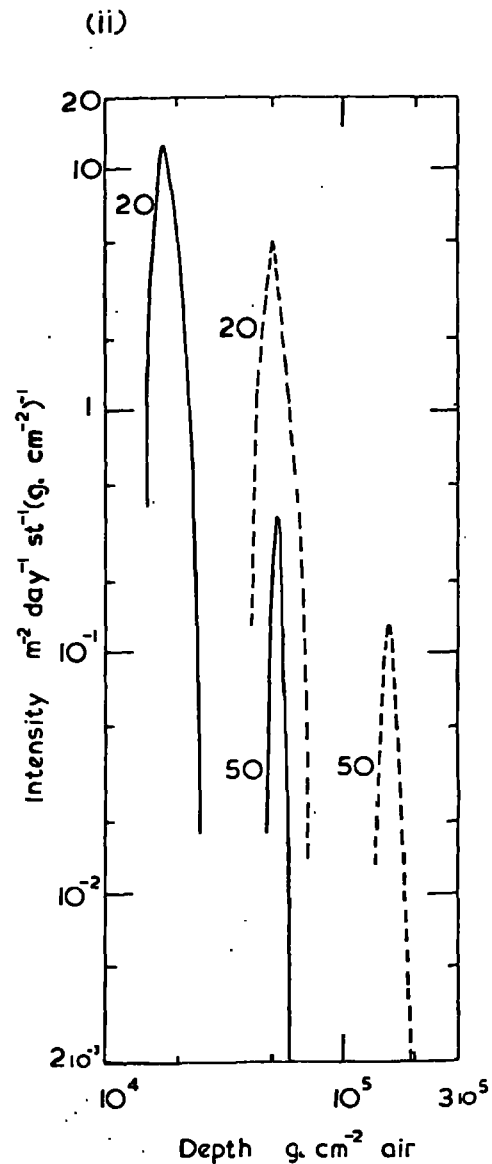
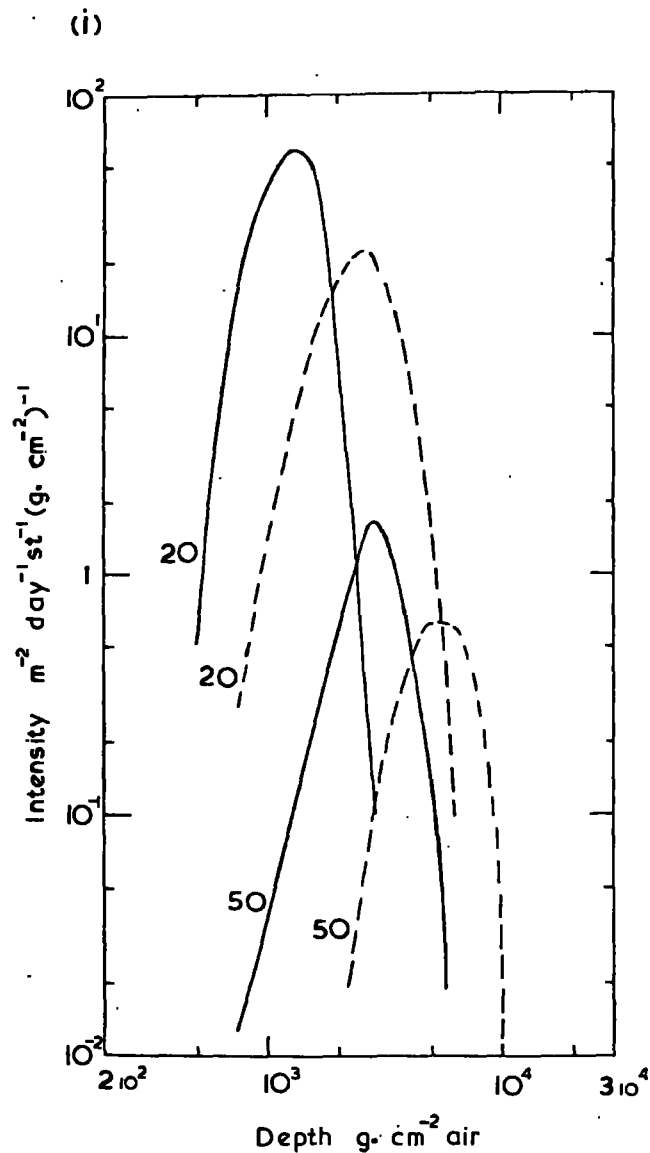


Figure 5.7

The stopping distributions of quarks.  
 (i)  $K_q=0.5$ ; (ii)  $K_q=0.5M_p/M_q$ ;

$\lambda_q=80\text{g.cm}^{-2}$  — full line;

$\lambda_q=240\text{g.cm}^{-2}$  - - - - - dashed line.

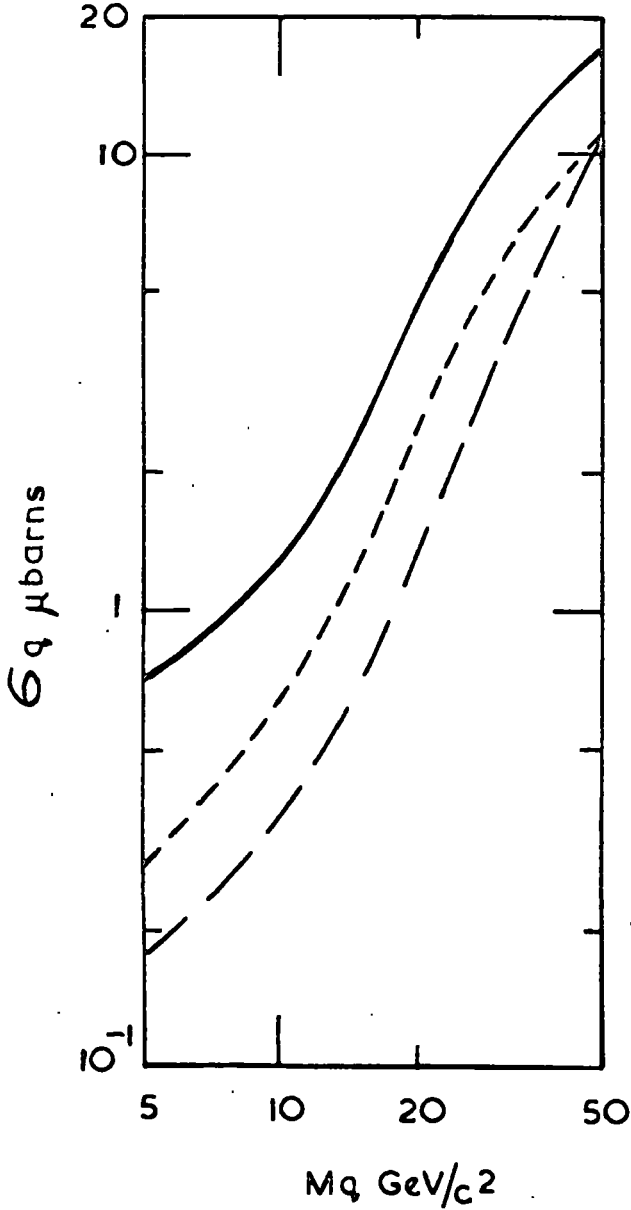
together with the sensitive velocity bands as a function of quark mass for charges of  $e$ ,  $\frac{2}{3}e$  and  $\frac{1}{3}e$ , given in Figure 4.8, for the heavy mass search can be used to evaluate the expected rate of quarks traversing the detector under the assumption of a 30 mb. cross section for quark production. The upper limits to their observed intensity of  $1.0 \cdot 10^{-9} \text{ cm.}^2 \text{ sec.}^{-1} \text{ sterad.}^{-1}$ , when compared with the calculated intensity, yields directly the upper limit to the production cross section at the 90% confidence level.

The results of such an analysis are shown in Figure 5.8, where the upper limit to the quark production cross section as a function of quark mass is given for charges of  $e$ ,  $\frac{2}{3}e$  and  $\frac{1}{3}e$ , for propagation models assuming the quark inelasticity to be 0.5 and the quark interaction length to be 80 g. cm.<sup>-2</sup> or 240 g. cm.<sup>-2</sup> of air. The present search would not have been sensitive to quarks having interaction properties, as discussed earlier, such that the quark inelasticity in an interaction was  $0.5M_p/M_q$  as such quarks at sea level would still have velocities very close to  $c$  as can be seen from Figure 5.1.

The cross section limits given in Figure 5.8 have not taken account of quarks lost through interactions in the telescope. Such losses will have the affect of increasing the derived limits and they must be estimated under the same model of quark interaction with matter as was used to obtain the propagation of quarks in the atmosphere and the cross section limits. Due to the energy loss through ionisation being sizeable at velocities encountered in the present experiment, the usual simple model of attenuation cannot be used here to determine the reduced detection efficiency resulting from interactions, and for this reason a Monte Carlo calculation was performed.

To simplify the calculation the telescope was assumed to be uniform and comprised 2.82 nucleon inelastic interaction lengths (Section 4.8) and, for purposes of energy loss through ionisation, 267 g. cm.<sup>-2</sup> water equivalent.

(i)



(ii)

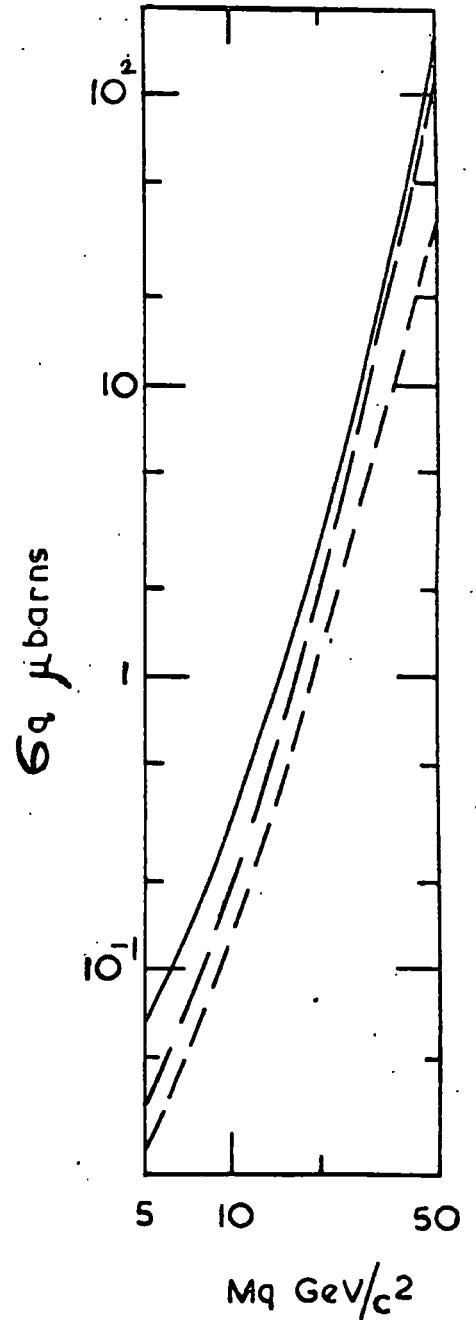


Figure 5.8

Limits on the quark production cross section, for production via  $NN \rightarrow NNq\bar{q}$ , derived from the heavy mass experiment (without corrections for interactions).

(i)  $K_q = 0.5$ ;  $\lambda_q = 80 \text{ g.cm.}^{-2}$       (ii)  $K_q = 0.5$ ;  $\lambda_q = 240 \text{ g.cm.}^{-2}$

—  $z = 1$ ;    - - - - -  $z = \frac{2}{3}$ ;    - · - · -  $z = \frac{1}{3}$ .

The method of calculation was as follows. An incident quark was chosen and its velocity at the telescope was chosen at random according to a procedure which established probabilities appropriate to the expected velocity spectrum of quarks for that particular propagation model being considered (Figure 5.1). A path length to its first interaction was chosen at random, again according to a procedure which gave probabilities appropriate to the quark mean free path being considered. If this interaction point fell within either of the Cerenkov counters, and the quark energy was greater than the pion production threshold (defined in Equation 5.8) the quark was assumed to be lost since a large veto pulse would be expected from the Cerenkov counters. If the above conditions were not satisfied the energy loss due to ionisation in reaching the interaction point was subtracted and the quark energy then further degraded by  $K_q E_q$ , where  $K_q$  is the inelasticity, if the quark energy was greater than the pion production threshold, or if not by the amount typical of an elastic interaction (Equation 5.9). A further path length to the next interaction was chosen and the quark subjected to the same conditions as before. This procedure was repeated until either the quark stopped, and was hence lost, or emerged from the detector and was accepted. After the quark had been lost or accepted the whole procedure was repeated, each repetition beginning with a new quark having a different velocity.

The calculation was performed for two models of the quark interaction with matter (a quark inelasticity of 0.5 and an interaction length the same as or three times that of a nucleon) for quark charges of  $e$ ,  $2e/3$  and  $e/3$ , having masses in the range  $5 - 50 \text{ GeV}/c^2$ . The resulting reduced detection efficiency as a function of mass for each charged state and for each propagation model is shown in Figure 5.9. The corrected quark production cross section limits are given in Figure 5.10 and are more valid than those



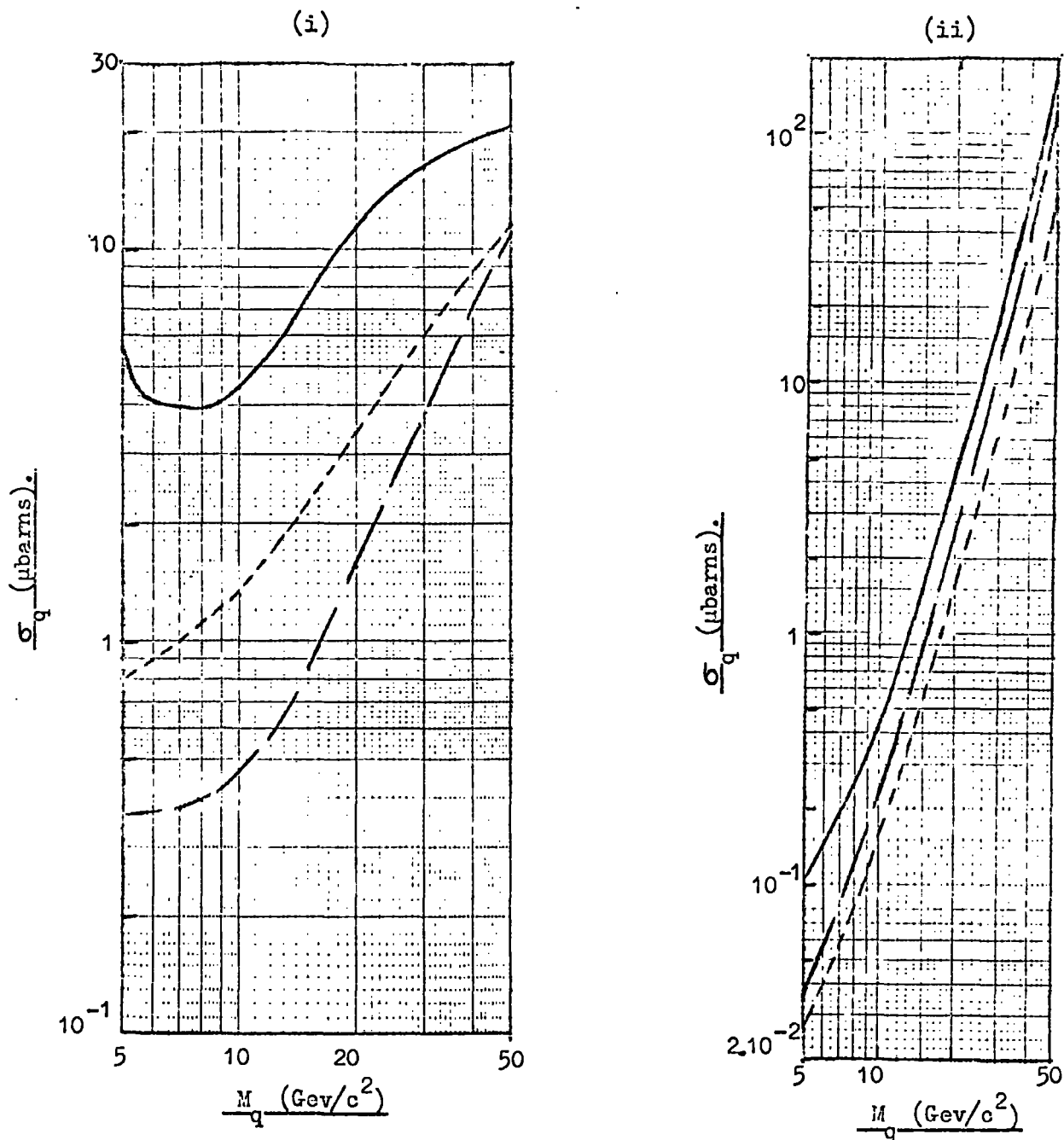


Figure 5.10

Limits on the quark production cross section, for quarks produced via  $NN \rightarrow NNq\bar{q}$ , from the heavy mass experiment after correction for interactions in the telescope.

(i)  $K_q = 0.5$ ;  $\lambda_q = 80 \text{ g. cm.}^{-2}$       (ii)  $K_q = 0.5$ ;  $\lambda_q = 240 \text{ g. cm.}^{-2}$

—  $z = 1$ ;      - - -  $z = \frac{2}{3}$ ;      - · -  $z = \frac{1}{3}$ .

given in Figure 5.8 in that they have been derived under a specific propagation model, and hence the quarks must be treated similarly while traversing the telescope.

### 5.7. Quark production via nucleon dissociation.

Finally it is relevant for the sake of completeness to consider the consequences of quark production occurring predominantly through nucleon dissociation, as opposed to production in particle-antiparticle pairs.

Considering the reaction  $N + N \rightarrow 6q$

then the proton energy threshold for such a process is given by

$$E_{p_T} = 2 \cdot \left[ 9 \cdot \left( \frac{M_q}{M_p} \right)^2 - 1 \right] \cdot M_p c^2$$

Assuming as before that the produced quarks have zero momentum in the centre of mass and that the production cross section is constant above the threshold energy, the production spectrum is identical with that given in Equation 5.4, apart from the factor of 2 which took account of quark-antiquark production. In the present case the situation is slightly different. Averaging over pp and pn collisions the average number of quarks produced per interaction is 6 in the unit charge representation, and 3.5 of charge  $2e/3$  and 2.5 of charge  $e/3$  in the fractional charge case. Thus the only difference in the spectrum is the factor of 2 which has to be replaced by one of the above numbers depending upon which quark representation is being considered. It should be further noted that the minimum quark energy at production is now  $\sim 3$  times greater than before and is given by

$$E_{q_{min}} = \left[ \frac{3M_q}{M_p} - 1 \right] M_q c^2.$$

The immediate consequence of considering production via this channel is that the total produced quark intensity of a specific charge is reduced, for  $M_q \gg M_p$ ,

by a factor of  $\sim 10$  (for unit charges) or  $\sim 20$  (for fractional charges) compared with production through quark-antiquark pairs, the reduction being due to the increased proton threshold energy and the integral energy spectrum of primary protons falling as  $E_p^{-1.58}$ . Assuming no attenuation of quarks in the atmosphere and that the quark remains in its produced charged state, the cross section limits from experiments sensitive to quarks suffering little or no attenuation, derived in terms of quark-antiquark production, should be increased by the reduction factors given above to be relevant to quark production through nucleon dissociation.

However the cross section limits imposed by the present experiment in terms of such production cannot be so simply evaluated, as they are particularly dependent upon the quark velocity distribution pertaining at sea level. For this reason the velocity distribution of quarks produced in this way has been evaluated at sea level using the same Monte Carlo methods as discussed in Section 5.4, for propagation models of the quark inelasticity being 0.5, and its interaction length being the same and three times that of a nucleon, for quark masses in the range 5 - 50 Gev/c<sup>2</sup>. For propagation models where the quark inelasticity is taken as  $0.5M_p/M_q$ , all quarks at sea level have velocities close to  $c$  and would not have been detected by the present experiment. The velocity distributions are given in Figure 5.11 and the absolute rates are for an assumed production cross section of 30 mb. and apply to the case of unit charged quarks. The rates have to be reduced by 1.7 and 2.4 to take account of fractional charges of  $2e/3$  and  $e/3$  respectively. In the manner described in Section 5.6 limits have been imposed on the production cross section for each charged state and have been corrected to take account of interactions in the telescope. The resulting limits are given in Figures 5.12 and 5.13 giving the limits before and

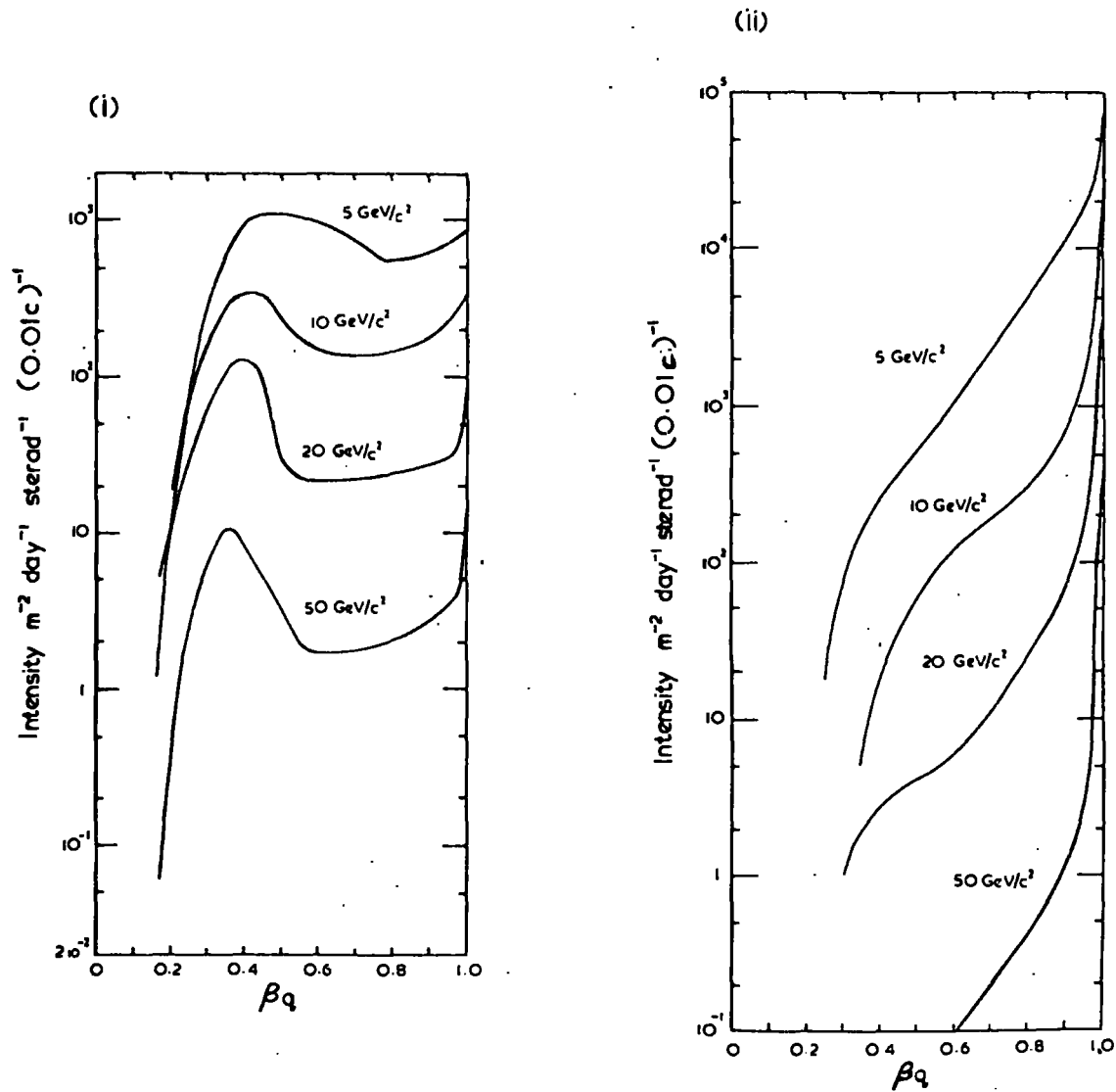


Figure 5.11

The velocity distributions of quarks, produced via total nucleon dissociation ( $NN \rightarrow 6q$ ), at sea level.

(i)  $K_q = 0.5$ ;  $\lambda_q = 80 \text{ g.cm}^{-2}$

(ii)  $K_q = 0.5$ ;  $\lambda_q = 240 \text{ g.cm}^{-2}$

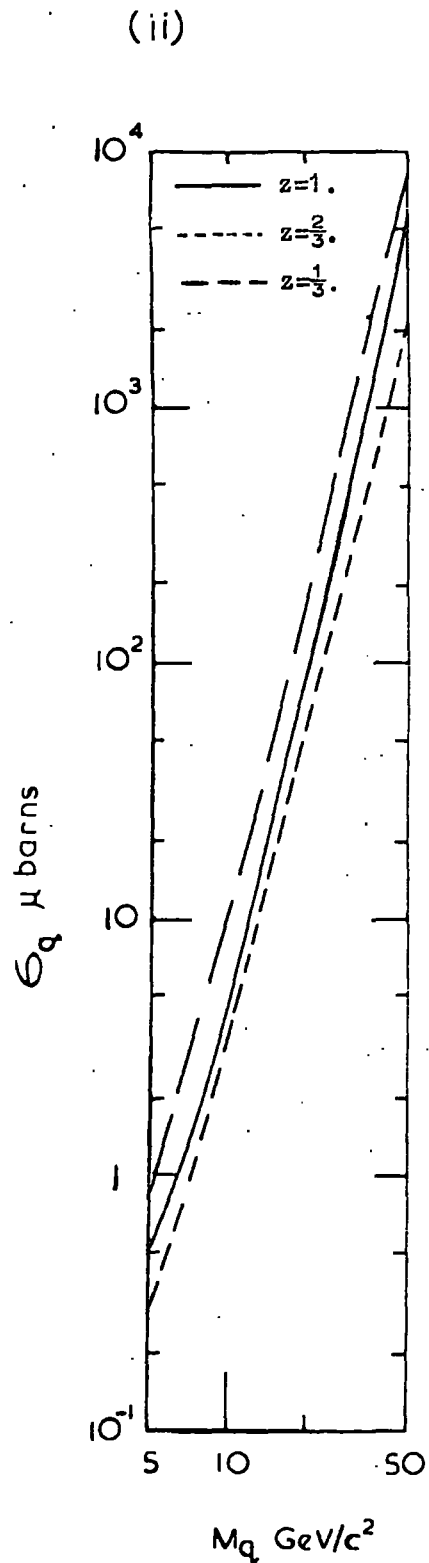
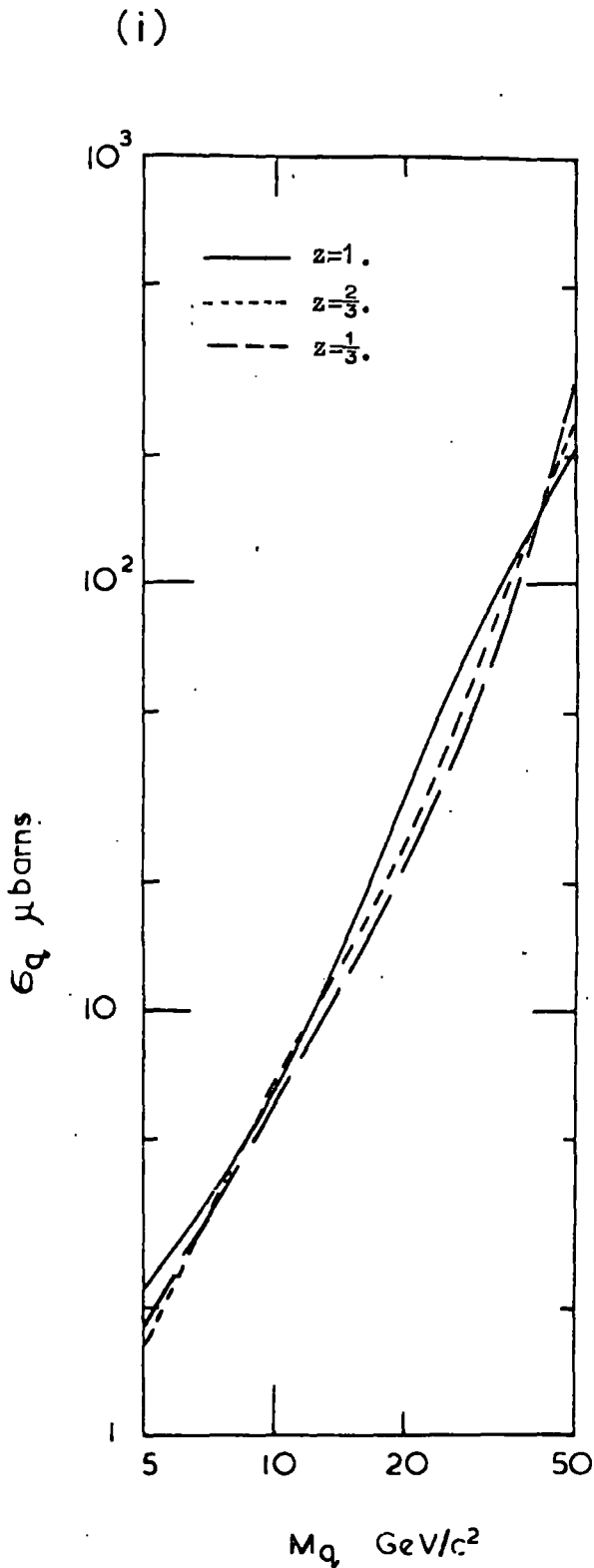


Figure 5.12 Limits on the quark production cross section, for production via total nucleon dissociation ( $NN \rightarrow 6q$ ), from the heavy mass experiment (before correction for interactions).

(i)  $K_q=0.5$ ;  $\lambda_q=80\text{g.cm.}^{-2}$       (ii)  $K_q=0.5$ ;  $\lambda_q=240\text{g.cm.}^{-2}$

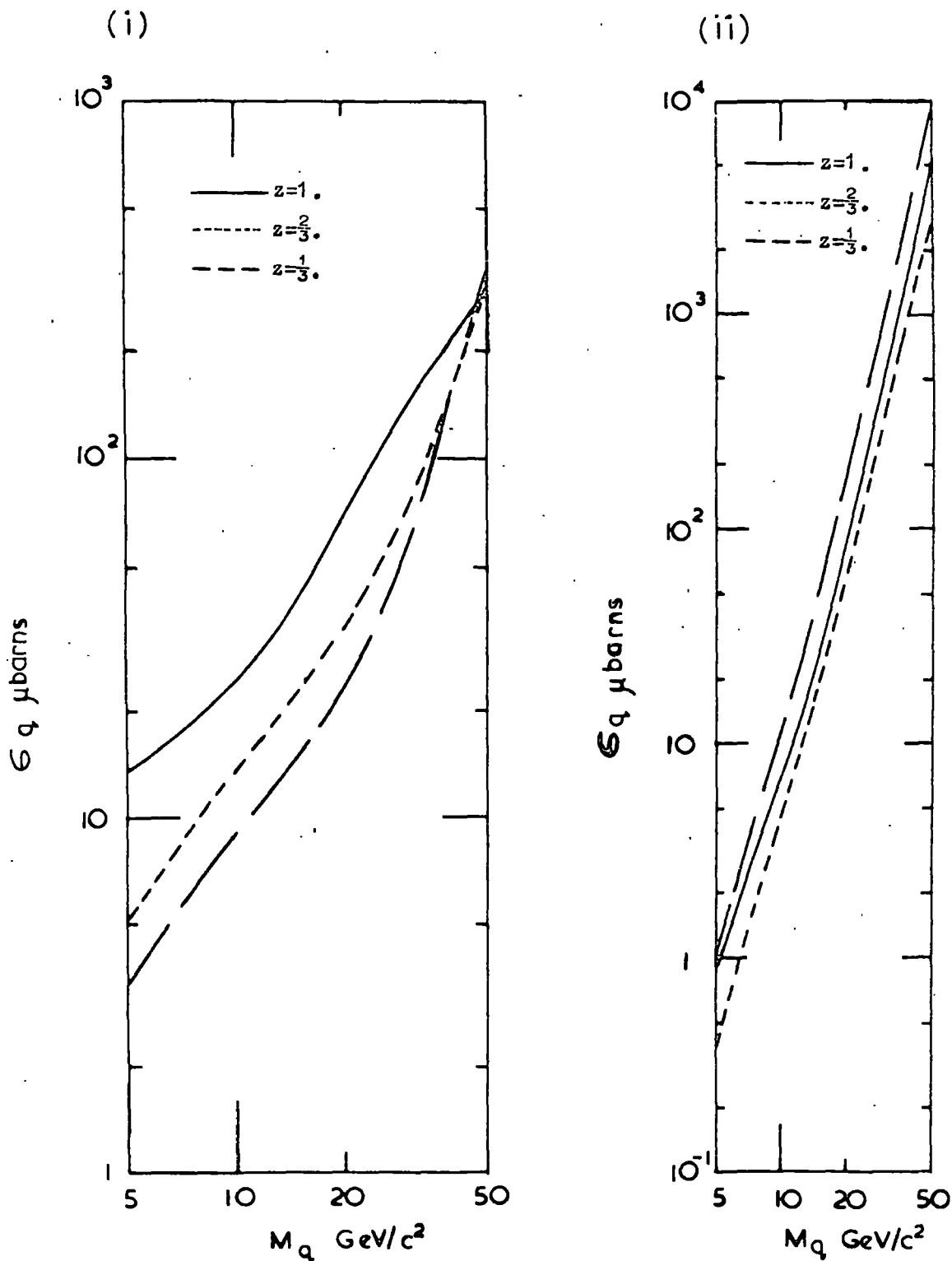


Figure 5.13

Limits on the quark production cross section, for production via total nucleon dissociation ( $NN \rightarrow 6q$ ), from the heavy mass experiment, after correction for interactions in the telescope.

(i)  $K_q=0.5; \lambda_q=80\text{g.cm.}^{-2}$

(ii)  $K_q=0.5; \lambda_q=24.0\text{g.cm.}^{-2}$

after correction for interactions respectively.

### 5.8. Summary.

Four plausible models of the quark interaction with matter have been considered and their consequences on the velocity distribution as a function of the amount of matter traversed and the stopping rate of quarks have been evaluated for a production model assuming quarks to be produced in particle-antiparticle pairs. The derived velocity distributions at sea level have been used to give limits on the quark production cross section subject to the interaction models to which the present experiment was sensitive. Quark production through nucleon dissociation has been more briefly considered and again cross section limits imposed as a consequence of the present experimental intensity limits and the predicted sea level velocity distributions. Further, in Appendix A, the intensity limits obtained in the experiment of Ashton et al., 1968 a, searching for relativistic fractionally charged particles, have been converted to cross section limits subject to these propagation models for quark production through nucleon dissociation, as well as through particle-antiparticle production.

It should be noted that the results obtained, when using a propagation model of the quark inelasticity being  $0.5M_p/M_q$  and the interaction length being  $80 \text{ g.cm.}^{-2}$  of air, are consistent with the results of Adair and Price who used similar values in their unique model of propagation.

The calculations, albeit for a limited number of quark interaction models, form the basis from which one can assess the most profitable areas for future quark searches, as well as assessing the relative merits of the experiments already performed. Further discussion will be given to this problem in Section 6.5 but at the same time one should not lose sight of the possibility of the quark having a much stronger interaction with matter

than has been considered here, as being the cause of their non-observation in cosmic ray experiments at sea level.

## CHAPTER 6

### REVIEW OF QUARK SEARCHES

#### 6.1. Introduction

The experiments performed in the pursuit of quarks are numerous and it is intended to review them with respect to establishing limits on their production cross section, subject to the propagation models proposed in Chapter 5, and to compare these with the various theoretical estimates as to what the cross sections might be. Such an analysis is necessary for quark searches in the cosmic radiation and in various materials; however the searches at the accelerators yield production cross sections directly.

#### 6.2. Review of quark searches.

##### 6.2.1. Searches at the proton accelerators.

The obvious place at which quark searches should begin was in the secondary beams at the proton accelerators, despite the limitations imposed there on the quark mass by presently available accelerator energies. The first experiments performed to search for fractional charges used bubble chambers where tracks exhibiting low bubble density were sought (typical bubble densities of 2.2/cm. and 8.8/cm. being expected for charges of  $\frac{1}{3}$  and  $\frac{2}{3}$  respectively, compared with 20/cm. for unit charged particles.) In such experiments precautions had to be taken against spurious events resulting from particles spilling out of the accelerator before the bubble chamber reached its maximum sensitivity. The earlier experiments, not specifically designed for detecting fractional charges, overcame this problem by an analysis of long  $\delta$  rays (typically 2 on a 2 metre track in a hydrogen chamber) accompanying tracks showing low bubble density

and of the bubble size in such tracks (the bubble size would be expected to be larger on tracks of early particles, having had a longer time to grow). However the later experiments employed electronic techniques to positively identify early particles by displaying the arrival times of the beam particles together with the bubble chamber pressure cycle on an oscilloscope. The results of these bubble chamber experiments are given in Table 6.1.

The other searches at the accelerators employed counter techniques and were of two types; those measuring  $dE/dx$  (searching for fractional charges making use of  $dE/dx \propto z^2$ ); and those making velocity measurements (such measurements being capable of accepting any charge and relying on the mass of the quark being large, hence reducing its velocity at production). The experiments utilising  $dE/dx$  are similar to cosmic ray searches in using several layers of scintillator to measure energy loss. Those relying on velocity measurements used time of flight selection and in some cases electrostatic separation as well.

The only other notable feature of the accelerator experiments is the work of Dorfan et al., 1965, who used time of flight selection but also extended measurements of the quark production cross section to higher quark mass values than attainable from a proton interaction with a zero momentum nucleon by considering the Fermi momentum of the nucleons in the target nuclei, which was obtained by measuring the production of antiprotons as a function of the primary proton energy. Typically in this particular experiment the probability of there being a sufficiently high centre of mass energy to create a  $5\text{Gev}/c^2$  quark pair, when the maximum mass from a zero momentum nucleon is  $3\text{Gev}/c^2$ , is  $10^{-5}$ . The results of all the counter experiments are given in Table 6.2. In Figure 6.1 the cross section limits from all the accelerator experiments are compared

Table 6.1.

## Quark searches at the proton accelerators using bubble chambers.

Workers	Primary beam Energy Gev.	Target	Secondary beam		Bubble Chamber	Mass Range assumed for $\sigma_t$ estimate	Charge Sensitivity	$\sigma_{\text{total}}^{**}$ cm. <sup>2</sup> at 90% C.L.
			Angle mrad.	Momentum Gev/c				
Morrison, 1964	24.8	Al	70	10.7	30cm.H <sub>2</sub>	0.5-2.0Gev/c <sup>2</sup>	$-\frac{2}{3}, -\frac{1}{3}$	$< 4.10^{-34}$
Bingham et al., 1964	21.0	Cu	77	16.0	1m.C <sub>2</sub> F <sub>5</sub> Cl	1.0-2.0Gev/c <sup>2</sup>	$-\frac{2}{3}, -\frac{1}{3}$	$< 5.10^{-35}$
Hagopian et al., 1964	31.0	W	120	8.5	80'' H <sub>2</sub>	*	$+\frac{2}{3}$	$< 3.10^5 \pi$
							$+\frac{1}{3}$	$< 6.10^5 \pi$
Blum et al. 1964	27.5	Cu	76	20.0	81cm.H <sub>2</sub>	1.0 Gev/c <sup>2</sup>	$-\frac{2}{3}, -\frac{1}{3}$	$< 6.5.10^{-35}$
						2.0 Gev/c <sup>2</sup>	$-\frac{2}{3}, -\frac{1}{3}$	$< 2.0.10^{-35}$

N.B \* The results of Hagopian et al. are presented in terms of the equivalent number of pions (see Figure 6.1. for cross section limits).

\*\* The total cross sections were obtained under the assumption of isotropic quark production and a four body phase space for the momentum spectrum of quarks produced in the reaction  $pp \rightarrow pp + q\bar{q}$  to enable the total cross sections to be obtained from the differential cross sections.

Table 6.2

Quark searches employing counter techniques at the proton accelerators

Workers	Primary beam energy Gev.	Target	Secondary beam		Method	Charge Sensitivity	Mass Range	$\sigma_{\text{total}} \text{ cm}^2$
			Angle mrad.	Momentum Gev/c				
Leipuner et al., 1964	28.0	Be	0	All	dE/dx behind 1.6Kg. shield	$\pm \frac{1}{3}$	$< 2.6 \text{ Gev}/c^2$	$< 10^{-34}$
			314	4.5	dE/dx in the beam	$+\frac{1}{3}$	$< 1.8 \text{ Gev}/c^2$	$< 10^{-34}$
Franzini et al., 1965	30.0	W	120	7.0	Electrostatic separator + time of flight	$-\frac{2}{3}$ to -1	3 Gev/c <sup>2</sup>	$\sigma_q/\sigma_p < 10^{-3}$
							4 Gev/c <sup>2</sup>	$\sigma_q/\sigma_p < 0.3$
Dorfan et al., 1965	30.0	Be	76	9.0	Time of flight	$-\gg \frac{2}{3}$	3-7Gev/c <sup>2</sup>	*
		Fe	76	10.0				

\*See Figure 6.1 for cross section limits.

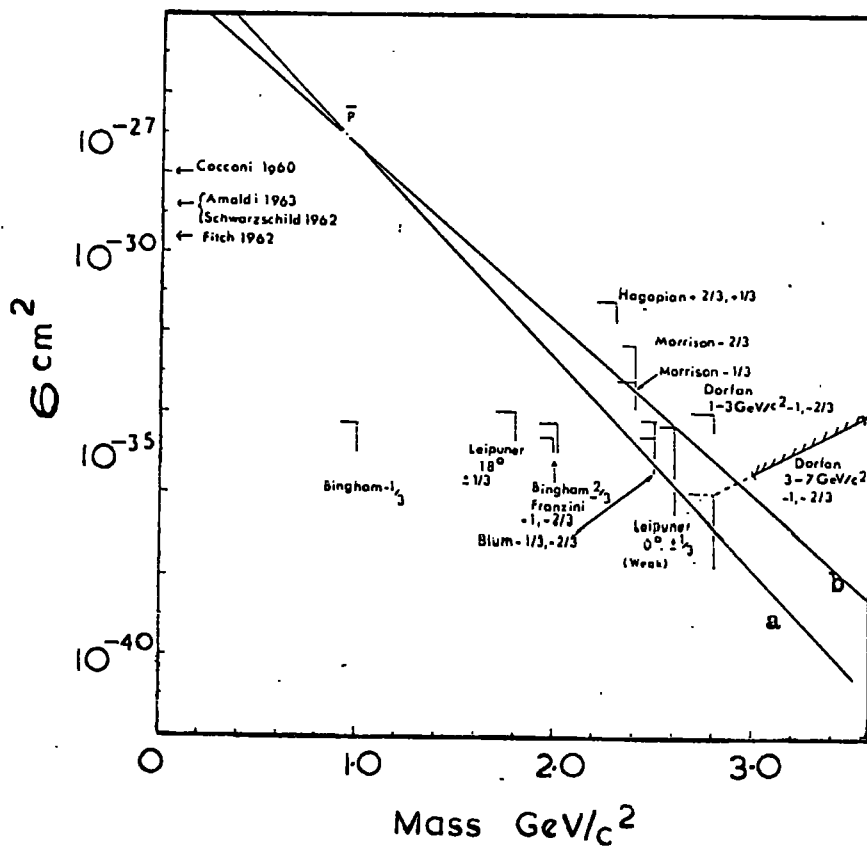


Figure 6.1

The experimental limits on the quark production cross section derived from searches at the proton accelerators (for quark production via  $NN \rightarrow NNq\bar{q}$ ). The vertical lines represent the maximum mass values that are kinematically possible, and the horizontal lines the upper limits to the cross section. The charged states to which each measurement applies are shown alongside the limit. The statistical model predictions of Masimenko et al. (a) and Hagedorn (b) are shown for comparison and they have been normalised to an antiproton production cross section of 1mb.. The Hagedorn curve has been drawn so as to pass half way between his two predictions at 3 GeV/c<sup>2</sup> (see Figure 6.11).

with the theoretical predictions of Masimenco et al., 1966, and Hagedorn, 1967, the figure being derived from a review of quark searches at the accelerators by Massam, 1968.

An analysis of Figure 6.1. shows that there is still room for improvement at the present accelerators, as even in the best cases the limits obtained are just about equal to the theoretical predictions. In fact for some of the possible charged states, particularly  $z = +\frac{2}{3}$ ,  $+1$ , the situation is very much worse, the limit for  $z = \frac{2}{3}$  being some  $10^3$  higher than the theoretical predictions at a mass of  $2.3 \text{ Gev}/c^2$ , and the limit for  $z = 1$  even worse than this. There is obviously a need for much improved experiments which should aim for limits significantly lower than the predicted cross sections in view of their uncertainties. However it may be felt that such searches are unjustified with the proton energies presently available, particularly if the quark mass is considered to be much higher than that kinematically possible from protons of such energies incident on zero momentum nucleons. Further consideration will be given later to possible future experiments at the proton accelerators.

#### 6.2.2 Searches at the electron accelerators.

If leptonic quarks existed then their production at the proton accelerators would be depressed relative to strongly interacting particles, as they would be predominantly produced in pairs through electromagnetic interactions. From an analysis of proton-antiproton annihilation into lepton pairs Massam, 1968, has shown that plausible estimates of the production cross section for leptonic quarks would be far too low for them to have been observed in the previously discussed searches at the proton accelerators. However such quarks would be more readily produced at the electron accelerators where photons are plentiful.

The production process comes from the photon flux (originating from electron bremsstrahlung in the target) producing pairs of charged particles by photoproduction on the nuclei and nucleons of the target. The pair production cross section is sharply dependent on mass (typically a reduction by a factor of  $10^9$  in going from a particle of mass  $0.105\text{Gev}/c^2$  to a particle mass of  $1.5\text{Gev}/c^2$ , both having integral charges), this arising predominantly from a  $q^4$  factor, where  $q$  is the four momentum transfer to the target, in the denominator of the production cross section, the value of  $q$  increasing with increasing mass of the produced pair. The reduction with mass is further intensified by form factors introducing polynomials in  $q^2$  to the denominator of the cross section. When searches are being made for sub-integral charges yet another reduction is experienced in the production, the cross section being dependent on  $z^4$ , where  $z$  is the particle charge. The cross section is relatively insensitive to other properties of the produced particles apart from whether or not they have a form factor, this again strongly reducing production.

Three experiments have been performed at the electron accelerators: Foss et al., 1967, using a 6 Gev bremsstrahlung beam incident on a target of 200 radiation lengths (r.l) of carbon; Bathow et al., 1967, using a 6 Gev electron beam incident on a target of 90 r.l. of lead followed by about 30 r.l of concrete; and Bellamy et al., 1968, using a 12 Gev electron beam incident on a target of 10 r.l. of copper followed by 6 r.l. of beryllium. Only the results of the experiment of Bellamy et al. will be discussed here in that their experiment, as well as establishing the lowest limits for  $z = \frac{2}{3}$  and  $\frac{1}{3}$ , also extended the search down to charges as low as  $z = 1/25$ . Further, they were also able to give limits even if the produced quarks were strongly interacting, due to the reduced amount of material in their beam compared with the other

workers. The sensitivity of the experiment down to charges of  $e/25$  was achieved by using 13 cm. thick sodium iodide crystals (giving a resolution of  $\pm 5\%$  for an energy deposit of 1Mev) rather than the commonly used plastic scintillator. The results of this experiment are given in Figure 6.2 where the lower mass limits imposed are shown as a function of  $z$  for cases of the produced particles being :- weakly interacting and stable; weakly interacting with a lifetime of  $10^{-8}$  seconds; and strongly interacting (assuming an interaction cross section of 25 mb/nucleon). The mass limits for  $z = \frac{2}{3}$  and  $\frac{1}{3}$  are summarised below in Table 6.3 for the several considered properties of the particles.

Table 6.3

Charge	Mass limits. $\text{Gev}/c^2$ at 95% confidence limits		
	weakly interacting and stable	weakly interacting, lifetime $10^{-8}$ sec.	strongly interacting.
$\frac{2}{3}$	1.5	1.1	0.75
$\frac{1}{3}$	1.0	0.75	0.5

It should be noted that in deriving these mass limits the produced particles were assumed to have spin  $\frac{1}{2}$  and to possess no form factor. If spins of  $< \frac{1}{2}$  are considered the mass limits should be slightly reduced while if spins  $> \frac{1}{2}$  are relevant the limits should be slightly raised. The assumption as to the absence of a form factor has more serious consequences. If a form factor reduction of about 500 is placed in the cross section, as observed in strong interactions (Massam, 1968; and Massam et al., 1966), the limits of 1.5 and 1.0  $\text{Gev}/c^2$  for assumed weakly interacting stable particles would be reduced to 1.1 and 0.65  $\text{Gev}/c^2$  for  $z = \frac{2}{3}$  and  $\frac{1}{3}$  respectively.

It would appear that searches for leptonic quarks at the electron accelerators cannot be improved by much when consideration is given to the

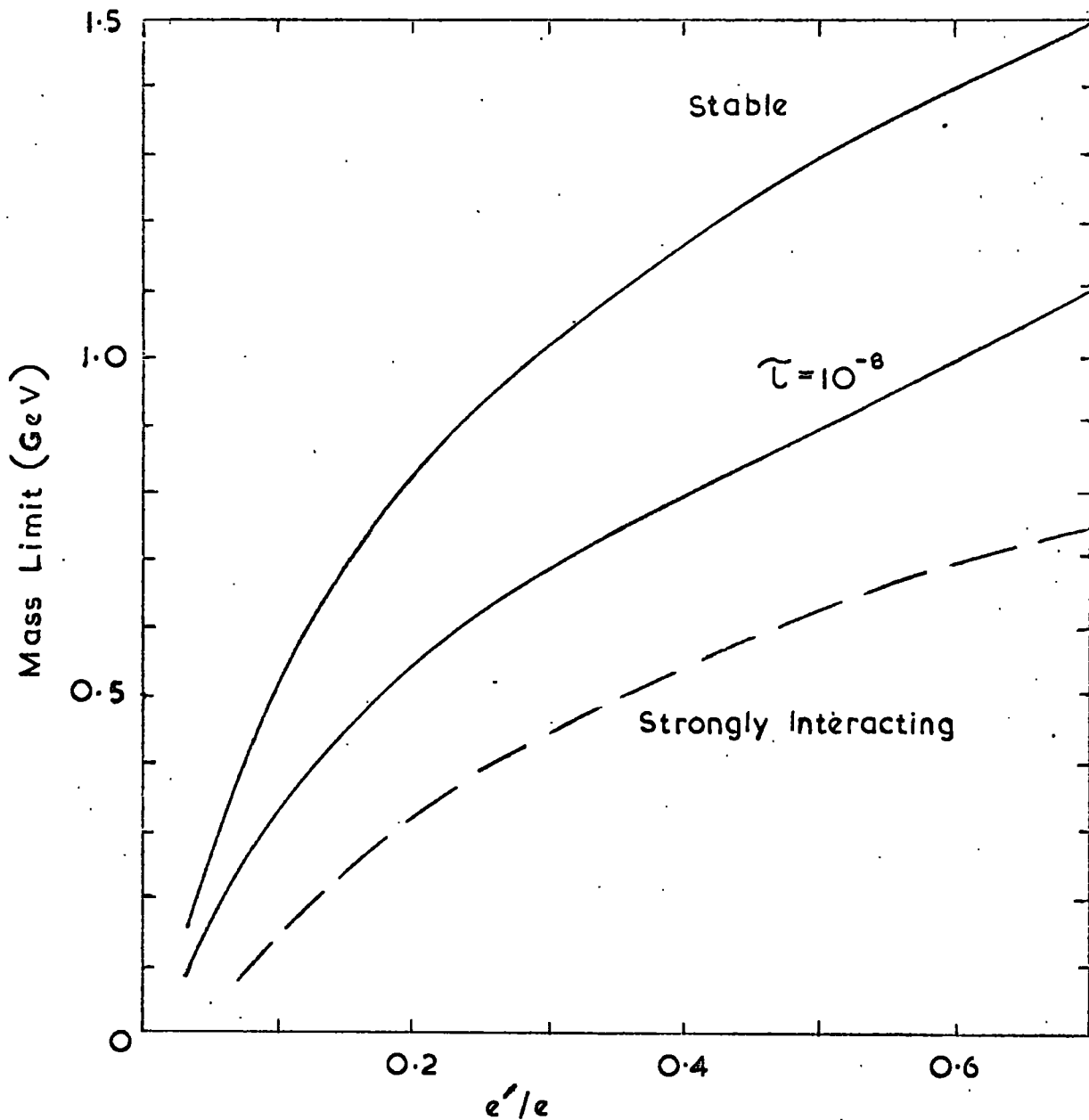


Figure 6.2

The mass limits, as a function of charge, obtained in a search for quarks via electromagnetic pair production at the electron accelerators (Bellamy et al.). The three curves are for stable leptonic quarks; leptonic quarks with a mean lifetime of  $10^{-8}$  sec.; and for stable quarks which are strongly interacting (25mb./nucleon) and are attenuated in the target.

maximum electron energies available and the pair production cross section varying with mass something like  $M^{-8}$ . However such experiments have been useful in searching for quarks produced via a different mode, the importance of establishing the existence (or non-existence) of quarks justifying any search, even if it proves to be negative, which increases or confirms their present understanding.

### 6.2.3 Searches in the cosmic radiation.

The negative results at the proton accelerators led to searches in the cosmic radiation where the effectively continuous primary proton spectrum obviates the restrictions placed on the quark mass at the accelerators. The experiments performed in the cosmic radiation can be categorised into three groups: those searching for relativistic fractionally charged particles; those searching for delayed particles of any charge in air showers; and those searching for sub-relativistic massive particles (typically  $\beta < 0.9, M > M_p$ ) of any charge. The experiments in each category will be treated in turn.

#### a) Relativistic fractionally charged particles.

Numerous experiments have been undertaken to search for such particles in the cosmic radiation, the first being performed in 1964 and others continuing or being contemplated at the present time. The principle of all these searches is the same, relying on the energy loss of a particle by ionisation being proportional to the square of its charge. Hence any detector which is sensitive to the amount of energy deposited in it would be capable of differentiating between unit and fractional charges, the relative energy losses being 1, 0.44 and 0.11 for charges of 1,  $\frac{2}{3}$  and  $\frac{1}{3}$  respectively, providing it had adequate resolution.

The initial experiments utilised scintillation counter telescopes which selected events where the energy deposited in each scintillator was character-

istic of that expected for the incident particle having a charge  $\frac{2}{3}$  or  $\frac{1}{3}$ , and discriminated against events where the energy deposit was greater than or equivalent to that expected for unit charged particles. Several scintillation counters were required, first to reduce background effects from weak electron-photon showers occurring at the lowest levels of ionisation, and secondly to reduce the probability of unit charged particles triggering the telescope and possibly being detected as having fractional charge by downward fluctuations in their recorded energy loss. Most of these experiments used a correlation analysis between the pulse heights produced in each scintillator to attempt to separate genuine particles from background effects, with a resulting decrease of the order of 2 in the efficiency of selecting good events. With this form of analysis many of the experiments in fact observed a positive signal but due to the lack of a full understanding of the background involved, and uncertainties in the statistical analysis arising out of uncertainties in the absolute scintillation line shapes, only upper limits could be quoted on the flux of fractionally charged particles.

Various attempts have been made to reduce background effects and to obtain unambiguous interpretations of individual events. Lamb et al., 1966, and Garmire et al., 1968, have incorporated gas proportional counters into their scintillation counter telescopes and have succeeded in greatly reducing background effects, due to proportional counters having a greater sensitivity to gamma radiation. Kasha et al., 1967 (b), have used a scintillation counter hodoscope and reduced background effects substantially by demanding that a straight line could be drawn through the triggered counters and that only one counter in each of the eight layers should be triggered. However all three of these experiments had finally to resort to statistical techniques to remove the remaining background. The most successful technique yet employed has been

the use of visual detectors in conjunction with scintillation counter telescopes (Ashton et al., 1968a, using flash tubes; Buhler-Broglin et al., 1966; Gomez et al., 1967; and Hanayama et al., 1967; all using spark chambers). In such experiments unambiguous detection of fractionally charged particles can be made by demanding the appearance of a track in the visual detectors correlated with the expected pulse heights for fractional charges in the scintillation counters. A further advantage of such a visual technique is that the pulse heights can be corrected for any non-uniformity of the counters and for obliquity of the incident particles. The only possible source of spurious events in these experiments is from particles traversing the telescope in the sensitive time of the visual detectors prior to the actual event triggering the scintillation counters. However suitable electronic techniques can be used to identify such spurious events.

A survey of all searches for relativistic fractionally charged particles is given in Table 6.4 (a, b and c) where the table has been subdivided into searches at, above and below sea level. Observation of the table shows that the majority of experiments have been conducted at sea level and that the limits imposed on the quark intensity in the cosmic radiation have been improved with time as larger and more sophisticated detectors were used. However the improvement has been far from dramatic, despite the number of experiments, since 1966. The underground experiments of Barton, while establishing the lowest limits on the quark intensity at that time, have been superseded by equivalent limits at sea level as it would be difficult to conceive a propagation model yielding a greater intensity of quarks at a greater depth. It is somewhat unfortunate that the intensity limits derived from the experiments of Bowen et al. and Delise et al. at mountain altitudes are some two orders of magnitude higher than the limits at sea level as if

Table 6.4

Searches for relativistic fractionally charged particles in the cosmic radiation.

a) Sea level measurements.

Workers	Telescope	Visual Technique employed	Thickness of telescope g·cm. <sup>-2</sup> * *	Intensity limits at 90% C.L. X 10 <sup>10</sup> cm <sup>-2</sup> sec <sup>-1</sup> sterad <sup>-1</sup> .		
				1/3	2/3	4/3
Sunyar et al. 1964.	7 p.s.c	No	> 28	2000	-	-
Massam et al. 1965 *	6 p.s.c	No	> 27	-	500	-
Kasha et al. 1966	3 p.s.c 3 l.s.c	No	~ 50	26 <sup>+21</sup> <sub>-13</sub>	21 <sup>+18</sup> <sub>-15</sub>	-
Buhler-Broglin et al. 1966 *	6 p.s.c 2 s.c.	Yes	> 22	15	14	-
Lamb et al. 1966	2 p.s.c 4 l.s.c 2 p.c	No	60	4.5	16	-
Kasha et al. 1967a	7 p.s.c	No	~ 50	-	20	-
(i) Buhler-Broglin et al. 1967a*	6 p.s.c 2 s.c.	Yes	> 22	-	-	1600±800
Gomez et al. 1967	8 p.s.c 2 s.c	Yes	> 15	1.7	3.4	-
Buhler-Broglin et al. 1967 b *	6 p.s.c 2 s.c	Yes	> 22	4.5	1.7±1.7	-
Hanayama et al. 1967	5 p.s.c 4 s.c	Yes	> 50	3.1	3.1	-
Kasha et al. 1967 b	48 l.s.c hodoscope	No	> 50	-	1.2	-
Kasha et al. 1968 a	48 l.s.c hodoscope	No	> 50	-	-	1.3
(ii) Garmire et al. 1968	2 p.s.c 1 l.s.c. 2 p.c.	No	> 46	1.5	2.0	-
Ashton et al. 1968a	6 p.s.c 48 layers F.T	Yes	81.8	1.2	0.8	-

cont/

b) Above sea level

Workers	Telescope	Visual techniques employed	Thickness of telescope $g \cdot cm^{-2}$	Thickness of atmos. above $g \cdot cm^{-2}$	Intensity limits at 90% C.L. $\times 10^{10}$ $cm^{-2} sec^{-1} sterad^{-1}$ .	
					$\frac{1}{3}$	$\frac{2}{3}$
Bowen et al. 1964	5 l.s.c	No	$\sim 40$	760	160	-
Delise et al. 1965	6 l.s.c	No	$\sim 48$	760	87	180

c) Underground.

Workers	Telescope	Visual technique employed	Thickness of Telescope $g \cdot cm^{-2}$	Depth underground m.w.e	Intensity limits at 90% C.L. $\times 10^{10}$ $cm^{-2} sec^{-1} st^{-1}$	
					$\frac{1}{3}$	$\frac{2}{3}$
Barton et al. 1966	1 p.s.c	No	$\sim 5$	2200	-	1.4
Barton 1967	6 l.s.c	No	$> 100$	60	-	1.4

Notes

\* These experiments were all performed 450 m. above sea level, an atmospheric depth of  $\sim 950 g \cdot cm^{-2}$ .

\*\* The telescope thickness where quoted as greater than a certain value has been estimated by the present author and includes only the scintillators in the telescope.

(i) This experiment was performed with  $790 g \cdot cm^{-2}$  of iron above the telescope.

(ii) The quoted intensity limits of Garmire et al. have been modified to give values at the 90% confidence limit in keeping with other workers.

Key to the detectors used.

- p.s.c - plastic scintillation counter.
- l.s.c - liquid scintillation counter
- p.c. - gas proportional counter.
- s.c. - spark chamber
- F.T. - neon flash tubes.

the quark interaction with matter is very strong then such experiments would be more sensitive than those performed at sea level. This situation however may be rectified in the near future as the Japanese group, Hanayama et al., proposed to take their large aperture detector to mountain altitudes.

The various experiments in Table 6.4 can be summarised to give the present intensity limits of relativistic fractionally charged particles in the cosmic radiation at the 90% confidence level as:-

Charge	Flux limit ( $\text{cm}^{-2} \text{sec}^{-1} \text{sterad}^{-1}$ )
$e/3$	$< 1.2 \cdot 10^{-10}$
$2e/3$	$< 0.8 \cdot 10^{-10}$
$4e/3$	$< 1.3 \cdot 10^{-10}$

where no regard has been taken as to where the experiment was performed (the location of the various experiments will be considered later when they will be used to establish quark production cross sections under various assumed propagation models). The limits for charges  $e/3$  and  $2e/3$  are from the work of Ashton et al., 1968a, in which the author was involved, and a summary of this experiment is given in Appendix A. The limit for  $z = 4/3$  is from work of Kasha et al., 1968(a), using a liquid scintillation counter hodoscope consisting of eight layers, each containing six counters. This experiment has been discussed in a different context in Section 4.9.3 and it would appear that their quoted limit is somewhat doubtful.

The experiment selected events subject to the following criteria; a set of counters, one in each layer and defining a straight line, should be triggered, where the discrimination level on each counter was  $1.4 I_{\min}$ ; further, no other counter in the hodoscope should record an energy deposit equivalent to  $> 0.4 I_{\min}$  at the same time. Under such an experimental

situation two events were recorded, both being attributed to two particles having traversed the same elements of the hodoscope simultaneously. However, using their quoted discrimination levels one would expect that no less than  $1.2 \cdot 10^6$  protons should have been observed to have traversed their detector having ionisation levels greater than  $1.4 I_{\min}$ , where in deriving this number their detector has been assumed to be equivalent to  $57 \text{ g. cm}^{-2}$  water (this is probably an overestimate; however a smaller value leads to a higher expected number of protons) and the proton intensity has been taken as  $8.4 \cdot 10^{-8} \text{ cm}^{-2} \text{ sec}^{-1} \text{ sterad}^{-1} (\text{Mev}/c)^{-1}$  at a mean momentum of  $1034 \text{ Mev}/c$  (Brooke and Wolfendale, 1964(a)). This momentum is the mean value of the contributing momentum band, the two limits being  $838$  and  $1230 \text{ Mev}/c$  which correspond to the minimum incident momentum required to traverse  $57 \text{ g. cm}^{-2}$  of water, and to the momentum equivalent to a proton ionising at  $1.4 I_{\min}$ . If it is assumed that 50% of these protons are accompanied and that 50% are scattered or lost in an interaction then the expected number can be reduced to  $\sim 10^5$ . To reduce this sizeable number, to unity say, the discrimination level on each counter must be such that only a fraction,  $f$ , of the protons would have an ionisation greater than this level at each counter; considering all eight counters then  $f^8 = 10^{-5}$ , giving  $f \sim 0.24$ . The average ionisation level of a proton, incident with the mean momentum, in traversing the hodoscope is  $1.78 I_{\min}$ , and since to reduce the expected number of protons to unity  $f$  must be of the order of  $0.24$  then the discrimination level on each counter must be greater than  $1.78 I_{\min}$ . Fortuitously perhaps the ionisation level of a relativistic particle of charge  $4e/3$  is also  $1.78 I_{\min}$  and hence the detection efficiency for these is the same as that for protons, namely of the order of  $10^{-5}$ . It could thus be suggested that the limits quoted by Kasha et al. should be increased by the order of  $10^5$  due to the reduced detection efficiency; however the present

discussion may well have underestimated the efficiency in that only the mean proton momentum and its corresponding mean ionisation have been considered. Despite this a simpler argument can be invoked to show that their detection efficiency was very much less than unity. If it is assumed that the only contributing protons come from a  $1\text{Mev}/c$  band about the minimum momentum required to traverse the hodoscope, then the expected number of observed protons would be  $\sim 10^3$ , where account has been taken of loss through accompaniment and interactions as before. Such protons would be incident with a level of ionisation of  $\sim 1.9 I_{\min}$  and this would increase as they traversed the hodoscope. If discrimination levels of  $1.4 I_{\min}$  pertained then surely all such protons would have been detected with 100% efficiency. The lack of such an observation suggests that the quoted discrimination levels must grossly underestimate the actual situation.

In conclusion little weight can be attached to the limit for quarks of charge  $4e/3$  quoted by Kasha et al., in light of the doubt regarding their detection efficiency which would appear to be as low as or even lower than  $10^{-3}$ . However their quoted limits will still apply to fractional charges greater than  $4e/3$  such that the actual discrimination levels were sufficiently far removed below the corresponding level of ionisation for that charge. Due to this uncertainty the measurement of Buhler-Broglin et al., 1967(a), of  $1.6 \pm 0.8 \cdot 10^{-7} \text{ cm}^{-2} \text{ sec}^{-1} \text{ sterad}^{-1}$  is perhaps a more reliable estimate as to the limit that can be placed on the intensity of particles of charge  $4e/3$  in the cosmic radiation at sea level. To enable a sizeable reduction to be obtained in this limit it would be necessary to incorporate Cerenkov counters in the telescopes to discriminate against sub-relativistic particles (these counters are necessary not only to reduce a sizeable background from triggering the telescope but also to enable spurious events initiated by sub-relativistic

particles to be recognised).

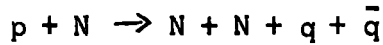
Returning to Table 6.4 the quoted limits have been derived without consideration of the possibility of quark interactions in the telescopes. Due to the strict discrimination levels used in these experiments any interaction would lead to the rejection of an incident fractionally charged particle; such effects will be considered later in Section 6.3. Finally it should be noted that the sensitivity of these experiments would be severely reduced if quarks in reaching sea level are heavily accompanied, any accompaniment within the sensitive area of the detector also leading to the rejection of the incident quark.

b). Delayed particles in air showers.

Such searches are capable of detecting massive particles irrespective of their charge, the method relying on heavy particles being delayed with respect to the much lighter particles constituting an air shower. The feasibility of this method in searching for heavy particles is demonstrated in the following discussion.

An air shower is initiated by a high energy particle, incident on the atmosphere, which interacts and produces both directly and indirectly many secondaries. Deep in the atmosphere these secondaries comprise mainly electrons, photons and muons whose  $\beta^3$  values are effectively unity providing they are capable of penetrating to sea level. Typically, at sea level, the secondaries are contained in a slightly curved disc of the order of 3m. thick, corresponding to a delay of the order of 10ns. between the shower front and tail. The particles present in the tail are normally of low energy, but if massive particles exist then they too would be expected to appear in the tail but with substantially larger energies, providing that their energy loss in

traversing the atmosphere was small. An estimate of likely delays to be expected for quarks in the tail of an air shower can be obtained from considering quarks produced in the reaction



At threshold (where most production will occur due to the rapidly falling proton spectrum) the kinetic energy of the quark is given by (Equation 5.5)

$$E_q = \frac{M_q^2 c^4}{M_p c^2} .$$

Hence the quark velocity at production is

$$\beta_q = \left\{ 1 - \left( \frac{M_q}{M_p} + 1 \right)^{-2} \right\}^{\frac{1}{2}} .$$

Taking  $M_q = 10 M_p$  then  $\beta_q = 0.996$ , which corresponds to the produced quark having a time lag of 0.013 ns/m. behind particles of  $\beta = 1$ . Assuming quarks to be produced predominantly in the first interaction of the primary protons then the production height is typically 16 km. (equivalent to an atmospheric depth of  $100 \text{ g. cm}^{-2}$ .) and the corresponding time lag of the quarks at sea level, assuming negligible energy loss in traversing the atmosphere, would be  $\sim 220$  ns. This quantity is obviously only suggestive of what might be expected, the absolute value varying appreciably with the assumed quark mass, the height of production, the energy loss in traversing the atmosphere and the momentum distribution of quarks in the centre of mass. However it shows that it is reasonable to expect to find massive particles (if they exist) which are sufficiently delayed so as not to be confused with the expected normal air shower tail.

Although the majority of normal shower particles arrive within  $\sim 10$  ns. of the shower front there is still a finite probability that some may arrive

at even greater delays. To avoid possible contamination of a heavy mass signal by such normal delayed particles all the experiments performed using this technique placed a minimum energy threshold on the delayed particle, such that the energy was significantly greater than that which could be carried by any of the normal particles, and at the same time be consistent with the observed delay of the particle.

Before considering the individual experiments in more detail it is relevant to assess their merits and disadvantages as a whole. Their obvious advantage is that they are not confined to searching only for fractional charges as they are also sensitive to unit charged massive particles. However their disadvantages would appear to be twofold; first that after quark production there needs to be sufficient remaining energy to create an air shower (this is particularly relevant if quarks are produced predominantly through nucleon dissociation), and second that the quark transverse momentum should be of the same magnitude as that acquired by nucleons in nuclear collisions, so that they will not be greatly displaced from their associated air showers when reaching the detection area.

Several experiments have been performed at various altitudes and each will be considered in turn.

Chatterjee et al., 1965 This experiment was performed 2.2 km (under  $\sim 810 \text{ g. cm}^{-2}$  of atmosphere) above sea level and used a total absorption spectrometer, of area  $1.5 \text{ m}^2$  containing  $\sim 800 \text{ g. cm}^{-2}$  iron, at the centre of an air shower array to detect delayed high energy interacting particles in a time interval 60 - 330 ns. The experiment was sensitive to particles having the following properties;  $5 < M_q < 10 \text{ Gev}/c^2$ ;  $40 < E_q < 100 \text{ Gev}$ ; an interaction length of  $\sim 80 \text{ g. cm}^{-2}$ , an inelasticity of  $\sim 5 - 10\%$ ; and that they were not more than 20 m. from the shower core. The result of the

experiment was negative, but the authors have not quoted an upper limit to the quark intensity.

Damgaard et al., 1965. Their detector, situated at sea level, comprised a scintillation counter telescope containing three counters separated by  $\sim 800 \text{ g. cm.}^{-2}$  steel (which imposed an energy threshold on the detected particle) having an aperture of  $0.25 \text{ m.}^2$  st. The air shower detector consisted of two adjacent scintillators and delayed particles were accepted in the time interval  $0-1 \mu\text{s}$ . A positive signal was obtained but this was not fully understood and is perhaps only useful in establishing an upper limit to the quark intensity of  $10^{-8} \text{ cm.}^{-2} \text{ sec.}^{-1} \text{ sterad.}^{-1}$ .

Jones et al., 1967 The search was performed 10,600 ft. above sea level (an atmospheric depth of  $715 \text{ g. cm.}^{-2}$ ) and used a total absorption spectrometer, of aperture  $0.78 \text{ m.}^2$  st., containing  $1,070 \text{ g. cm.}^{-2}$  of iron which was interleaved between seven layers of scintillators. Above the spectrometer were proportional counters and spark chambers to assist in the charge identification of an accepted particle. The source of the air shower trigger was  $130 \text{ ft.}^2$  of scintillator which was divided into four groups and placed adjacent to the spectrometer. Particles, whose energy was greater than 10 Gev, which traversed the spectrometer were selected subject to an air shower trigger being obtained within  $\pm 200 \text{ ns.}$  of the spectrometer signal, where the air shower signal comprised a pulse from each group of scintillator such that at least two of these should be coincident within 40 ns. of each other. (the energy threshold of 10 Gev was achieved by summing the pulses from the six lower scintillators in the spectrometer and demanding that this was  $> 30 I_{\text{min}}$ ).

Essentially the experiment was sensitive to heavy particles with masses in the range  $5 - 15 \text{ Gev}/c^2$  which were strongly interacting (this is necessary

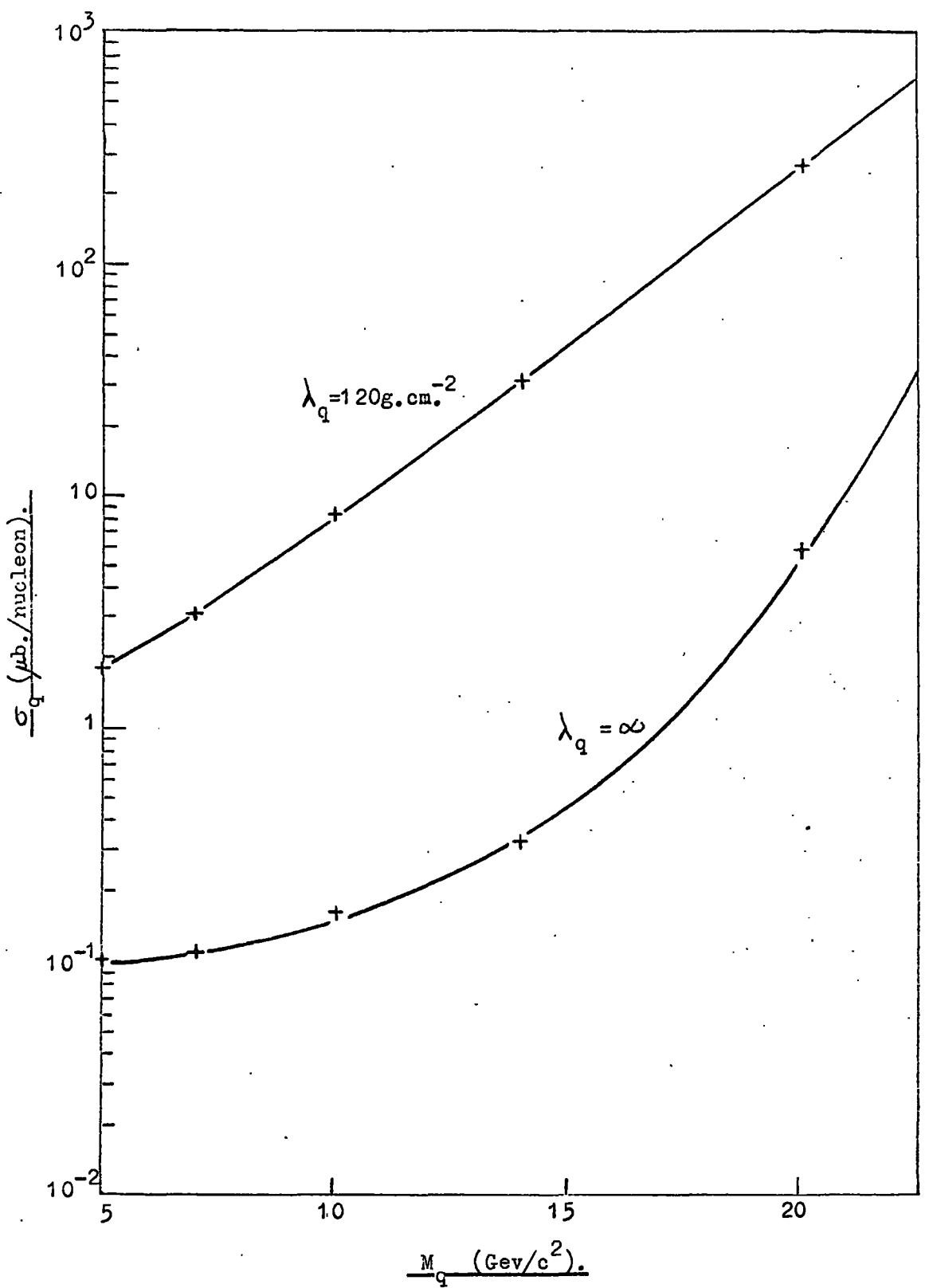


Figure 6.3

The upper limits, at the 99% confidence level, of the quark production cross section (for production via  $NN \rightarrow NNq\bar{q}$ ) from the experiment of Jones et al..

to obtain a signal from the absorption spectrometer) and whose energy loss per interaction was greater than 5%. Only one event was recorded whose behaviour was atypical of a nucleon or nucleus and as the probability of this being a nucleon was 8% it was used only to set an upper limit of  $\sim 10^{-10}$   $\text{cm}^{-2} \text{sec}^{-1} \text{st}^{-1}$  to the intensity of heavy particles. The authors have transformed this limit into a cross section for quark production using a quark production spectrum equivalent to that proposed in Chapter 5, and have assumed that the quark attenuation length is the same as that for nucleons (that is an interaction length of  $80 \text{ g. cm.}^{-2}$  of air and an inelasticity of 0.5). They have also evaluated cross section limits under the assumption of an infinite quark attenuation length; however, apart from demonstrating the effect on the cross section of an increasing attenuation length, this derived limit is not useful in that under such conditions the particle would not be detected by the spectrometer. The cross section limits for the two cases of attenuation length are shown in Figure 6.3.

Biornboe et al., 1968 These workers have carried out a search at sea level with their delayed particle detector placed underground in a tunnel to shield it from muons incident at sea level with energies less than several Gev. The experiment was performed in two distinct parts, each part being sensitive to different interaction properties of the delayed particles.

The first part of the experiment, A, was designed to search for unit charge or neutral particles which were delayed with respect to an air shower and were capable of penetrating  $\sim 3 \text{ kg. cm.}^{-2}$  of rock, or of interacting in a detector placed at such a level underground. The air shower detector, situated at sea level, comprised two horizontal sheets of plastic scintillator ( $S_1$  and  $S_2$ ) of area  $0.4 \text{ m.}^2$  having a vertical separation 0.8m. The delayed

particle detector consisted of 1.6 tons of liquid scintillator (T) in a tank of dimensions  $1 \times 2 \times 0.8\text{m}^3$ . which was sandwiched between two layers of plastic scintillator (X and Y), and was placed in a tunnel vertically below the air shower detector at a depth of  $3.6 \text{ kg.cm.}^{-2}$  of rock. Events were selected under a  $S_1 S_2$  coincidence which was followed by an XY coincidence or a large pulse in T (defined as twice that produced by an incident muon traversing the tank) in a time interval 20-520 ns. after the  $S_1 S_2$  coincidence. Their observations were consistent with the expected rate from chance coincidences and, as the delay distribution of the events showed no significant deviation from uniformity, they concluded that there was no evidence from this experiment for delayed massive particles and imposed a limit of  $< 0.3 \text{ day}^{-1}$  incident on their detector.

The second part, B, of the experiment was designed to search for particles, associated with air showers, which were capable of producing pions at depths where pion production by nucleons is negligibly small. In this case the air shower detector comprised a single layer of plastic scintillators (S), of total area  $2\text{m}^2$ , placed at sea level and vertically above the delayed particle detector, which was situated at a depth of  $1.6 \text{ kg. cm.}^{-2}$  of rock. It consisted of the liquid scintillator (T), as used in A, which was shielded above by  $200 \text{ g.cm.}^{-2}$  cement, and beneath the tank were 2.5cm. of lead, 2 cm. of iron and then a plastic scintillator, (Y), of area  $2\text{m}^2$ . Events were selected where a signal in S was coincident with ( $-30 < \tau < 20$  ns, prompt signals) or followed by ( $20 < \tau < 470$  ns, delayed signal) a TY coincidence, which in turn was followed by a delayed signal T' ( $0.18 \mu\text{s.} < \tau < 5.18 \mu\text{s.}$ ) in the tank (this being attributable to an electron from a  $\pi-\mu-e$  decay). As well as chance coincidences from unrelated events satisfying these selection criteria, further signals could be obtained from either particles

interacting in the tank and producing a pion which stops and decays, as well as at least one other charged particle which traverses the tank and scintillator Y, or from two or more muons associated with an air shower, one of which traverses the tank and Y, while the other stops and decays in the tank. If the TY signal is delayed with respect to the S signal then the event cannot be attributed to muons and must be due to a massive particle or a random coincidence. However if the TY signal is prompt then muons cannot be ruled out and in such cases both the S and TY signal may have been produced by the same particle. The result of the search was negative and upper limits, at the 95% confidence level, to the flux of massive particles incident on the detector are given as

$$\begin{aligned} &< 0.2 \text{ day}^{-1} && \text{for 'delayed particles'} \\ \text{and} &< 6 \text{ day}^{-1} && \text{for 'prompt particles'}. \end{aligned}$$

As pointed out above the prompt particles also include background due to muons and, while a precise calculation is complex, a rough estimate by these workers shows that all the observed signals could be accounted for by background.

Limits on the quark production cross section have been derived from the negative results of experiments A and B. The production model used assumes quark-antiquark pairs to be produced by the decay of fireballs (produced in nucleon-nucleon interactions) and has considered cases of the quarks being produced with centre of mass velocities of 0 and  $0.87c$  (the latter crudely taking into account the effects of fireball motion in the centre of mass and the quark motion in the fireball rest frame) in the direction of the incoming nucleon or opposite to it, and having average transverse momenta of either 0.15, 0.3 or 1.5 Gev/c. Quark propagation in the atmosphere was taken into account by assuming the quark-nucleon cross section to be 30 mb.

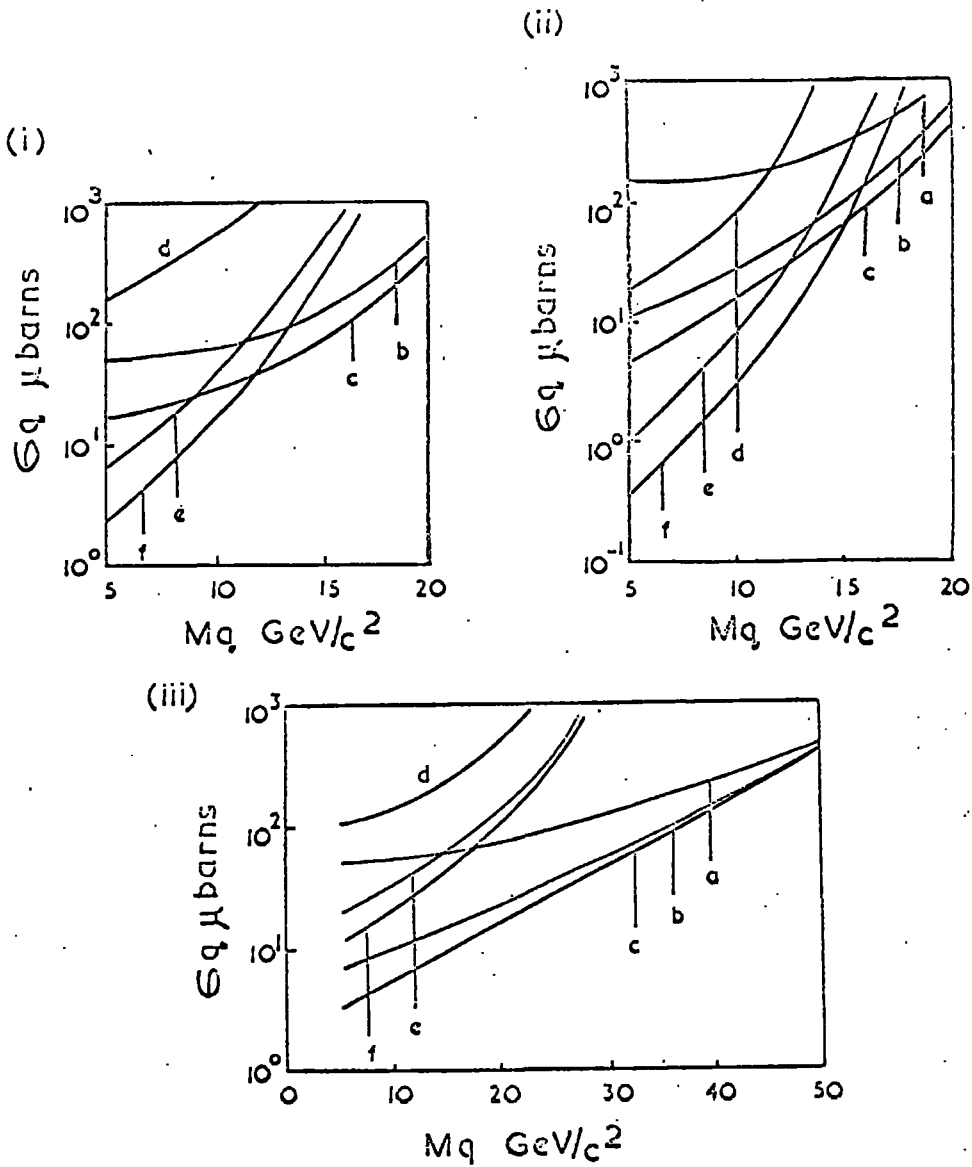


Figure 6.4 Limits on the quark production cross section (production via  $NN \rightarrow NNq\bar{q}$ ) from the experiments of Bjornboe et al..

(i) Experiment A; (ii) Experiment B (delayed signals);  
 (iii) Experiment B (prompt signals).

The key to each curve refers to the following assumed values of the quark velocity in the C.M. system,  $\beta_q$ , and the quark transverse momentum;  $p_{\perp}$ , at production.

- |                        |                                    |                        |                                    |
|------------------------|------------------------------------|------------------------|------------------------------------|
| (a) $\beta_q = 0.87$ ; | $p_{\perp} = 1.5 \text{ GeV}/c^2$  | (b) $\beta_q = 0.87$ ; | $p_{\perp} = 0.3 \text{ GeV}/c^2$  |
| (c) $\beta_q = 0.87$ ; | $p_{\perp} = 0.15 \text{ GeV}/c^2$ | (d) $\beta_q = 0$ ;    | $p_{\perp} = 1.5 \text{ GeV}/c^2$  |
| (e) $\beta_q = 0$ ;    | $p_{\perp} = 0.3 \text{ GeV}/c^2$  | (f) $\beta_q = 0$ ;    | $p_{\perp} = 0.15 \text{ GeV}/c^2$ |

and the inelasticity to be 0.05. The limits are shown in Figure 6.4 for each experiment and for each assumed model of production.

Dardo et al., 1968 This experiment was performed at a depth of 70 m.w.e. and the apparatus consisted of an air shower detector of six two-scintillation counter trays of total area  $5.5 \text{ m}^2$ , with 5 cm. of lead between the scintillators, and a delayed particle telescope, of aperture  $0.75 \text{ m}^2$  sterad., comprising four scintillation counters each separated by 13 cm. of lead. Initially the selection criterion was that a signal should be obtained from at least one of the air shower counters, which was then followed in a time interval 40-520 ns. by a coincidence between at least the two inner counters in the telescope. The interesting nature of the results obtained at short time delays led to the selection criterion being changed to accept signals from the air shower counters and telescope that were coincident within  $\pm 250$  ns. of each other, to enable a more detailed investigation of events occurring at very short delays. Under this latter selection the vast majority of events ( $> 90\%$ ) fell within time delays of  $\pm 20$  ns. The time delay distribution was not symmetric about zero and was biased somewhat to positive delays (where a positive delay refers to the telescope signal coming after the shower signal). An analysis of the events showed the presence of a nuclear active component contributing to the signals from observations of interactions occurring in the telescope. However this component at negative delays was found to have an interaction mean free path of  $165 \pm 25 \text{ g. cm}^{-2}$  of lead while at positive delays a mean free path of  $\geq 375 \text{ g. cm}^{-2}$  was found. Further the angular and lateral distributions for positive and negative delays were also found to be significantly different. This deviation between the nuclear active component at positive and negative delays was further investigated by including a further  $115 \text{ g. cm}^{-2}$  of lead below both the second and third

scintillators in the telescope. While the component at negative delays was strongly attenuated that at positive delays showed little attenuation loss.

These observations led them to suggest that in fact they were dealing with two distinct types of nuclear active particles; those appearing at negative delays being pions originating from nuclear interactions of single muons in the rock above the array; and the most likely interpretation of those appearing at positive delays is that they are particles of mass  $10-15 M_p$ , having unit charge, an interaction length some two to three times larger than pions and having an inelasticity of  $0.5 M_p/M_q$ . If the triggering conditions of the array had been symmetric it would have been possible to subtract the pion component from the positive delays (pions should contribute equally to both positive and negative delays) but as it was not an estimate of the flux of these massive particles was made by subtracting off the calculated rate of muon produced pion showers, this giving the intensity of massive particles as  $\sim 10^{-7} \text{ cm.}^{-2} \text{ sec.}^{-1} \text{ sterad.}^{-1}$

Such an intensity is apparently inconsistent with the upper limits of  $\sim 10^{-10} \text{ cm.}^{-2} \text{ sec.}^{-1} \text{ sterad.}^{-1}$  derived from other experiments. However Dardo et al. suggest that the discrepancy can be explained by assuming the particles to be created in catastrophic processes involving the dissociation of the colliding nucleons with subsequent decay of the unstable triplets into muons, hence leaving little or no energy for the production of a conventional air shower. They go on to suggest that the muon showers accompanying these triplets are small, typically of the order of ten muons, and they are contained within a few metres of the triplet.

Accepting that the particles have unit charge and are produced in the manner suggested by Dardo et al., the inconsistency between their experiment and those performed to search for relativistic fractional charges (Ashton et al. 1968a, etc) is readily removed. Further the inconsistency with the

results of Jones et al. is also removed as the efficiency of that experiment in detecting weakly accompanied massive particles would be substantially reduced, due to the relatively large air shower trigger (a four fold coincidence) required to trigger the detector. It would however be somewhat more difficult to reconcile their measurements with the observations of Bjornboe et al., who in one of their experiments, as described earlier, looked for particles capable of pion production, at a depth where pion production by nucleons is negligible, which were coincident with an air shower trigger at sea level in a time interval - 30 ns. to + 20ns. The air shower trigger was particularly liberal requiring only one particle in a sensitive area of  $2m^2$ . (in fact this experiment would be sensitive to unaccompanied massive particles since the same particle could trigger both the shower detector and the detector in which pion production was required). Taking the upper limit at the 95% confidence level of the observed rate of events by Bjornboe et al. of  $6 \text{ day}^{-1}$  and using the assumption of Dardo et al. that the massive particles are accompanied by  $\sim 10$  muons within a few metres, the intensity limit imposed by the experiment of Bjornboe et al. on such particles would be  $< 10^{-8} \text{ cm}^{-2} \text{ sec}^{-1} \text{ sterad.}^{-1}$ . If the extreme case is taken of the massive particles not being accompanied at all (in which case Dardo et al. would not have observed any events) the limit would be increased to  $< 3 \cdot 10^{-7} \text{ cm.}^{-2} \text{ sec.}^{-1} \text{ sterad.}^{-1}$ , where the massive particle is assumed to trigger both detectors. In fact both these limits should be substantially reduced as the observed rate of events was compatible with them all being initiated by muons. There would thus appear to be a contradiction between these two experiments, and perhaps the only way of resolving the inconsistency would be to suggest that the pions produced are of such high energy (and further do not interact to produce lower energy pions) as not to decay in the detector of Bjornboe et al.

This however would appear unlikely.

In light of this discrepancy it is perhaps justifiable to examine the results of Dardo et al. more critically and look for a more plausible interpretation. Before considering their analysis procedure it is relevant to discuss the experimental data itself. The major criticism in this respect is that it is difficult to understand the appearance of the heavy mass signal only at positive delays, when the most probable expected delay is  $\sim 3$  ns. and the electronic resolution something like 5-10 ns. Returning to their mode of data analysis the strength of their argument in favour of an interpretation in terms of massive particles relies on the differing nature of interactions occurring at positive and negative delays. A table is given below summarising their interaction data for delays  $> 5$  ns. and  $< -5$  ns, where  $I_i$  represents the percentage of interactions occurring in the  $i$ 'th lead absorber, and L is the percentage of non-interacting particles.

Delay	$I_1$	$I_2$	$I_3$	L
$> 5$ ns.	$16.0 \pm 1.2$	$11.5 \pm 1.3$	$9.5 \pm 1.2$	$63.2 \pm 1.8$
$< -5$ ns	$34.3 \pm 3.4$	$16.3 \pm 2.8$	$4.8 \pm 1.5$	$44.5 \pm 4.5$

The events triggering the telescope were assumed to comprise muons and a nuclear active component. The relative abundance and interaction length of the nuclear active component at delays of each sign were evaluated by optimising the fit of the experimental data to assumed values of these two parameters, where the probability of a muon producing a detectable interaction per layer was taken as 0.015, this value having been measured by observations of the interactions of single muons selected to traverse the telescope.

The justification of this latter value would appear to be dubious.

Measurements of muon showers (pairs and triples) by Barton, 1965, using an arrangement somewhat similar to that of Dardo et al., show that the mean muon energy recorded when triggering under a twofold coincidence is  $\sim 150$  Gev, when the extension tray is 2.7m from the telescope, and  $\sim 100$  Gev for a separation of 6.3m. Such energies are to be compared with the mean energy at 70 m.w.e of single muons of 17 Gev. The extension trays of Dardo et al. are at distances of 1.5, 3 and 5m. from the telescope, and hence muon energies significantly greater than 100 Gev would be expected for muons traversing their telescope under the twofold coincidence criterion used in their experiment. At energies of  $\sim 17$  Gev the predominant contribution to muon accompaniment is from knock on electrons but at energies of  $\sim 100$  Gev the effect of pair production becomes appreciable, and the probability of muon accompaniment increases substantially above that at 17 Gev. Depending on the typical energy transfer required to register the occurrence of an interaction in their telescope the probability of accompaniment at 100 Gev would be some 5 to 10 times greater than that at 17 Gev (Barton, 1965). Obviously the interaction probability of 0.015 (corresponding to a mean muon energy of 17 Gev) which was measured for single muons is not applicable to the muon component traversing the telescope when selected under a twofold coincidence, and the effect of increasing this probability has the effect of invalidating the analysis and interpretation of Dardo et al..

In view of this underestimate in their analysis an alternative interpretation of their data is proposed which would seem more plausible than that in terms of massive particles. It is suggested that the observed events comprise only muon showers and an admixture of muon produced pion showers. The pion component being nuclear active will be severely attenuated before reaching the third absorber and it would thus seem a reasonable assumption

that interactions in  $I_3$  and non-interacting particles are all muons. Under this assumption the muon interaction probability can be derived from the data in the previous table and this yields a value of  $0.1 \pm 0.01$  per layer, which is compatible with the expected value of some 5-10 times that observed for single muons at 70 m.w.e. Subtracting the interacting muon component from the interaction data one is left with the pion interaction rates, and these values are consistent with this remaining component having the expected interaction length of  $\sim 150 \text{ g.cm.}^{-2}$  of lead at both positive and negative delays.

Such an interpretation seems quite satisfactory in requiring no new concepts but only the expected cosmic ray components at the detecting level. Further supporting evidence can be obtained from the angular distributions of events at positive and negative delays, where the measurements suggest a steeper angular distribution for positive delays. Due to the triggering asymmetry of the detector the pion component appears predominantly at negative delays, and as it is produced primarily by single muons the angular distribution at negative delays will be biased towards that of single muons, having a form of  $\sim \cos^2 \theta$ . At positive delays the muon component is dominant and this is expected to have angular distribution something like  $\cos^4 \theta$  (Higashi, 1962, from observations of muon pairs) this predicting a steeper angular distribution in keeping with the observations. Consistency is also found with the measurement made with increased lead absorber in the telescope, the muon component at positive delays suffering little or no attenuation, while at negative delays the pion component is substantially attenuated.

In conclusion the interpretation in terms of massive particles by Dardo et al. would seem unjustified in that they have underestimated the interaction

rate of detected muons, and that a more viable explanation of their data is in terms of the commonly expected particles, that is muon showers and muon produced pion showers.

### c) Searches for sub-relativistic massive particles.

Only two searches of this type have been performed; one having been performed by Kasha et al. 1968(e) and the other already described in Chapter 4 forming the basis of the present work.

Kasha et al, used a magnetic spectrograph, of aperture  $10^{-2} \text{ m}^2$  sterad., inclined at  $75^\circ$  to the zenith and incorporated time of flight techniques to enable a determination of the particle mass to be made. Particles incident with velocities in the range  $0.5c - 0.75c$  were accepted. The result of the search was negative and established an upper limit to the quark intensity of  $2.4 \cdot 10^{-8} \text{ cm}^{-2} \text{ sec}^{-1} \text{ sterad}^{-1}$ . The corresponding cross section limit imposed by this intensity will be discussed later.

### 6.2.4 Searches for fractionally charged quarks concentrated in matter.

There have been two approaches to this problem, one searching for quarks produced in the atmosphere, thermalised and then absorbed into the nucleus of some atom, and the other searching in optical spectra for shifted lines which might be expected for 'quarked atoms'. It is not intended to review this subject fully, due to the many problems involved in the interpretation of the experiments performed and in the nature of quark behaviour in matter, but to present briefly the limits of quark concentration in various materials and to consider the major difficulties involved in such searches.

The purpose of extending quark searches to matter in the earth is that, while the quark flux in the cosmic radiation has been shown to be small, the relatively long irradiation time of the earth ( $\sim 10^9$  years) may render such searches more sensitive than those performed directly in the cosmic radiation.

The geophysical aspects of quark searches have been discussed at length by Nir, 1967, who has derived a merit factor,  $M$ , for quark concentrations in various materials (where  $M = \frac{TE}{D}$ , where  $T$  is the irradiation time,  $E$  the enrichment in collection and  $D$  the dilution by non-irradiated matter) using the model of quark production and propagation derived by Adair and Price, 1966, who assumed the quark-nucleon cross section to be 30 mb/nucleon and the inelasticity of quark interactions to be  $0.5M_p/M_q$ .

These derived merit factors, together with experimental limits on the quark/nucleon concentration, are given in Table 6.5. The upper limit derived corresponding to an 'ideal' material (i.e.  $E = 1$  and  $D = 1$ ) is due to Massam, 1968, who took the quark intensity limit of  $<10^{-10} \text{ cm.}^{-2} \text{ sec.}^{-1} \text{ sterad.}^{-1}$  in the cosmic radiation and assumed the flux to have been incident for  $10^9$  years and that all quarks are stopped uniformly in the first kilometre of the earth's crust. The last column in the table shows the relative sensitivity of these experiments to those performed in the cosmic radiation and have been obtained by dividing the upper limit of the concentration by the merit factor, and normalising the sensitivity of the 'ideal' material (corresponding to the cosmic ray case) to unity. This shows that apart from measurements on tropospheric aerosol (giving a sensitivity of  $10 - 10^7$ ) that cosmic ray experiments are in general still the most sensitive at the present time. The value derived for the aerosol is perhaps not particularly meaningful with respect to grave doubts expressed by Chupka et al. of their lack of knowledge of the collection efficiency in the sampling procedure. It can be concluded however that if experiments of this type can be improved and fully understood then they will be able to give better limits on the existence of quarks more readily than the more direct cosmic ray experiments.

Searches for shifted lines in optical spectra have been carried out by

Table 6.5

Quark searches in matter.

Material	Typical value of the merit factor M	Range of M	Quark/nucleon concentration limits	Relative Sensitivity
Sea Water	10	$1 - 10^7$	$5 \cdot 10^{-27}$ (a)	$2 \cdot 10^{-4}$
Stratospheric aerosol	$3 \cdot 10^9$	$10^9 - 10^{10}$	-	-
Tropospheric aerosol	$3 \cdot 10^5$	$10^5 - 10^6$	$3 \cdot 10^{-27} - 10^{-33}$ (a)	$10 - 10^7$
Rock	$10^7$	$10^6 - 10^8$	-	-
Marine sediments	$2 \cdot 10^7$	$10^6 - 10^8$	-	-
Meteorites	$2 \cdot 10^8$	$10^8 - 5 \cdot 10^9$	$10^{-17}$ (a)	$10^{-6}$
Graphite	-	-	$10^{-18}$ (b)	$< 10^{-4}$
'Ideal Material'	$3 \cdot 10^9$	-	$10^{-22}$	1

a) Chupka et al., 1966, using charge separation and mass spectrometer techniques.

b) Gallinaro and Morpurgo, 1966; and Morpurgo, 1968, using a magnetic levitometer.

Sinanoglu et al., 1966, who studied the far ultraviolet spectrum of the sun, and Vainshtein et al., 1966, who looked for lines predicted for quarked calcium and magnesium, and both have found hitherto unidentified lines. Bennett, 1966, however has pointed out that there may be many weak dipole transitions and has made a systematic prediction of spectral lines from normal, unquarked atoms, and has found a total of 21 predicted lines within the line widths observed by Sinanoglu et al. Interpretations of searches of this type would thus appear remarkably difficult. Finally Bocaletti et al., 1966, have suggested the possibility that the red shift of spectral lines in quasars may be due to a very high quark concentration rather than to a source motion. However there would be some difficulty in identifying the unshifted lines which should also exist.

### 6.3 Summary of the experimental quark production cross section limits.

The summary will be directed solely towards the limits derived from experiments performed in the cosmic radiation. The reasons for this are that the limits from the accelerator experiments have already been given in Figure 6.1, and, as well as not covering all the possible charged states (particularly  $z = \frac{2}{3}$  and  $z = 1$ ) equally well, they are in most cases (with the exception of Dorfan et al. sensitive to  $z = -\frac{2}{3}$  and  $-1$ ) about comparable with the cosmic ray limits at quark masses well below those attainable in the cosmic radiation. Further the uncertainties involved in the searches for fractional charges in matter (that is uncertainties in the mode of quark capture and subsequent behaviour as well as the same uncertainty as experienced in cosmic ray experiments, that of quark propagation in the atmosphere) prevent satisfactory conclusions to be drawn about cross sections obtained in this manner.

The experiments performed in the cosmic radiation will be considered with respect to the four plausible propagation models discussed in Chapter 5.

For a given propagation model only the experiment, of a given type, yielding the lowest cross section will be included in the survey. The reason for including the lowest limits from each type of experiment carried out is to present a more complete picture of the situation, as each type of experiment has a different sensitivity to the degree of accompaniment of the quark at the detecting level. Obviously searches for delayed particles in air showers demand a high degree of accompaniment to be efficient, while searches for relativistic fractional charges necessitate zero accompaniment within the detector volume. Searches, such as the present work, for sub-relativistic particles are relatively insensitive to accompaniment due to the quark being substantially delayed with respect to its accompaniment because of its low velocity. Thus the several limits given for each model are independent of each other and when taken together enable limits, insensitive to the degree of quark accompaniment, to be achieved.

The limiting cross sections are given in Figures 6.5 - 6.7 for quarks of charge  $1$ ,  $\frac{2}{3}$  and  $\frac{1}{3}e$  respectively for production via quark-antiquark pairs in the reaction  $NN \rightarrow NN q\bar{q}$ , and Figures 6.8 - 6.10 give the limiting cross sections for quark production through total nucleon dissociation ( $NN \rightarrow \mathbb{E}_q$ ) where in each case limits have been derived for each of the four propagation models previously considered. While limits from the air shower experiments have been included in the survey of quark production through nucleon dissociation they must remain extremely doubtful, since there would be little remanent energy to create an air shower (essential in such experiments to provide the triggering source) unless the energy to this component was furnished by the quarks themselves. Inspection of Figures 6.5-6.10 shows that in general the cross section limits obtained are lower for

Table 6.6

Experiments from which cross section limits were derived,  
and the key to Figures 6.5 - 6.10.

Z	Propagation model		Experiments.		
	Interaction length g.cm <sup>-2</sup>	Inelasticity	R.F.C.	D.P.A.S.	S.R.P.
1	80	0.5	-	c	b
	240	0.5	-	c	b
	80	0.5M <sup>p</sup> /M <sup>q</sup>	-	d	e
	240	0.5M <sup>p</sup> /M <sup>q</sup>	-	d	-
0.5-0.9	80	0.5	a	c	b
	240	0.5	a	c	b
	80	0.5M <sup>p</sup> /M <sup>q</sup>	a	d	e
	240	0.5M <sup>p</sup> /M <sup>q</sup>	a	d	-

Notes:

- 1) R.F.C. - searches for relativistic fractional charges.
- 2) D.P.A.S - searches for delayed massive particles in air showers.
- 3) S.R.P. - searches for sub-relativistic massive particles.
- 4) Key to the experiments:
  - a - Ashton et al, 1968a.
  - b - Present work.
  - c - Jones et al., 1967.
  - d - Bjornboe et al., 1968.
  - e - Kasha et al., 1968c.
- 5) The cross section limits for (a) and (b) have been derived in Appendix A and Chapter 5 respectively, subject to the calculated sea level velocity distributions and are presented after correction for interactions in the respective telescopes. It should be further noted that (a) was also sensitive to sub-relativistic fractional charges (see Appendix A).
- 6) The cross section limits for (c), (d) and (e) have been given by the authors concerned for quark production via  $NN \rightarrow NN + q\bar{q}$  and for a specific propagation model. Where these experiments were sensitive to any other of the models presently considered the quoted cross sections were accordingly altered by the author, in particular when limits were obtained for quark production through nucleon dissociation. Again it is mentioned that the limits (c) and (d) in Figures 6.8 - 6.10 are suspect due to the lack of energy available to create an air shower.

- 7) The limit quoted as (d) is the lowest quoted by Bjornboe et al. for quarks produced with zero momentum in the centre of mass and with a transverse momentum of 0.3 Gev/c (see Figure 6.4).
- 8) For each Figure (6.5 - 6.10) each individual diagram (i-iv) refers to different assumed properties of the quark interaction with matter.

$$(i) K_q = 0.5; \quad \lambda_q = 80 \text{ g. cm.}^{-2} \text{ air.}$$

$$(ii) K_q = 0.5; \quad \lambda_q = 240 \text{ g. cm.}^{-2} \text{ air.}$$

$$(iii) K_q = 0.5 M_p/M_q; \quad \lambda_q = 80 \text{ g.cm.}^{-2} \text{ air.}$$

$$(iv) K_q = 0.5 M_p/M_q; \quad \lambda_q = 240 \text{ g. cm.}^{-2} \text{ air.}$$

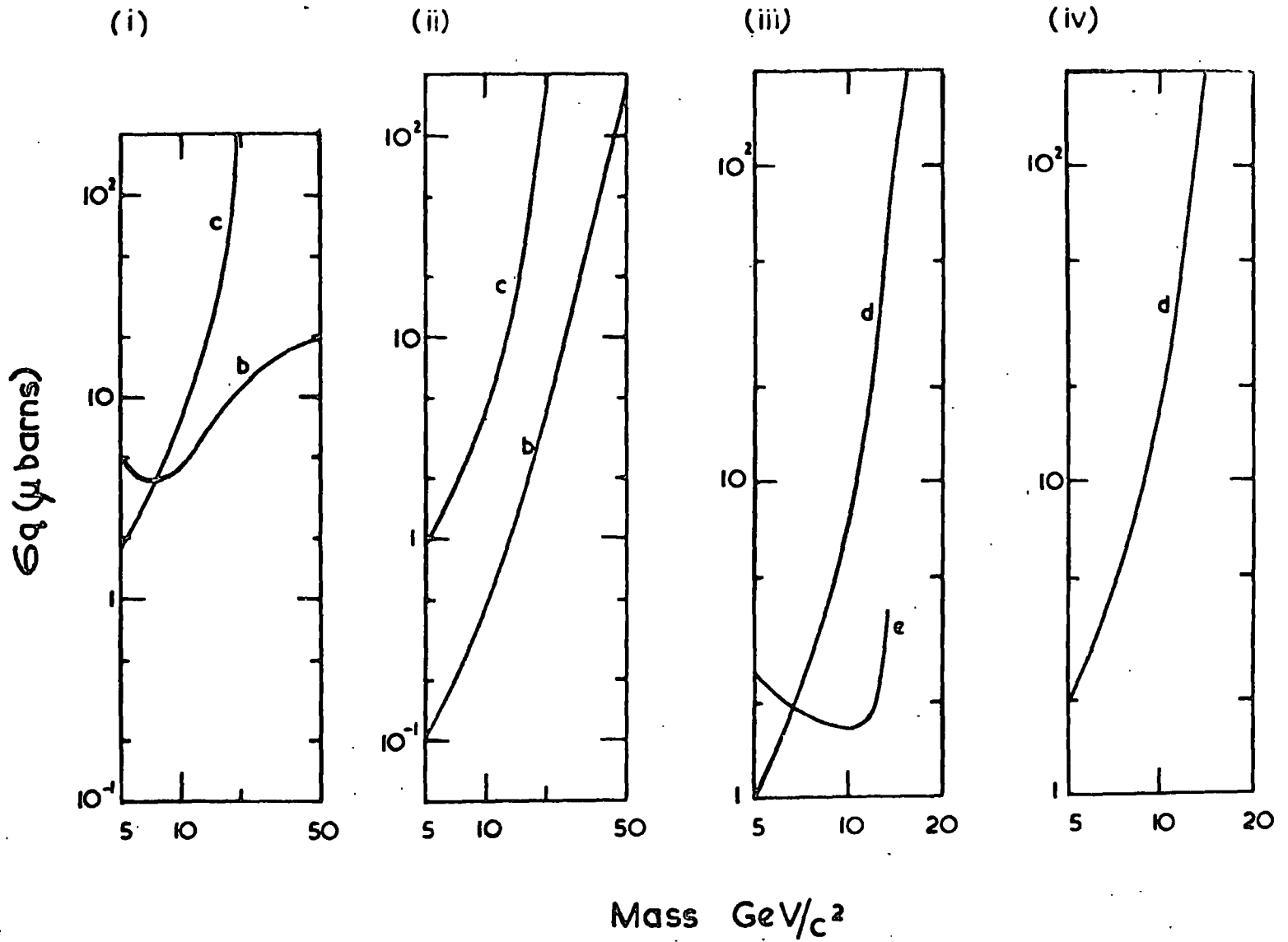


Figure 6.5

A review of the quark production cross section limits (production via  $NN \rightarrow NNq\bar{q}$ ) derived from cosmic ray experiments for  $z = 1$  quarks. A key to the various curves is given in Table 6.6.

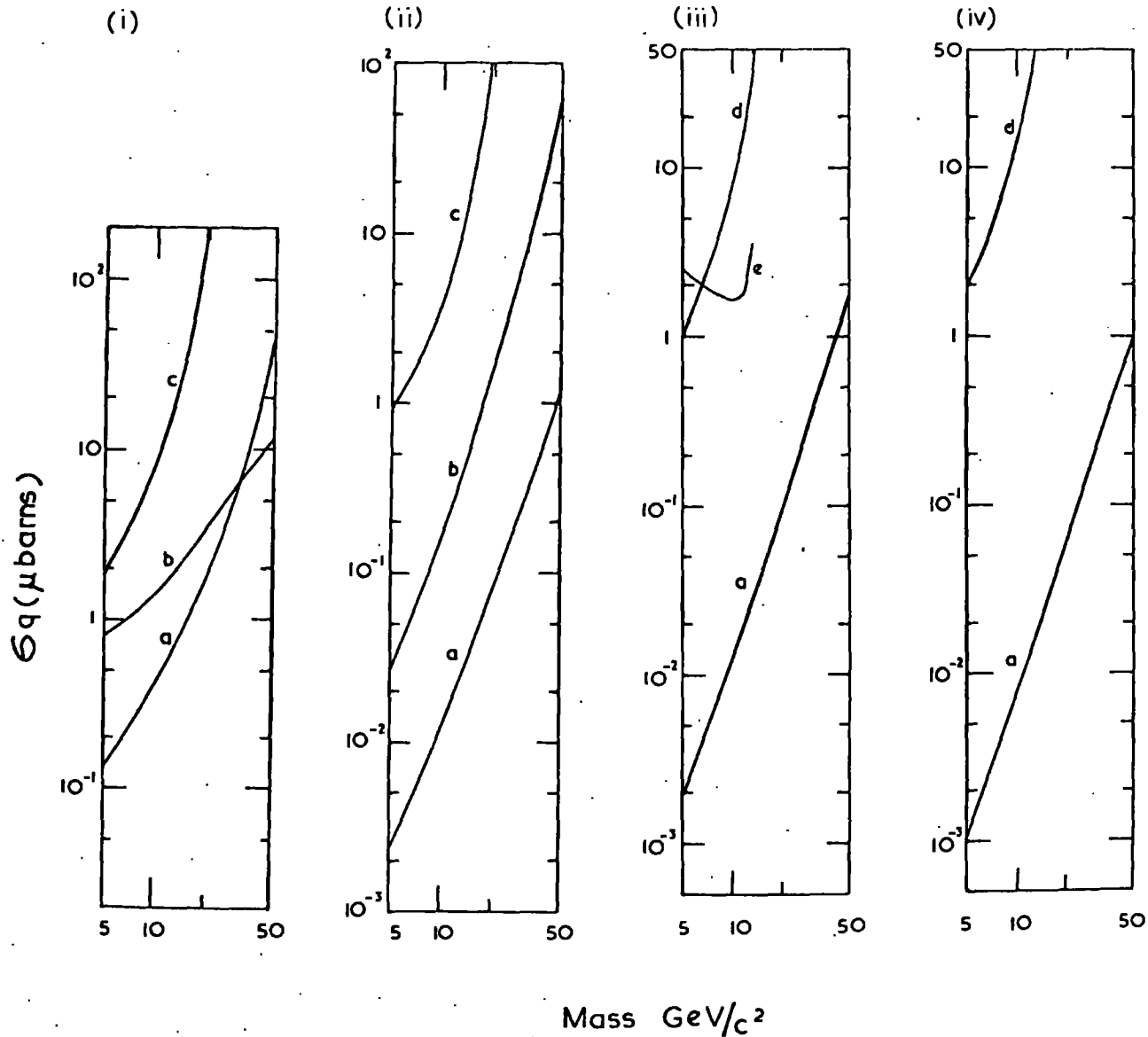


Figure 6.6

A review of the quark production cross section limits (production via  $NN \rightarrow NNq\bar{q}$ ) derived from the cosmic ray experiments for  $z = \frac{2}{3}$  quarks. A key to the various curves is given in Table 6.6.

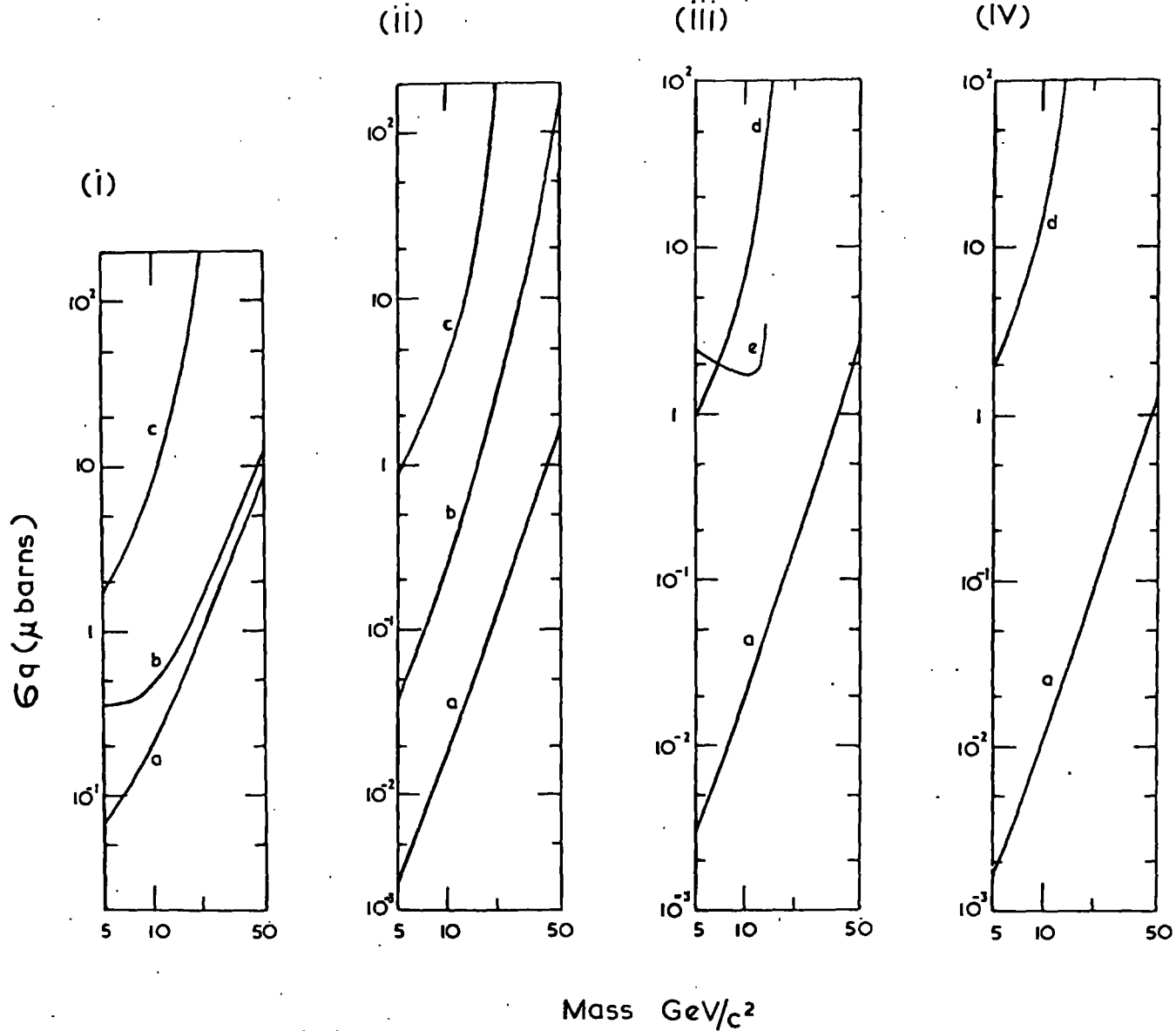


Figure 6.7 A review of the quark production cross section limits (production via  $NN \rightarrow NNq\bar{q}$ ) derived from cosmic ray experiments for  $z = \frac{1}{3}$  quarks. A key to the various curves is given in Table 6.6.

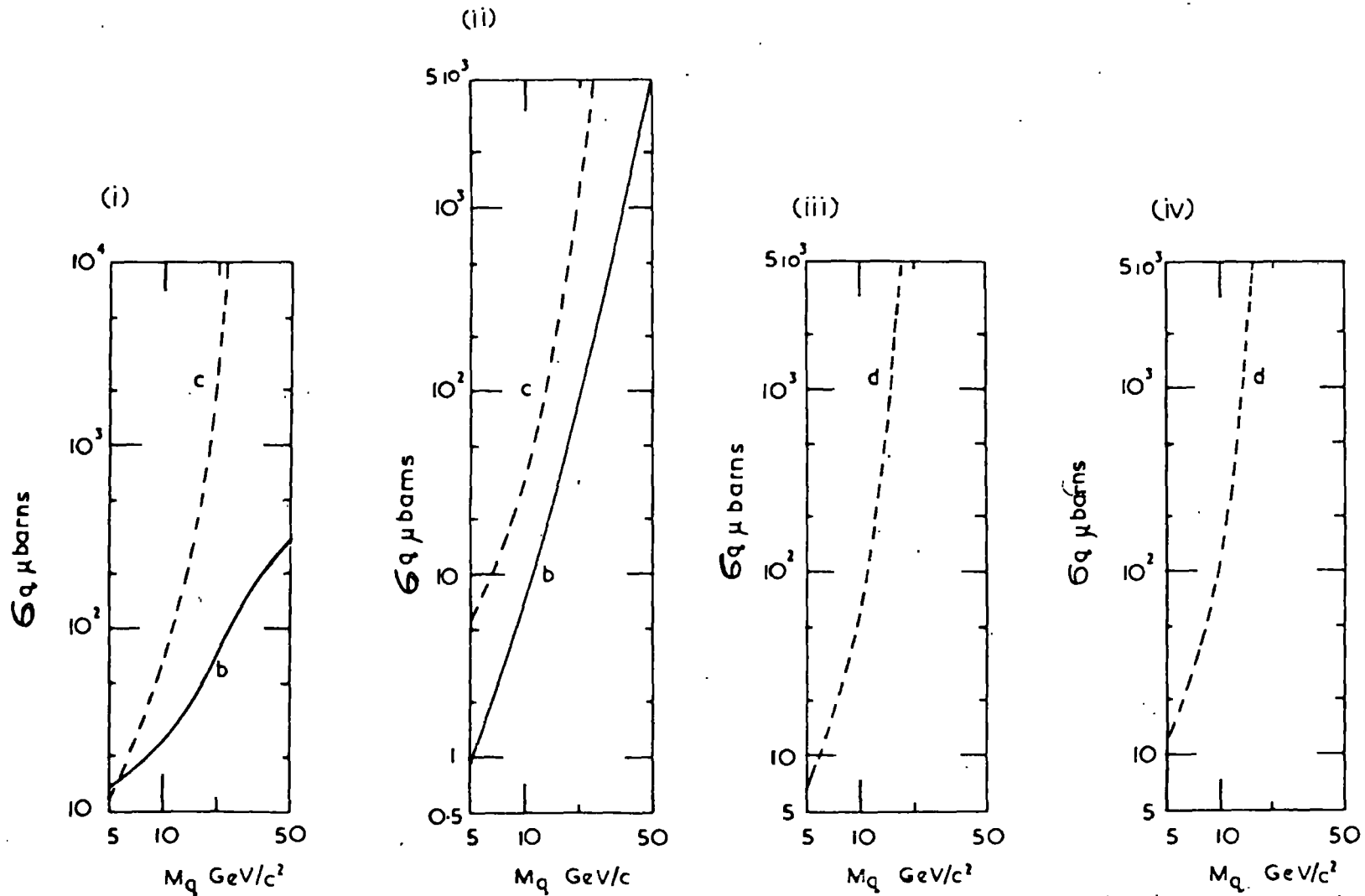


Figure 6.8

A review of the quark production cross section limits (production via  $NN \rightarrow 6q$ ) derived from cosmic ray experiments for  $z = 1$  quarks. A key to the various curves is given in Table 6.6. The dashed curves are from experiments searching for delayed particles in air showers and they must remain doubtful, due to the lack of energy left to create an air shower, for production via this mode.

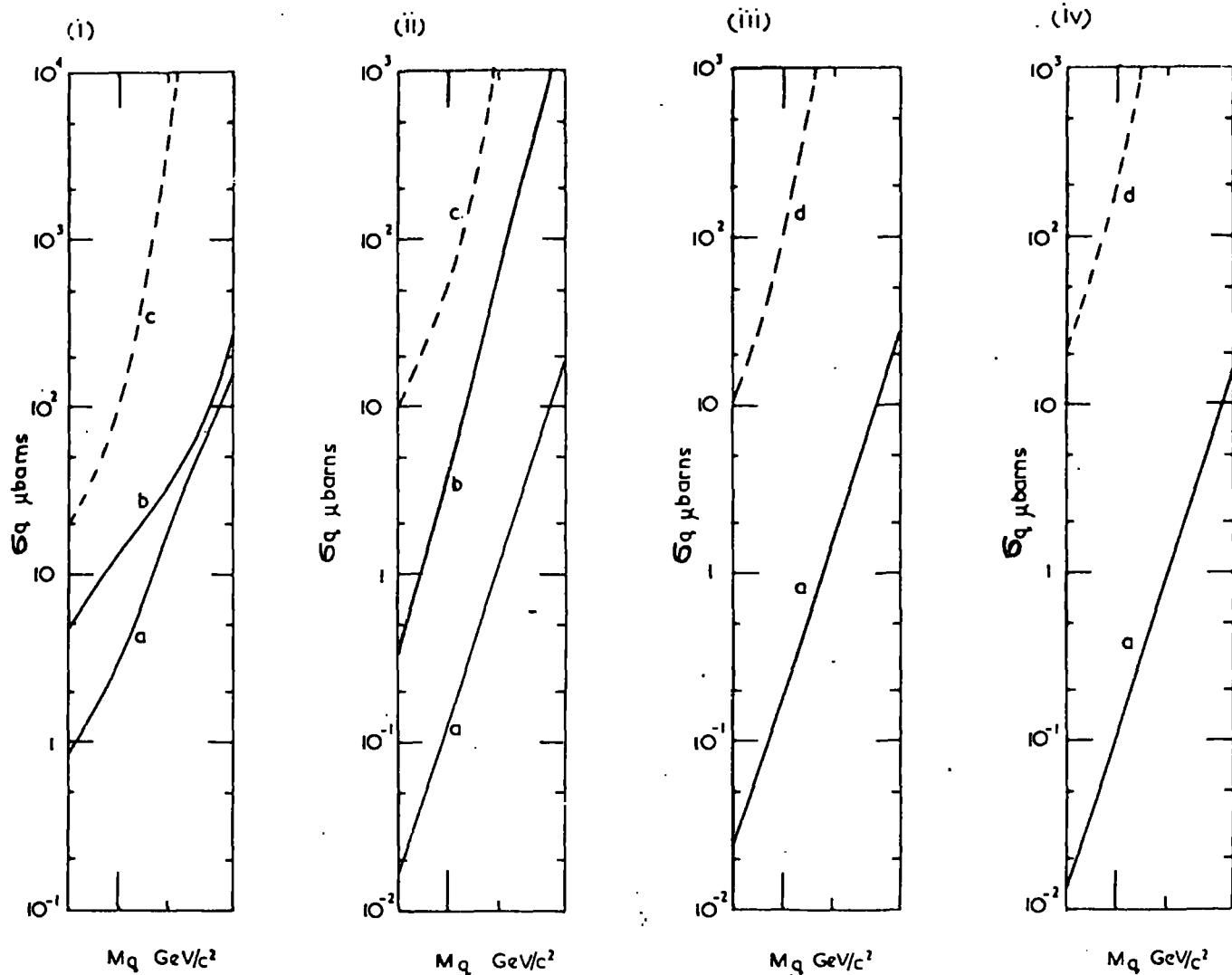


Figure 6.9

A review of the quark production cross section limits (production via  $NN \rightarrow 6q$ ) derived from cosmic ray experiments for  $z = \frac{2}{3}$  quarks. A key to the various curves is given in Table 6.6. The dashed curves are from experiments searching for delayed particles in air showers and they must remain doubtful, due to the lack of energy left to create an air shower, for production via this mode.

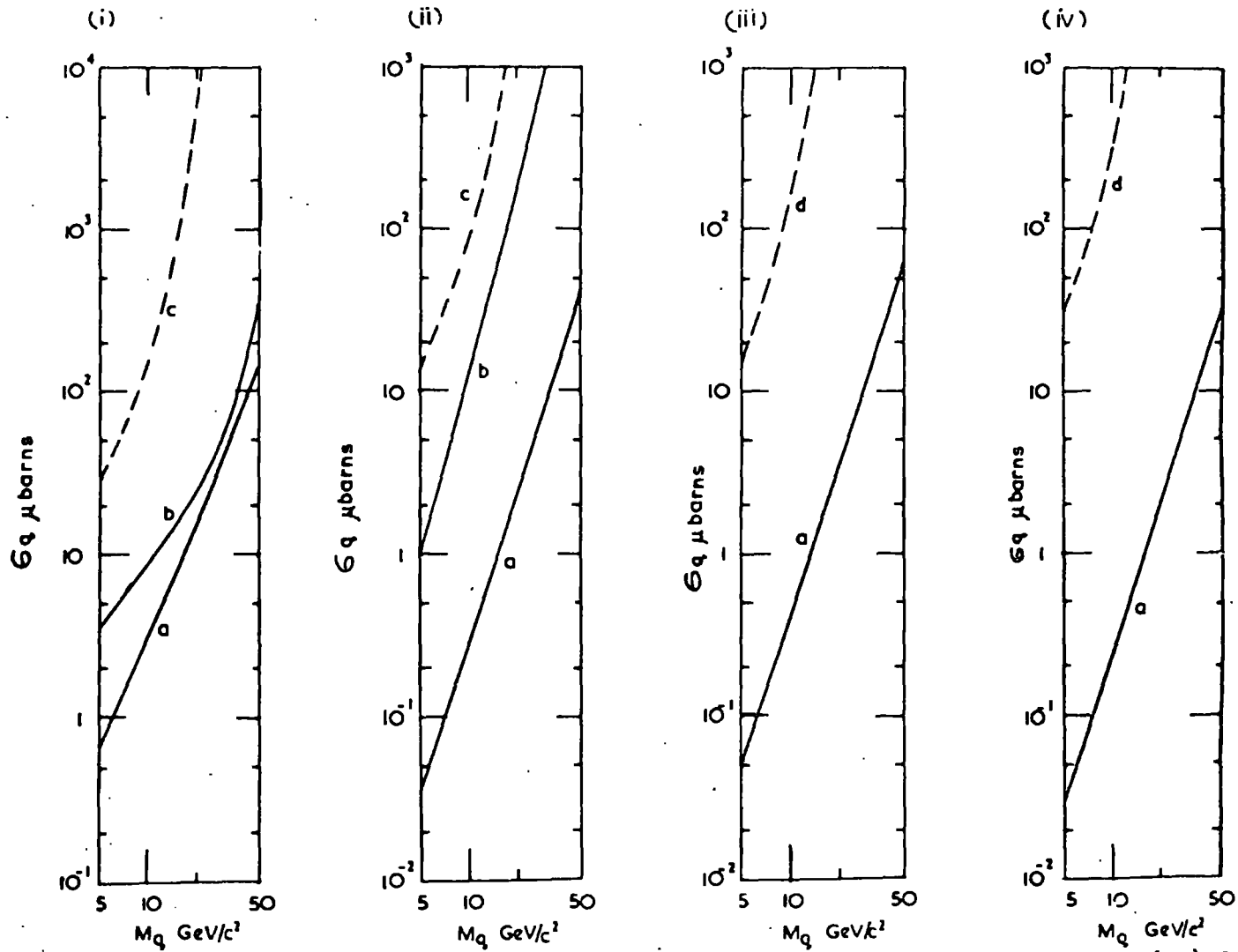


Figure 6.10

A review of the quark production cross section limits (production via  $NN \rightarrow 6q$ ) derived from cosmic ray experiments for  $z = \frac{1}{3}$  quarks. A key to the various curves is given in Table 6.6. The dashed curves are from experiments searching for delayed particles in air showers and they must remain doubtful, due to the lack of energy left to create an air shower, for production via this mode.

searches for single particles than for delayed particles in air showers and also lower for fractional charges, such experiments being easier to perform, than for unit charged particles. Table 6.6 shows the experiments from which the cross sections were derived and gives a key for the subsequent Figures 6.5 - 6.10.

#### 6.4 Theoretical estimates of the quark production cross section.

While establishing experimental limits on the quark production cross-section a quantity of greater significance is the quark mass. To evaluate limits on the quark mass it is essential to know what the production cross section is and several workers have been involved in this field using a variety of production models.

Chilton et al., 1966, have calculated the production cross section of quark-antiquark pairs in nucleon-nucleon collisions using a peripheral model and found a cross section smoothly dependent on the quark mass such that above the threshold energy,  $\sigma_q \propto M_q^{-2}$ . However Hagedorn, 1967, has pointed out that peripheral model calculations are not justified as there must be a strong damping in the  $q\bar{q}$  vertex which was not taken into account by Chilton et al.

Domokos and Fulton, 1966; Masimenko et al., 1966; and Hagedorn, 1967, have all used a statistical model to predict the cross section, where the quarks have been assumed to behave similarly to other hadrons. Domokos and Fulton found an exponential dependence of the cross section with mass, but Hagedorn suggests that their absolute values are overestimates due to ignoring the conservation law which requires quarks to appear in pairs, and to using a temperature which was about twice as high as that suggested by experimental evidence. For this reason only the predictions of Masimenko et al., and Hagedorn are given in Figure 6.11, where the curves have been normalised to an antiproton production cross section of  $10^{-27}$  cm.<sup>2</sup>. The obvious feature

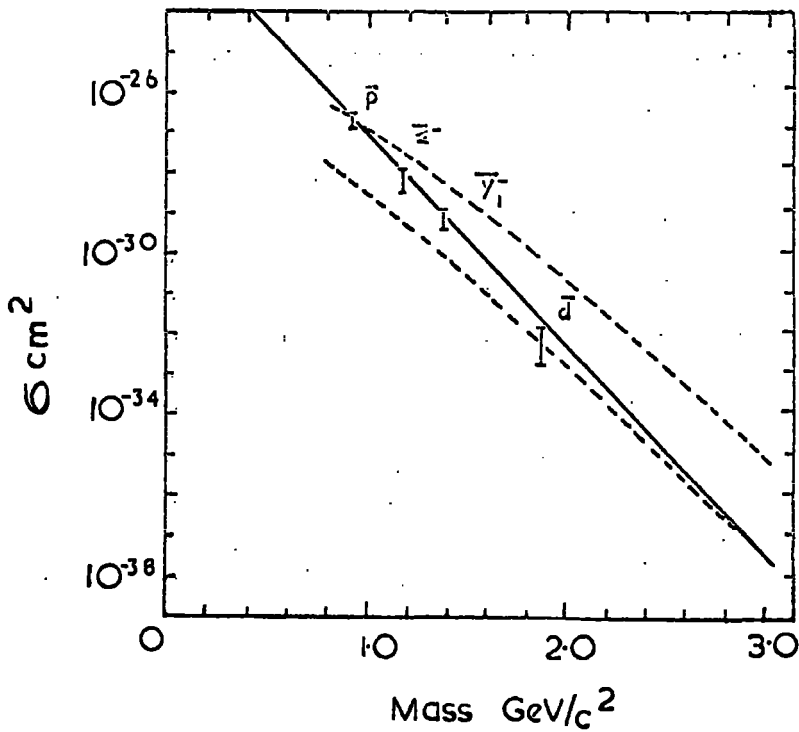


Figure 6.11 Statistical model predictions for the quark production cross section in reactions such as  $NN \rightarrow NN + q\bar{q} + \text{anything}$ . The curves have been normalised to a  $\bar{p}$  cross section of  $10^{-27} \text{ cm}^2$  and the measured cross sections for  $\bar{p}$ ,  $\bar{\Sigma}$ ,  $\bar{Y}$ , and  $\bar{d}$  production are shown for comparison. The full line is due to Masimenko et al., and the dashed curves are due to Hagedorn, the upper of the two being for particles in the ground state of a series of resonances, and the lower for particles which are not.

of these statistical model predictions is a decrease in cross section of about five orders of magnitude for every Gev increase in mass. The results of the two workers are slightly different. Masimenko et al. have fitted  $\bar{p}$ ,  $\bar{\Sigma}^-$ ,  $\bar{Y}_1^-$ , and  $\bar{d}$  with an unique curve, while Hagedorn has pointed out that there are two groups of particles, those which are the ground states of a series of resonances and those which are not, and not knowing into which group the quarks fall he has evaluated two curves, one for each case, with one through the antiproton point and the other through the antideuteron point. Further it should be noted that the Hagedorn curves have a lower slope than that of Masimenko et al. by about a factor of 7 for each Gev increase in mass.

If these predicted cross sections are in fact representative of the true state of affairs then the possibility of experimentally detecting quarks is particularly weak. The presently available experimental cross section limits (Figures 6.1 and 6.5 -6.10) are only able to place a lower limit of  $\sim 3 \text{ Gev}/c^2$  on the quark mass when consideration is given to the theoretical cross sections. To raise this limit by as little as  $1 \text{ Gev}/c^2$  would require an experiment which would be some  $10^5$  times better than those already performed. This is by no means an easy task. Further, if the quark mass is as high or higher than  $5 \text{ Gev}/c^2$  and the theoretical cross sections correct, it is inconceivable that quarks will ever be observed, at least within the capabilities of present day technology. If these cross sections are accepted then the situation may be somewhat reassuring to the theoreticians since no conclusion on the non-existence of quarks can ever be drawn from negative experimental results, only the lower limit on the quark mass can be increased a little, but probably not much above  $4 \text{ Gev}/c^2$ . In this respect theoretical work on quark models can proceed with quark masses as low as  $4 \text{ Gev}/c^2$  without being hindered by arguments that quarks should be treated as 'mathematical entities'

since they have not been observed.

However from an experimental standpoint not too much emphasis should be placed on these theoretical calculations, as so little is known regarding the quarks and their production mode may be completely alien to anything presently understood. While the calculations of Hagedorn and Masimenco et al. are in good agreement with the cross sections for particle-antiparticle production at the accelerators, the interactions of very high energy cosmic ray protons may be substantially different and there is always the possibility of nucleon-nucleon dissociation into their constituent quarks, a problem that has had little theoretical treatment. In conclusion any experiment which is capable of yielding significantly lower limits on the quark production cross section, or which searches via a method yet unexplored, is still justified despite the meagre production cross sections suggested on the basis of the statistical model.

### 6.5 Conclusions and possible future quark searches.

Perhaps the greatest scope for further searches is at the proton accelerators. Even with presently available proton energies there is room for improvement in the present limits, particularly for the charged states  $+le$  and  $+_{\frac{2}{3}}e$ , but it would probably be more sensible to await the higher energy accelerators before intensive searches are renewed (the 70 Gev machine at Serpukov, now in operation, and the proposed 200 Gev U.S.A and 300 Gev CERN machines). A search has been proposed by Massam and Zichichi, 1968, to be carried out at the CERN intersecting storage rings (I.S.R), which should enable cross section limits of  $10^{-9}$  mb. to be achieved over a large range of quark masses. Such limits would be  $10^2$  better than present values at masses around  $3 \text{ Gev}/c^2$  and some  $10^5$  better than the most favourable cosmic ray limit pertaining at  $20 \text{ Gev}/c^2$ . This proposal seems to be the most

promising to have been considered at the accelerators as it is capable of giving low limits to masses even greater than  $\sim 12 \text{ Gev}/c^2$ , the maximum quark mass that will be attained with the CERN 300 Gev proton synchrotron.

While experiments performed in the cosmic radiation at present yield the lowest cross section limits their future with respect to the proposal of Massam and Zichichi is not favourable, particularly if quarks are in fact characterised by any one of the four propagation models proposed in Chapter 5. The lack of an unambiguous observation of a quark in the cosmic radiation, apart from the obvious case of their non-existence, can be due to one of two factors; either the production cross section is much lower than the measured limits or the quark interaction with matter is very much stronger than has previously been considered. If the former is the case then cosmic ray searches will be unable to compete with future machine experiments unless the quark mass is greater than that attainable even at the new accelerators (this might well be the case if the dominant quark production mode is dissociation of both colliding nucleons, when the maximum mass able to be created, even at the I.S.R., would be  $\sim 8 \text{ Gev}/c^2$ ). If this were so there would then still be justification for further cosmic ray experiments, and with such a proviso there appear to be three areas into which further searches should be concentrated, two of which would yield lower cross section limits than so far determined, and the third which would search in a region hitherto only weakly investigated.

The first and obvious region in which further progress can be made is in the search for relativistic fractional charges. To be useful a decrease by a factor of  $10^2$  in the limits should be aimed for and this would demand a detector of aperture  $\sim 100 \text{ m.}^2$  sterad. to enable the search to be completed in a reasonable time. The cost of such a detector comprising scintillator

would be prohibitive but one made up of much less expensive cylindrical gas proportional counters, 10m. long, as suggested by Ashton et al., 1967b, would be much more viable.

Reference to Figures 6.5 - 6.10 shows that the limits are highest for particles having unit charge and having interactions characterised by an inelasticity of  $0.5 M_p/M_q$ . These limits could be substantially reduced by taking a detector of the type used in the present experiment underground to search for sub-relativistic massive particles. A much larger and less sophisticated instrument could be used in a search below sea level due to the then severely attenuated proton contamination which is experienced and must be discriminated against at sea level. A telescope of aperture  $\sim 10\text{m}^2$  sterad. could be readily achieved at moderate cost, comprising Cerenkov counters and a suitable amount of absorber sandwiched between two layers of scintillation counters, and would be capable of giving limits at least  $10^3$  better than presently available over a wide range of possible masses, provided the detector was operated at a variety of depths (see Figures 5.4 and 5.5) in the range  $10 - 10^3$  m.w.e. Such a search would also be sensitive to fractional charges having the same interaction characteristics and, although it would only yield limits approximately 10 times better than already obtained, it would be useful in that the possibility of quark rejection due to accompaniment at the detector would be greatly reduced from that pertaining in sea level experiments.

The final approach to be considered is to search for quarks whose interaction characteristics are much stronger than so far proposed in Chapter 5, such that the velocity distributions at sea level are degraded to even lower velocities than obtained in Figures 5.1 and 5.11. The present work itself has been involved in a search for low velocity quarks but its

disadvantages have been the sizeable quantity of material in the telescope (equivalent to 2.82 nucleon interaction lengths) and the limiting lower velocities to which it was sensitive (typically  $\beta \sim 0.5$  for quarks of mass  $10\text{Gev}/c^2$  and  $z = \frac{2}{3}$ ). These problems can be surmounted by using an air gap magnetic spectrometer to search in the vertical direction for low velocity massive particles, employing time of flight or Cerenkov threshold selection techniques. A spectrometer of aperture  $\sim 0.5\text{m}^2$ .sterad. appears a viable proposition and although it is unlikely that cross sections of a factor of 10 better than in the present work could be obtained (in terms of the same propagation models) such an experiment would be sensitive down to much lower velocities (typically  $\beta = 0.1$ ) and further would contain much less material (it should be possible to construct a spectrometer containing less than 0.5 of a nucleon interaction length). Hence measurements can be made in a velocity region yet unexplored as well as enabling unambiguous interpretations of events such as event H40/6, observed in the present experiment, and minimising the correction of any results obtained for loss due to interactions. In conclusion with regard to further cosmic ray searches it again must be stressed that they will only be useful if the quark mass is higher than that attainable at the new accelerators, otherwise they compete very unfavourably with limits that can be obtained there.

As yet, apart from the uncertain results of Chupka et al. on measurements on air, searches for a fractional charge content in matter are not as sensitive as cosmic ray experiments. However, while there are many media yet unstudied and while the limits on those already measured can be reduced, an interpretation of these experiments in terms of a limiting quark cross section appear particularly difficult. As well as there being uncertainties in the mechanisms of quark capture itself and in the subsequent enhancement and degradation of

a given material the results are also sensitive to the mode of quark propagation in the atmosphere; for example (see figure 5.6) if quarks have an inelasticity of 0.5 then the majority, if  $M_q < 10 \text{ Gev}/c^2$ , will be stopped in the atmosphere before reaching the earth and this will severely affect the conclusions of Nir on the expected concentrations in rock and in the oceans. However it would be useful if such searches were continued in the hope that a greater understanding of the problems involved will be forthcoming.

At present there are two proposals for experiments of this type that appear quite appealing. McDowell and Hasted, 1967, have considered the case of negative quarks absorbed into oxygen nuclei of the oceans, with the capture resulting in the dissociation of the water molecule and the 'quarked oxygen' eventually leaving the oceans and being carried to a height of  $\sim 50 \text{ km}$ . by the vertical component of the atmospheric field. They have suggested that collection of air in  $10^4 \text{ g}$ . of charcoal at such a height and subsequent analysis of it by mass spectrometric techniques would give limits on the quark production cross section at least  $10^2$  lower than those at present, providing of course that their model of quark capture and subsequent transfer to the top of the atmosphere is correct.

The other interesting suggestion is due to Marshall-Libby and Thomas, 1968, who suggest that negative stable quarks should be very effective catalysts of Coulomb fission in stockpiles of heavy metals. Their estimates suggest that a stable quark of mass  $5 \text{ Gev}/c^2$  and  $z = -\frac{1}{3}$  should induce on average more than  $6 \cdot 10^9$  fissions when stopped in a block of  $^{235}\text{U}$  or  $^{238}\text{U}$ , this giving rise to more than 0.4 curie of neutrons in a time  $\gg 0.6 \text{ m. sec}$ . The non-observation of such radioactivity has led them to conclude an upper limit of  $2 \cdot 10^{-30}$  for the concentration of such quarks per nucleon of heavy

metal. However Morpurgo, 1968, has suggested that before conclusions are drawn the rate of Coulomb fission and the number of fissions should be calculated in more detail, and that the situation for Coulomb fission induced by  $\mu^-$  should be considered since this is an experimentally accessible problem.

In conclusion the most fruitful area for further searches is at the new proton accelerators (particularly at I.S.R. because of the greater quark mass available there) and only if the quark mass is greater than the maximum kinematically possible at these machines are further cosmic ray searches useful or justified. The searches for quarks concentrated in matter suggest many interesting possibilities but will remain somewhat unsatisfactory until a greater confidence can be attached to the interpretation of their results.

## CHAPTER 7

### MUONS FROM NEUTRAL PRIMARIES

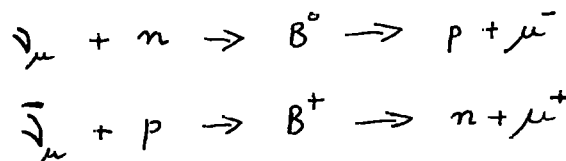
#### 7.1 Introduction

As mentioned in Chapter 4 several events were observed in the heavy mass experiment which appeared to have had neutral origins, and a few of these exhibited single particle tracks which were apparently lacking in strong interactions. The interesting nature of these events and the repeated reports by the Cosmic Ray group of the Catholic University of America (see Section 1.5) of observations of muons produced by neutral primaries at a rate much greater than that expected from neutrino induced muons (at least for neutrinos having their typical interaction cross section) stimulated further investigation of this neutral component in more detail.

The observations of Cowan et al, 1964, suggested the occurrence of a process:



where the presence of a muon has been inferred from observations of decay electrons at time delays consistent with the muon lifetime, and it has been further suggested that the high rate of occurrence can be reconciled with the predictions of Tanikawa and Watanbe, 1958, and Kinoshita, 1960, as to the existence of a resonance in the neutrino-nucleon cross section of  $\sim 10^{-26} \text{ cm}^2$  having a half width of  $\sim 200 \text{ ev.}$ ; and occurring at a neutrino energy of several hundred Mev. The observed muons are then assumed to have been produced in the following processes:-



However, what Cowan et al. may conceivably have underestimated is the muon signal coming from the decay of neutron induced pions.

The purpose of the present work was thus to study neutral induced low energy muons using a detection method similar to that of Cowan et al., and to extend the measurements to higher energy penetrating secondaries (since if such a neutrino resonance existed then the effect of the Fermi motion of a target nucleon in a nucleus would bring both higher and lower energy neutrinos into the resonance, with the result that the contributing neutrino energy spectrum and the produced muon energy spectrum would be quite broad) with the intention of establishing whether or not there was definite evidence for a directly produced muon signal of the magnitude suggested by Cowan et al., or whether more sophisticated techniques would be required to isolate such a signal from the expected muons from the decay of neutron induced pions.

In the short time available for such an investigation, at the end of the heavy mass experiment, it was realised that the telescope itself, while obviously not designed for this purpose, with suitable modification would be capable of such a search and be relatively efficient in discriminating against unwanted charged background. The telescope in three modified forms was used to make three series of measurements, N, M and C, on the neutral primaries and each will be discussed in the ensuing sections. No further discussion will be afforded to the neutral induced events obtained in the heavy mass search, in that a more precise analysis can be performed on similar events observed in the following investigation under somewhat more controlled experimental conditions.

## 7.2. A study of penetrating charged secondaries from neutral primaries.

### 7.2.1 Modifications to the heavy mass telescope.

As the initial objective was to further investigate charged particles induced by neutral primaries in the heavy mass detector it was essential that

preliminary modifications should be kept to a minimum. For this reason the only alteration was the inclusion of a smaller scintillation counter, (V), to enable selection of incident neutral events at the exclusion of charged primaries. The revised telescope is shown in Figure 7.1.

The extra scintillator (NE102A), denoted by V, of dimensions 75 x 30 x 5 cm.<sup>3</sup> was included in the telescope between CI and F<sub>3</sub>, and it can readily be seen that an electronic selection of the type  $VCDEF\overline{BCI}$  would lead to the acceptance of neutral particles traversing A to CI and subsequently charged particles traversing V to F, with a high rejection efficiency for charged particles incident upon the detector. The scintillation light produced in V was viewed through triangular perspex light guides, cemented to the 30 cm. edge of the phosphor, by two 53 AVP photomultipliers, one at each end, where the outputs from each were added.

#### 7.2.2 Selection of events: N and M series.

The experimental arrangement used in the N series is that given in Figure 7.1. Events were selected using fast electronic logic, basically similar to that shown in Figure 4.2., with a coincidence requirement of  $VCDEF\overline{BCI}$ . The discrimination levels used on each counter were as follows:-

B	CI	V	C	D	E	F
0.05	0.5	0.2	0.25	0.25	0.25	0.25

where they are expressed in terms of  $E_s$  and  $E_c$ , the most probable and median pulse height respectively produced in that counter by a relativistic muon.

On a particle satisfying the electronic logic the train of events (e.g. photographing the counter pulse heights, pulsing the flash tubes etc.) was identical with that described in Section 4.3 apart from the display mode of the counter pulse heights, where only the amplified versions of the Cerenkov pulses were displayed and the pulse from V being incorporated into the display train.

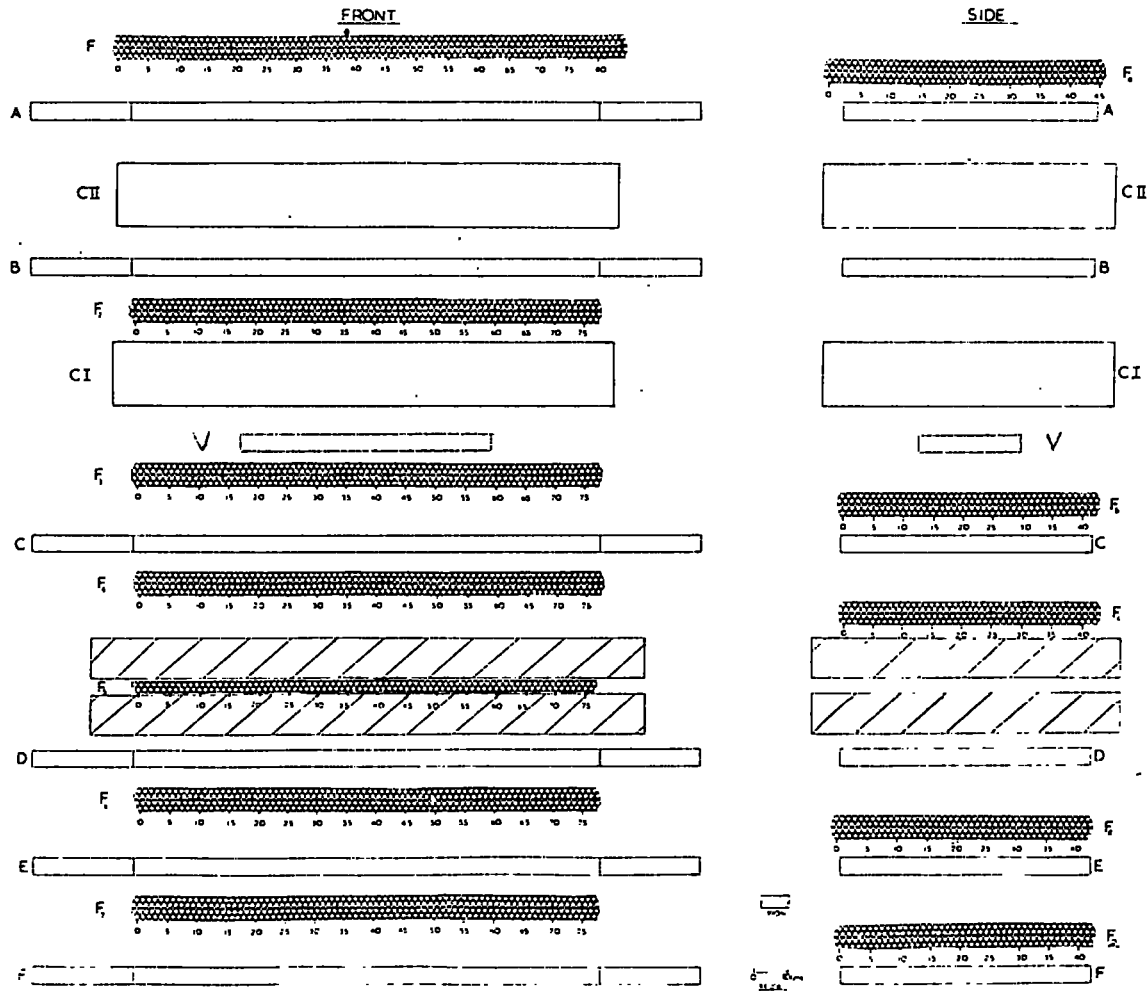


Figure 7.1 The modified telescope used in the N series. A, B, C, D, E, F are plastic scintillators (NE102A); CII, CI are water Cerenkov counters; and F<sub>1</sub>-F<sub>7</sub> and F<sub>a</sub>-F<sub>e</sub> are neon flash tube trays.

It should be noted that the pulses from A and CII were also displayed despite not forming part of the electronic logic, as in this way one had two independent witnesses of the event, unbiased by electronic selection, to verify that the incident particle was truly neutral.

On completion of the N series of measurements it was decided to extend the investigation to lower energy penetrating secondaries, the M series. This was accomplished by removing the steel absorber and flash tube tray  $F_5$  from the telescope, so as to create a lower energy particle threshold which was able to satisfy the electronic selection. Otherwise the telescope and electronic selection were identical with that which pertained in the N series.

### 7.2.3 The basic data.

Analysis of individual events was achieved by projection of the three films (two of the flash tubes and one of the counter pulse heights) onto scanning tables as discussed in Section 4.3. The selection criteria for selecting events from the film were based solely on the flash tube information and were as follows:- a track or burst should be observed to traverse the flash tube trays,  $F_3$ - $F_7$ ,  $F_b$ - $F_e$  as well as scintillator V, and that the upward projection of the track (or burst) should intersect scintillator B. Such criteria established that an observed event had emanated from a neutral primary (apart from a small contamination from highly scattered charged primaries producing the observed secondaries). Each event selected in this way was classified according to the number of charged secondaries emerging from the production region and whether or not a scattering occurred when a single particle only was observed to emerge. The pulse height information for the selected events was measured and this served as a further check that the incident particle was neutral.

The basic data referring to the two series of measurements, N and M, are tabulated below, where n refers to the number of observed charged prongs leaving the interaction region.

	N series	M series.
Running time (hours)	140.75	6.03
Mean pressure (mbars)	1003	997
VCDEF rate/hour	$2.00 \cdot 10^4$	$2.33 \cdot 10^4$
$\bar{B} \bar{C} \bar{I}$ veto rate/hour	$1.25 \cdot 10^7$	$1.25 \cdot 10^7$
Total number of triggers	1865	547
No. of accepted events	363	290
No. of events with n = 1	93	86
No. of events with n = 2	70	72
No. of events with n > 2	200	132

The difference between the total number of triggers and the accepted number of events is accounted for by angled tracks and showers traversing C-F accompanied by a random pulse in V, and by weak electron-photon showers triggering the telescope. The flash tube and pulse height information for a representative set of events selected in the N and M series are given in Figure 7.2 (a-e).

#### 7.2.4 The observed rate of events

To be useful the absolute rates must be expressed in terms of the target thickness in which the charged secondaries could have been produced. The region where the neutral primaries could interact was in the material between CI and V as well as within parts of CI and V themselves, depending upon the discrimination levels used on each counter. As the identity of the neutral particles is essentially unknown it is difficult to assess the multi-material

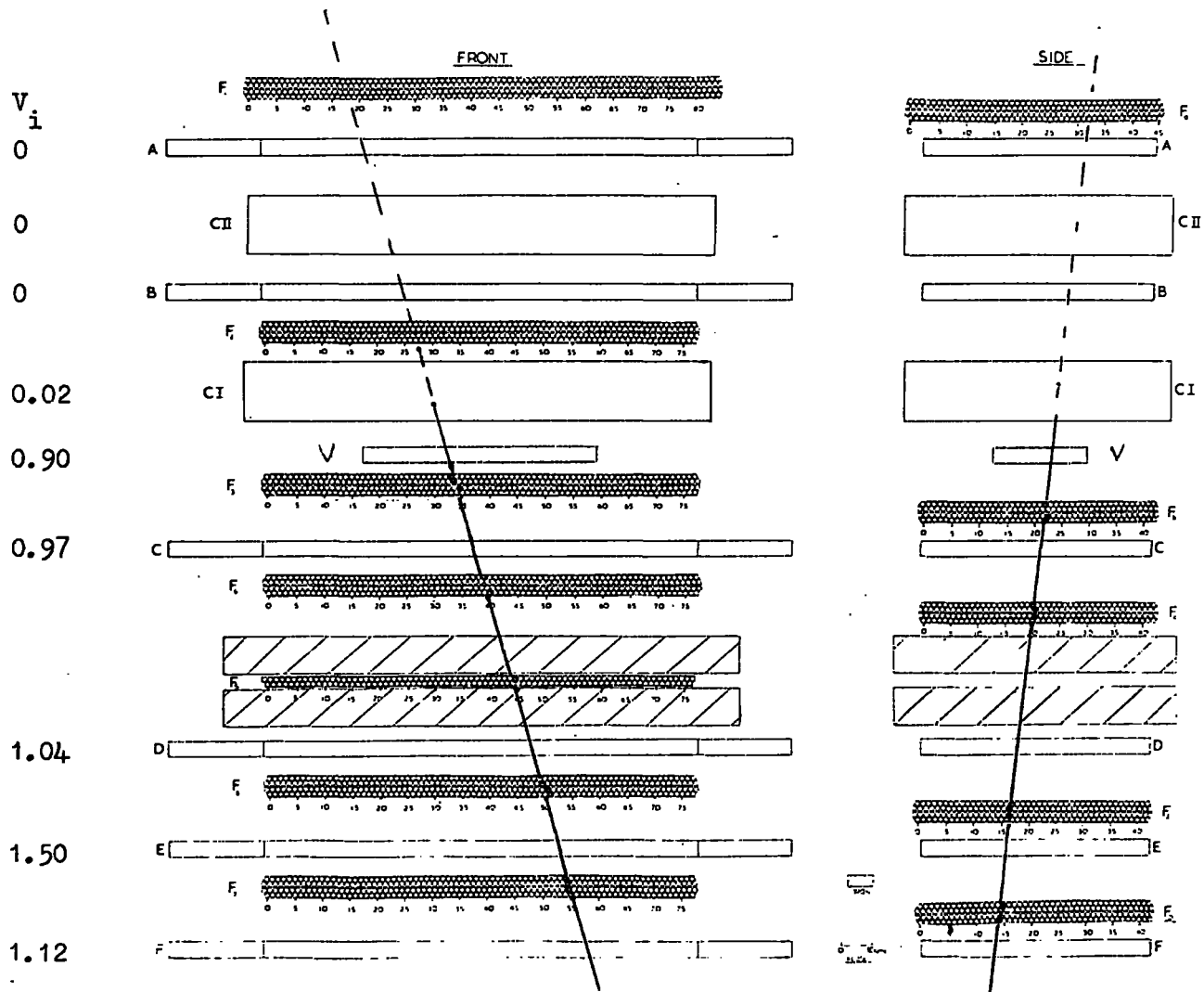


Figure 7.2(a) Event N10/12 showing the production of a neutrally induced single unscattered particle. The normalised pulse height from each counter, in terms of E, is also shown.



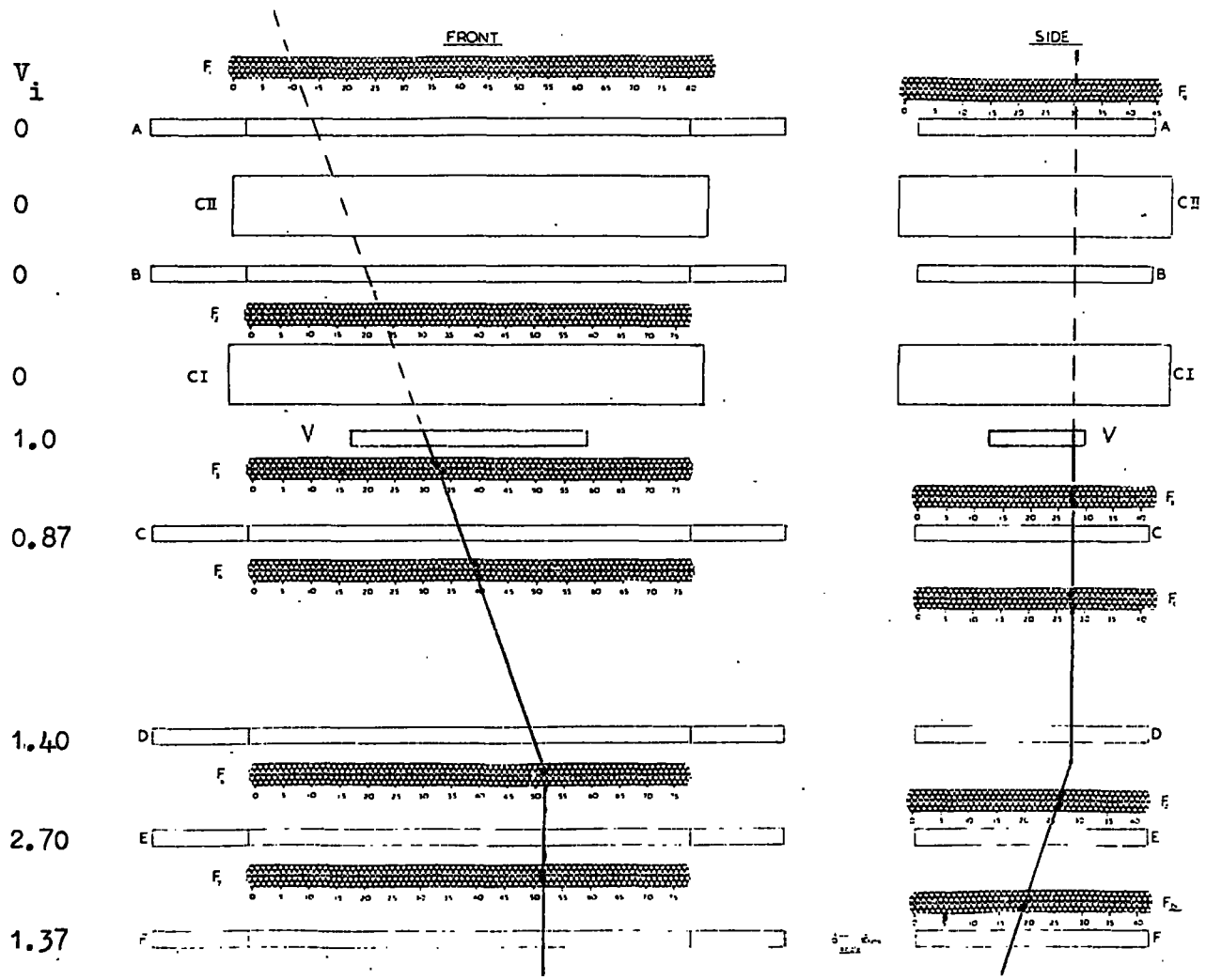


Figure 7.2(c) Event M1/29 showing the production of a single neutrally induced scattered particle. The normalised pulse height in each counter, in terms of  $E$ , is also given.

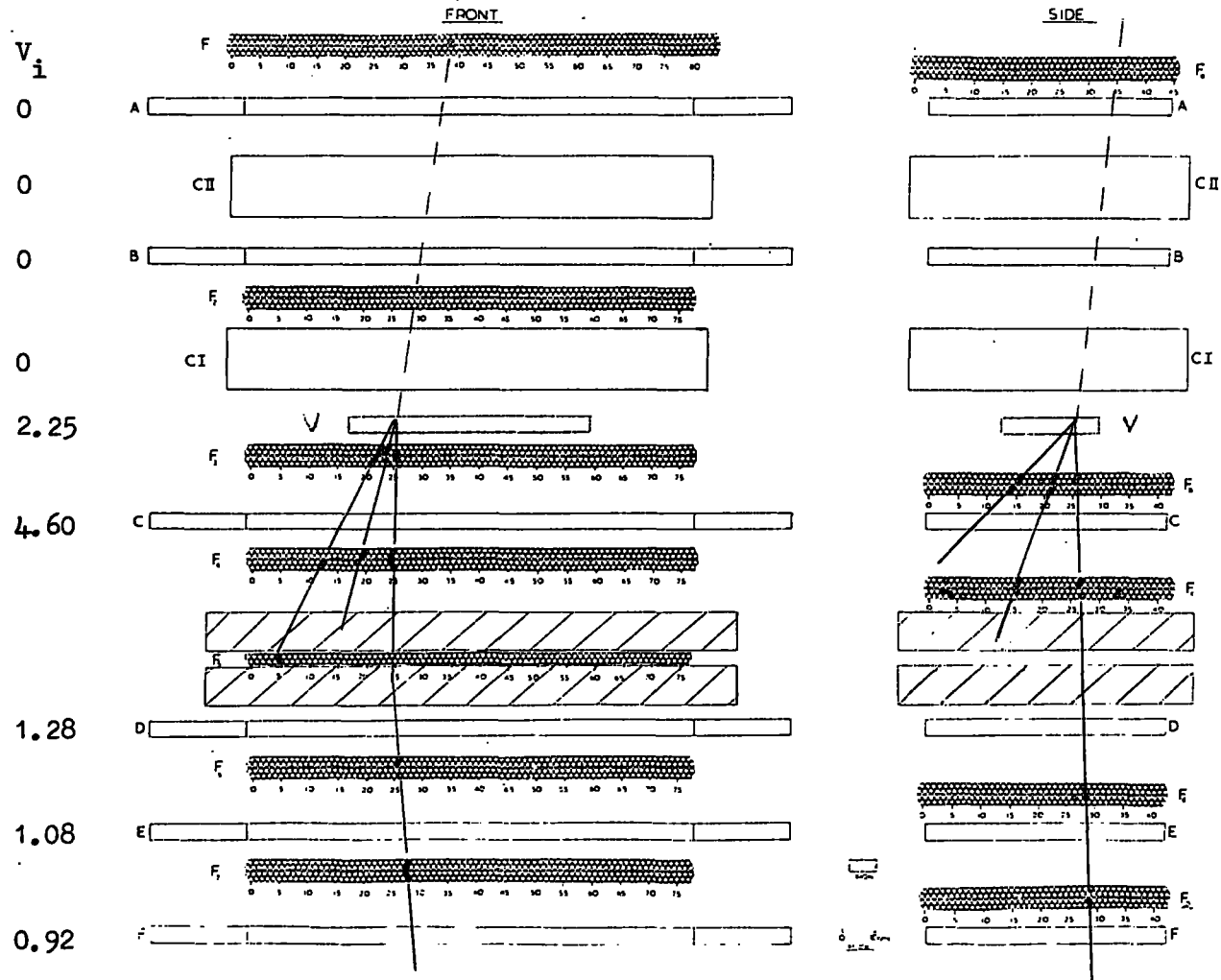


Figure 7.2(d) Event N2/172 showing the production of a single penetrating neutrally induced charged secondary with two further charged prongs also emerging from the target region. The pulse height from each counter, in terms of  $E$ , is also shown.

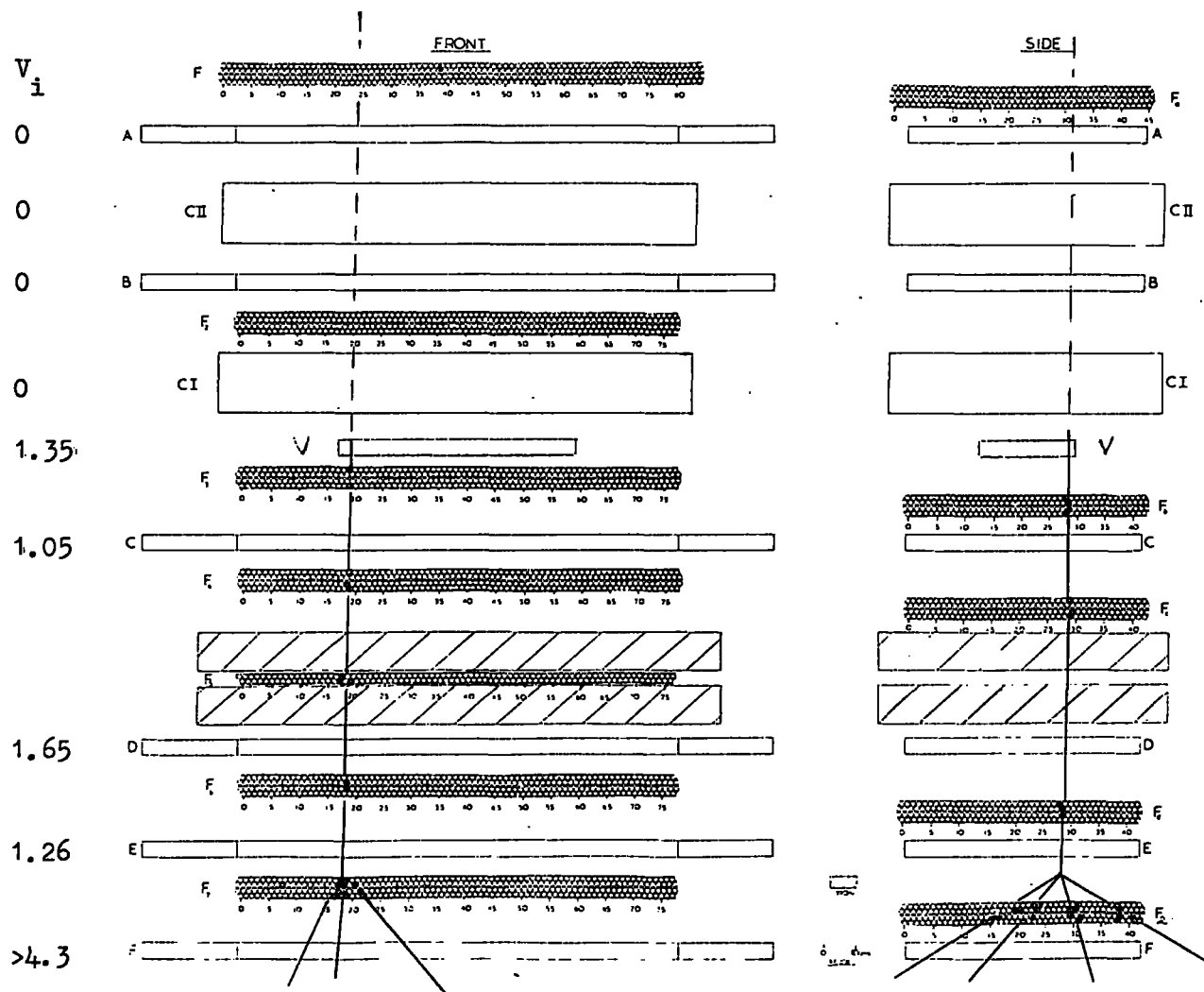


Figure 7.2(e) Event N2/207 showing the production of a neutrally induced single particle which later interacts and produces further charged prongs. The pulse height from each counter, in terms of  $E_i$ , is also given.

target in terms of one element since some form of A dependence must be assumed for the cross section (if the neutral particles are neutrons a dependence of  $\sim A^{\frac{2}{3}}$  could be taken whereas if they are neutrinos a linear dependence on A would be more valid). For this reason it is perhaps sufficient to note the relative composition of the target and to evaluate the rates per  $\text{g. cm.}^{-2}$  of target irrespective of the materials it contains. Under such an analysis the total target is equivalent to  $23.1 \text{ g.cm.}^{-2}$  and its composition is tabulated below.

Target element	$\text{g. cm.}^{-2}$
Water (0.5 of CI)	8.0
Perspex (base of CI container)	1.15
Wood (base of CI container)	1.03
Steel plate (support for CI)	8.37
Aluminium (top of V container)	0.44
Phosphor (0.8 of V)	4.13
Total target	23.12

The aperture of the telescope, now defined by the scintillators V and F, has been evaluated by normalising to the aperture calculated for the heavy mass telescope in Section 4.7 (defined by A and F) by comparing the respective counting rates VCDEF and ABCDEF, this giving a value of  $(7.1 \pm 0.7) 10^2 \text{ cm.}^2$  sterad., where the error limits correspond to the neutral radiation having an angular exponent of 8 (as might be expected if it comprises neutrons) and an exponent of 0 (typical of low energy atmospheric neutrinos). In fact the secondary particles may well have an angular distribution significantly different from that of the incident neutrals due to the angular spread between the incident and emergent particles in the interaction. However the quoted

errors should take account of any such effects.

The only other important parameter to be considered in the present context is the minimum energy required by the charged secondaries to satisfy the electronic selection. This is approximately the minimum kinetic energy required by a particle, produced at the centre of the target, so that it can just traverse the remainder of the telescope. From the previous normalisation of the telescope materials to  $\text{g. cm.}^{-2}$  water equivalent (Chapter 3) the minimum kinetic energies required by protons, pions or muons can easily be evaluated from range - energy tables due to Serre, 1967, and the limiting values are given below.

Particle	Minimum Kinetic Energy (Mev)	
	N Series	M Series
P	701	344
$\pi$	449	185
$\mu$	435	173

The rates of events with greater than zero, one, and two prongs emerging from the interaction region have been evaluated in units of  $\text{cm.}^{-2}\text{sec.}^{-1}\text{sterad}^{-1}$  ( $\text{g. cm.}^{-2}$ )<sup>-1</sup> and are tabulated below as a function of the minimum visible kinetic energy carried away by the observed prongs from the neutral interaction, where it has been assumed that the penetrating particle is a pion and that the other prongs are protons and that the interaction occurred at the centre of the target.

	M Series			N Series		
	Rate of events with a visible energy transfer greater than E Mev $\text{cm.}^{-2}\text{sec.}^{-1}\text{sterad}^{-1}(\text{g. cm}^{-2})^{-1}$ $\times 10^7$	7.8 $\pm 0.46$	5.49 $\pm 0.39$	3.55 $\pm 0.31$	0.44 $\pm 0.02$	0.33 $\pm 0.02$
E Mev	>185	>325	>465	>449	>589	>729
Number of emergent charged prongs, n.	>0	>1	>2	>0	>1	>2

### 7.2.5 Preliminary conclusions and a more refined analysis.

The results so far, by virtue of the fraction of events observed with multiple prongs leaving the target region of 0.74 and 0.7 for the N and M series respectively, are suggestive of the majority of triggers being initiated by neutral nuclear active particles (neutrons), since events induced by neutrinos should in general exhibit only one emergent charged prong, a muon. In fact the quoted numbers are most likely underestimates of multiple prong production in that they refer only to visible prongs, and as the telescope does not have continuous visual sensitivity many low energy prongs will be missed.

Accepting the presence of a strong neutron component, responsible for the production of the multi-prong events, a more refined analysis of the single prong events is warranted with respect to establishing the identity of the individual particles and determining whether or not there is any evidence for a directly produced muon signal. It is relevant first to consider which particles may be expected among the secondary products. Assuming an admixture of neutrons and neutrinos as constituting the neutral primaries it would seem justifiable to expect single pions, protons and muons to comprise the observed secondaries. The crux of the problem is thus to separate the nuclear-active component of pions and protons from a possible weakly interacting muon signal, and while it should be relatively easy to separate out the proton component (if it occurs with sub-relativistic velocities) a separation of pions from muons is not, in the optimum circumstances, simple and perhaps not even possible with the present experimental arrangement. Despite the obvious difficulties an attempt has been made to analyse the single secondaries in more detail with the hope of obtaining their identities.

The single prong events have been classified into three categories according to whether they are unscattered, scattered (where the scattering

does not result in further charged particle production) or whether they interact, resulting in the production of other particles while traversing the telescope. A 'scattering' is defined as that in which a projected angle of scatter of greater than  $4^{\circ}$  is observed in either flash tube elevation, this being the minimum angular deviation that can be efficiently detected. A breakdown of the events is tabulated below for both series of measurements.

	N series	M series
Total number of singles	93	86
Number 'unscattered'	17	30
Number 'scattered'	47	22
Number 'interacting'	29	34.

The nature of the interactions observed was atypical of muonic behaviour and suggests that the component in this category is nuclear active, with the consequence that its neutral origins were most probably neutrons. An analysis of the scattered and unscattered events taken together yields a somewhat different result. When resort was taken to the pulse heights measured in each counter it was possible to subdivide the events into two distinct groups; those which showed fairly high levels of ionisation in each counter, the level increasing as the particle traversed the telescope, and those which remained minimally ionising throughout the telescope, apart from a few which registered a high level of ionisation in counter F only. The particles in the former group from their rate of change of ionisation in traversing the telescope were found to be consistent with the majority of them being protons (they could not be pions or muons since the recorded levels of ionisation were too great to allow such particles to traverse the telescope to the next scintillator - typically a pion ionising at  $1.7 I_{\min}$  has a residual range of only  $11 \text{ g. cm.}^{-2}$

of water) and hence presumably produced in neutron interactions, while the particles in the latter group exhibiting relativistic properties could be either pions, muons or even protons. The breakdown of the events into the two groups is given below.

	N series	M series
Sub-relativistic protons	25	28
Minimum ionising particles	39	24

A more striking result was obtained when the distribution of true scattering angle was considered for each group, and this can be seen in Figure 7.3 where the distributions for each series are given. It is immediately apparent that there is a significant difference, in both cases, between the scattering distribution for sub-relativistic protons and that for the relativistic particles, the protons having a much higher probability of being scattered. The fact that protons are observed to have a higher scattering probability and that they are nuclear active is suggestive of the relativistic particles perhaps being predominantly weakly interacting. Further it can be realised that the scattering distribution for the relativistic particles in the N series is not particularly inconsistent with the majority of them being muons, when the expected root mean square true angle of scatter, for muons of energy just sufficient to traverse V-F, of  $\sim 13^\circ$  is considered. However a conclusion at this stage in terms of these particles being muons would be somewhat premature.

So far the multi-prong, interacting, and sub-relativistic proton events can be attributed to having neutron origins, and there remain only the relativistic particles whose origins need further discussion. Having observed the production of protons in the sub-relativistic sample then they must also be present in the relativistic sample, since it is inconceivable that the energy

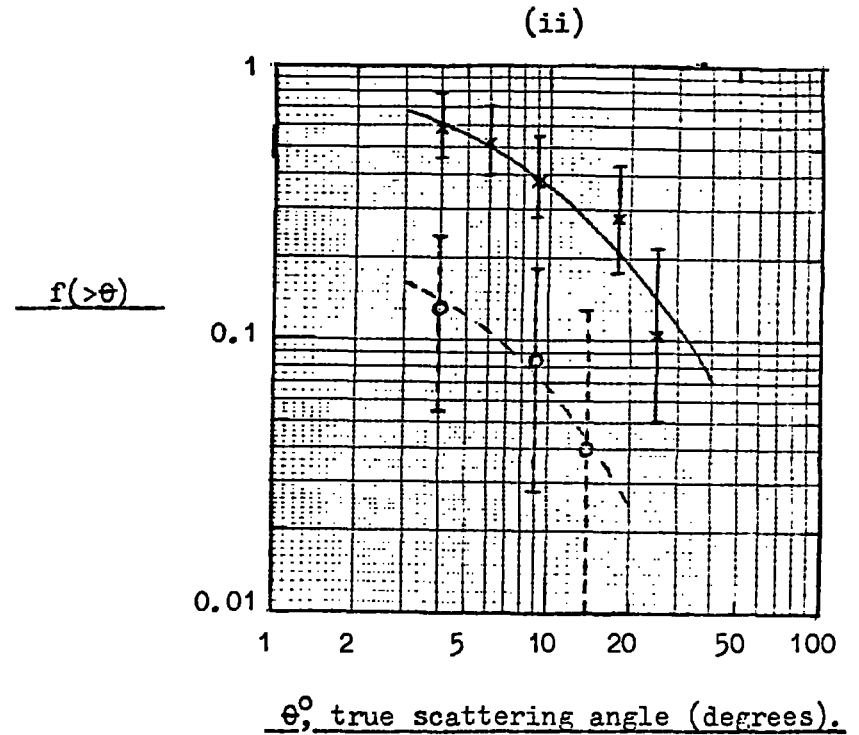
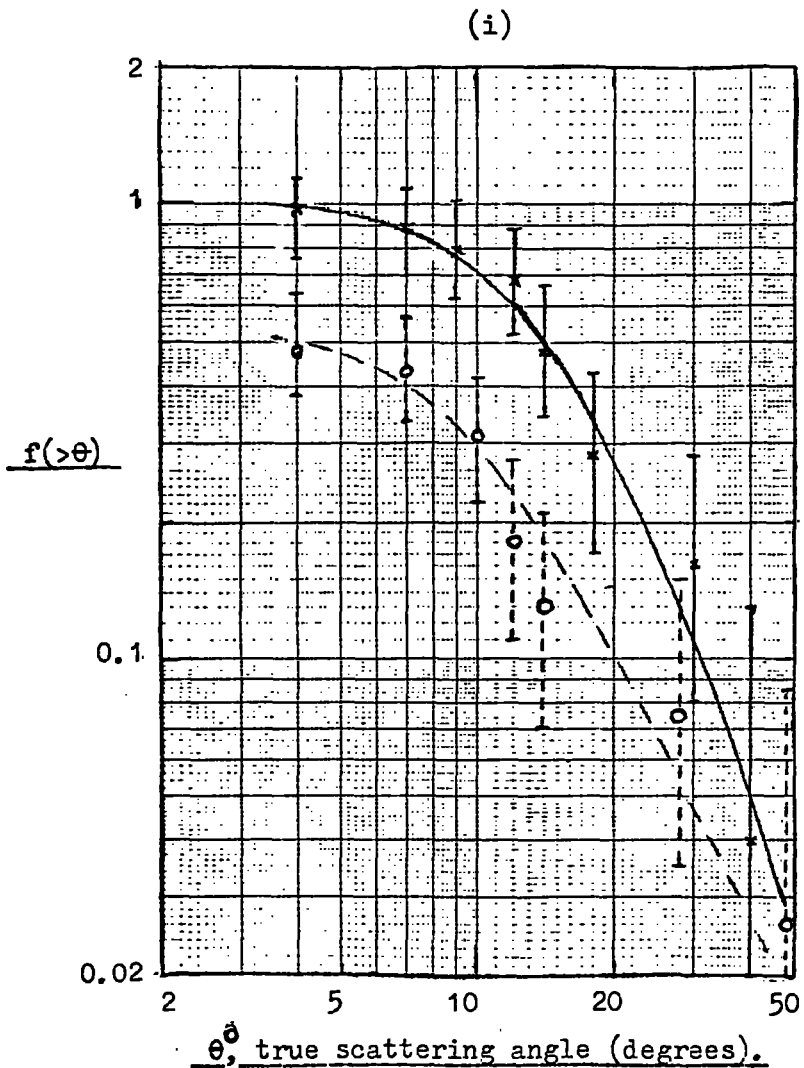


Figure 7.3

The true angle scattering distributions for neutrally induced single particles accepted in the N series (i) and in the H series (ii). The crosses refer to sub-relativistic particles and the open circles to minimum ionising particles ( $\pi, \mu$ , or  $p$ ).

spectrum of protons produced in neutron interactions is discontinuous. Further, a signal from relativistic pions would also be expected from the interactions of incident neutrons. However to suggest the presence of protons and pions to a large extent in the relativistic sample would appear at first sight to be particularly difficult, due to the differences obtained in the scattering analysis between the relativistic and sub-relativistic proton sample. This deviation however can be reconciled when consideration is given to the expected scattering characteristics of pions and protons in this sample.

A review by Major, 1959, of low energy pion interactions in emulsion shows that the probability of a pion suffering absorption or charge exchange (resulting in the loss of the pion) in an inelastic interaction is 0.7 and 0.85 for pion energies of 250 Mev and 110 Mev respectively (where the energies refer to a pion at the centre of the telescope which was incident with just sufficient energy to penetrate from V-F for the N and M series respectively). Thus pions undergoing inelastic interactions in the telescope will have a high probability of not being selected, and those having interactions other than in which absorption or charge exchange occurs will be predominantly in the 'interacting' category by virtue of the other charged particles produced. It can be concluded therefore that single pions observed in the experiment will be biased towards those not suffering any inelastic interactions in the telescope, and any scattered pions that are observed will have come primarily through elastic and multiple Coulomb processes.

Returning to protons there are several factors which render those in the relativistic sample to be less strongly scattered than those in the sub-relativistic sample: the elastic scattering cross section falling with increasing energy; the scattering angle decreasing with increasing energy for

a fixed energy transfer, coupled with the minimum scattering angle that could be efficiently observed of  $4^{\circ}$ ; and the probability of further charged particle production in a proton interaction increasing with increasing energy (resulting in higher energy interacting protons having a greater probability of being classified in the 'interacting' category). It can thus be realised that, due to the experimental bias towards non-interacting pions and the changing nature of the characteristics of proton interactions with increasing energy, the scattering distribution obtained for the relativistic sample, while appearing at first sight to be uncharacteristic of nuclear active particles, is in fact not inconsistent with what might be expected for pions and protons, with the result that no separation of a non-nuclear active component is possible in terms of a scattering analysis.

There is, however, evidence for a nuclear active component in the relativistic sample from observations of the scatterings, since the majority show single point scattering which is characteristic of elastic scattering rather than multiple Coulomb scattering, as would be expected if the sample was dominantly muonic. Despite this it is not possible to conclude that the whole sample is nuclear active, and the only remaining method of establishing the magnitude of a possible muon signal would be to calculate the expected number of neutron induced pions and protons and use subtraction techniques. However such a calculation is complex, and although it is treated in some detail in Section 7.7 the uncertainties involved are such that no firm conclusions can be drawn as to the presence or otherwise of a muon signal. For this reason perhaps all that is justifiable is to assume all the events in the relativistic sample to be muons, and use this number to set an upper limit to their produced intensity (this will be a particularly liberal upper limit in that there is

evidence for a sizeable proton and pion component from observations of single point scatters and from the analysis in Section 7.7). Under this assumption the upper limits of muon production are then  $1.4 \cdot 10^{-7}$  and  $7.7 \cdot 10^{-9}$   $\text{cm.}^{-2}\text{sec.}^{-1}\text{sterad}^{-1}(\text{g. cm.}^{-2})^{-1}$  for muon energies greater than 173 Mev and 435 Mev respectively.

### 7.3. Muons resulting from the interactions of neutral primaries.

#### 7.3.1 The experimental arrangement and electronic selection.

This series of measurements, the C series, was designed to detect the presence of muons produced directly or indirectly in the interactions of neutral primaries, using a method similar to that of Cowan et al., 1967, where the presence of a stopping muon is inferred from observations of its decay electron.

To improve the visual efficiency of the detector for locating the decay electrons a slight modification was made to the telescope from its form in the M series, a further four layered flash tube tray being included in the front elevation. The revised telescope is shown in Figure 7.4. Events were selected by means of a VC  $\bar{\text{CI}} \bar{\text{B}}$  coincidence, having a resolving time of 55 ns., (this selecting incident neutrals interacting in the region of V and producing a charged particle or particles) which was followed in a time interval 0.26 - 5.5  $\mu\text{s.}$  by a further pulse from C, D or E (this selecting the decay electron from a  $\mu^- \rightarrow e$  decay). The discrimination levels used throughout the search are given below, where they are expressed in terms of  $E_s$  and  $E_c$  as before

Counter	B	CI	V	C	D	E
Discrimination level	0.05	0.3	0.1	0.2	0.2	0.2

The electronic logic employed was similar to that previously used with the addition of a further coincidence unit of longer resolving time to afford the



selection of the delayed decay electron.

On an event satisfying the electronic logic the sequence of events was as described in the earlier experiments, apart from significant changes to the mode in which the counter pulse heights were displayed. As the coincidence was now defined by the arrival time of the decay electron, a delay line of  $5.5 \mu\text{s}$ . had to be incorporated into the pulse height display to avoid losing parts of the pulse train, and the flash tubes were pulsed after a time delay of  $15 \mu\text{s}$ . to avoid pick-up problems (such a delay results in a negligible reduction in the flash tube efficiency, as can be seen in Figure 2.1, from that pertaining at a  $5 \mu\text{s}$ . delay, the value previously used).

### 7.3.2 The basic data and film analysis.

The telescope was operated for 140 hours in which time 1,046 events satisfied the electronic logic. Because of interpretation problems the analysis was restricted to events satisfying a  $VCD \bar{B} \bar{C} I$  coincidence which was followed by a delayed pulse from D or E, this reducing the effective number of triggers to 253. From this sample events were accepted from the film which satisfied the following selection criteria: a charged particle (or particles) should emerge from the target region and the upward projection of its trajectory should intersect scintillator B; the particle should be observed to stop in the telescope region D,  $F_6$ ,  $F_d$ , E,  $F_7$ ,  $F_e$  and in stopping give rise to a visible decay electron emerging from the stopping point (a visible decay electron was defined as a minimum of two flashed tubes, one in each of two adjacent layers).

In all 10 events satisfied the selection criteria, five of which showed a single particle leaving the target region and the other five showing either two or three emergent prongs, one of which stopped in each case and showed a visible decay electron. The remaining 243 events comprised the following:-

single (and multiple) neutrally induced tracks stopping in the required region but not giving rise to a visible electron; neutrally induced bursts in which a decay electron could not be observed even if it were present, due to the flash tube saturation in the stopping region; and angled tracks or bursts traversing C-E accompanied by a random pulse in  $V_1$ , which were of no interest since they were probably not neutrally induced nor were they within the defined telescope acceptance.

For each of the ten events accepted the trajectories of the neutral induced secondaries and the decay electron were recorded and the relevant pulse height information measured. This information, as well as giving evidence that the incident particle was truly neutral (from measurements of the pulse heights in A, CII, B and CI), also served as a check on the visual information regarding the decay electron, in that the source of the delayed pulse could be shown to be consistent with the location of the electron. The only other parameter measured was the time delay between the prompt coincidence and the decay electron, this being determined with a precision of  $0.1 \mu\text{s}$ , the oscilloscope sweep speed being  $1 \mu\text{s}/\text{cm}$ .

Three of the selected events are shown in Figure 7.5 (a-c), and the properties of all ten events are tabulated in Table 7.1.

### 7.3.3 Calibration of the telescope with stopping atmospheric muons.

The purpose of this calibration, beyond ensuring the correct functioning of the electronic logic in selecting  $\mu^- - e$  decays, was to establish the detection efficiency under the stringent acceptance criteria imposed (these were given in the last section and were necessary to avoid distortion of the sample by ambiguous events), and to study the behaviour of low energy muons, with respect to scattering on traversing the telescope.

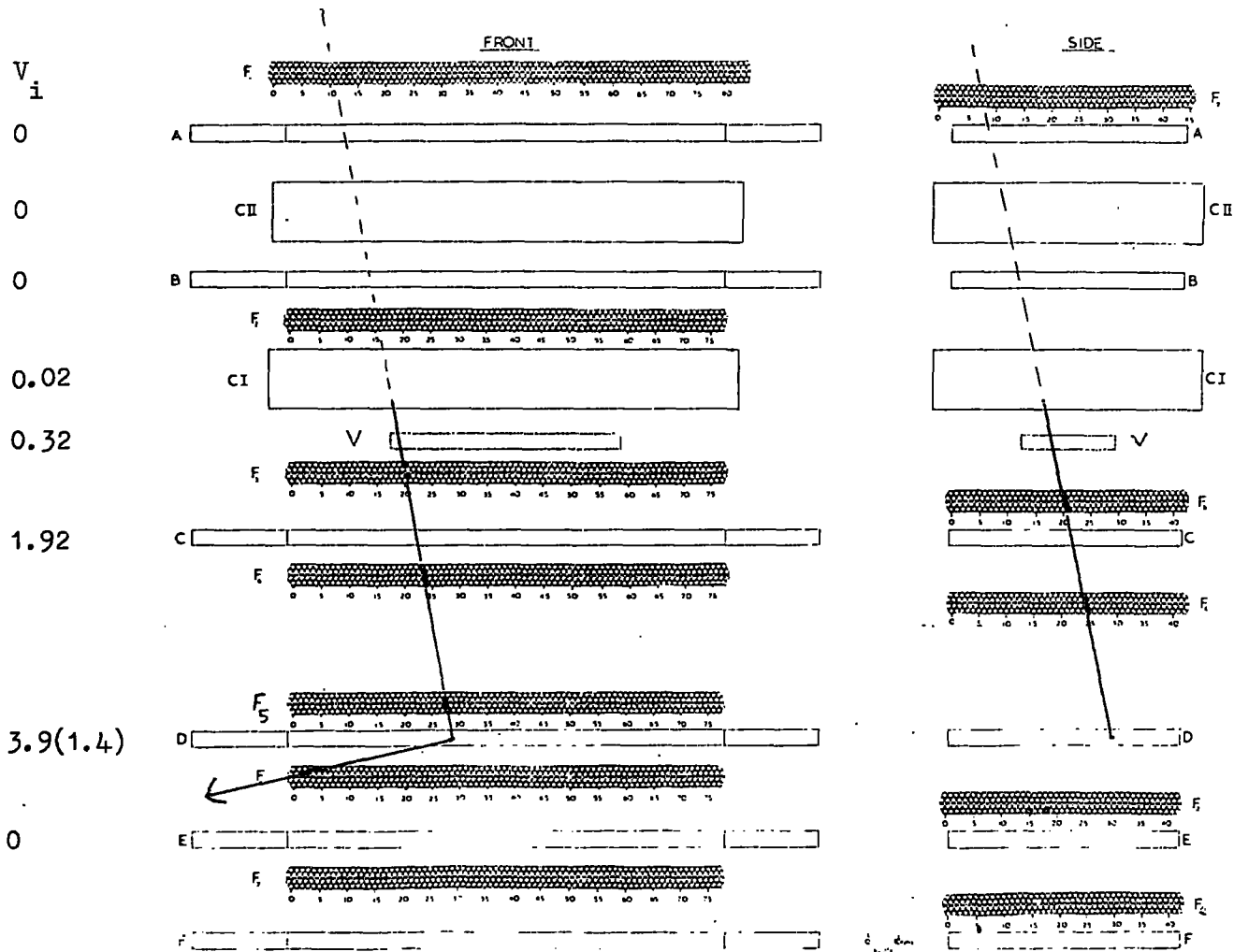


Figure 7.5(a) Event C8/70 showing the production of a single unscattered neutrally induced particle which stops and leads to a  $\mu$ - $e$  decay. The pulse height, in terms of  $E$ , from each counter is shown and the value in brackets refers to the delayed decay electron.

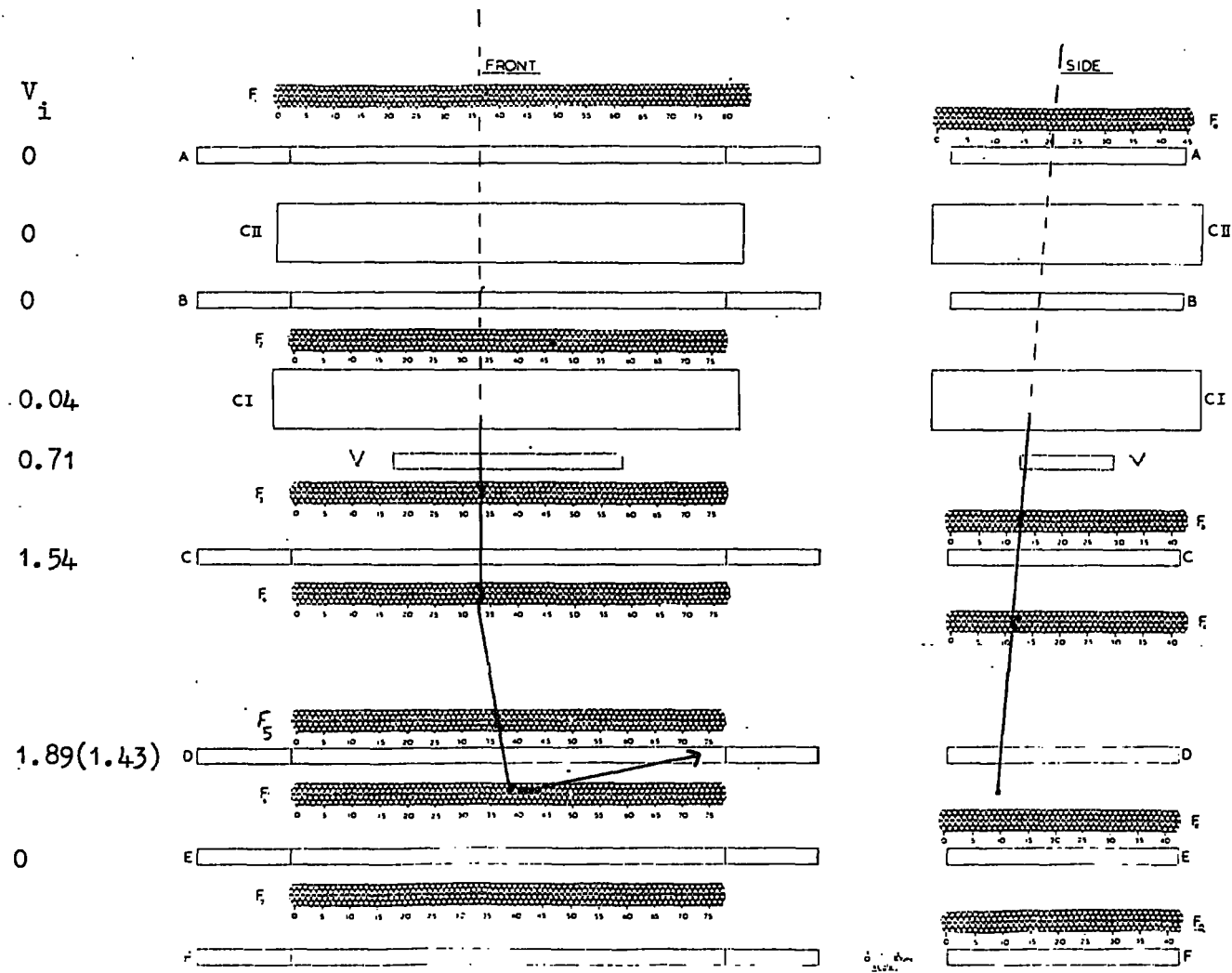


Figure 7.5(b)

Event C7/17 showing the production of a single neutrally induced scattered particle which leads to an observed  $\mu$ - $e$  decay. The pulse height, in terms of  $E$ , from each counter is shown and the value in brackets refers to the delayed decay electron pulse.



Table 7.1

Events accepted in the C series showing a visible

decay electron

a) Single prong events

Event No.	Angle of scatter			Location of the decay	Time delay of the decay electron $\mu$ s.
	Front elevation	Side elevation	True angle		
C5 / 101	0°	N.O.	N.O.	D	1.2
C7/17	12°	N.O.	$\gg 12^\circ$	F <sub>6</sub>	2.1
C8/70	0°	N.O.	N.O.	D	1.3
C11/48	17°	35°	37.5°	E	1.1
C11/115	11°	11°	15.3°	F <sub>d</sub>	2.7

b) Multiple (n = 2 or 3) prong events.

Event No.	Angle of scatter			Location of the decay	Time delay of the decay electron $\mu$ s.
	Front elevation	Side elevation	True angle		
C5/8	0°	N.O.	N.O.	F <sub>6</sub>	3.7
C8/36	4.5°	N.O.	$\gg 4.5^\circ$	D	2.9
C10/20	3°	3°	4.3°	F <sub>7</sub>	1.2
C10/163	3°	N.O.	$\gg 3^\circ$	D	0.6
C10/219	17°	21°	26.2°	F <sub>6</sub>	1.6

N.O. - scattering not observable in side elevation due to only two available flash tube coordinates.

Stopping and decaying incident muons were selected by a coincidence  $BVCD\bar{F}$  which was followed in a time interval  $0.26 - 5.5 \mu s.$  by a pulse from C, D or E. With this arrangement the same conditions pertained as in the neutral induced muon search, the adding of scintillator F in anticoincidence having no more effect than reducing the rate of random triggers. The telescope was operated in this mode for 1.383 hours in which 240 events were recorded. The events were categorised as follows:- random events in which a second spurious track was observed to traverse scintillator C,D or E and provided the delayed signal; those in which the particle stopped without the observation of a decay electron, despite the occurrence of a delayed pulse from the scintillator in which the particle stopped; and those which stopped and showed the appearance of a visible electron, events of this type being subdivided into two groups of those stopping in the scintillators, and those stopping in the flash tube trays. The basic data and classification of the events are tabulated below.

Total running time (hours)	1.383
Useful running time (hours)	0.883
Total number of events	240
Observed 'randoms'	39
Stopping particles without visible e	107
Events with visible e emerging from D,E; $F_6 F_7 F_d F_e$ ;	58
	36

From the counting rates of  $BVCD\bar{F}$  of  $157 \text{ min}^{-1}$  and  $(C+D+E)$  of  $3.1 \cdot 10^4 \text{ min}^{-1}$  the expected number of random events in the running time was  $45 \pm 7$ , and as the observed number was 39 it is reasonable to assume that the 107 events showing no visible decay electron are in fact stopping muons, where the decay electron triggers the scintillator but does not penetrate the flash tubes. The delay distribution between the prompt coincidence and the decay electron for the events

attributed to a  $\mu^-e$  decay is shown in Figure 7.6 and a least squares fit to the points yields a value of  $1.9 \pm 0.25 \mu\text{s}$  for the muon lifetime, a value not inconsistent with the accepted value of  $2.2 \mu\text{s}$ . In fact a slightly reduced value might be expected in the experimental situation due to the possibility of  $\mu^-$  capture, although such effects would be slight in that the majority of particles are observed to stop in the scintillators which comprise predominantly hydrogen and carbon. This agreement with the expected muon lifetime shows the correct operation of the instrument.

A quantity of more importance is the efficiency with which  $\mu^-e$  decays are detected on demanding the appearance of a visible decay electron. The mode of selection of  $\mu^-e$  decays is heavily biased towards muons stopping in the scintillators, as in these cases the decay electron is automatically registered (provided its energy is greater than 2 Mev, the discrimination level on the scintillators), whereas for muons stopping in the flash tubes the decay electron has to emerge in a favourable direction and not stop before reaching a scintillator which can record its presence. From the relative amounts of material in the scintillators (D and E) and the flash tube trays ( $F_6, F_7, F_d$  and  $F_e$ ) of 10.2 and 19.2 g. cm.<sup>-2</sup> water equivalent respectively, one would expect that in the absence of selection biases, and assuming a uniform stopping distribution of particles in this region, that the number of  $\mu^-e$  decays occurring in the flash tube trays should be 1.88 times those stopping in the scintillators. The results of the calibration give this ratio to be  $0.23 \pm 0.045$ , and assuming the scintillators to be 100% efficient in electronically recording a  $\mu^-e$  decay for a muon stopping in a scintillator (this is reasonable in that those lost will be decay electrons having energies less than 2 Mev (<1%) and  $\mu^-$  captures, also very small), the efficiency of recording a  $\mu^-e$  decay in the flash tube trays ( $F_6, F_7, F_d$  and  $F_e$ ) is  $0.122 \pm 0.023$ . It should

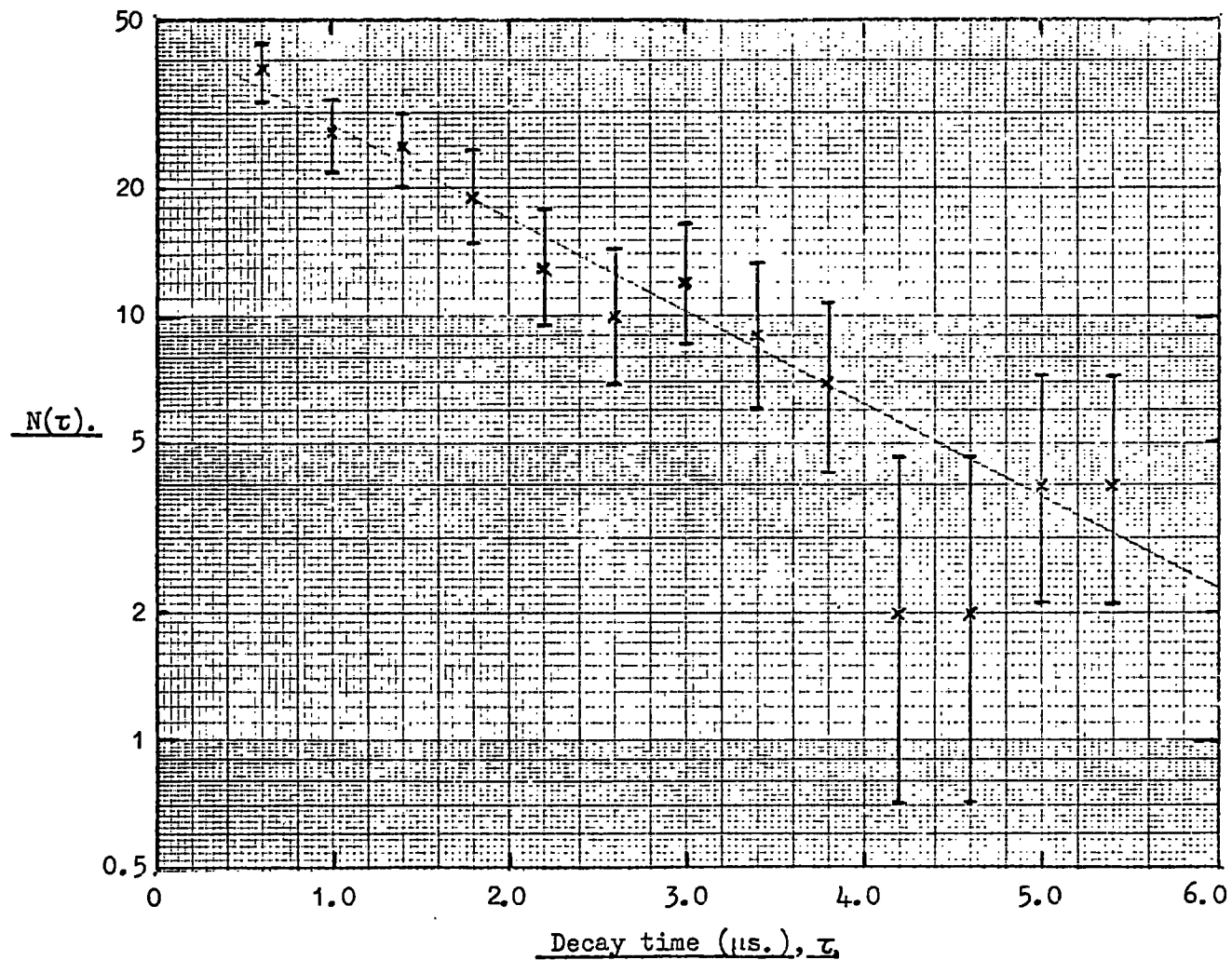


Figure 7.6 The decay time distribution for  $\mu - e$  decays in which the electron was observed. A least squares fit to the data gives a muon lifetime of  $1.9 \pm 0.25 \mu\text{s.}$

be noted that this quantity, as well as taking account of the reduced efficiency due to the previously discussed selection biases, also takes account of the increased probability of  $\mu^-$  capture in the flash tube trays. Considering the number of  $\mu^-e$  decays observed with and without observed decay electrons (35% with observed electrons for muons stopping in the scintillators and effectively 100% for those stopping in the flash tubes) the overall efficiency of accepting a muon stopping in the telescope region D-F<sub>e</sub>, when the presence of a visible decay electron is demanded, is  $20.5 \pm 5.5\%$ , which is further reduced to  $16.5 \pm 4.5\%$  when account is taken of the finite time interval in which the decay electrons were accepted.

Support for the validity of this calculated efficiency can be obtained by evaluating the intensity of muons detected in this calibration and comparing it with other measurements of the low energy muon flux. The telescope was sensitive to muons incident in the momentum band 352 - 412 Mev/c and the telescope aperture has been derived as  $9.3 \cdot 10^2 \text{ cm}^2 \text{ sterad.}$ , using a method of normalising the counting rates as discussed in Section 7.2.4. The observed intensity was  $5.3 \cdot 10^{-7} \text{ cm.}^{-2} \text{ sec.}^{-1} \text{ sterad.}^{-1} (\text{Mev/c})^{-1}$  and correcting for the calculated efficiency this yields an intensity of  $(3.2 \pm 0.9) \cdot 10^{-6} \text{ cm.}^{-2} \text{ sec.}^{-1} \text{ sterad.}^{-1} (\text{Mev/c})^{-1}$  at a mean muon momentum of 382 Mev/c. This is to be compared with the measurement of the low energy muon spectrum by Gardener et al., 1962, the measurement being made at the same location as the present work, which gives an intensity of  $\sim 2.5 \cdot 10^{-6} \text{ cm.}^{-2} \text{ sec.}^{-1} \text{ sterad.}^{-1} (\text{Mev/c})^{-1}$  at the same momentum. The apparent agreement signifies that the calculated efficiency can be used with confidence when applied to correct the observed rate of neutrally induced  $\mu^-e$  decays.

Information obtained on the scattering of the muons selected in this

calibration will be presented in the next section.

#### 7.3.4 The analysis and identity of the neutral induced events.

While there can be little doubt that the decay of a muon has been observed in the 10 events previously extracted from the film records of the neutral search (Section 7.3.2), a question of greater importance is whether the muon was produced directly as the consequence of a neutral interaction or whether it was the progeny of a neutron induced stopping positive pion. Although the pulse height in each counter was displayed for each event the resolution was not sufficient to separate a direct  $\mu \rightarrow e$  decay from that arising initially from a pion decay, and lacking such information other means had to be sought to attempt to resolve this problem.

Of the ten events accepted five emerged from the target with further particle accompaniment and it would seem reasonable to assume these to have been neutron induced, with the  $\mu \rightarrow e$  decay being the result of a decay of a stopping pion. No such conclusion could be drawn regarding the remaining five singly produced events and resort was made to an analysis of their scattering in the telescope. A calculation of the expected scattering distribution for pions or muons traversing the multi-medium telescope is obviously complex, and for this reason it was decided to measure the scattering of the muons obtained in the calibration and compare this, as being representative of what would be expected for muons, with the distributions of the neutrally induced events. To preserve the same conditions as pertained in the neutral search only the 94 muon decays in which a visible decay electron was observed were analysed, and scatterings were looked for in the telescope region  $F_3 - F_e$ , where the flash tube information from  $F_1, F_2$  and  $F_a$  was disregarded in determining whether a scattering had occurred, this information not being available in

the neutral experiment. This sample is expected to comprise solely muons apart from perhaps one or two atmospheric pions at the most. (Barton and Slade, 1965, have measured the low energy  $\pi/\mu$  ratio at sea level and underground and found a value of  $\sim 1\%$ ). The projected angle scattering distribution of this muon sample is given in Figure 7.7 and is compared with the scattering distributions of the singly and multiple produced events observed in the neutral experiment.

The scattering distributions of both types of neutrally induced events show a divergence from that obtained for stopping muons, and are suggestive of the produced secondaries not in fact being muons but perhaps pions which stop and lead to a  $\pi - \mu - e$  decay. However the statistical significance that can be attached to such an analysis is quite weak, and while suggesting the presence of pions it precludes an interpretation of all the neutral events in these terms. Again, as in the N and M series of measurements, perhaps the only valid conclusion to be drawn is an upper limit to the intensity of produced muons. Three of the singly produced particles suffered single large angle scatters of  $37^\circ$ ,  $15^\circ$  and  $>12^\circ$  respectively, values which are atypical of those expected of muons, and it would seem reasonable to conclude that the number of directly produced muons observed in the search was  $\leq 2$ .

Making the assumption that all the produced secondaries originated from the centre of the target the search was sensitive to muons in the energy band 120 - 179 Mev (an energy band of 130 - 191 Mev for pions). The target in which the interactions could occur was slightly less than that in the N and M series, due to the different discrimination levels employed on counters V and CI, and was equal to  $20.6 \text{ g. cm.}^{-2}$  having a mean atomic weight of 25.3. Based on the assumption that the two unscattered events are muons this number

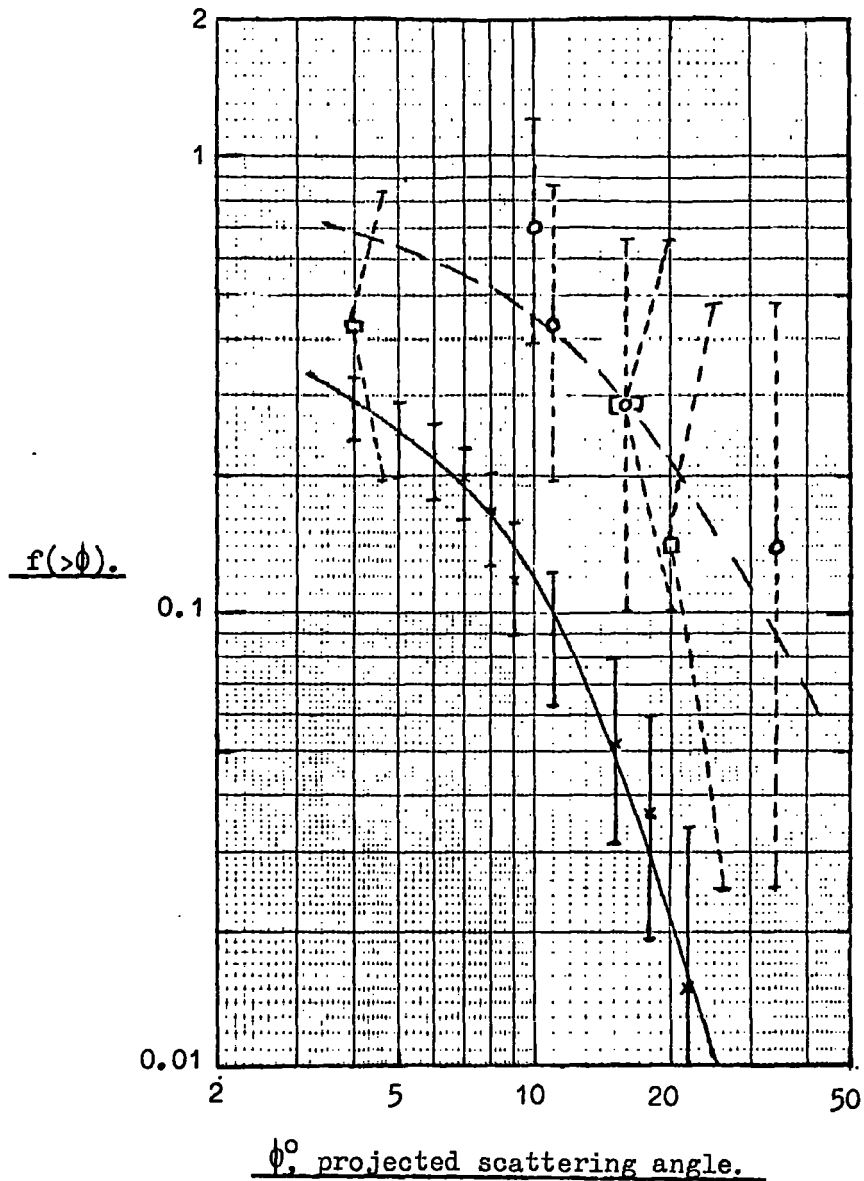


Figure 7.7

The projected angle scattering distribution of muons selected in the telescope calibration (crosses) compared with that of the neutrally induced  $\mu$ -e decays. The open circles refer to the single prong events and the open squares to events where 2 or 3 charged prongs emerged from the target.

has been used to set an upper limit to their intensity of  $2.15 \cdot 10^{-11} \text{ cm.}^{-2} \text{ sec.}^{-1} \text{ sterad.}^{-1} \text{ Mev}^{-1} (\text{g. cm.}^{-2})^{-1}$ , where the telescope aperture has been taken as  $9.3 \cdot 10^2 \text{ cm.}^2 \text{ sterad.}$ , and a correction applied for the efficiency of observing a  $\mu \rightarrow e$  decay.

#### 7.4 Summary of the N, M and C series

In each series of measurements single secondaries have been observed as the products of neutral interactions, and in the C series the presence of muons has been concluded from the observation of their decays. Unfortunately in none of the experiments has an analysis been forthcoming that could reliably separate out a neutron induced pion or proton component from possible directly produced muons, and while evidence has been found for the presence of pions and protons (single point scatterings in the N and M series and large angle scatters atypical of muons in the C series, as well as the theoretical analysis in Section 7.7) no definite conclusion, neither for nor against, could be made regarding a possible admixture of directly produced muons among the secondary particles. For this reason only upper limits have been imposed on the produced muon intensity and these are summarised below.

Muon Energy (Mev)	Intensity Limit
$E_{\mu} > 173$	$< 1.47 \cdot 10^{-7} \text{ cm.}^{-2} \text{ sec.}^{-1} \text{ sterad.}^{-1} (\text{g. cm.}^{-2})^{-1}$
$E_{\mu} > 435$	$< 7.7 \cdot 10^{-9} \text{ cm.}^{-2} \text{ sec.}^{-1} \text{ sterad.}^{-1} (\text{g. cm.}^{-2})^{-1}$
$120 < E_{\mu} < 179$	$< 2.15 \cdot 10^{-11} \text{ cm.}^{-2} \text{ sec.}^{-1} \text{ sterad.}^{-1} \text{ Mev}^{-1} (\text{g. cm.}^{-2})^{-1}$

The intensities are necessarily liberal upper limits in the absence of suitable techniques for extracting the pion background. In conclusion, experiments of the present type are not particularly successful in looking for a neutrino induced muon signal in the presence of a high background of neutron induced pions and protons, and any conclusions drawn as to the existence of

such a muon component from these types of experiments must be extremely doubtful in the absence of precise calculations of the neutron induced background.

#### 7.5. Comparison with the work of Cowan et al.

These workers began their searches, initially in 1964, with large volume scintillation tanks completely surrounded by anticoincidence shields and looked for neutrally induced muons within the tanks, the presence of the muon being inferred from measurements of its decay electron (Cowan et al., 1964; Cowan et al., 1965; Ryan et al., 1966; and Buckwalter et al., 1966). More recently they have constructed a much more elaborate multiplate scintillation counter-spark chamber telescope, and the present discussion will be confined to their results obtained with this detector.

Their telescope comprised 36 spark chamber gaps (width of  $\frac{1}{2}$ " ) with a  $\frac{3}{4}$ " plastic scintillator of area 4'x4' inserted between each pair of spark gaps. This whole arrangement was contained within a box, all six sides of which were also made of plastic scintillator, and the resulting chamber was continually flushed with a neon-helium gas mixture. The spark chambers and each internal scintillator were viewed through the surrounding anticoincidence shield. Events were selected such that a neutral particle entered the chamber and produced a charged particle which later, still within the chamber, resulted in a muon decay.

Results of this work have been given by Hesse et al., 1967, and Cowan et al., 1967. They have concluded from an analysis of the scattering distribution of the produced particles, and from measurements of the decay electron delay distribution that they were observing muons directly produced in the interactions of neutral primaries (private communication), and further

they have produced maps of the celestial sphere, in the declination range  $-10^{\circ}$  to  $+70^{\circ}$ , showing the celestial coordinates of several possible sources of the neutral particles which produce the observed muons.

However they have recently looked more carefully at their telescope, and have found gross inefficiencies in their spark gaps and scintillators, with the result that the majority of events that they had observed were in fact atmospheric muons leaking through the anticoincidence detectors (private communication and Cowan et al., 1969). This reappraisal of their experiment invalidates their conclusion, based on a scattering analysis, that the events observed were neutrally induced muons (since muons would be expected to exhibit a scattering distribution characteristic of muons), and further no weight can be attached to their maps of the celestial sphere showing possible point sources of the neutral primaries. In an attempt to re-establish their data approximately 60% of the events have been rejected as attributable to atmospheric muons, but even then the remaining 1070 events are highly suggestive of still containing a large atmospheric muon background. Of this more severely sorted sample approximately 63% of the supposed neutrally induced secondaries commence in the sixth scintillator, while the starting points of the remainder are distributed over a further 13 scintillators. Such a situation is consistent with the spark gaps above the sixth scintillator being very inefficient, with the result that even their reappraised data contain a high proportion of atmospheric muons responsible for the excess of secondaries emerging from the sixth scintillator. Further it would seem a not unreasonable assumption that a sizeable fraction of the other events may also be due to incident muons.

With respect to the severe inefficiencies in the spark gaps and the anticoincidence shield negligible weight can be assigned to the results of this

experiment as any analysis of the data will always be subject to extreme uncertainty. Perhaps if the pulse height from each scintillator had been recorded such a situation could have been avoided. However it is worth noting that their initial data and that after re-appraisal, despite still containing a sizeable atmospheric ~~muon~~ background, both showed a strong sidereal correlation, and while most effects one can imagine would tend to smear such a result it must remain particularly interesting but somewhat surprising. Our own data in this respect (N, M and C series) were too weak statistically to be useful.

More recently Cowan et al., 1969, have modified the detector by placing a further anticoincidence detector above the telescope (a liquid scintillator of dimensions 6' x 6' x 5") and tuning the spark gaps individually to achieve an improved efficiency. The major modification however has been the replacing of four of the scintillators by  $\frac{3}{4}$ " aluminium plates, the purpose of which was to examine the Z dependence of the neutral particle cross section, and to try and identify the produced secondaries from an analysis of the  $\mu$ -e decays observed to occur in the aluminium plates to those occurring in the adjacent scintillators (if the signal is pionic only the positive mode will contribute to  $\mu$ -e decays in each material, with perhaps a small contribution from negative pions decaying in flight; if the signal is muonic both positive and negative modes will contribute, but the  $\mu^-$  contribution in the aluminium will be decreased to approximately one half due to the increased capture probability).

This revised instrument has only recently been put into operation and only very preliminary data are available. In a running time of 687 hours some 22 singly produced events and 18 multiple events, the latter having been attributed to neutron induced pions, have been observed (this rate of singly

induced events of  $\sim 0.8 \text{ day}^{-1}$  when compared with their previous rate of  $\sim 10 \text{ day}^{-1}$  suggests that in the earlier experiment at least 90% (and not 60% which were extracted) were due to atmospheric muons). As yet the data are too weak statistically to allow any conclusions to be drawn regarding the identity of the particles or the Z dependence of the production cross section. It is interesting to note however that their observed ratio of single to multiple events is consistent with unity, as was found in the C series, and one could perhaps speculate that as multiple pion events are observed then there must also be a sizeable production of singles.

From this preliminary data Cowan et al. have imposed a limit on  $f\sigma$  (where  $f$  is the intensity of the primary neutrals in the cosmic radiation responsible for muon production in units of  $\text{cm}^{-2}\text{sec}^{-1}\text{sterad}^{-1}$  and  $\sigma$  is the production cross section in units of  $\text{cm}^2/\text{nucleon}$ ) of  $3 \cdot 10^{-33} \text{sec}^{-1}\text{sterad}^{-1}$  per nucleon of target under the assumption that all the singly produced events are muons. A limit in these terms is not particularly meaningful in that it takes no account of the sensitive energy range of the detector, and for this reason the limit on  $f\sigma$  has been modified to  $< 10^{-34} \text{sec}^{-1}\text{sterad}^{-1} \text{Mev}^{-1}$  per nucleon, where the sensitive energy band has been taken as 30 Mev (private communication) and  $f$  is now expressed in units of  $\text{cm}^{-2}\text{sec}^{-1}\text{sterad}^{-1} \text{Mev}^{-1}$ . A limit in these same terms can be directly obtained from that given for the present work (the C series) given in Section 7.4, since 1g. of target contains  $\sim 3 \cdot 10^{23}$  nucleons useful for a neutrino or antineutrino interaction, and the resulting limit on  $f\sigma$  is  $7.3 \cdot 10^{-35} \text{sec}^{-1}\text{sterad}^{-1} \text{Mev}^{-1}$  per nucleon.

These limits, derived from the present work and from the latest experiment of Cowan et al., are in good agreement considering the statistical errors involved and the uncertainty expressed by Cowan et al. of their detection

efficiency while they are in marked disagreement with the earlier results reported by these workers. At this time however there is yet no evidence of an observation of a directly produced muon signal and the quoted values are necessarily liberal upper limits in that they contain a background, presumably pionic, of unknown magnitude (recent estimates by Cowan et al., 1969, of single pion production by neutrons have yielded background rates in the range 0.1 to several times the observed rate).

The intensity limits on neutrally induced muons evaluated from the N and M series can also be modified to give limits in terms of  $f\sigma$ , where  $f$  is now the neutral intensity in units of  $\text{cm}^{-2}\text{sec}^{-1}\text{sterad}^{-1}$ , of  $4.9 \cdot 10^{-31}$  and  $2.57 \cdot 10^{-32} \text{ sec}^{-1}\text{sterad}^{-1}$  per nucleon for neutrals of energy  $> 278 \text{ Mev}$  and  $> 540 \text{ Mev}$  respectively (assuming the muon to take all the energy of the neutral, which is assumed here to be a neutrino). Again these limits contain an undoubted pion and proton background, and while they do not give such low limits as that obtained from the C series they are useful in referring to higher energy neutrals, and furthermore it should be noted that they are integral rather than the previously used differential limits.

#### 7.6. Limits on the suggested neutrino resonance cross section.

The implications of the present measurements on the neutrino resonance suggested by Tanikawa and Watanabe, 1959, and Kinoshita, 1960, can now be considered. Kinoshita has suggested that the expected resonance cross section of  $\sim 7 \cdot 10^{-27} \text{ cm}^2$  will be smeared out to an effective cross section of  $\sim 2 \cdot 10^{-32} \text{ cm}^2$  for neutrino interactions with target nucleons in a nucleus, and consequently the contributing energy band of neutrinos will be increased.

Recent estimates of the cosmic ray muon neutrino energy spectrum below 1 Gev have been made by Wolfendale and Young, 1969, and give an intensity

of  $4.5 \cdot 10^{-4} \text{ cm.}^{-2} \text{ sec.}^{-1} \text{ sterad}^{-1} \text{ Mev.}^{-1}$  at a neutrino energy of  $\sim 260 \text{ Mev}$  (i.e. the mean neutrino energy required to produce a muon which would be selected in the C series, assuming the muon to take all the neutrino energy). From this intensity a limit of  $1.6 \cdot 10^{-31} \text{ cm}^2/\text{nucleon}$  can be imposed on the neutrino cross section in the energy range 230 - 290 Mev, a similar limit being attained if the result of the most recent experiment of Cowan et al. is used. If the muon is assumed to take a smaller fraction of the neutrino energy then a slightly increased limit for the cross section would pertain at higher neutrino energies. It is readily apparent that the measured limits are a factor of 10 greater than the expected cross section, which is further suggestive of the signal observed being predominantly pionic background. If the expected cross section is correct then such muon production through the neutrino resonance would be particularly difficult to detect in cosmic ray experiments, having to be separated from a background of neutron induced pions some ten times greater in magnitude.

Of course the situation can be reversed and one might assume the rather high limits to be due to a greatly intensified flux of neutrinos from various point sources on the celestial sphere, as was suggested by Cowan et al., 1967, from observations of a strong sidereal effect emerging from each of their several experiments (this has yet to be confirmed for their latest experiment). Taking a typical neutrino cross section of  $10^{-38} \text{ cm}^2/\text{nucleon}$  the flux of such neutrinos, subject to the previously evaluated limits on  $f\sigma$  would have to be  $\sim 10^4 \text{ cm.}^{-2} \text{ sec.}^{-1} \text{ sterad}^{-1} \text{ Mev.}^{-1}$  at a neutrino energy of  $\sim 260 \text{ Mev}$ , some  $2 \cdot 10^7$  times greater than the intensity of neutrinos produced in the atmosphere (Wolfendale and Young). If such a neutrino intensity pertained it is inconceivable that it would not have been observed by the K.G.F. and Case

With neutrino experiments, and for this reason an interpretation in terms of enormous neutrino fluxes from point sources appears very unlikely.

### 7.7. Interpretation of the present results in terms of neutron induced protons and pions.

Consideration will be given to the expected number of singly produced pions and protons which should have been observed in each experiment, in an attempt to resolve whether the observed rate of events is inconsistent with what might be expected in terms of neutron induced pions and protons. The analysis is to be confined to singly produced events and hence only the following two reactions are to be considered:-



since other reactions lead to further charged particle production giving multiple prong events, and in general such events would not be contained in the extracted single prong sample.

While both reactions will contribute to the observed events in the N and M series, only the latter will contribute in the C series, in that in this experiment the decay of a muon was the selection criterion.

#### 7.7.1 The sea level neutron spectrum.

An analysis in these terms at the present time can at the best be only approximate since the most important parameter in such a calculation, the sea level neutron spectrum is not known with any great precision, nor has it been measured in the relevant energy region. Recent measurements of the high energy sea level neutron spectrum ( $E_n > 50 \text{ Gev}$ ) have been made by Ashton and Coats, 1968, and they were found to be in good agreement with the measurements of Brooke and Wolfendale, 1964, of the proton spectrum in the same energy region. Results of Hess et al., 1959, give the neutron to proton ratio at sea

level energies greater than 80 Mev as 8, but there is little information on the variation of this ratio between such an energy and 50 Gev, the region where Ashton and Coats found the ratio to be unity. In the absence of any absolute information in this intermediate energy region, this being the important region in the present calculation, an approximate neutron spectrum has been derived by extrapolating the sea level proton momentum spectrum (Brooke and Wolfendale, 1964a) from momenta above which energy loss through ionisation is not important to lower momenta, this giving a differential neutron spectrum of the form  $N_n(p)dp = 1.6 \cdot 10^{-4} p^{-2.6} dp \text{ cm}^{-2} \text{ sec}^{-1} \text{ sterad}^{-1} (\text{Gev}/c)^{-1}$ .

#### 7.7.2 The expected number of neutron induced single protons.

The major contribution to the observed number of protons can be seen to come through charge exchange of the incident neutron, when consideration is given to the rapidly falling neutron spectrum and to the emergent proton taking almost all of the incident neutron energy. The expected number of protons has been evaluated from the following expression:

$$N_n(p)dp \cdot e^{-y} \cdot \sigma_{c.e.}(p) \cdot N_{\text{eff}} \cdot e^{-x} \cdot A \Omega t.$$

where it is assumed that the proton takes all of the incident neutron energy; and where  $N_n(p)dp$  is the derived sea level neutron momentum spectrum;

$y$  is the number of nucleon interaction mean free paths from the top of the telescope to the beginning of the target region, this taking account of the degradation of the neutron flux in reaching the target;

$\sigma_{c.e.}(p)$  is the charge exchange cross section ( $n+p \rightarrow p+n$ ), the variation of which is shown in Figure 7.8 as a function of momentum;

$N_{\text{eff}}$  is the effective number of protons in the target available for the charge exchange process after taking account of shadowing effects;  
 $x$  is the number of nucleon interaction mean free paths from the centre of the target to scintillator F;

$p_1$  and  $p_2$  are the limits of integration over the neutron spectrum;

$A\Omega$  is the telescope aperture in  $\text{cm}^2$  sterad for an incident radiation having an angular exponent of  $n = 8$ ,

and  $t$  is the running time of the experiment in seconds.

The quantities used in the calculation for each series are given below.

	$y$	$N_{\text{eff}}$	$x$	$A$ ( $\text{cm}^2$ sterad.)	$t$ (sec.)	$p_1$ (MeV/c)	$p_2$ (MeV/c)
N series	0.73	$3.65 \cdot 10^{24}$	1.98	$6.4 \cdot 10^2$	$5.05 \cdot 10^5$	1344	1542
						1542	$\infty$
M series	0.73	$3.65 \cdot 10^{24}$	0.72	$6.4 \cdot 10^2$	$2.17 \cdot 10^4$	874	1156
						1156	$\infty$

The values of  $x$  and  $y$  have been derived from the data of Chen et al., 1955, (Figure 3.19) and the telescope composition given in Section 4.8. The values of  $N_{\text{eff}}$  have been derived assuming the np total cross section to be 40 mb. and from a review of shadowing corrections by Alexander and Yekutieli, 1961, this resulting in reducing the number of protons in the target of  $6.65 \cdot 10^{24}$  to an effective number of  $3.65 \cdot 10^{24}$ . The integration has been carried out over two distinct momentum bands for each series, the lower one in both cases referring to protons that would have been categorised into the sub-relativistic sample, and the upper band referring to those appearing in the relativistic sample.

The results of the calculation are shown in Table 7.2 where the expected numbers of produced protons are compared with the experimental observations.

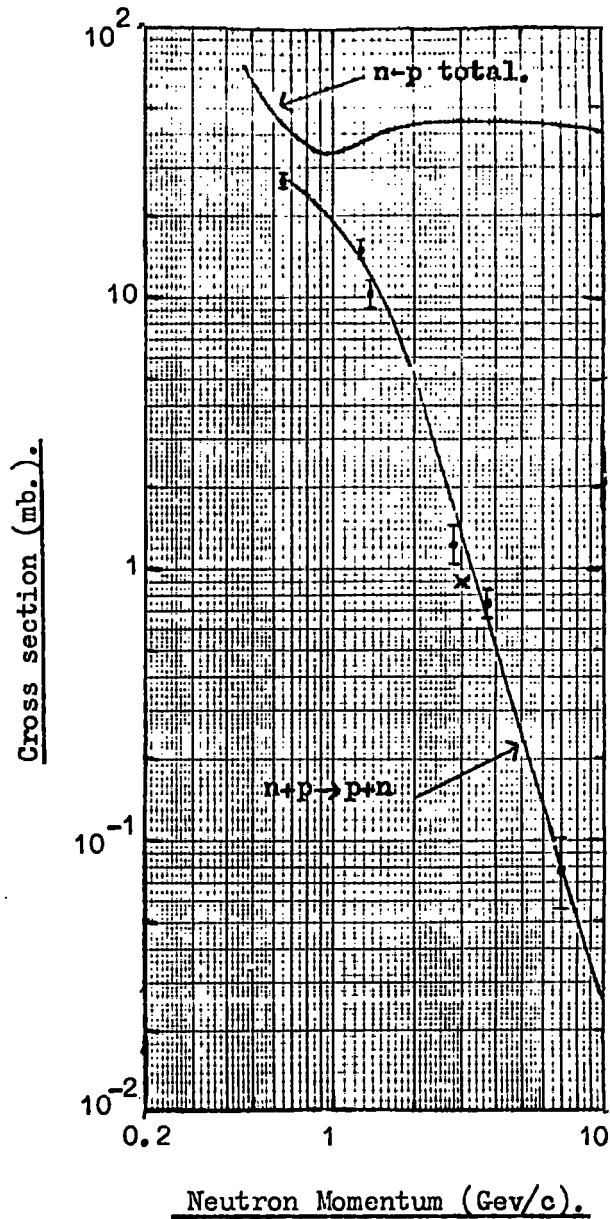
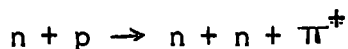


Figure 7.8

The variation of the charge exchange cross section ( $n+p \rightarrow p+n$ ) as a function of the neutron momentum. Also shown is the variation of the total np cross section. The points (circles) refer to values calculated from a summary of differential cross sections by Manning et al., 1966. The cross corresponds to a theoretical estimate of the charge exchange cross section by Narayan, 1966.

### 7.7.3 The expected number of neutron induced single pions.

As discussed earlier the only reaction to be considered is that of



in that other reactions would lead to the production of multiprong events. The cross section for single pion production via this reaction has been evaluated from a consideration of the possible channels for np inelastic interactions and their isotopic spin weights (Fermi, 1953 and 1954), the total np inelastic cross section, and the probability of such an interaction leading to the production of a single pion, as opposed to multiple pions, which is given by Lindenbaum, 1957. The resulting cross section as a function of the neutron momentum is shown in Figure 7.9.

The number of pions expected in each experiment can then be written as

$$\int_{E_{\pi}} \int_{p_n}^{p_n^2} N_n(p) dp \cdot f(p_n, E_{\pi}) dE_{\pi} \cdot e^{-y} \cdot \sigma_{\pi}(p) \cdot N_{eff} \cdot e^{-x} \cdot A \Omega t \cdot \mathcal{I}$$

where the symbols have the same meaning as in Section 7.7.2 apart from

$\sigma_{\pi}(p)$  which is the cross section for single pion production via the reaction  $n + p \rightarrow n + n + \pi^{\pm}$ ;

$x$  which is now the number of pion interaction mean free paths from the centre of the target to scintillator F (N and M series), and to the centre of the stopping region in the C series.

$\mathcal{I}$  which is the efficiency of detecting a pion by demanding the observation of a decay electron from a  $\pi \rightarrow \mu + e$  decay (applicable only to the C series);

and  $f(p_n, E_{\pi}) dE_{\pi}$  is the probability of a neutron of momentum  $p_n$  producing a pion in the energy range  $E_{\pi} \rightarrow E_{\pi} + dE_{\pi}$ .

The kinematics of the reaction have been considered under the assumption of equipartition of energy between the pion and two nucleons in the centre of mass system, and that the energy spectrum of produced pions in the laboratory

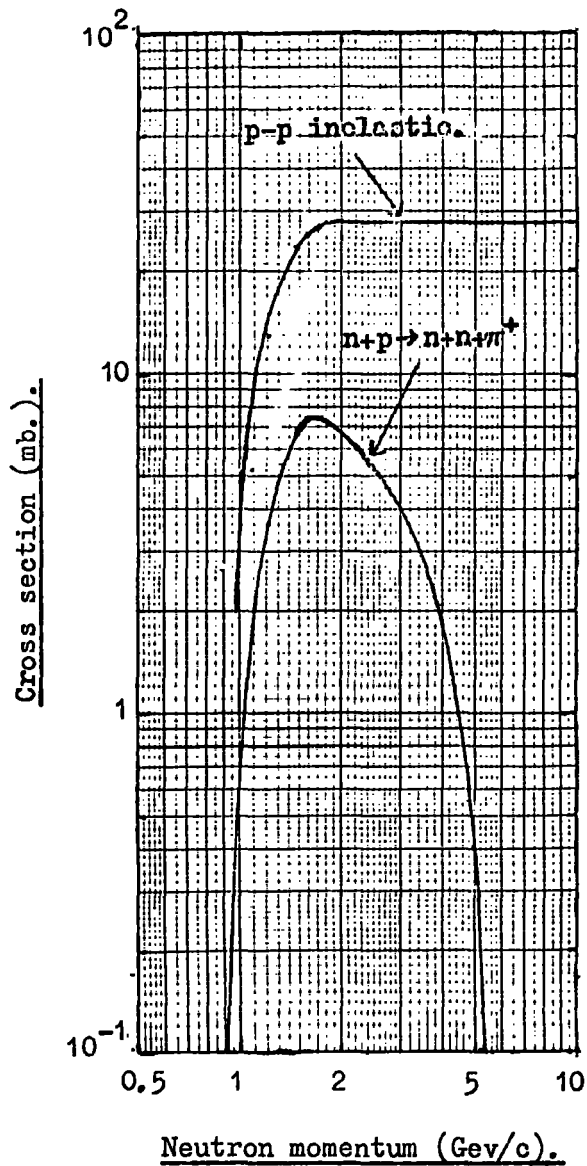


Figure 7.9

The variation of the cross section for single pion production via the reaction  $n+p \rightarrow n+n+\pi^+$  as a function of the neutron momentum. Also shown for comparison is the total p-p inelastic cross section.

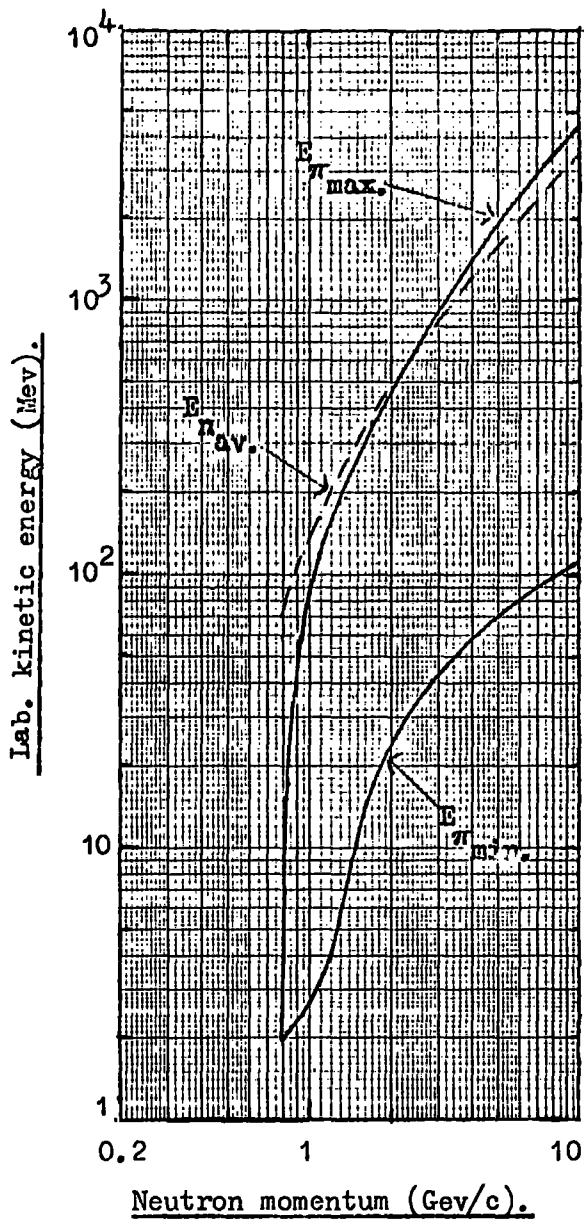


Figure 7.10

The maximum and minimum kinetic energies of a pion (in the laboratory system) which is produced in the reaction  $n+p \rightarrow n+n+\pi^+$ , under the assumption of equipartition of energy in the centre of mass, as a function of the primary neutron momentum. Also shown is the average kinetic energy of the secondary neutrons (dashed line) in the lab. system under the same assumptions.

system, from a neutron of a given incident energy, is uniform between the minimum and maximum energies that the pion can take. Under the assumption of equipartition of energy in the centre of mass the minimum and maximum pion energies are shown as a function of the incident neutron momentum in Figure 7.10, together with the mean nucleon energy produced under the same assumptions. From the minimum and maximum pion energies as a function of  $p_n$ , the quantity  $f(p_n, E_\pi) dE_\pi$  can be evaluated for each series of measurements under the assumption of a uniform pion energy spectrum in the laboratory system between these two limits.

The values of the various terms used in the calculation are given below

	$\gamma$	$N_{\text{eff}}$	$x$	$A_{\Omega}$ ( $\text{cm}^2 \text{sterad}$ )	$t$ (sec.)	$\eta$	$p_1$ ( $\text{Mev}/c$ )	$p_2$ ( $\text{Mev}/c$ )
N series	0.73	$3.65 \cdot 10^{24}$	2.55	$6.4 \cdot 10^2$	$5.05 \cdot 10^5$	1	1920	$\infty$
M series	0.73	$3.65 \cdot 10^{24}$	1.1	$6.4 \cdot 10^2$	$2.17 \cdot 10^4$	1	1325	$\infty$
C series	0.77	$3.15 \cdot 10^{24}$	0.85	$9.3 \cdot 10^2$	$5.04 \cdot 10^5$	0.165	1155	$\infty$

The pion energy bands to which each experiment was sensitive and over which the integration was applied have already been given in Sections 7.2.4 and 7.3.4. The values of  $N_{\text{eff}}$  have been derived in the same manner as before, and the values of  $x$  have been obtained from the theoretical work of Sternheimer, 1956(b), on the absorption cross sections of pions on various nuclei. The results of the calculation are given in Table 7.2 together with the experimental observations and the expected numbers of protons.

#### 7.7.4 Comparison between the observed and predicted numbers.

Reference to Table 7.2 shows that, apart from the C series where the observed and expected numbers of singly produced events are not inconsistent, the observed numbers of events are approximately twice the expected numbers. Having obtained such a result one might presume that there is evidence for a neutrino induced muon signal to make up the deficit in the calculated numbers.

Table 7.2

	M series			N series			C series	
Proton kinetic energy that would be detected from $n + p \rightarrow p + n$	> 344 Mev			> 701 Mev			-	
Pion kinetic energy that would be detected from $n + p \rightarrow n + p + \pi^+$	> 185 Mev			> 449 Mev			130-191 Mev	
	Observed	Expected		Observed	Expected		Observed	Expected
		$\pi^+$	p		$\pi^+$	p		$\pi^+$
No. of identified protons	28	-	11.5	25	-	12.9	-	-
No. of minimum ionising particles	24	1.7	8.5	39	2.2	15.2	-	-
Total	52	21.7		64	30.3		5	6.3

Comparison of the observed number of events with the expected number from  $n + p \rightarrow p + n$  and  $n + p \rightarrow n + n + \pi^+$  reactions.

The secondary particles were identified as protons if their kinetic energies at production were in the range 344 - 551 Mev for the M series, and 701 - 867 Mev for the N series. Minimum ionising particles refer to all produced pions and to protons with production energies > 551 Mev and > 867 Mev for the M and N series respectively.

However the inherent error in the neutron spectrum assumed invalidates any such conclusion, and in fact there is evidence that the calculated numbers are small due to an underestimated neutron spectrum rather than anything else. This arises from the observed numbers of identified sub-relativistic protons being approximately twice the calculated numbers. The suggestion of a muon contamination of the signal would not restore agreement in this area in that a muon could not be interpreted as a sub-relativistic proton, since its residual range is small once it reaches sub-relativistic velocities. The only way in which agreement could be restored in this area would be to increase the np charge exchange cross section by a factor of  $\sim 2$ , which would be unreasonable in that it would then be larger than the total np cross section, or to increase the neutron intensity by  $\sim 2$  in the momentum range  $\sim 0.5 - 1.5$  Gev/c. Such an increase would give better overall agreement in each sample of events, the expected number of pions not increasing as much as the expected number of protons, since in general the main contribution to the pion component comes from higher incident neutron energies than does the proton component.

An increase in the neutron intensity of this order is not unreasonable considering how little is known about it in the presently considered energy region, and the observations are suggestive of such an increase rather than the discrepancy between the observed and predicted numbers being due to the presence of a neutrino induced muon component. However the precision of the calculations is not sufficient to conclude the absence of a muon signal, but it can be said that the results themselves are not inconsistent, under the assumption of an increased neutron intensity, with all the observed events being initiated by neutrons.

## 7.8. Conclusions

The observation in the heavy mass experiment of several neutral induced single and apparently weakly interacting particles can be reconciled when one considers that the selection of events is heavily biased towards non-interacting pions, due to their high probability of suffering absorption or charge exchange in an inelastic interaction (Section 7.2.5). Further the scattering distributions obtained in the N and M series for the relativistic samples of events, while showing much lower scattering probabilities than for the sub-relativistic samples, are not inconsistent with the observed particles being protons and pions when consideration is given to the scattering characteristics of the particles in these two samples (Section 7.2.5).

From the analysis in Section 7.7 it has been shown that the observed rates of events are not particularly inconsistent with them all being the products of neutron interactions. Further support for the presence of a significant proton and pion component comes from the majority of observed scatterings being single point scatters, which is characteristic of a nuclear active rather than a muonic signal. However a categorical conclusion cannot be drawn that there is not an admixture of muons in the data and, in the absence of an exact knowledge of the proton and pion component, only upper limits have been imposed on their presence under the assumption that all the observed events are in fact muons. A cross section of  $\sim 2 \cdot 10^{-31} \text{ cm}^2/\text{nucleon}$  has been derived for neutrinos producing these muons which is a factor of 10 greater than the suggested resonance value, and such a result is further evidence for the events being initiated predominantly by neutrons (even more so if the resonance does not exist or occurs in a different energy region than that currently studied). A further investigation of the occurrence of a neutrino resonance in this energy region via cosmic ray experiments would appear unfavourable in view of the

high background from neutron induced events.

The evidence (from a scattering analysis of the observed particles) reported by Cowan et al. in support of their interpretation in terms of directly produced muons has recently been retracted (Cowan et al, 1969) and preliminary results from their revised telescope are in good agreement with the present work. Even with their latest detector it is doubtful whether absolute conclusions will be possible on the presence or otherwise of a directly produced muon signal, at least above that expected from neutrinos having their typical cross section, unless the observed rate of events is significantly greater than the muon component arising from neutron induced pion decays in flight. Similar difficulties would be experienced if a pion-muon separation was attempted by using fast timing to resolve the  $\pi-\mu$  part of the  $\pi-\mu-e$  decay. The situation could be improved by shielding the telescope with several hundred  $\text{g. cm}^{-2}$  of absorber so as to filter out the neutron component. However an equilibrium would soon be set up as the amount of absorber was increased since a neutron signal from the nuclear interactions of muons would be obtained. The inclusion however of a scintillator and perhaps visual detectors above the shielding would probably be sufficient to isolate such events induced initially from a muon interaction by the observation of an incident charged particle. The disadvantage of course of using shielding or performing such an experiment underground is that the rare events one is looking for may also be filtered out if their interaction cross section were sufficiently large. In fact an experiment of this type has been performed by Novey, 1965, using only a scintillator to identify the incident charged particle, and the results obtained (although only  $\sim 40\%$  of the events were correlated with an incident charged particle, due to the

detector not having continuous sensitivity to the total incident radiation) were shown to be not inconsistent with all the events arising initially from a muon interaction.

With regard to the sidereal effect reported by Cowan et al., it is difficult to comprehend how so pronounced an effect was obtained in the presence of  $\sim 90\%$  atmospheric muons (and the remainder presumably containing a high pion background). Further it has been shown (Section 7.6) that the neutrino intensity (for neutrinos having their typical cross section) required from suggested point sources would have to be so great that they would surely have been observed copiously elsewhere. On the other hand, it is difficult to imagine experimental biases which would lead to a strong sidereal effect and one must await results from their present detector to see whether such an effect is confirmed. Should it be confirmed it would appear that, due to the undoubted high neutron induced pion background in these experiments, there is a strong sidereal variation of the low energy neutron flux, which would be a rather important and novel phenomenon.

In conclusion, in the present author's view, there is no evidence for the direct production of muons at a level above that expected from neutrinos having their 'normal' cross section, and it is doubtful if future experiments in the cosmic radiation will be capable of resolving an anomalous muon signal (if it exists) unless it is observed at a rate significantly greater than that expected from neutron induced pion decays in flight.

APPENDIX AA search for relativistic fractionally charged particles in the cosmic radiation at sea level.

This experiment has been described in detail by Simpson, 1967, and by Ashton et al., 1968a, and only a brief summary will be given here, but a more detailed analysis will be given of the implications on the quark production cross section of the upper limits obtained for the quark intensity, subject to the models of quark propagation proposed in Chapter 5.

A diagram of the scintillation counter-neon flash tube telescope is shown in Figure A.1 and it is essentially that which was used in the heavy mass search, less the Cerenkov counters, further flash tube trays and steel absorber which were added later. The scintillators A-F and flash tubes have been discussed in Chapter 2 and the other two scintillators,  $V_1$  and  $V_2$  are identical with counter V as described in Chapter 7, and were used as an anticoincidence against particles generating spuriously low Cerenkov pulse heights when traversing the perspex light guides of the main scintillators. The electronic logic employed was similar to that used in the heavy mass search.

Two series of measurements were made, the first selecting only particles with charge  $2e/3$  by means of a coincidence  $ABDEF\bar{V}_1\bar{V}_2$  where the output pulse from counters A,B,D,E,F had to be in the range  $0.2 - 0.85E$  (where E was the most probable pulse height from a muon traversing that counter), and C was left free of the electronic selection to act as an independent witness of the event; and the second which selected both  $e/3$  and  $2e/3$  particles, where  $e/3$  were selected by a coincidence  $ABCDEF\bar{V}_1\bar{V}_2$  where all six coincident pulses

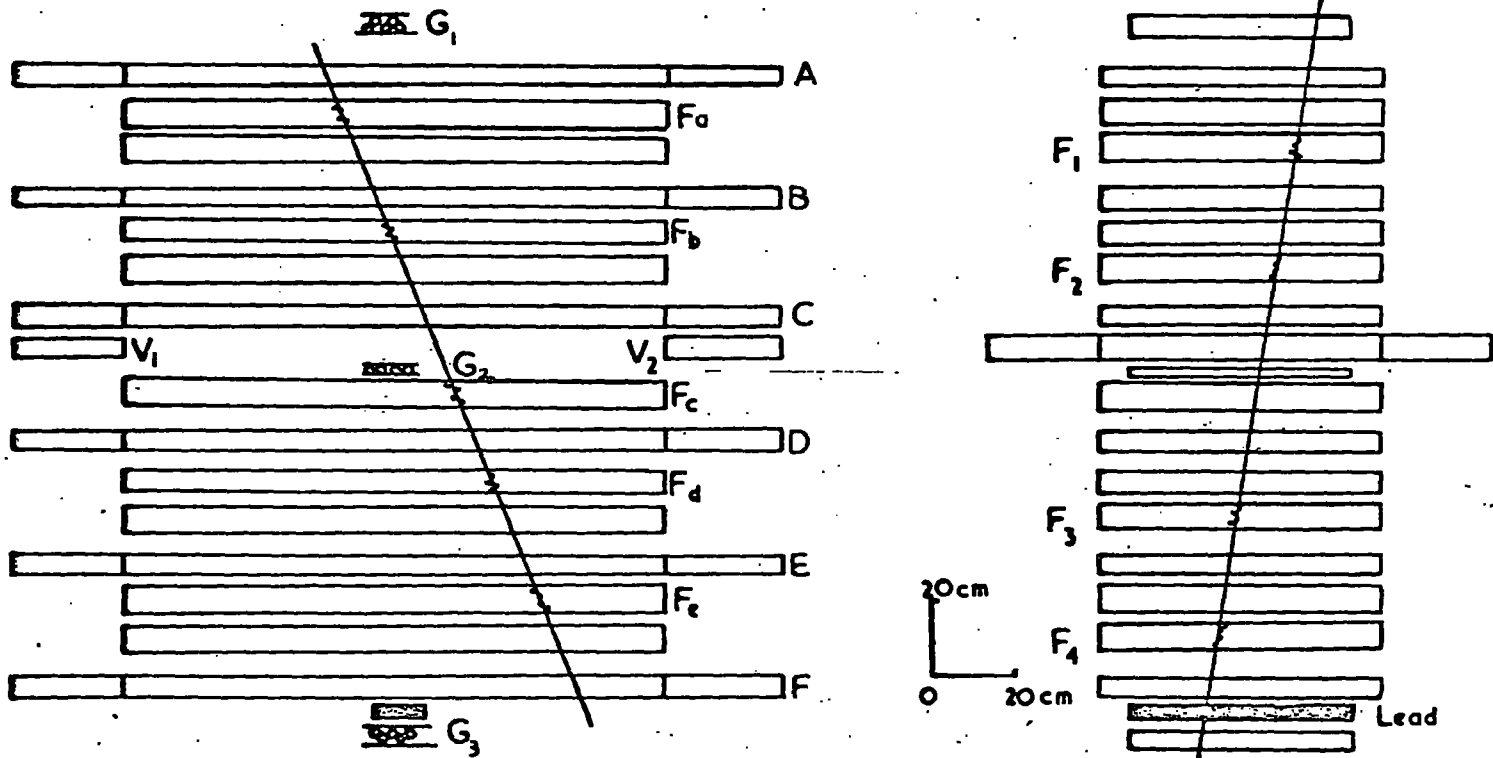


Figure A.1 The 'scintillation counter-neon flash tube telescope'.  
 A,B,C,D,E,F are plastic scintillation counters (NE102A);  
 F<sub>a</sub>-F<sub>e</sub>, F<sub>1</sub>-F<sub>4</sub> are neon flash tube trays;  
 and G<sub>1</sub>, G<sub>2</sub>, and G<sub>3</sub> are geiger counter trays.

were in the region  $0.05 - 0.3E$ , and  $2e/3$  by a coincidence  $ABCDEF\bar{V}_1\bar{V}_2$  with all six pulses being greater than  $0.3E$  and, apart from C on which no upper discrimination was afforded, less than  $0.85E$ . The results of both series were negative and limits at the 90% confidence level were imposed on the intensity of relativistic fractionally charged quarks in the sea level cosmic radiation of  $1.2 \cdot 10^{-10}$  and  $8.0 \cdot 10^{-11}$   $\text{cm.}^{-2}\text{sec.}^{-1}\text{sterad.}^{-1}$  for  $e/3$  and  $2e/3$  quarks respectively.

The experiment, while being specifically designed to search for relativistic fractionally charged quarks, was also sensitive to quarks with sub-relativistic velocities, by virtue of the width of the discrimination windows employed, and sub-relativistic quarks of  $z = \frac{1}{3}$  looking like relativistic quarks with  $z = \frac{2}{3}$ . From the discrimination levels used on each counter and the predicted scintillation line shapes for quarks with  $z = \frac{1}{3}$  and  $\frac{2}{3}$ , the effective running time of the experiment has been calculated for both charged states as a function of their velocity, and the resulting operating times are given in Figure A.2. From the aperture of the telescope,  $0.47\text{m.}^2\text{sterad.}$ , and the velocity distributions expected for quarks at sea level for four different models of quark interaction with matter, and for quark production via quark-anti-quark pairs and via total nucleon dissociation (Figures 5.8 and 5.11), the expected number of quarks in the experiment was calculated on the basis of a 30 mb. nucleon-nucleon cross section for quark production. Having observed no events, limits at the 90% confidence level were derived on the quark production cross section for each production model and for each model of propagation, and the resulting limits are shown in Figures A.3 and A.4.

The limits given in Figures A.3 and A.4 have not been corrected for the

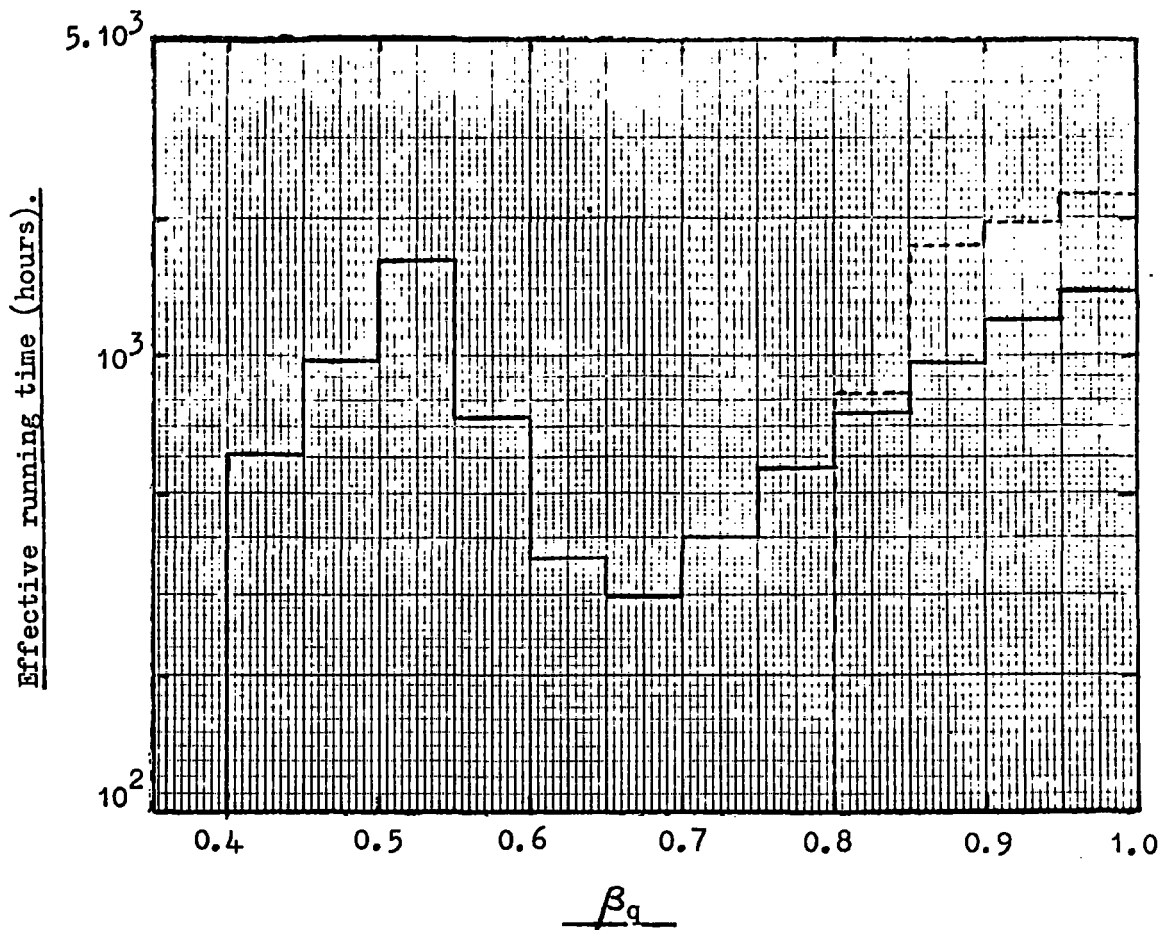


Figure A.2

The effective running time of the experiment as a function of the quark velocity. The full line is for quarks with  $z = \frac{1}{3}$  and the dotted line for  $z = \frac{2}{3}$ .

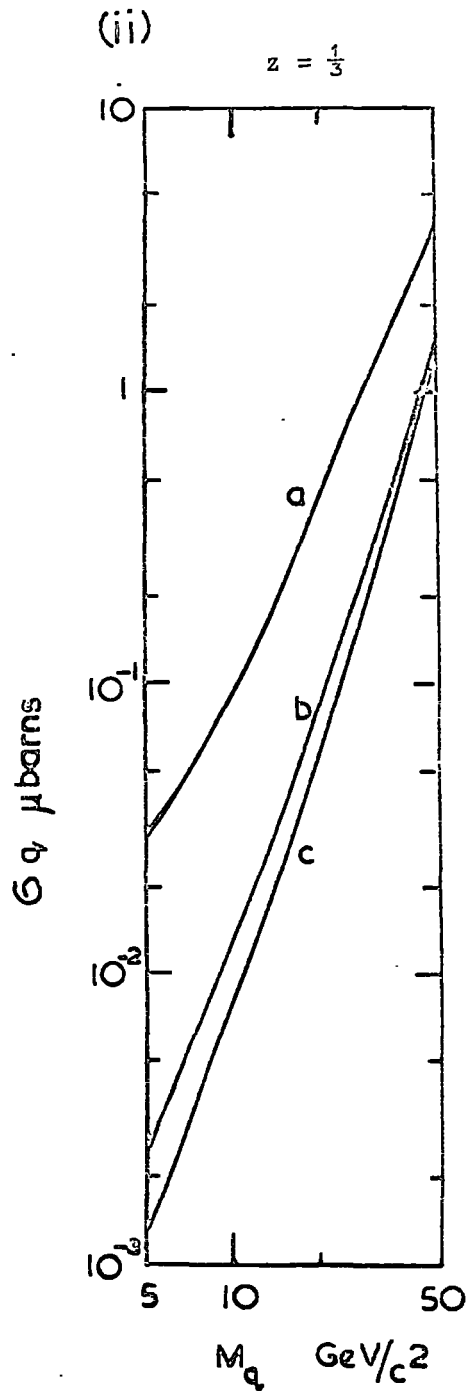
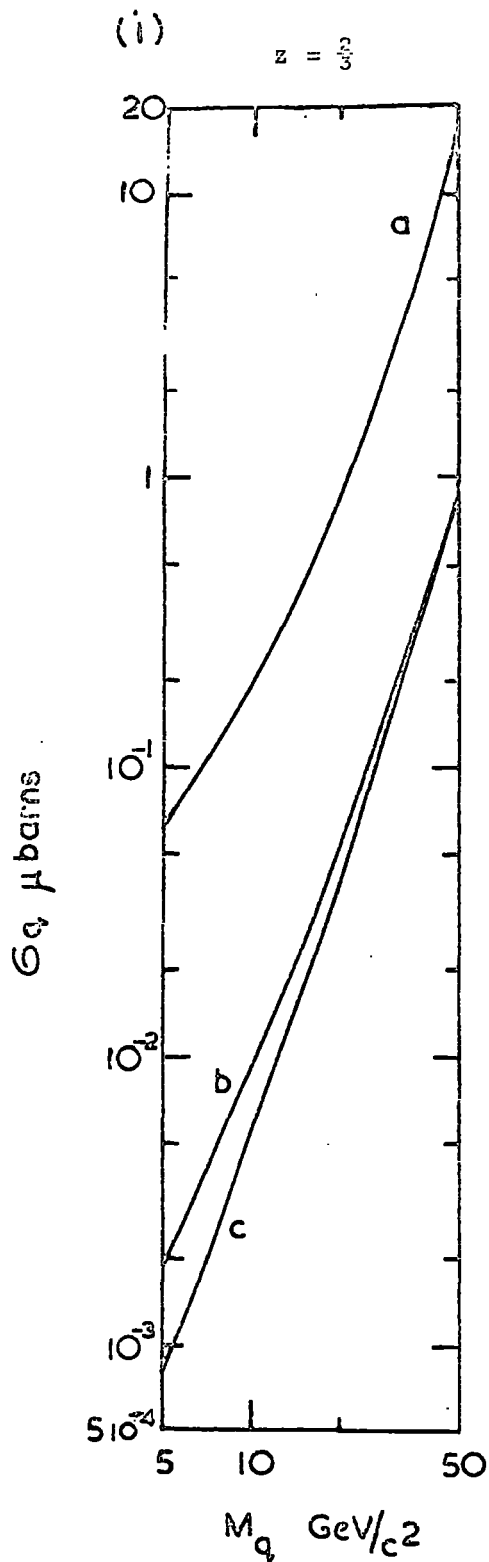


Figure A.3

The cross section limits imposed on quark production in reactions such as  $NN \rightarrow NNq\bar{q}$ , where no correction has been applied for interactions in the telescope.

(a)  $K_q = 0.5$ ;  $\lambda_q = 80 \text{ g. cm.}^{-2}$       (b)  $K_q = 0.5$ ;  $\lambda_q = 240 \text{ g. cm.}^{-2}$

(c)  $K_q = 0.5 M_p / M_q$ ;  $\lambda_q = 80$  or  $240 \text{ g. cm.}^{-2}$

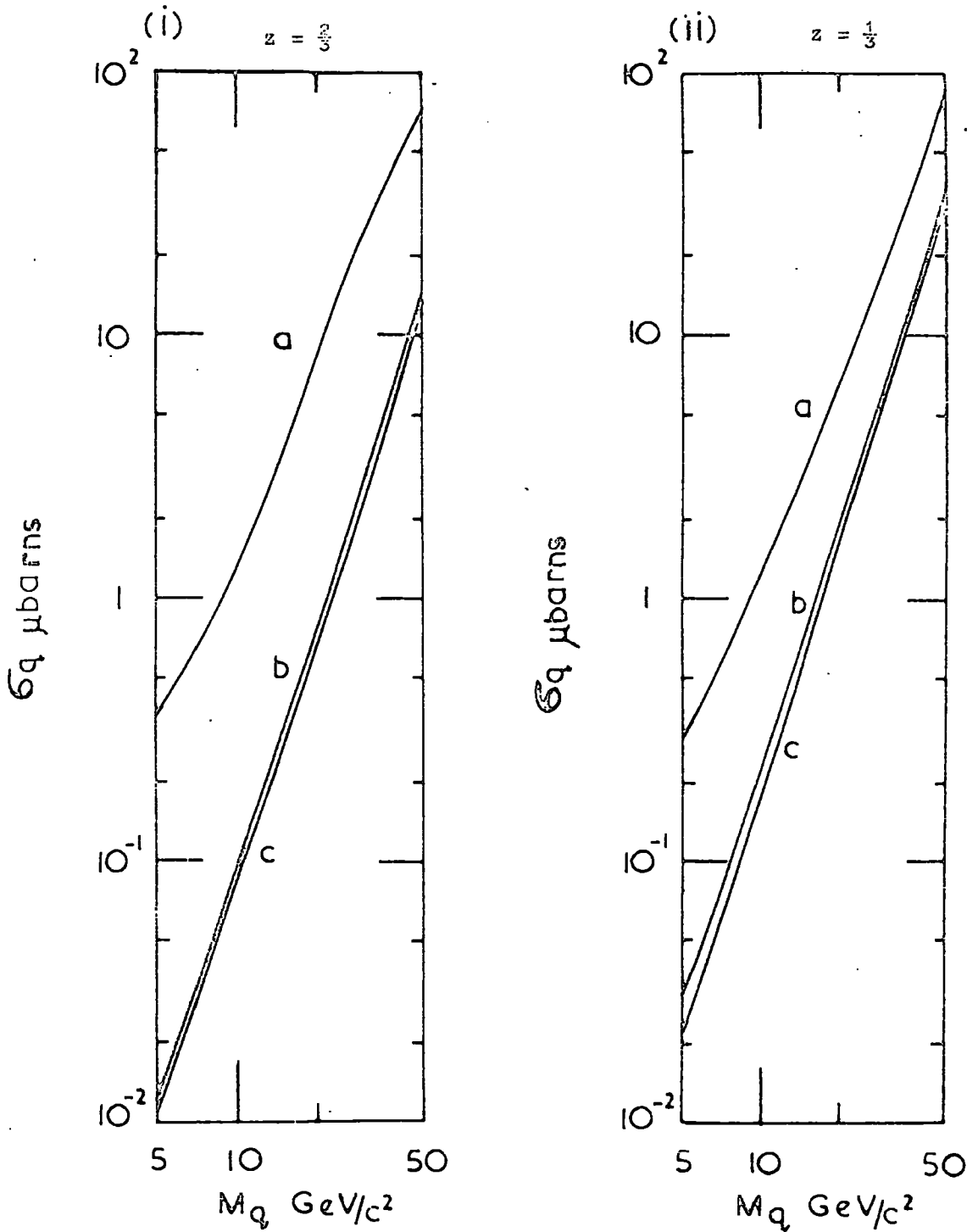


Figure 1.4. The cross section limits imposed for quark production via total nucleon dissociation ( $MN \rightarrow 6q$ ), where no correction has been applied for interactions in the telescope.

(a)  $K_q=0.5$ ;  $\lambda_q=80 \text{ g.cm.}^{-2}$  (b)  $K_q=0.5$ ;  $\lambda_q=240 \text{ g.cm.}^{-2}$  (c)  $K_q=0.5 M_p/M_q$ ;  $\lambda_q=80$  or

$240 \text{ g.cm.}^{-2}$

possibility of quark interactions in the telescope, and if these are taken into account the limits should be increased by 2.3 or 1.32 for the cases of a quark interaction length in air of  $80 \text{ g. cm.}^{-2}$  and  $240 \text{ g.cm.}^{-2}$  respectively, the telescope containing 0.83 nucleon interaction lengths. At present these cross section limits are the best available from cosmic ray searches for fractionally charged quarks and they are included in the cross section survey in Figures 6.5 - 6.10, where they have been corrected for interactions subject to the propagation model to which they apply. The limits derived from this experiment are subject to only one qualification that if the quark is heavily accompanied then the calculated limits should be severely increased, since any accompaniment within the detector volume would lead automatically to the rejection of the incident quark due to the strict discrimination levels used on the scintillation counters.

## APPENDIX B

Deuteron production through the reactions  $NN \rightarrow d\pi$ .B.1. The deuteron production momentum as a function of the primary nucleon energy.

With the cosmic ray nucleon component comprising both neutrons and protons, of approximately equal numbers at moderate depths in the atmosphere, deuteron production can occur through the following channels for nucleon-air nucleus collisions, where the interaction is considered as a collision with an individual nucleon in the nucleus.



The cross section for reactions (i) and (iii) is a factor of 2 greater than that for (ii) and (iv) since in the former case the isospin has only one possible value of  $I = 1$ , whereas for (ii) and (iv)  $I$  can be 1 or 0.

By virtue of only two secondary particles being produced (ignoring the participation of the nucleus) their momenta in the centre of mass system are uniquely defined. Thus  $p_{\pi}^1 c = p_d^1 c$ , where the dash signifies a centre of mass (C.M.) value, and since

$$p^2 c^2 = (\gamma^2 - 1) M^2 c^4$$

$$\text{then } (\gamma'_{\pi}{}^2 - 1) M_{\pi}^2 c^4 = (\gamma'_d{}^2 - 1) M_d^2 c^4 \quad \dots \dots \dots (B1)$$

The total centre of mass energy,  $U'$ , is given by

$$U' = \gamma'_{\pi} M_{\pi} c^2 + \gamma'_d M_d c^2 \quad \dots \dots \dots (B2)$$

and substituting in (B1) for  $\gamma'_{\pi} M_{\pi} c^2$  from (B2) then

$$\gamma'_d = \frac{M_d^2 c^4 - M_\pi^2 c^4 + U'^2}{2 U' M_d c^2} \approx \frac{M_d c^2}{2 U'} + \frac{U'}{2 M_d c^2}$$

Thus the total energy,  $E'_d$ , and momentum,  $p'_d c$ , of the deuteron in the centre of mass system are given by

$$E'_d = \frac{M_d^2 c^4}{2 U'} + \frac{U'}{2}$$

$$\text{and } p'_d c = \gamma'_d \cdot \left(1 - \frac{1}{\gamma'^2}\right)^{\frac{1}{2}} M_d c^2$$

where  $U'$ , in terms of the total energy,  $T_N$ , of the incident nucleon, is given by

$$U' = \left[ 2 M_N c^2 (T_N + M_N c^2) \right]^{\frac{1}{2}}$$

The deuteron momentum in the laboratory system (L.S) can be obtained by the usual Lorentz transformation of

$$p_{d_x} = \gamma_c (p'_{d_x} + \beta_c \cdot E'_d)$$

where  $\gamma_c$  and  $\beta_c$  refer to the C.M. system.

Obviously the deuteron momentum in the L.S depends upon the emission angle in the C.M. and assuming this to be isotropic the median momentum can be approximated to

$$p_d = p_{d_x} \quad \text{where } p'_{d_x} = 0$$

and the contributions to  $p_d$  from the transverse components have been ignored as being small. Under this approximation a nucleon of a given incident energy is assumed to produce a deuteron with a unique momentum in the L.S., that is the median value, and the variation of this momentum with the incident nucleon kinetic energy is shown in Figure B.1. For comparison the maximum and minimum deuteron momenta are also shown.

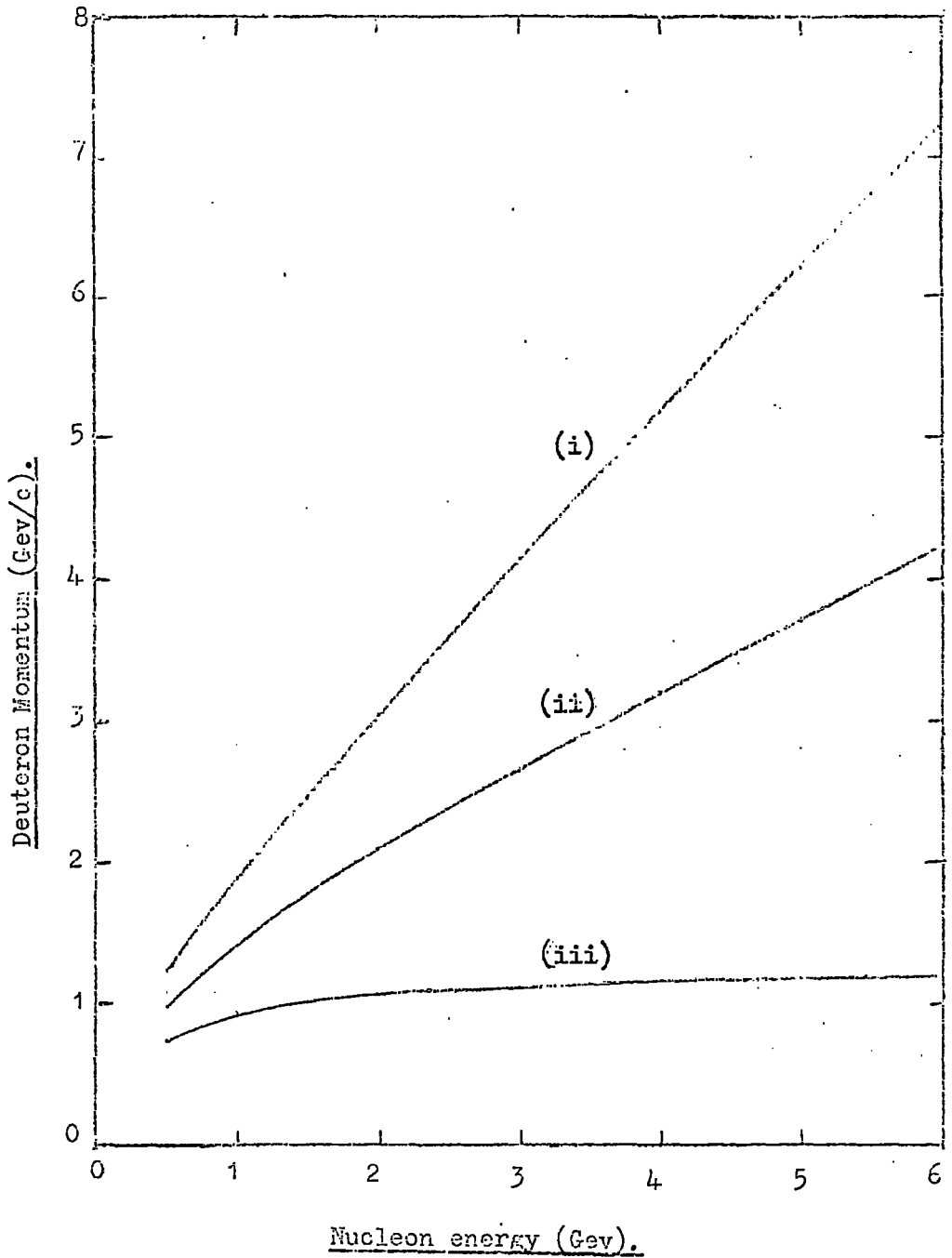


Figure B.1

The variation of the momentum of a deuteron, produced in a reaction  $NN \rightarrow d\pi$ , as a function of the kinetic energy of the incident nucleon. Three limiting cases are considered:-

(i)  $p'_x = p'_d$ ;      (ii)  $p'_x = 0$ ;      (iii)  $p'_x = -p'_d$ .

## B.2 The observed cross section for deuteron production.

For a detector accepting deuterons in the momentum band defined by  $p_1$  and  $p_2$  the corresponding nucleon energy band capable of such production ( $E_1 \rightarrow E_2$ ) can be derived from Figure B.1. Then the sea level deuteron intensity in the momentum band  $p_1 - p_2$  can be written as

$$N_d(p_1 \rightarrow p_2) = \int_x N_N(E_1 \rightarrow E_2) \cdot \exp \left[ \left( \frac{1000-x}{\lambda_{aN}} \right) + \left( \frac{x-1000}{\lambda_{id}} \right) \right] \cdot \frac{dx}{\lambda_{Nd}}$$

where  $x$  is the depth in  $\text{g. cm.}^{-2}$  of air from the top of the atmosphere,

$N_N(E_1 \rightarrow E_2)$  is the sea level nucleon intensity in the energy band defined by  $E_1$  and  $E_2$  and is in the same units of  $N_d(p_1 \rightarrow p_2)$ ,

$\lambda_{aN}$  is the nucleon attenuation length,

$\lambda_{Nd}$  is the nucleon mean free path for deuteron production.

and  $\lambda_{id}$  is the deuteron interaction length,

and where energy loss through ionisation has been ignored (this will be shown later to be a reasonable approximation).

Integrating over the whole atmosphere then  $\lambda_{Nd}$  is given by

$$\lambda_{Nd} = \frac{N_N(E_1 \rightarrow E_2)}{N_d(p_1 \rightarrow p_2)} \cdot \frac{\lambda_{aN} \cdot \lambda_{id}}{(\lambda_{aN} - \lambda_{id})}$$

The nucleon-air nucleus cross section for deuteron production can be obtained from

$$\sigma(d)_{N\text{-}NUCL} = \frac{A}{N_0 \lambda_{Nd}}$$

where  $N_0$  is Avagadros' number and as the cross section is likely to be small the nucleon-nucleon cross section can be approximated to

$$\sigma(d)_{N\text{-}N} \approx \frac{\sigma(d)_{N\text{-}NUCL}}{A}$$

Thus

$$\sigma(d)_{N-N} = \frac{1}{N_0 \lambda_{Nd}} = \frac{N_d(p_1 \rightarrow p_2)}{N_N(E_1 \rightarrow E_2)} \cdot \frac{(\lambda_{aN} - \lambda_{id})}{\lambda_{aN} \cdot \lambda_{id}} \cdot \frac{1}{N_0}$$

The nucleon-nucleon cross section for deuteron production has been evaluated, using values of  $\lambda_{aN} = 120 \text{ g.cm.}^{-2}$  air and  $\lambda_{id} = 40 \text{ g.cm.}^{-2}$  of air, from the two measurements of the deuteron intensity given in Section 4.9.2, and the various other parameters used are tabulated below.

Accepted deuteron momentum band (Gev/c)	$\bar{p}_d$ (Gev/c)	Contributing nucleon energy band (Gev)	$\bar{E}_{\text{Gev}}$	Intensity $\text{cm}^{-2} \text{sec}^{-1} \text{sterad}^{-1}$	
				$N_d(p_1-p_2)$	$N_N(E_1-E_2)$
1.565 - 1.725	1.65	1.23 - 1.45	1.34	$6.75 \cdot 10^{-7}$	$4.89 \cdot 10^{-6}$
2.28 - 2.61	2.45	2.33 - 2.91	2.62	$1.58 \cdot 10^{-7}$	$3.59 \cdot 10^{-6}$

The nucleon sea level intensity,  $N_N(E_1 \rightarrow E_2)$ , has been taken as twice the proton intensity as measured by Brooke and Wolfendale, 1964a. The analysis yields cross section values of  $1.9^{+1.3}_{-1.0}$  mb/nucleon and  $0.6^{+0.9}_{-0.4}$  mb./nucleon for nucleon energies of 1.34 and 2.62 Gev respectively. These values are averaged over proton-proton and proton-neutron as well as neutron-neutron and neutron-proton interactions since air nuclei (predominantly oxygen and nitrogen) contain equal numbers of protons and neutrons. Since the nn and pp cross sections for deuteron production are twice those for np and pn interactions, the calculated cross sections have to be increased by 1.33 before comparison can be made with direct measurements of the nn or pp cross section at the accelerators. The experimental observations would thus suggest cross sections of  $2.5^{+1.8}_{-1.4}$  mb./nucleon and  $0.8^{+1.2}_{-0.5}$  mb./nucleon for nn or pp interactions leading to the production of a deuteron and pion, and they are compared with a review of the total cross section as a function of the nucleon momentum for  $pp \rightarrow \pi^+ d$  given

by Cocconi et al., 1963, in Figure B.2.

It can be seen that the cross sections evaluated from the present work are significantly (at least a factor of 10) greater than those expected for deuteron production via  $NN \rightarrow \pi d$  reactions. In fact the calculated cross sections are lower limits in that no account has been taken of shadowing effects in the nucleus or of the loss of deuterons due to their not being able to escape from the nucleus, and further the assumption of a unique deuteron momentum being produced from a nucleon of a given energy reduces the cross sections by a factor of  $\sim 2$  from those that would have been obtained if the spectrum of deuteron energies which can be produced had been considered. It can thus be concluded that the deuterons observed in the present experiment were not produced (apart perhaps from a small fraction) from any of the processes (i-iv) listed in Section B.1.

Finally, it should be noted that the approximation of ignoring energy loss through ionisation can be seen to be justified when consideration is given to the mean depth at which deuterons are produced of only  $\sim 60 \text{g.cm}^{-2}$  of air above the detection level, and further the resonance in the  $pp \rightarrow d\pi^+$  cross section, while occurring at an energy below that to which the present experiments were sensitive, would not have been observed even if the experiments had been sensitive to such nucleon energies, in that the resonance would be smeared out by the Fermi motion of the target nucleons in the air nuclei.

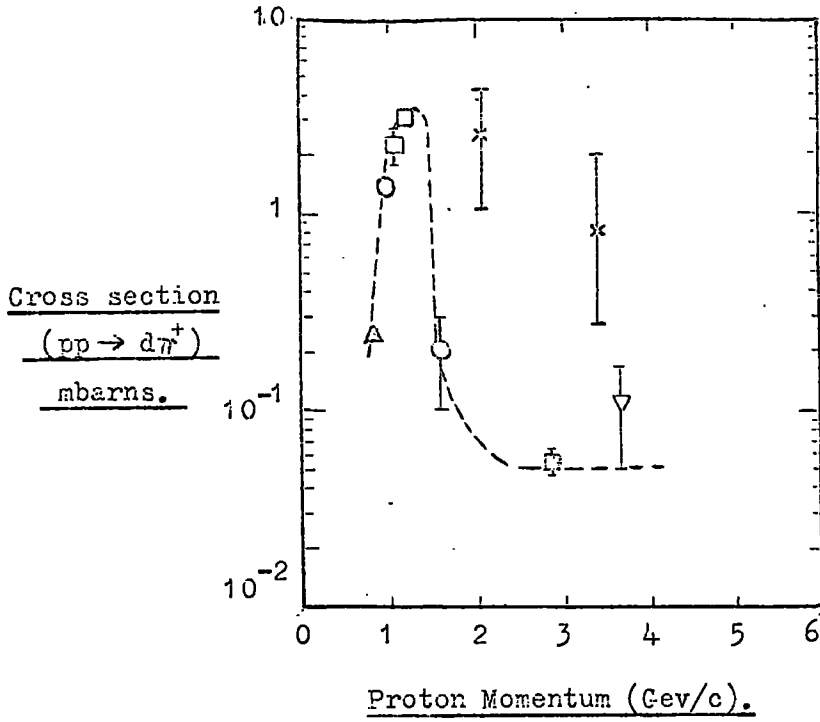


Figure B.2

A review of the  $pp \rightarrow d\pi^+$  cross section (dotted line) by Cocconi et al., 1963. The present measurements suggest cross section values given by the crosses if such a process was responsible for the observed deuterons.

APPENDIX CDiscussion of recently published quark searches.

The results of several quark searches in the cosmic radiation have been published since the survey in Chapter 6 was compiled. Brief discussion will be given to each of these.

Briatore et al., 1968. These workers have performed an experiment at 63 m.w.e. to search for relativistic leptonic quarks of charge  $e/3$ ,  $2e/3$  and  $4e/3$  and used a telescope comprising 6 plastic scintillation counters. The result of the search was negative and they have placed upper limits on the intensity of quarks at this depth (at the 90% confidence level) of

$$< 1.8 \cdot 10^{-10} \text{ cm.}^{-2} \text{ sec.}^{-1} \text{ sterad.}^{-1} \quad \text{for } z = \frac{1}{3},$$

$$< 1.8 \cdot 10^{-10} \text{ cm.}^{-2} \text{ sec.}^{-1} \text{ sterad.}^{-1} \quad \text{for } z = \frac{2}{3},$$

$$\text{and } < (1.1 \pm 1.8) \cdot 10^{-8} \text{ cm.}^{-2} \text{ sec.}^{-1} \text{ sterad.}^{-1} \quad \text{for } z = 4/3.$$

The limits refer to quarks with energies greater than the threshold energies  $(2.1 \pm 0.1)$  Gev,  $(8.5 \pm 0.6)$  Gev and  $(22 \pm 1)$  Gev for  $z = \frac{1}{3}$ ,  $\frac{2}{3}$  and  $4/3$  respectively.

Fukushima et al., 1969. They have carried out a search, at sea level, for relativistic quarks of charge  $z = \frac{1}{3}$  or  $\frac{2}{3}$  using 12 scintillation counters (of which 6 were plastic of dimensions  $100 \times 100 \times 5 \text{ cm.}^3$  and 6 liquid of dimensions  $100 \times 100 \times 10 \text{ cm.}^3$ ) and a streamer chamber placed above the telescope. The result was negative and the following upper limits were placed on the sea level quark intensity at the 90% confidence level.

$$< 0.5 \cdot 10^{-10} \text{ cm.}^{-2} \text{ sec.}^{-1} \text{ sterad.}^{-1} \quad \text{for } z = \frac{1}{3},$$

$$\text{and } < 7.5 \cdot 10^{-10} \text{ cm.}^{-2} \text{ sec.}^{-1} \text{ sterad.}^{-1} \quad \text{for } z = \frac{2}{3},$$

Bowen et al., 1968 The results of this work were reported by Morpurgo, 1968. The experiment was performed at 700 m. above sea level and was sensitive

to  $e/3$  and  $2e/3$  relativistic quarks. The following limits have been placed on the quark intensity (at the 90% confidence level) of :-

$$< 3.4 \cdot 10^{-10} \text{ cm.}^{-2} \text{ sec.}^{-1} \text{ sterad.}^{-1} \quad \text{for } z = \frac{1}{3},$$

$$\text{and } < 2.6 \cdot 10^{-10} \text{ cm.}^{-2} \text{ sec.}^{-1} \text{ sterad.}^{-1} \quad \text{for } z = \frac{2}{3}.$$

Franzini et al., 1968 This experiment was sensitive to sub-relativistic massive particles arriving in the near horizontal direction at sea level. Particles of mass greater than  $2 \text{ Gev}/c^2$  and having velocities in the range  $0.5 - 0.9c$  were selected by time of flight and demanding that they were able to traverse  $195 \text{ g.cm.}^{-2}$  of aluminium. The result was negative and an upper limit of  $< 2.2 \cdot 10^{-8} \text{ cm.}^{-2} \text{ sec.}^{-1} \text{ sterad.}^{-1}$  was placed on the intensity of sub-relativistic massive particles incident in the defined velocity bands.

The effect of these recent measurements on the conclusions drawn as to the limits that could be placed on the quark production cross section (Chapter 6) from a summary of the searches in the cosmic radiation is negligible. The intensity limits reported by Bowen et al. and Briatore et al. for relativistic quarks of  $z = \frac{1}{3}$  and  $\frac{2}{3}$  are not as low as those obtained by Ashton et al., 1968a, the values adopted in the summary. The intensity limit reported by Franzini et al. is equivalent to that reported by Kasha et al., 1968c, who performed almost an identical experiment, the result of the latter workers having been used in the summary. The limit reported by Fukushima et al. for  $z = \frac{1}{3}$  quarks is about a factor of 2 lower than that obtained by Ashton et al., 1968a, but due to the larger amount of material in their telescope ( $> 100 \text{ g. cm}^{-2}$ ) the limits that can be imposed on the quark production cross section will be almost the same for both experiments. The results of Briatore et al., however, for  $z = 4/3$  are a factor of  $\sim 10$  better

than those reported by Buhler -Broglin et al., 1967a, but a factor of  $\sim 10^2$  higher than the rather doubtful limit (see Chapter 6) reported by Kasha et al., 1968a.

Thus the conclusions drawn in Chapter 6 on the quark production cross sections that can be imposed on  $z = \frac{1}{3}$  and  $\frac{2}{3}$  quarks are not affected by these more recent searches, this demonstrating further the saturation point that has been reached in searching for relativistic fractional charges in the cosmic radiation with scintillation counter telescopes. The intensity limit on leptonic  $4e/3$  relativistic quarks has been reduced by a factor of  $\sim 10$  to  $< (1.1 \pm 1.8) 10^{-8} \text{ cm.}^{-2} \text{ sec.}^{-1} \text{ sterad.}^{-1}$  by Briatore et al. However this is still some  $10^2$  higher than the limits obtained for  $z = \frac{1}{3}$  and  $\frac{2}{3}$  quarks, and it further shows that Cerenkov counters must be used in such searches to discriminate against sub-relativistic background if the limits are to be substantially reduced (discussed in Chapter 6).

ACKNOWLEDGEMENTS

The author wishes to thank Professor G.D. Rochester, F.R.S., for the provision of the facilities for this work and for his interest and support.

He is particularly grateful to his supervisor, Professor A.W. Wolfendale, for initially creating an interest in this subject. Dr. F. Ashton and Professor A.W. Wolfendale are thanked for their willing help and guidance throughout the work and for many stimulating and invaluable discussions.

Members of the Cosmic Radiation and High Energy Physics Research Groups are thanked for helpful discussions and especially Mrs. H.J. Edwards for her assistance during the latter two years of this work.

The technical staff of the Physics Department, in particular Mr. G. Young, Mr. W. Leslie, Mr. M. Lee, and in the earlier stages of the work Mr. K. Tindale and Mr. J. Webster, are thanked for their willing help. The author is indebted to Miss P. Wallace for carrying out much of the routine and more tedious work involved in the various experiments in such a conscientious manner.

The Durham Computing Unit is thanked for the provision of facilities as well as for advice at various times.

The author is grateful to Mrs. D. Anson for her patient work in typing this thesis.

Finally the Science Research Council is thanked for the provision of a Research Studentship, and the National Institute for Research into Nuclear Science (Rutherford Laboratory) is thanked for providing much of the equipment.

REFERENCES

- Adair, R.K., and Price, N.J., (1966), Phys. Rev., 142, 844.
- Akimov, Yu. K., (1965), 'Scintillation Counters in High Energy Physics,' published by Academic Press, p.5.
- Alexander, G., and Yekutieli, G., (1961), Nuovo Cimento, 19, 103.
- Alikhanov, A.I., Eliseev, G.P., Kamalyan, V.Sh., Lyubimov, V.A., Moisseev, B.N., and Khrimyan, A.V., (1960), Sov. Phys., J.E.T.P., 2, 280.
- Ashton, F., (1965), Proc. Int. Conf. Cosmic Rays (London), p. 1108.
- Ashton, F., Coats, R.B., and Simpson, D.A., (1967a), Proc. Int. Conf. Cosmic Rays, (Calgary), Canad. J. Phys., 46, S 361.
- Ashton, F., Coats, R.B., Kelly, G.N., Simpson, D.A., Smith, N.I., and Takahashi, T., (1967b), Proc. Int. Conf. Cosmic Rays (Calgary), Canad. J. Phys., 46, S 1125.
- Ashton, F., and Coats, R.B., (1968), J. Phys. A., 1, 169.
- Ashton, F., Coats, R.B., Kelly, G.N., Simpson, D.A., Smith, N.I., and Takahashi, T., (1968a), J. Phys. A., 1, 569.
- Ashton, F., Edwards, H.J., Kelly, G.N., and Wolfendale, A.W., (1968b), Phys. Rev. Letts., 21, 303.
- Ashton, F., Edwards, H.J., and Kelly, G.N., (1969a), CERN Neutrino Meeting, Jan. 1969, to be published as a CERN report.
- Ashton, F., Edwards, H.J., and Kelly, G.N., (1969b), Phys. Letts., 29B, 249.
- Baccalini, C., Bassi, P., and Manduchi, C., (1955), Nuovo Cimento, 1, 657.
- Badalian, G.V., (1959), Sov. Phys., J.E.T.P., 8, 209.
- Ballam, J., and Lichtenstein, P.J., (1954), Phys. Rev., 93, 851.
- Barton, J.C., Barnaby, C.F., Jasani, B.M., and Thompson, C.W., (1962), J. Sci. Instrum., 39, 360.
- Barton, J.C., (1965), Proc. Int. Conf. Cosmic Rays (London), p. 621.
- Barton, J.C., and Slade, M., (1965), Proc. Int. Conf. Cosmic Rays (London), p. 1006.
- Barton, J.C., and Stockel, C.T., (1966), Phys. Letts., 21, 360.

- Barton, J.C., (1967), Proc. Phys. Soc., 90, 87.
- Bathow, G., Freytag, E., Schulz, D.H., and Tesch, K., (1967), Phys. Letts., 25B, 163.
- Batty, C.J., (1961), Nuc. Phys., 23, 562.
- Belcher, E.H., (1953), Proc. Roy. Soc., A216, 90.
- Bellamy, E.H., Hofstadter, R., Lakin, W.L., Perl, M.L., and Toner, W.T., (1968), Phys. Rev., 166, 1391.
- Bennett, W.R., (1966), Phys. Rev. Letts., 17, 1196.
- Bergeson, H.E., Keuffel, J.W., Larson, M.O., Martin, E.R., and Mason, G.W., (1967), Phys. Rev. Letts., 19, 1487.
- Bernardini, G., Booth, E.T., and Lindenbaum, S.J., (1952), Phys. Rev., 85, 826.
- Bingham, H.H., Dickinson, M., Diebold, R., Koch, W., Leith, D.W.G., Nikolic, M., Ronne, B., Huson, R., Musset, P., and Veillet, J.J., (1964), Phys. Letts., 9, 201.
- Bjornboe, J., Damgard, G., Hansen, K., Chatterjee, B.K., Greider, P., Korning, A., Lillethun, E., and Peters, B., (1968), Nuovo Cimento, 53B, 241.
- Blum W., Brantd, S., Cocconi, V.T., Czyzewski, O., Danysz, J., Jobses, M., Kellner, G., Miller, D., Morrison, D.R.O., Neale, W., and Rushbrooke, J.G., (1964), Phys. Rev. Letts., 13, 353a.
- Boccaletti, D., de Sabitta, V., Gualdi, C., (1966), Nuovo Cimento, 45, 513.
- Bowen, T., Delise, D.A., Kalbach, R.M., and Mortara, L.B., (1964), Phys. Rev. Letts., 13, 728.
- Bowen, T. et al., (1968), 14th Int. Conf. on High Energy Physics, (Vienna), paper 170, unpublished.
- Bransden, B.H., (1952), Proc. Phys. Soc., A65, 738.
- Briatore, L., Castagnoli, C., Bollini, D., Massam, T., Palmonari, F., and Zichichi, A., (1968), Nuovo Cimento, 57, 850.
- Brooke, G., and Wolfendale, A.W., (1964a), Proc. Phys. Soc., 83, 843.
- Brooke, G., and Wolfendale, A.W., (1964b), Proc. Phys. Soc., 83, 853.
- Buckwalter, G., Cowan, C.L., and Ryan, D., (1966), Phys. Letts., 21, 478.
- Bugg, D.V., Salter, D.C., Stafford, G.H., George, R.F., Riley, K.F., and Tapper, R.J., (1966), Phys. Rev., 146, 980.

- Buhler-Broglin, A., Fortunato, G., Massam, T., Muller, T., and Zichichi, A., (1966), *Nuovo Cimento*, 45, 120.
- Buhler-Broglin, A., Fortunato, G., Massam, T., and Zichichi, A., (1967a), *Nuovo Cimento*, 49, 209.
- Buhler-Broglin, A., Dalpiaz, P., Massam, T., and Zichichi, A., (1967b), *Nuovo Cimento*, 51A, 837.
- Gallan, C.G., and Glashow, S.L., (1968), *Phys. Rev. Letts.*, 20, 779.
- Chatterjee, B.K., Murthy, G.T., Naranan, S., Sreekantan, B.V., Srinivasa Rao, M.V., and Tonwar, S.C., (1965), *Proc. Int. Conf. Cosmic Rays (London)* p805.
- Chen, F.F., Leavitt, C.P., and Shapiro, A.M., (1955), *Phys. Rev.*, 99, 857.
- Chilton, F., Horn, D., and Jabbur, R.J., (1966), *Phys. Letts.*, 22, 91.
- Chupka, W.A., Schiffer, J.P., and Stevens, C.M., (1966), *Phys. Rev. Letts.*, 17, 60.
- Cocconi, G., (1962), *Proc. Int. Conf. on High Energy Physics (CERN)*,
- Cocconi, G., Lillethun, E., Scanlon, J.P., Ting, C.C., Walters, J., and Wetherell, A.M., (1963), *CERN report 63-6*.
- Cowan, C.L., Ryan, D., and Szydlek, P.P., (1964), *Report of the Physics Department, Catholic University of America*.
- Cowan, C.L., Ryan, D., and Buckwalter, G., (1965), *Proc. Int. Conf. Cosmic Rays (London)*, p. 1041.
- Cowan, C.L., Hesse, P.W., and Talbott, F.L., (1967), *Proc. Int. Conf. Cosmic Rays (Calgary)*, unpublished paper.
- Cowan, C.L., Hesse, P.W., Johnston, R.L., Maciorowski, F.L., O'Sullivan, C.T., Shelby, R.N., and Talbott, F.L., (1969), *CERN Neutrino Meeting, Jan. 1969*, to be published as a CERN report.
- Coxell, H., and Wolfendale, A.W., (1960), *Proc. Phys. Soc.*, 75, 378.
- Crispin, A., and Hayman, P.J., (1964), *Proc. Phys. Soc.*, 83, 1051.
- Damgard, G., Grieder, P., Hansen, K.H., Iversen, C., Lohse, E., Peters, B., and Rengarajan, T., (1965), *Phys. Letts.*, 17, 152.
- Dardo, M., Penengo, P., and Sitte, K. (1968), *Nuovo Cimento*, 58A, 59.
- Delise, D.A., and Bowen, T., (1965), *Phys. Rev.*, 140, B458.
- Domokos, G., and Fulton, T., (1966), *Phys. Letts.*, 20, 546.
- Dorfan, D.E., Eades, J., Lederman, L.M., Lee, W., and Ting, C.N., (1965), *Phys. Rev. Letts.*, 14, 999.

- Fermi, E., (1953), Phys. Rev., 92, 452.
- Fermi, E., (1954), Phys. Rev., 93, 1435.
- Filthuth, H., (1955), Z. Naturforsch, Part a, 10, 219.
- Foley, K.J., Jones, R.S., Lindenbaum, S.J., Love, W.A., Ozaki, S., Platner, E.D., Quarles, C.A., and Willen, H., (1967), Phys. Rev. Letts., 19, 857.
- Foss, J., Garelick, D., Homma, S., Lobar, W., Osborn, L.S., and Uglum, J., (1967), Phys. Letts., 25B, 166.
- Franzini, P., Leontic, B., Rahm, D., Samios, N., and Schwartz, M., (1965), Phys. Rev. Letts., 14, 196.
- Franzini, P., and Shulman, S., (1968), Phys. Rev. Letts., 21, 1013.
- Fukushima, Y., Kifune, T., Kundo, T., Koshiha, M., Naruse, Y., Nishikama, T., Orita, S., Suda, T., Tsunemoto, K., Kimura, T., (1969), Phys. Rev., 178, 2058.
- Galbraith, W., Jenkins, E.W., Kycia, T.F., Leontic, B.A., Phillips, R.W., Read, A.L., and Rubinstein, R., (1965), Phys. Rev., 138, B913.
- Gallinaro, G., and Morpurgo, G., (1966), Phys. Letts., 23, 609.
- Gardener, M., Kisdnasamy, S., Rossle, E., and Wolfendale, A.W., (1957), Proc. Phys. Soc., 70, 687.
- Gardener, M., Jones, D.G., Taylor, F.E., and Wolfendale, A.W., (1962), Proc. Phys. Soc., 80, 697.
- Garmire, G., Leong, C., and Sreekantan, B.V., (1968), Phys. Rev., 166, 1280.
- Gell-Mann, M., (1962), Phys. Rev., 125, 1067.
- Gell-Mann, M., (1964), Phys. Letts., 8, 214.
- Goldwasser, E.L., and Merkle, T.C., (1951), Phys. Rev., 83, 43.
- Gomez, R., Kobrak, H., Moline, A., Mullins, J., Orth, C., Van Putten, J., and Zweig, G., (1967), Phys. Rev. Letts., 18, 1022.
- Gursey, F., Lee, T.D., and Nauenberg, M., (1964), Phys. Rev. Letts., 135, B467.
- Hagedorn, R., (1967), CERN report TH. 751.
- Hagopian, V., Selove, W., Ehrlich, R., Leboy, E., Lanza, R., Rahm, R., and Webster, M., (1964), Phys. Rev. Letts., 13, 280.
- Hanayama, Y., Hara, T., Higashi, S., Kitamura, T., Miono, S., Miyamoto S., Nakagawa, M., Ozaki, S., Takahashi, T., Tsuji, K., and Watase, Y., (1967), Proc. Int. Conf. Cosmic Rays (Calgary), Canad. J. Phys., 46, S 734.

- Hayman, P.J., and Wolfendale, A.W., (1962), Proc. Phys. Soc., 80, 710.
- Heiberg, E., and Marshall, J., (1956), Rev. Sci. Instrum., 27, 618.
- Heidman, J., (1950), Phys. Rev., 80, 171.
- Hess, W.N., Patterson, H.W., Wallace, R., and Chupp, E.L., (1959), Phys. Rev., 116, 445.
- Hesse, P.W., Talbott, F.L., and Cowan, C.L., (1967), Ap. J., 148, L 73.
- Higashi, S., Kitamura, T., Mishima, Y., Miyamoto, S., Oshio, T., Shibata, H., and Watase, Y., (1962), J. Phys. Soc. (Japan), 17, 209.
- Jelley, J.V., (1958), 'Cerenkov Radiation and its Applications', published by Pergamon Press.
- Jones, L.W., Lyon, D.E., Ramana Murthy, P.V., De Meester, G., Hartung, R.W., Mikamo, S., Reeder, D.D., Subramanian, A., Cork, B., Dayton, B., Benvenuti, A., Marquit, E., Kearney, P.D., Bussian, A.E., Mills, F., Radmer, C., and Winter, W.R., (1967), Phys. Rev., 164, 1584.
- Kasha, H., Leipuner, L.B., and Adair, R.K., (1966), Phys. Rev., 150, 1140.
- Kasha, H., Leipuner, L.B., Wangler, T.P., Alspector, J., and Adair, R.K., (1967a), Phys. Rev., 154, 1263.
- Kasha, H., Larsen, R.C., Leipuner, L.B., and Adair, R.K., (1967b), Proc. Int. Conf. Cosmic Rays (Calgary), Canad. J. Phys., 46, S730.
- Kasha, H., Larsen, R.C., Leipuner, L.B., and Adair, R.K., (1968a), Phys. Rev. Letts., 20, 217.
- Kasha, H., and Stefanski, R.J., (1968b), Phys. Rev. Letts., 20, 1256.
- Kasha, H., and Stefanski, R.J., (1968a), Phys. Rev., 172, 1297.
- Kelly, G.N., MacKeown, P.K., Said, S.S., and Wolfendale, A.W., (1967), Proc. Int. Conf. Cosmic Rays (Calgary), Canad. J. Phys., 46, S365.
- Kelly, G.N., MacKeown, P.K., Said, S.S., and Wolfendale, A.W., (1967b), Proc. Int. Conf. Cosmic Rays (Calgary), Canad. J. Phys., 46, S309.
- Kerns, Q.A., Kirstein, F.A., and Cox, G.C., (1959), Rev. Sci. Instrum., 30, 34.
- Khachatryan, M.N., and Pantuev, V.S., (1963), Sov. Phys., J.E.T.P., 18, 1239.
- Kinoshita, T., (1960), Phys. Rev. Letts., 4, 378.
- Krishnaswamy, M.R., Menon, M.G.K., Narasimham, V.S., Kawakami, S., Kino, S., and Miyake, S., (1968), 14th Int. Conf. High Energy Physics, (Vienna), unpublished.
- Lamb, R.C., Lundy, R.A., Novey, T.B., and Yovanovitch, D.D., (1966), Phys. Rev. Letts., 17, 1068.

- Landau, L., (1944), J. Phys. (U.S.S.R.), 8, 201.
- Lattes, C.M.G., Muirhead, H., Occhialini, G.P.S., and Powell, C.F., (1947), Nature, 159, 694.
- Leipuner, L.B., Chu, W.T., Larsen, R.C., and Adair, R.K., (1964), Phys. Rev. Letts., 12, 423.
- Lemaitre, G., and Vallarta, M.S., (1933), Phys. Rev., 43, 87.
- Lindenbaum, S.J., (1957), Ann. Rev. Nuc. Sci., 7, 317.
- Lloyd, J.L., (1960), Proc. Phys. Soc., 75, 387.
- Longo, M.J., (1968), CERN Report 68-7, Topical Conference on High Energy Collisions of Hadrons, p 523.
- Major, J.V., (1959), Ph.D Thesis, (Manchester), unpublished.
- Manning, G., Parham, A.G., Jafar, D.J., van der Raay, H.B., Reading, D.H., Ryan, D.G., Jones, B.D., Malos, J., and Lipman, N.H., (1966), Nuovo Cimento, 40, 167.
- Marshall, J., Marshall, L., and Nedzel, V.A., (1953), Phys. Rev., 93, 767.
- Marshall-Libby, L., and Thomas, F., (1968), 14th Int. Conf. High Energy Physics, (Vienna), unpublished.
- Masimenko, V.M., Sisakyan, I.N., Feinberg, E.L., and Chernavskii, D.S., (1966), Zh. Eksper. Teor. Fiz. Pis'ma., 3, 340.
- Massam, T., Muller, Th., and Zichichi, A., (1965), Nuovo Cimento Suppl., 3, 1268.
- Massam, T., and Zichichi, A., (1966), Nuovo Cimento, 43, 227.
- Massam, T., (1968), CERN report 68-24.
- Massam, T., and Zichichi, A., (1968), 'Quark Search at I.S.R.', I.S.R. Users Meeting (CERN).
- McDiarmid, I.B., (1959), Canad. J. Phys., 37, 79.
- McDowell, M.R.C., and Hasted, J.B., (1967), Nature, 214, 235.
- Menon, M.G.K., Naranan, S., Narasimham, V.S., Kinotani, K., Ito, N., Miyake, S., Craig, R., Creed, D.R., Osborne, J.L., and Wolfendale, A.W. (1967), Proc. Roy. Soc. (London), A301, 137.
- Miller, C.H., and Hincks, E.P., (1957), Canad. J. Phys., 35, 363.
- Morpurgo, G., (1968), 14th Int. Conf. on High Energy Physics (Vienna), p.224.

- Morpurgo, G., (1968), 'The Quark Model- Results and Problems' (to be published by Academic Press Inc., New York).
- Morrison, D.R.O., (1964), Phys. Letts., 2, 199.
- Mylori, M.G., and Wilson, J.G., (1951), Proc. Phys. Soc., A64, 404.
- Narayan, D.S., (1966), Nuovo Cimento, 44, 213.
- Nedzel, V.A., (1954), Phys. Rev., 94, 174.
- Neeman, Y., (1961), Nuc. Phys., 26, 222.
- Nir, A., (1967), Phys. Rev. Letts., 19, 336.
- Novey, T.B., (1965), CERN report 65-32, Informal Conf. on Experimental Neutrino Physics, p.71.
- Ogilvie, K.W., (1955), Canad. J. Phys., 33, 746.
- Osborne, J.L., (1967), Ph.D. Thesis, (Durham), unpublished.
- Palevsky, H., Friedes, J.L., Sutter, R.J., Chrien, R.E., and Muether, R.H., (1964), Proc. Cong. Int. Phys. Nucl., (Paris), p.162.
- Pathak, K.M., (1967), Ph.D. Thesis, (Durham), unpublished.
- Peyrou, C., and Legarrigui, A., (1950), J. Phys. Rad., 11, 666.
- Ryan, D., Acosta, V., Buckwalter, G., Carey, W., Cowan C.L., and Curtin, D., (1966), Phys. Letts., 21, 457.
- Saito, K., and Suga, K., (1959), Nuovo Cimento, 11, 600.
- Schopper, E., (1967), Handbuch der Physik, 46/2, 414.
- Serre, C., (1967), CERN report 67-5.
- Simpson, D.A., (1967), Ph.D Thesis, (Durham), unpublished.
- Sinanoglu, O., Skutnik, B., and Tousey, A., (1966), Phys. Rev. Letts., 17, 785.
- Sternheimer, R.M., (1953), Phys. Rev., 91, 256.
- Sternheimer, R.M., (1956b), Phys. Rev., 101, 384.
- Sternheimer, R.M., (1956), Phys. Rev., 103, 511.
- Sternheimer, R.M., (1960), Phys. Rev., 118, 1045.
- Sunyar, A.W., Schwarzschild, A.Z., and Connors, P.I., (1964), Phys. Rev., 136, B1157.

Symon, K.R., (1948), Ph.D Thesis (Harvard), unpublished.

Takahashi, T., (1967), private communication.

Tanikawa, Y., and Watanbe, S., (1959), Phys. Rev., 113, 1344.

Vainshtein, L.A., and Pikel'ner, S.B., (1966), Zh, Eksper. Teor. Fiz. Pis'ma., 4, 307.

Wolfendale, A.W., and Young, E.C.M., (1969), CERN Neutrino Meeting, Jan. 1969, to be published as a CERN report.

York, G.M., (1952), Proc. Phys. Soc., A65, 559.

Yukawa, H., (1935), Proc. Phys. Math. Soc., Japan, 17, 48.

Zweig, G., (1964), CERN reports 8182/Th 401 and 8419/Th 412.

